Activity-Directed Fragment-Based Ligand Discovery

Samuel James Liver

Submitted in accordance with the requirements for the degree of

Doctor of Philosophy

The University of Leeds

School of Chemistry

March, 2019

The candidate confirms that the work submitted is his own and that appropriate credit has been given where reference has been made to the work of others.

Acknowledgements

I am extremely grateful to Adam and Stuart for the opportunity to undertake a PhD under their supervision. Their support and guidance throughout the 3.5 years of my PhD have been invaluable and have allowed me to develop and flourish both professionally and personally. My time in the Nelson group has been a truly rewarding and enjoyable experience and I have met an extraordinary group of people, many of whom I hope will be friends with for life.

To the members of the Nelson group I would like to say a huge thank you. You have been great to work with and I have learnt something from each and every one of you. You have made my time in the group all the more enjoyable. I am sure you will all continue doing great things for the rest of your time in G56 and beyond. I have to give special mention to Chloe, Shiao and Adam with whom I have formed great friendships. Adam, you are one of the most intelligent people to grace the lab while I have been in G56 and you deserve all the success in the rest of your PhD and beyond. I will cherish those moments in pottery class with Chloe and Shiao. Chloe undoubtedly won top potter! I look forward to future road trips with the two of them and I will never forget the moment Shiao managed to squeeze inside a glass waste bin!

And to Jacob Masters, the one who has been there since day one. We went through four years of undergraduate together and barely spoke to one another, yet after 3.5 years later I consider you one of my closest friends. My time in G56 would undoubtedly have been less enjoyable without your presence. You are probably the most quick witted person I've ever met and you are finally free from the torment of doing a column!

I am also extremely grateful to Adam and Shiao for their contributions for the diazoamides I used in ADS and Chloe for being my proof-reader. I would also like to thanks members of Dr Anastasia Zhuravleva's group in FBS for their guidance with expressing and purifying protein.

Finally, I would like to thank all my family and friends who have supported me throughout my PhD. Your love and support have allowed me to live happily and made my time away from home all the easier.

Abstract

Biologically active small molecules are typically discovered in design-synthesis-purify-test cycles. These workflows are underpinned by a remarkably narrow toolkit of robust and reliable chemical transformations and place equal resources on all molecules regardless of their biological function. Activity-directed synthesis harnesses the potential of chemical reactions that can form more than one possible product and allows resources to be focussed on small molecules with biological activity. The discovery of small molecules through activity-directed synthesis emerge in parallel to their associated synthetic routes. A feedback mechanism can serve to optimise the range of bioactive products, analogous to the emergence of natural products through the evolution of biosynthetic pathways found in nature.

The implementation of fragments as substrates in activity-directed synthesis has the potential to enable their optimisation into lead-like compounds without the target molecule being predefined, contrasting starkly to typical structure-guided fragment-to-lead studies. A range of C-H functionalisation chemistry was configured in microscale parallel reaction array format, for its implementation as a fragment elaboration strategy in activity-directed synthesis. This chemistry, along with the previously established metal-catalysed carbenoid chemistry, was assessed for its potential to elaborate Hsp90 fragments. To ensure a streamlined workflow for activity-directed synthesis a series of protocols, for scavenging of metal catalysts and electrophiles and removal of fragment protecting groups, was established for use in parallel reaction array format.

To enable the elaboration of Hsp90 fragments with the chosen chemistries in activity-directed synthesis, a set of fragments designed for biological activity against Hsp90 was prepared. The fragments were screened in the established high-throughput assay and led to the discovery of analogues of Hsp90 fragments with previously unreported activity. The use of the high-throughput assay and LC-MS enabled the biological activity and success rate of the crude reaction mixtures from the arrays to be rapidly assessed. The study highlighted the poor functional group tolerance of modern chemical

methodologies and the need for robust and reliable chemical transformations in medicinal chemistry workflows.

List of Abbreviations

Ac	acetyl
Ac_2O	acetic anhydride
AcOH	acetic acid
ADP	adenosine diphosphate
ADS	activity-directed synthesis
app.	apparent
Ar	aromatic
ATP	adenosine triphosphate
b.p.	boiling point
Bn	benzyl
Boc	tert-butyloxycarbonyl
BODIPY-GM	BODIPY-labelled geldanamycin
BQ	benzoquinone
ca	around, about
CAS	Chemical Abstracts Service
CD	carboxy terminal domain
CH_2Cl_2	dichloromethane
CHK1	serine/threonine-protein kinase
COSY	correlation spectroscopy
δ	chemical shift
d	doublet
DCC	dynamic combinatorial chemistry
DEL	DNA-encoded libraries
DG	directing group
DIPEA	*N*,*N*-diisopropylethylamine
DMF	*N,N'*-dimethylformamide
DMSO	dimethyl sulfoxide
DOS	diversity-oriented synthesis

e.g.	*example gratia*; for example
ES	electrospray ionisation
Et	ethyl
etc.	*et cetera*; and so forth
ether	diethyl ether
EtOAc	ethyl acetate
FA	fluorescence anisotropy
FBDD	fragment-based drug discovery
FDA	United States Food and Drink Administration
GM	geldanamycin
h	hour
HCV	hepatitis C virus
hept	heptet
HFIP	hexafluoro-2-propanol
HIF1α	hypoxia-inducible factor 1α
HPLC	high performance liquid chromatography
HRMS	high resolution mass spectrometry
HSF1	heat-shock factor 1
Hsp70	Heat shock protein 70
Hsp90	Heat shock protein 90
HTS	high-throughput screening
Hz	Hertz
i.e.	*id est;* that is
IC_{50}	half-maximal inhibitory concentration
in silico	via computer simulation
in vivo	within the living
IR	infrared
ITC	isothermal titration calorimetry
J	spin-spin coupling constant

K_d	dissociation constant
LC-MS	liquid chromatography mass spectrometry
LE	ligand efficiency
logP	octanol-water partition coefficient
LOS	lead-oriented synthesis
m	multiplet
Me	methyl
MeCN	acetonitrile
MeOH	methanol
MIDA	*N*-methyliminodiacetic acid
MS	mass spectrometry
MTD	middle terminal domain
NME	new molecular entity
NMP	*N*-methyl-2-pyrrolidone
NMR	nuclear magnetic resonance
nOe	nuclear Overhauser effect
NOESY	nuclear Overhauser effect spectroscopy
NTD	amino terminal domain
Nu	nucleophile
PDB	protein data bank
Petrol	petroleum spirit
P_i	inorganic phosphate
ppm	parts per million
Pr	propyl
q	quartet
R_f	retention factor
rt	room temperature
s	singlet
SAR	structure-activity relationship

SDS PAGE	sodium dodecyl sulfate polyacrylamide gel electrophoresis
sext.	sextet
S_NAr	nucleophilic aromatic substitution
SPR	surface plasmon resonance
t	triplet
tert	tertiary
TFA	trifluoroacetic acid
THF	tetrahydrofuran
TIPS	triisopropylsilane
TLC	thin layer chromatography
TM	transition metal

Table of Contents

Chapter 1.
Chemical Approaches to Enable the Exploration of Chemical Space

Biologically active small molecules are of immense value in medicinal chemistry and chemical biology.[1,2] They rank highly in the top FDA approved prescription drugs[3] and can enable fundamental biomedical research.[4] However, the discovery of bioactive small molecules is extremely challenging. Bioactive small molecules are typically discovered in design-synthesis-purify-test workflows, which are underpinned by a narrow toolkit of chemical transformations. This has led to a lack of productivity in the pharmaceutical industry,[5] encouraging the development and uptake of new molecular discovery practices.

Herein, an overview of current and emerging approaches for molecular discovery is given, followed by the recent revolution in automated high-throughput microscale experimentation for increasing productivity within the pharmaceutical industry. Function-driven approaches, which have the potential to disrupt practices within current discovery workflows, are discussed, followed by an outline of the proposed project – Activity-Directed Fragment-Based Ligand Discovery.

1.1 Bioactive Small Molecule Discovery

1.1.1 The Pharmaceutical Industry

The ability to treat disease is largely driven by biologically active small molecules, with nine of the top ten prescribed drugs in the US in 2014 being small molecules.[3] However, the discovery of bioactive small molecules remains an enduring challenge in both medicinal chemistry and chemical biology. The discovery process, and associated costs, have come under greater scrutiny in recent years[5] and despite increased investment, the rate of drug discovery has remained roughly constant for the last 60 years.[6] Estimates for bringing a new molecular entity (NME) to market, when accounting for costs incurred in failed drug campaigns, lie at *ca.* $2 billion.[5] This enormous cost can be attributed to two key areas of the drug discovery

pipeline. Firstly, the pre-clinal (lead discovery) phase accounts for a third (32%) of all associated costs in drug discovery, as a large number of programmes fail to lead to marketed drugs. Secondly, attrition rates in clinical trials are extremely high, with rates of attrition in phases II and III being estimated at 66% and 30% respectively.[5] As a result, marketed drugs have to carry the costs of failed drug campaigns to recoup the huge investments in research and development. These enormous costs and high attrition rates are evidence that more high-quality, cost-effective candidates, that are able to evade attrition in clinical trials, are needed. Indeed, increasing productivity has been identified as the pharmaceutical industry's grand challenge.[5]

1.1.2 Exploration of Biologically Relevant Chemical Space

The discovery of high-quality chemical probes is paramount for understanding the fundamental biology of a protein, however, the historical exploration of protein biology has been highly uneven.[4] To enable the underpinning biology of new and challenging targets, e.g. protein-protein interactions, to be understood, new classes of small molecules will likely be required.[7] Chemical space is the total number of possible compounds that confirm to a given set of conditions (e.g. <500 Da and number of heavy atoms). Chemical space is multidimensional and is defined by multiple descriptors such as charge, surface area and number of hydrogen bond donor/acceptors, not simply the three dimensional space that the compound fills. The ability to explore biologically relevant chemical space (often described by Lipinksi's 'Rule of 5'[8]) in search of novel bioactive small molecules is arguably the medicinal chemists greatest challenge. Chemical space is vast and based on extrapolation from an enumerated library of molecules with up to 17 heavy atoms (GDB17), there are 10^{33} possible molecules with up to 36 heavy atoms.[9] The historical exploration of chemical space by chemists has been highly uneven and unsystematic, highlighted by the fact that half of the small molecules in the CAS registry are based on just 0.25% of the known molecular frameworks.[10] This has resulted in a lack of scaffold diversity in medicinal chemistry space[11] and drugs.[12] This unsystematic approach to chemical space exploration can be attributed to the

workflows, and their underpinning chemistries, employed during drug discovery.

Early-stage drug discovery is initiated by a variety of strategies. A review of clinical candidates published in the *Journal for Medicinal Chemistry* (in 2016 and 2017)[13] concluded the most common lead generation strategies, amongst others, were; known starting points derived from previous campaigns (44%), high-throughput screening (HTS) of compound libraries (29%) and structure-based drug design (14%). HTS of large compounds libraries is routine in drug discovery and generates series of hit compounds against a specific biological target.[14] Hit compounds provide starting points for drug discovery and the development of detailed structure-activity relationships (SAR) can facilitate lead discovery and optimisation. The potency, selectivity and physiochemical properties of the compounds are improved through iterative design-synthesis-purification-test cycles (Figure 1.1).[15] This empirical approach of design, synthesis and testing usually all takes place in isolation from assessment of function, meaning that equal resources and time are spent on all molecules regardless of biological function.[16,17]

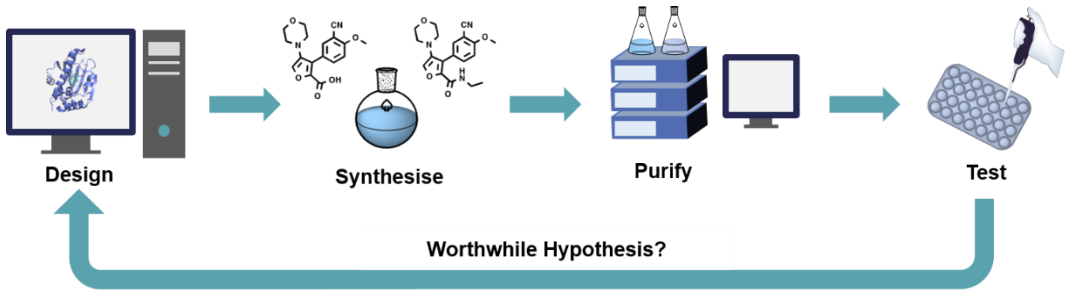

Figure 1.1 *Overview of current workflows in bioactive small molecule discovery*

Medicinal chemists have relied on a remarkably narrow toolkit of robust and reliable chemical transformations in drug discovery workflows,[18–22] which has contributed to the lack of structural diversity and uneven exploration of chemical space. Medicinal chemists reliance on a limited suite of chemical reactions, such as amide formations, Suzuki-Miyaura and S_NAr reactions, has resulted in densely populated areas of chemical space with structurally similar compounds.[20] These reaction types typically contribute to the increased

exploration of more lipophilic and flat (sp^2-rich) compounds,[23,24] which typically have higher attrition rates compared with more sp^3-rich compounds.[25] For compounds to have desirable molecular properties for successful drug discovery,[8,26] libraries need to be prepared from highly functionalised and polar substrates.[26,27] Given that such substrates systematically fail synthesis and can prove challenging for purification, compound libraries can suffer from 'logP drift', resulting in compounds moving away from their intended molecular properties.[27] The pharmaceutical industry has highlighted the need to explore a wider range of reaction classes,[18,28] for example, photoredox catalysis to enable C(sp^3)-H functionalisation[29,30] for fragment optimisation studies [31] and indeed, the range of reactions published in US patents over the last 40 years has gradually been increasing.[24]

To address some of the challenges of chemical space exploration, there has been an increased focus on strategies that enable the efficient development of more diverse compound libraries, containing scaffolds that have the potential to explore previously untouched areas of chemical space. More structurally diverse compound libraries are believed to increase the odds of addressing a broad range of biological targets. Diversity-Oriented Synthesis (DOS) is the divergent construction of distinctive scaffolds using minimal synthetic steps,[32] which has been applied in the creation of fragment,[33] small molecule,[34] peptide[35] and macrocylic[36] libraries (Figure 1.2). An analogous approach, Lead-Oriented Synthesis (LOS), relies on a similar divergent approach for compound library preparation, but places greater emphasis on the molecular properties of the compounds,[37] by focussing attention on compounds which lie within lead-like chemical space (Figure 1.2). Lead compounds can act as stronger starting points in drug-discovery, as ligand optimisation ensures final compound libraries maintain their desired molecular properties. While DOS/LOS libraries can enable underexplored areas of chemical space to be studied, there are no guarantees library compounds will lead to the identification of biological activity during the screening phase.

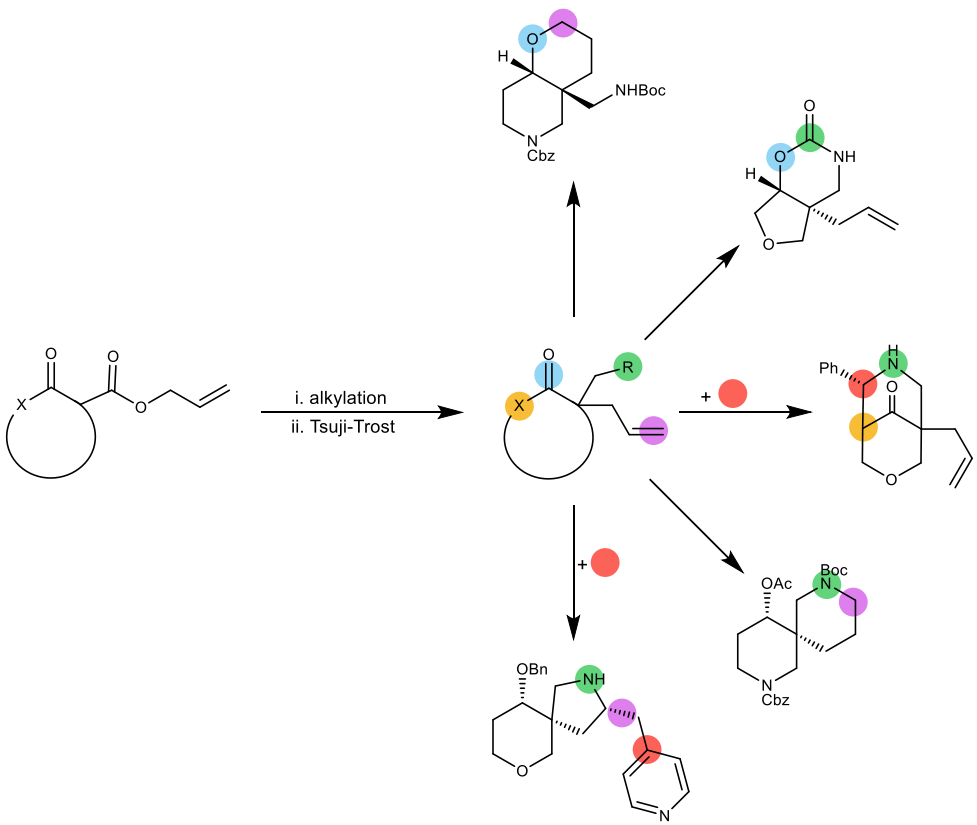

Figure 1.2 *Overview of the synthetic strategy utilised in Diversity- and Lead-Oriented Synthesis. Colours represent pair-wise cyclisation strategies to generate diverse molecular scaffolds.*[38]

Alternative high-throughput technologies have emerged as potential sources for novel compound collections, such as Dynamic Combinatorial Chemistry (DCC), which is the preparation of compound libraries synthesised from building blocks based on their affinity for a protein,[39] and DNA-encoded libraries (DEL) which enables the deeper sampling of chemical space by four or five times compared to traditional high-throughput screening methods (Figure 1.3).[40] However, both approaches suffer from a limited range of chemistries applicable to their respective technologies, most notably DCC, which relies on reversible chemistry that must be suitable for protein stability, limiting the potential diversity of products possible. While these strategies can help address the lack of scaffold diversity in screening libraries (typical library size 10^6), they fail to address the issue of how to most efficiently sample biologically relevant chemical space (10^{33} compounds with 36 heavy atoms).

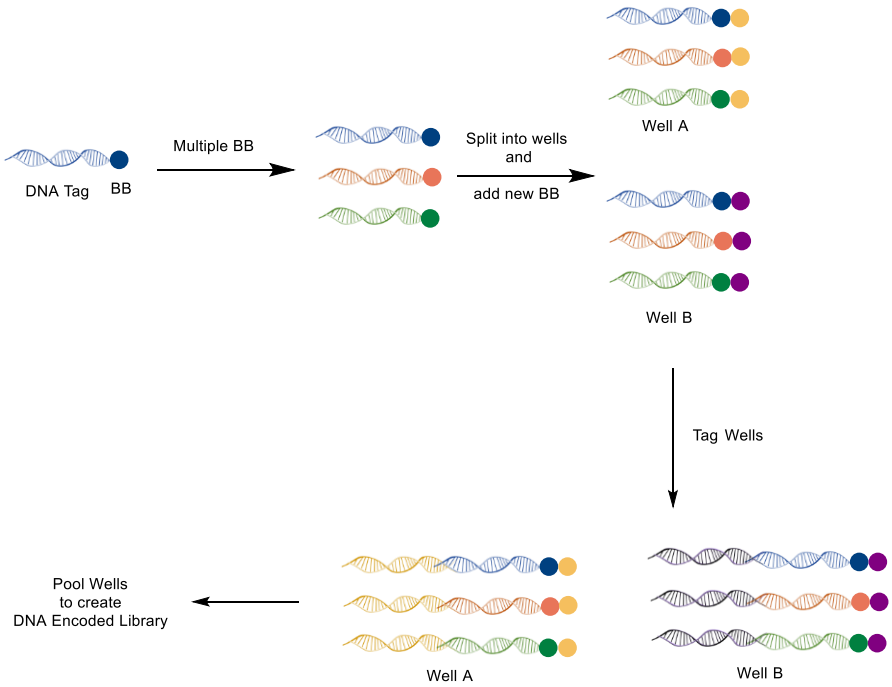

Figure 1.3 *Overview of the preparation of DNA-Encoded Libraries. BB – Building Blocks.*

1.1.3 Fragment-Based Drug Discovery

Fragment-based drug discovery (FBDD) has become a widely adopted strategy in the pharmaceutical industry (5% of leads come from fragment screens),[32,41,42] as a means of efficiently sampling biologically relevant chemical space. This is because the size of chemical space increases exponentially with molecular size, and so there are only ~10^7 possible fragment-sized compounds.[41,43] There have been several metrics proposed for capturing fragment space, for example, Astex restrict fragment libraries to compounds with molecular weight 140-230 g mol^{-1}, 10-16 non-hydrogen atoms and clogP: 0.0 to 2.0.[44] Fragments typically have lower complexity, compared to traditional screening libraries, and are more likely to form favourable interactions with a biological target.[45] FBDD typically undergoes (1) fragment library design, (2) screening of the fragment library and (3) fragment elaboration and optimisation.[46]

Fragments tend to have lower affinities (0.1 – 10 mM) towards biological targets, compared to traditional screening compounds, but it is believed the interactions between the fragment and the target tend to be of higher quality

i.e. have high ligand efficiency (see below).[47] Fragment binding reveals protein hot-spots which drive high affinity ligand binding.[48] However, detecting weaker fragment-protein interactions can be challenging and so biophysical screening techniques such as X-ray crystallography, NMR, ITC and SPR are routinely used in fragment screens, which detect binding rather than inhibition.[46,48] It is the specificity of the binding interactions and the potential to build or grow off the hit that needs to be considered when analysing a fragment hit.

Once a fragment hit has been identified, validated and binding mode established, the fragment undergoes cycles of elaboration to develop the hit into a lead.[49] Fragment linking involves connecting multiple fragments together that bind at adjacent sites in the target (Figure 1.4).[46] When a fragment's binding mode has been identified, it has revealed its preferred orientation to the target. Maintaining each fragments binding mode and ensuring the linker itself makes favourable interactions within the binding site can be extremely challenging.[46] Fragment growing is seen as a more tractable approach in FBDD which involves growing a fragment synthetically along one or many vectors to establish new interactions with the target (Figure 1.4). Structural information is often key for developing a successful fragment.[46]

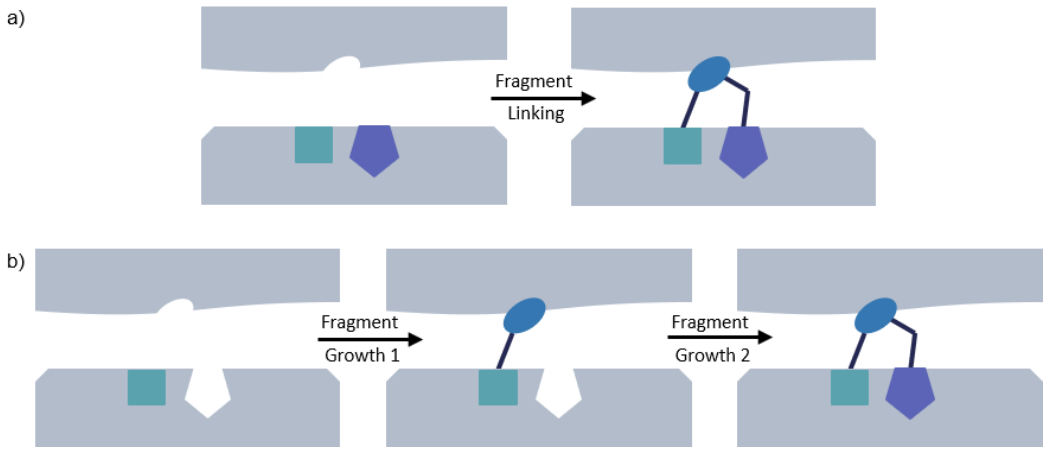

Figure 1.4 *Overview of fragment elaboration. a) Fragment linking of two fragments hits bound in adjacent sites of protein binding pocket. b) Fragment growth by synthetically elaborating along one (or many) vector(s) of the fragment into adjacent binding sites.* [46,49]

At each stage of the design, synthesis, testing and evaluation in the fragment growth cycle, ligand efficiency (LE) can be used to assess the success of the newly evolved fragment.[48,50] Ligand efficiency is defined as the free energy of binding of the ligand, divided by the number of heavy atoms in the ligand (or average binding per heavy atom), which can be used to assess whether the additional molecular mass has contributed significantly to fragment-protein binding.[50] Ultimately the choice of fragments to pursue will be selected based on the potency, ligand efficiency, synthetic tractability and more general medicinal chemistry considerations.

The value of FBDD has been realised with two drugs discovered in fragment programmes now marketed, Vemurafenib[51] and Venetoclax[52], as well as numerous clinical candidates (Figure 1.5)[41,42]. However, there are still some challenges that must be overcome if FBDD is to fulfil its promised potential. FBDD relies on knowledge of the fragments binding mode to the target and often requires the development of synthetic routes at each stage of the fragment elaboration cycle. These fragment elaboration cycles can be extremely iterative and hence both money and time-consuming. One attractive concept in FBDD is the opportunity to synthetically grow the fragment in three-dimensions, i.e. accessibility to all vectors of the fragment, allowing for the broader exploration of chemical space.[44] The development of methodologies that allow for synthetic growth along multiple vectors, such as C-H bond functionalisation at sp^2- and sp^3-centres, that incorporate protentional problematic polar binding groups in synthetic methodologies,[53] can only enhance the potential of FBDD.[31]

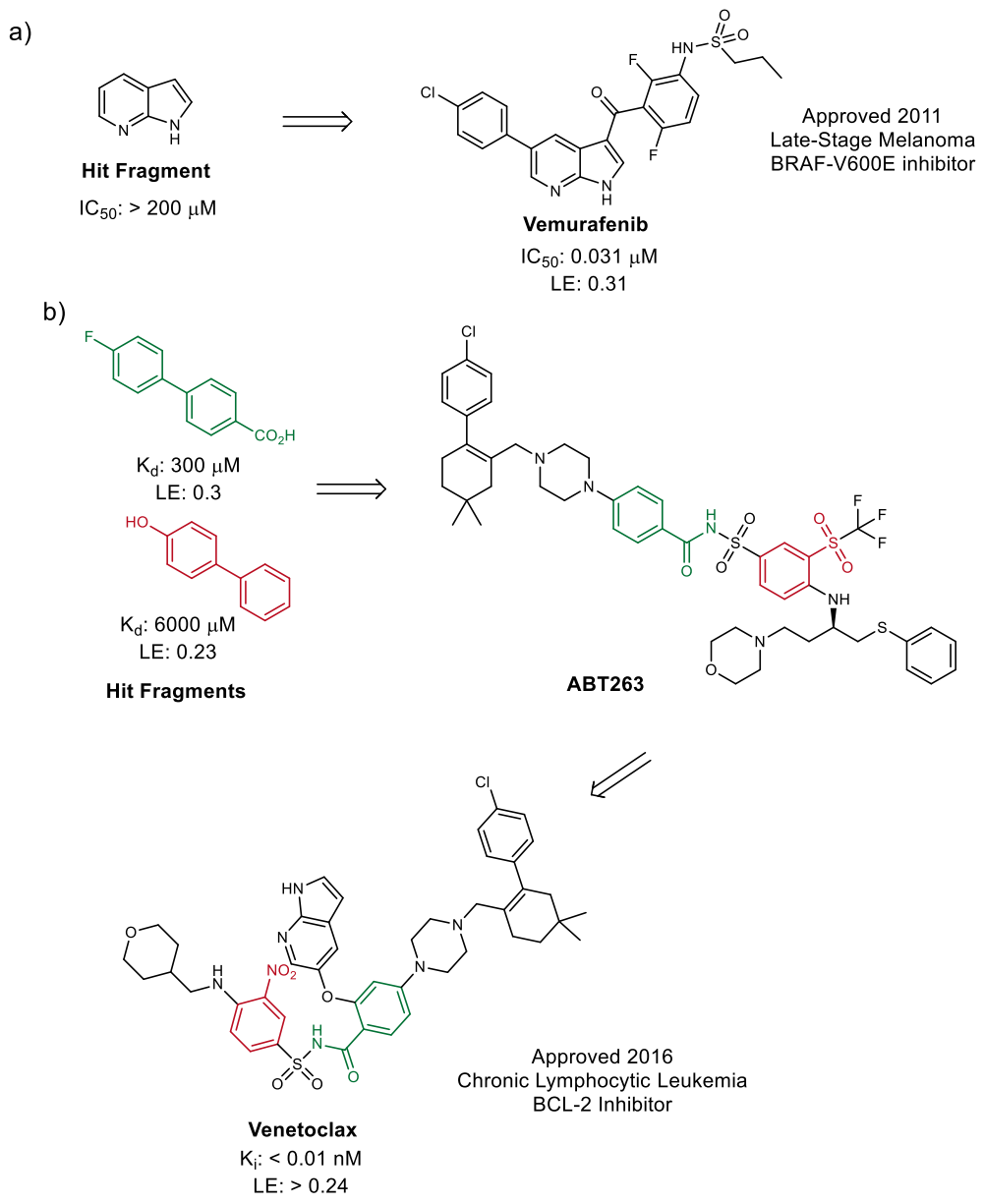

Figure 1.5 *The two current marketed drugs, a) Vemurafenib and b) Venetoclax, that have been discovered from fragment-based drug discovery programmes.*[51,52]

1.1.4 Automation in Drug-Discovery to Enable High-Throughput Experimentation

Automation has played a key role in the pharmaceutical industry for many years,[54] most notably in the high-throughput screening of compound libraries to generate hit compounds.[14] More recently there has been a marked increase in the use of automation and high-throughput experimentation in drug discovery workflows. Automation of chemical synthesis has been aided by technological advancements,[55] and has been applied, for instance, in the

synthesis of an array of small molecules using a single automated process.[56] *N*-methyliminodiacetic acid (MIDA) boronate building blocks (protected to enable greater stability and prevent polymerisation) were iteratively coupled in a linear fashion, using a technology which incorporated coupling, deprotection and purification modules to give a library of diverse small molecules. The linear compounds were cyclised to give a range sp^3-rich macro- and polycyclic natural product and natural product-like cores (Figure 1.6).[56]

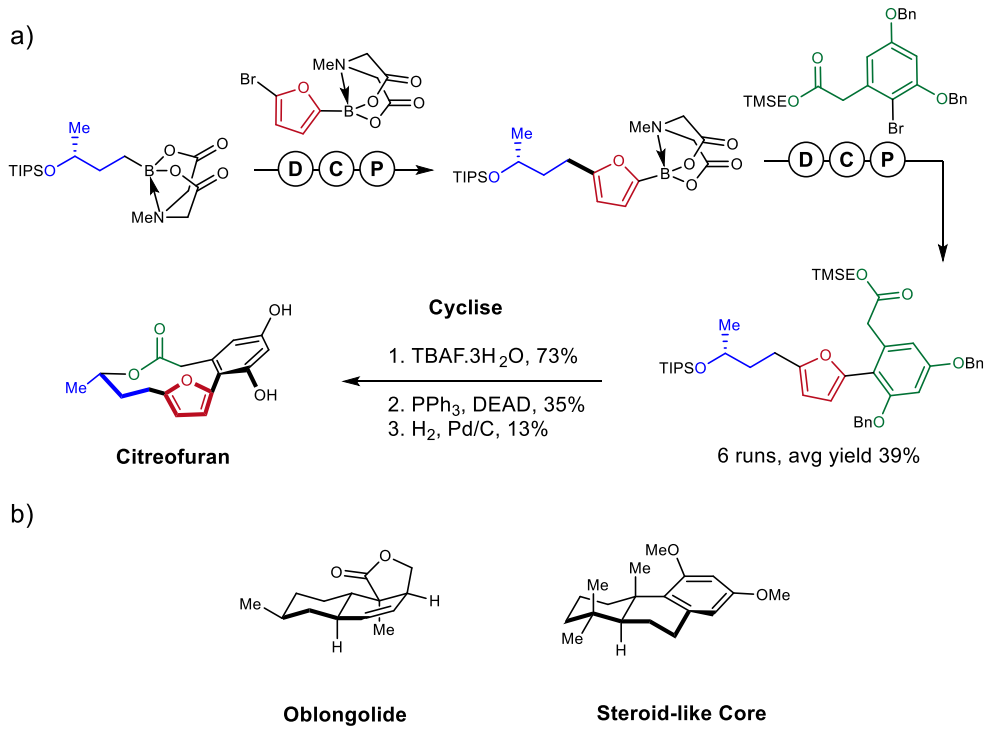

Figure 1.6 Overview of the automated *synthesis of an array of small molecules using MIDA boronate building blocks. a) Automated linear synthesis and cyclisation of Citreofuran b) Exemplar sp^3-rich macro- and polycyclic natural products and natural product-like cores.* ***D****: Deprotection of protected boronate building block,* ***C****: Couple and* ***P****: Purification.*

Given that target molecules in medicinal chemistry need to be prepared from polar and highly functionalised substrates, they tend to perform poorly in chemical reactions and often require bespoke reaction conditions for each specific combination of substrates.[19,26,57] Automated high-throughput experimentation has enabled the rapid exploration of multiple reaction parameters, to optimise conditions for specific reaction classes, using only small amounts of material.[57,58] A range of palladium catalysed coupling

reactions (C-C, C-N and C-O cross couplings) was, on nanomole scale, optimised in batch[57] and flow-based[58] systems, by exploring discrete (catalysts and bases) and continuous (reagent stoichiometry and catalyst loading) parameters. The optimisation study enabled a broader scope of substrates to be used, enabling a greater number of compounds to be successfully prepared, thus increasing the value of the specific reaction class. Automated high-throughput experimentation has also enabled the discovery of novel reaction classes e.g. in the nickel catalysed variant of alkyne diarylation.[59]

The automation of these processes has almost always been performed on isolated stages of discovery workflows,[60] as ensuring all stages of the discovery workflows for full integration, have a high- and matched-throughput is challenging. The major bottleneck in integrating stages of discovery workflows is almost always purification, due to widely adopted purification technologies (e.g. mass-directed HPLC, which is performed in series), in the industry.[60] However, there are reported examples in which automated synthesis and biological evaluation have been integrated.[61–68] One approach, ‘nanoscale synthesis and affinity ranking’,[68] integrated reaction optimisation, library synthesis and affinity ranking of library compounds in the discovery of serine/threonine-protein kinase (CHK1) inhibitors (Figure 1.7).

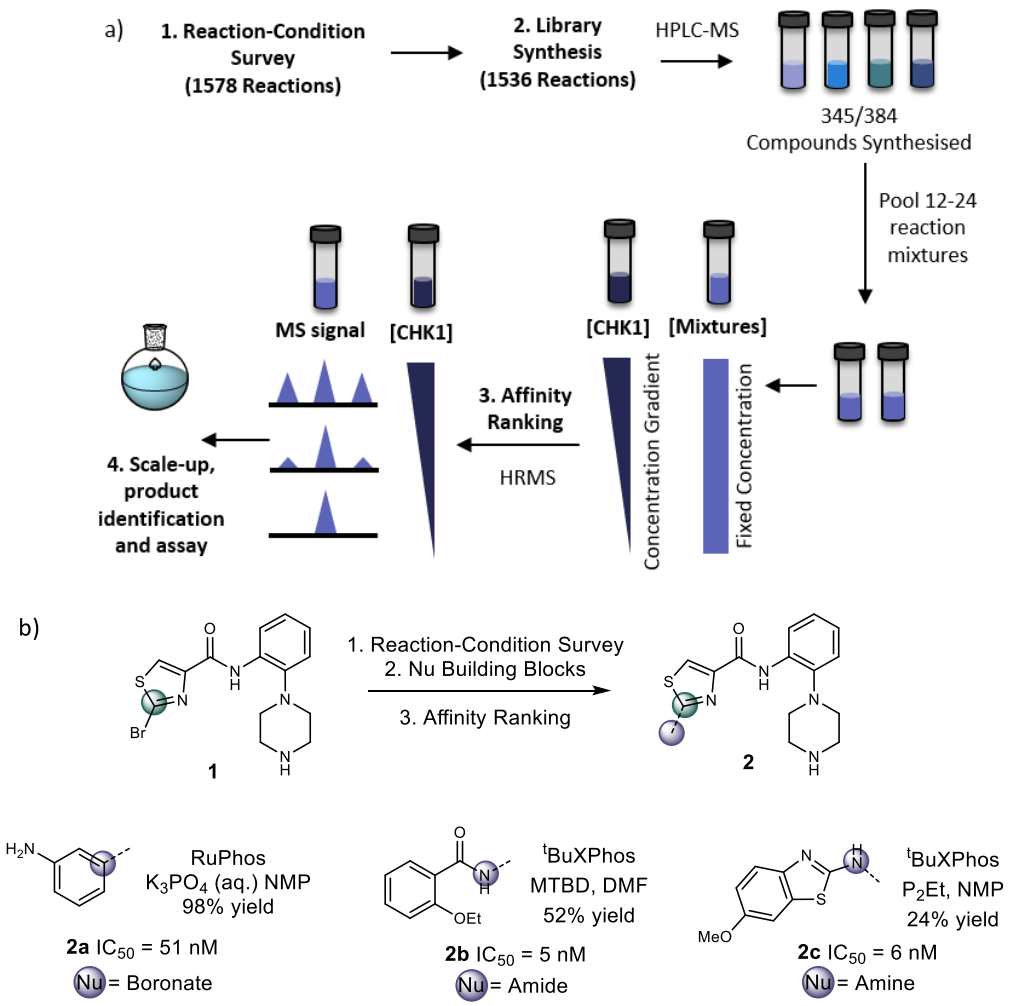

Figure 1.7 *Overview of nanoscale synthesis and affinity ranking. a) The integrated workflow in which reaction conditions were assessed, a library of 345/384 compounds synthesised, mixtures pooled and the library products assessed and ranked against CHK1 using affinity-selection mass spectrometry. b) Exemplar CHK1 inhibitors discovered from nanoscale synthesis and affinity ranking studies.*[60,68]

Palladium-catalysed cross couplings, C-C, C-O, C-S and C-N, were exploited in the preparation of a small compound library. Four sets of reaction conditions were identified for each class of nucleophile (thiols, alkynes, boronates, alcohols, amides, amines and sulphonamides) for reaction with bromothiazole **1** to enable the synthesis of 384 target compounds. Of the 384 target compounds, 345 were successfully synthesised (compared to 158 under the single best reaction conditions) on a 100 nmol scale (Figure 1.7). Reaction mixtures (12-24) were pooled together and incubated with the target protein, CHK1, at range of protein concentrations. The mixtures were eluted through a size-exclusion column to remove unbound compounds, and the

identity of the bound compounds identified by HRMS (Figure 1.7a). By incubating compounds along a concentration gradient of the target protein, ligands were ranked based on their affinity to CHK1. A range of CHK1 inhibitors, **2a-c**, was discovered following successful scale up, product identification and biological activity confirmation (Figure 1.7b).

The ability to initially assess the biological function of crude reaction mixtures can eliminate purification bottlenecks in integrated discovery workflows. Indeed, the direct screening of crude reaction mixtures has been performed in the 'off-rate' screening, by SPR, of unpurified reaction products, containing designed test compounds, in the fragment-to-hit phase of FBDD.[69] The rapid assessment of crude reaction products performed in high-throughput microscale reaction arrays, that incorporate previously underutilised reaction classes, could disrupt current practices within the pharmaceutical industry, enabling the increase in productivity and in chemical and biological innovation.

1.2. Function-Driven Approaches to Bioactive Small Molecule Discovery

1.2.1 Emergence of Natural Products through Biosynthetic Pathway Evolution

Natural products have been a huge inspiration in drug discovery programmes, inspiring around third of FDA approved drugs between 1980 and 2010.[70] Atorvastatin is a microbial natural product used for the treatment of hypocholesterolemia, and has inspired a range of other statin drugs, e.g. Lovastatin.[70] Natural products provide a source of biologically-relevant chemical diversity, with a broad range of pharmacophores and inherently higher fraction of sp^3-hybrisided carbons, compared to synthetic compounds.[71] Natural product emergence through biosynthetic pathways[72,73] is remarkably different to the discovery of synthetic bioactive small molecules. Natural products arise based on their benefit to the host organism. Nucleic acids are transcribed and translated to produce biosynthetic enzymes, which use simple bioavailable molecules (primary metabolites) as building blocks for natural product synthesis. Evolutionary pressure provides a feedback loop

that serves to optimise the range of natural products produced. As a result, bioactive products emerge in parallel to their biosynthetic routes (Figure 1.8). Two function-driven approaches for bioactive small molecule discovery, Synthetic Fermentation[74] and Activity-Directed Synthesis[16,17], have some parallels to the emergence of natural products.

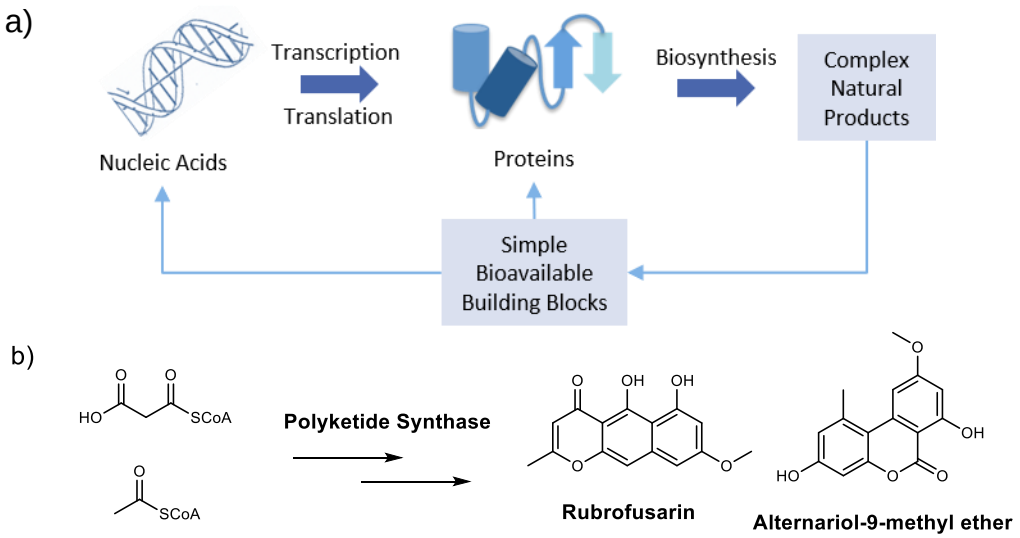

Figure 1.8 a) *Evolution of biosynthetic pathways found in nature. b) Exemplar natural products that arise through biosynthetic pathways.*[75,76] *Rubrofusarin and Alternariol-9-methyl ether have been reported as having antimicrobial effects.*

1.2.2 Synthetic Fermentation

Synthetic fermentation is a function-driven bioactive small molecule discovery approach that enabled the discovery of bioactive *β*-peptide inhibitors of HCV NS3/4A protease.[74] Products were prepared by reacting simple building blocks in arrays of plate-based reactions termed 'cultures'. Aqueous-tolerant amide-forming ligations were exploited, by reaction of α-keto acid initiators (**I**) with isoxazolidine elongation monomers (**M**) to yield α-keto acid oligomers, which upon reaction with terminator (**T**) building blocks stopped the elongation process (Figure 1.9a). The sequences, structures and compositions of the products could be modified by altering the building blocks and conditions used. Thousands of compounds were readily prepared by combining suitable building blocks in aqueous solution and screened directly, without purification, in the biological assay. Each well contained several major

products, which could be identified from the building blocks used. Active compounds were then identified using combinatorial deconvolution strategies.

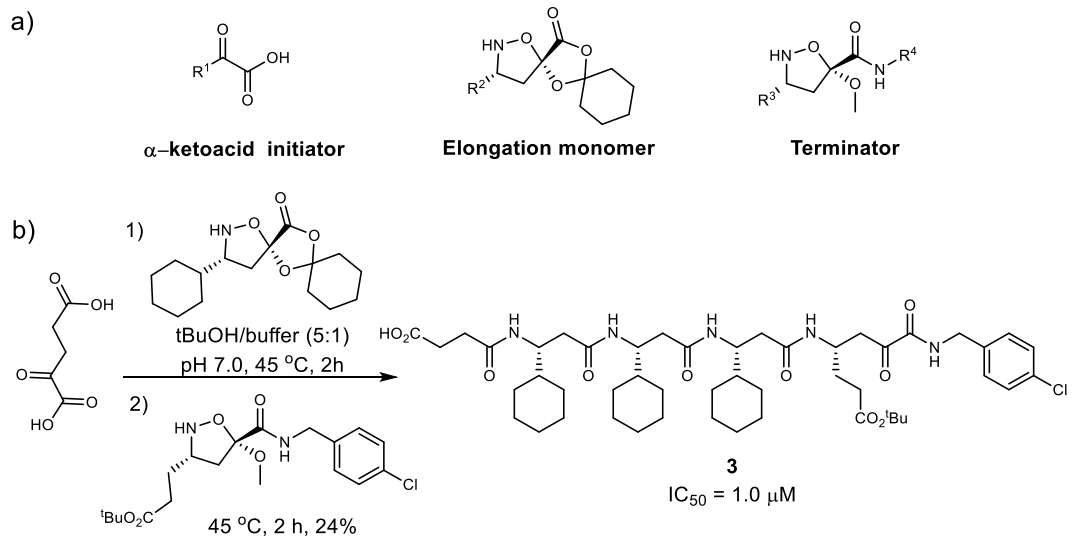

Figure 1.9 *Overview of synthetic fermentation a) Representative initiator (**I**), elongation monomer (**M**) and terminator (**T**) building blocks. b) Discovery of a hepatitis C virus N53/4A protease inhibitor **3**, (IC_{50} = 1 μM).*[74]

Three rounds of reactions were performed and after each round, analysis and identification of active mixtures was performed to reveal how effective moieties had performed. Poorly performing moieties were eliminated in subsequent rounds and only functional building blocks were taken forward for further study, ensuring subsequent rounds focussed only on producing bioactive mixtures. The approach resulted in the discovery of a hepatitis C virus N53/4A protease inhibitor **3** (IC_{50}: 1 μM), that was readily identified and characterised from around 6000 unnatural peptides that were synthesised from just 23 building blocks (Figure 1.9b). However, the necessity for aqueous chemistry limits the range of compatible chemical transformations, greatly reducing the diverse range of products possible.

1.2.3 Activity-Directed Synthesis

Activity-directed synthesis (ADS) is the function-driven discovery of bioactive small molecules, in which the target molecule is not predefined at the outset of the discovery phase.[16,17] Reactions with many possible outcomes

are deliberately chosen, which can be steered by the specific reaction conditions used. Arrays of microscale reactions are performed, in which the components (substrates, catalysts, solvents etc.) are varied. Following reaction completion, the crude mixtures are scavenged, evaporated, and screened, without purification, for biological activity. Reactions that yield active products inform the design of subsequent reaction arrays, by varying the components of those reactions. Finally, after multiple rounds of ADS, promising reaction mixtures are scaled-up to enable purification, structural elucidation and characterisation of the responsible bioactive small molecules (Figure 1.10). Unlike conventional medicinal chemistry workflows, ADS enables resources to be focussed solely on small molecules with biological function. The approach is iterative, and enables the function-driven discovery of biologically active small molecules in parallel with their associated synthetic routes.

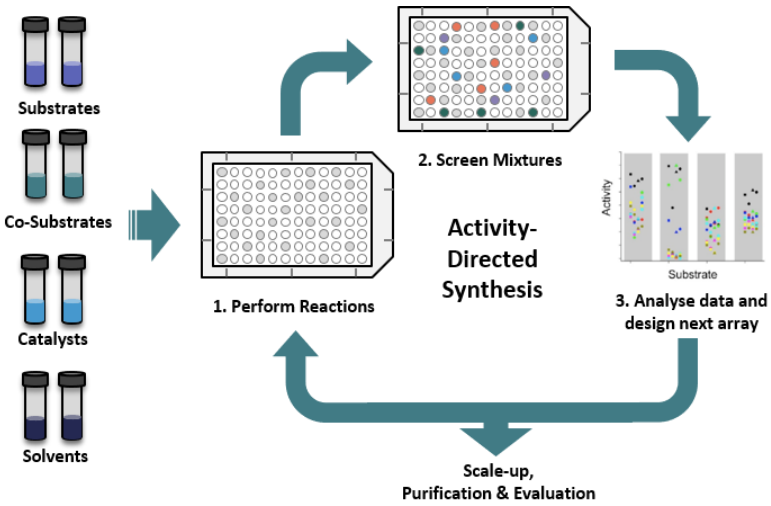

Figure 1.10 *Overview of the workflow in Activity-Directed Synthesis: Reaction arrays are performed, scavenged and screened for biological activity. Subsequent reactions arrays are designed by varying the components of active product mixtures. The most promising reactions are scaled-up to identify the bioactive small molecules.*[16,17]

ADS has been demonstrated as a powerful small molecule discovery approach, in a series on intra-[16] and intermolecular[17] studies, that enabled the efficient discovery of novel ligands with submicromolar activity against the androgen receptor. Metal-catalysed carbenoid chemistry, exploiting a range of α-diazoamide compounds, was chosen as many possible reaction modes

are possible, including intermolecular C-H, N-H and O-H insertions, cyclopropanations, ylide formation/cycloaddition as well as intramolecular variations that yield varying ring sizes, enabling the possible evaluation of a wide-range of chemotypes.[77–79]

The initial intramolecular study of ADS employed a range α-diazoamides **4**-**19**, bearing a known (4-cyano 3-trifluromethyl phenyl) binding group of the androgen receptor (Figure 1.11). Reaction arrays were performed in which the diazo substrate, catalyst and solvent were varied.

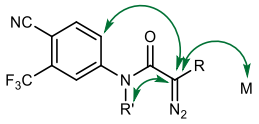

	R'	R	
		Ac	**H**
Round 1 Diazoamides for Intramolecular series	^{n}Pr	**4**	**5**
	CH_2Ph	**6**	**7**
	$(CH_2)_2Ph$	**8**	**9**
	$(CH_2)_2CH{=}CH_2$	**10**	**11**
	$(CH_2)_2{}^{i}Pr$	**12**	**13**
	$CH_2CONMe(CH_2)_2CH{=}CH_2$	**14**	**15**
Round 2 Diazoamides for Intramolecular series	^{n}Pr	**4**	**-**
	CH_2Ph	**6**	**-**
	$(CH_2)_2Ph$	**-**	**9**
	$(CH_2)_2CH{=}CH_2$	**10**	**-**
	$CH_2CONMe(CH_2)_2CH{=}CH_2$	**14**	**15**
Round 3 Diazoamides for Intramolecular series	^{n}Pr	**4**	**-**
	CH_2Ph	**6**	**-**
	$(CH_2)_2OMe$	**16**	**-**
	4-pyridylmethyl	**17**	**-**
	$(CH_2)_2CN$	**18**	**-**
	Propargyl	**19**	**-**
Diazoamides for Intermolecular series	Me	**20**	**21**
	Cyclopropyl	**22**	**23**

Figure 1.11 *α-Diazoamides, with many possible intra/intermolecular reaction modes, that were utilised in activity-directed synthesis.* ***4-19*** *were used for intramolecular reactions and* ***20-23*** *for intermolecular reactions in the discovery of androgen receptor agonists.*

In the first array 36 reactions were explored, in which twelve diazoamides **4**-**15** and three catalysts in dichloromethane were varied. After 48 h, reactions were scavenged for metal catalysts, evaporated and screened (total product concentration: 10 μM) directly, without purification, for agonism of the androgen receptor. Of the 36 reactions, substrates **4**, **6**, **9** and **10** yielded product mixtures with biological activity, which were used to inform the design of the second array. The four most promising substrates **4**, **6**, **9** and **10**, along with two control substrates, **14** and **15** were explored with an expanded range of eight catalysts and four solvents. Following scavenging and evaporation, the product mixtures were screened (total product concentration: 1 μM) for activity. Only substrates **4** and **6**, with specific combinations of catalysts and solvents, yielded product mixtures with biological activity, suggesting the reaction conditions are critical in steering substrates towards bioactive products.

A final array exploited substrates **4** and **6** and built on promising combinations of catalyst and solvent. Four additional structurally-related substrates **16**-**19**, were also included and reacted combinatorially with six rhodium carboxylate catalysts and three different solvents. The reaction mixtures were screened (total product concentration: 100 nM) for activity. Reactions of three of the substrates, **4**, **6** and **18**, yielded the most active product mixtures.

Ten reactions involving the three substrates **4**, **6** and **18**, were selected for scale-up (50-fold increase) based on their biological activity from round three. From the ten reactions, three distinct products were discovered. Diazo substrates **6** and **18** underwent intramolecular C–H insertion to yield the β-lactams **24** and **25** respectively and diazo substrate **4** also underwent intramolecular C–H insertion to yield γ-lactam **26** (Scheme 1.1). The three isolated products were all sub-micromolar modulators of the androgen receptor, with none of the chemotypes previously reported with activity against the androgen receptor. Remarkably, of the 336 reaction performed, ten were only ever scaled up and only three products, which were biologically active, needed to be purified, highlighting the efficiency of ADS.

Following the intramolecular study, the use of intermolecular reactions in activity-directed synthesis was explored. Intermolecular reactions allowed

fewer fragments, loaded with the core-binding moieties, to be synthesised, which can undergo reactions with huge numbers of commercially available co-substrates. In this case just four diazo substrates **20**-**23**, each armed with the 4-cyano 3-trifluoromethyl phenyl group, were prepared (Figure 1.11).

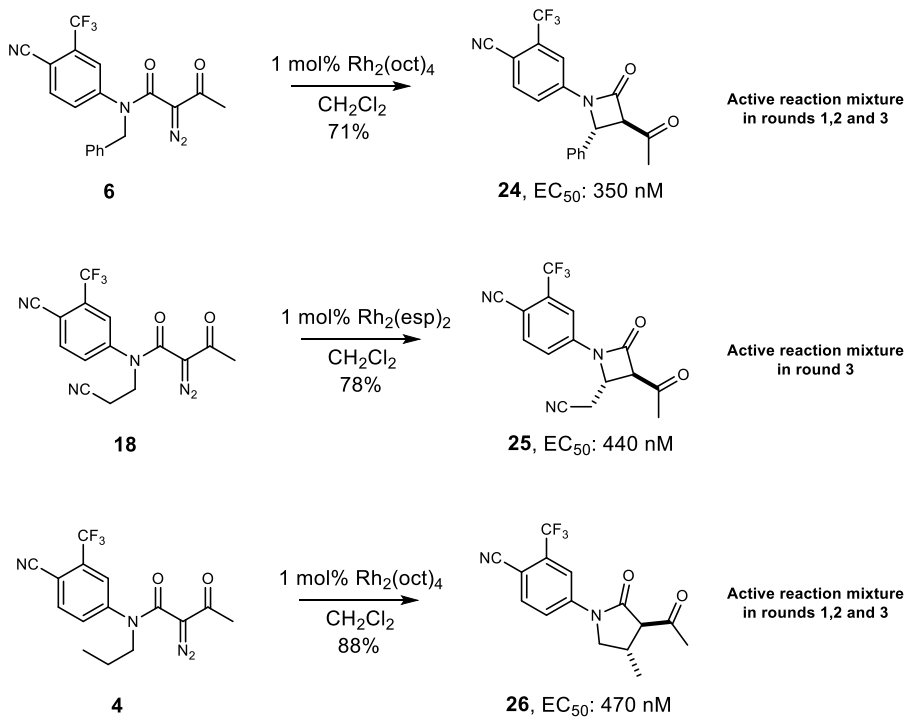

Scheme 1.1 *Reactions selected for scale-up from ADS, which enabled the discovery of three novel submicromolar agonists, with previously unreported activity, of the androgen receptor.*

Arrays were performed in which the diazos **20**-**23**, commercially available co-substrates which possess multiple possible reaction modes, catalysts and solvents were varied. Following reaction completion and scavenging, reactions mixtures were screened without purification for agonism of the androgen receptor. A total of three rounds of ADS was performed and reactions with promising biological activity from all three rounds were chosen for scale up (50-fold larger scale), to enable the identification of the products responsible for biological activity.

Over the three rounds, products were identified from alternative patterns of reactivity. Rounds one and two yielded active products formed from intermolecular C-H insertions and cyclopropanations. However, products from round three emerged from new patterns of reactivity, highlighting the value in exploiting reactions with many possible outcomes. The dihydropyran **27** and the benzopyran **29** (Scheme 1.2) were chosen on the basis of their similarity

to promising co-substrates from round two and were expected to undergo similar cyclopropanation reactions. However, the bioactive molecules **28** and **30** were produced as a result of different modes of reactivity (Scheme 1.2). Amide **28** was the product of an enantioselective O-H insertion reaction, the first reported example of its kind. Interestingly, the enantioselective reaction was inferred in the activity data in round three. Reaction of diazo substrate **20** with dihydropyran **27** resulted in an active product with Rh_2(*R*-DOSP)$_4$, but there was no observed activity using same substrates and the enantiomeric catalyst Rh_2(*S*-DOSP)$_4$. Finally, oxazole **30** was formed by reaction of diazo substrate **20** with the nitrile group in co-substrate **29.**

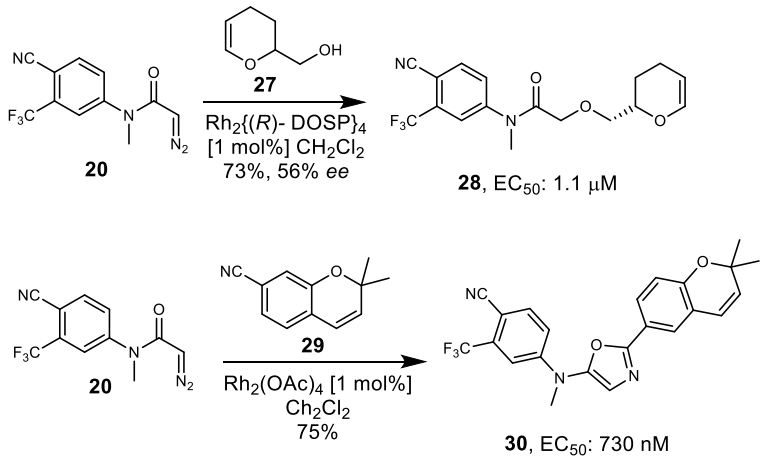

Scheme 1.2 B*iologically active products discovered from ADS with intermolecular metal-catalysed carbenoid reactions.*

Function-driven approaches have the potential to address bottlenecks in discovery workflows and ensure resources are focussed solely on biologically small molecules. However, to maximise the impact of such discovery workflows, the range of applicable chemistries would need to be expanded in order to allow a broad range of chemotypes to be discovered.

1.3 Summary

The historical uneven exploration of chemical space can largely be attributed to the narrow toolkit of reactions employed during drug discovery workflows, which has resulted in densely populated areas of chemical space. This often results in compound libraries with undesirable molecular properties

for successful drug discovery. The pharmaceutical industry has recognised the need for the development of robust synthetic strategies that incorporate the use of highly functionalised substrates in compound library preparation. This has resulted in the development and uptake of technologies that enable automated high-throughput experimentation for reaction optimisation, reaction discovery and compound library preparation. To fully automate and integrate all stages of drug discovery workflows, purification bottlenecks, which are performed in series, need to be addressed. Function-driven approaches, such as activity-directed synthesis, allow direct evaluation of crude reaction mixtures and have the potential to disrupt current practices within discovery workflows. To maximise the impact of activity-directed synthesis, the range of applicable chemistries must be expanded to enable diverse regions of chemical space to be explored.

1.4 Project Outline: Activity-Directed Fragment-Based Ligand Discovery

Activity-directed synthesis has been demonstrated as powerful approach for bioactive small molecule discovery. Intermolecular reactions in activity-directed synthesis have potentially greater impact in the search for bioactive small molecules, as fewer fragments loaded with core-binding moieties need to be synthesised, which can undergo reaction with huge numbers of commercially available co-substrates.

Elaboration of fragments in conventional FBDD workflows is greatly assisted by knowledge of a fragments binding mode to its biological target and often requires the development of synthetic routes at each stage of the fragment elaboration cycle. In stark contrast, activity-directed synthesis has the potential to enable fragment-to-lead optimisation studies to be performed without predefining the target molecule. However, a limitation in employing a fragment loaded with a diazotised-carbon, for metal-catalysed carbenoid chemistry, is that reaction is only possible on the carbon loaded with the diazo. This reduces the number of accessible vectors for fragment elaboration, limiting the potential to explore broad swathes of biologically-relevant chemical space.

For activity-directed synthesis to be employed for fragment elaboration, new chemistry must be utilised which enables synthetic elaboration at multiple reaction sites of the fragment. It was proposed that metal-catalysed C-H functionalisation has the potential to elaborate along one or many C-H vector(s) of a fragment to produce a range of regioisomers for biological evaluation.

It was proposed that the establishment of C-H functionalisation chemistry for activity-directed synthesis in the discovery of novel bioactive small molecules would enable the establishment of a multistep discovery platform. The platform would enable the function-driven discovery of novel bioactive small molecules, at each stage of the discovery phase, without any bioactive molecule being designed at the outset. The establishment of multiple chemistries in activity-directed synthesis would then allow extrapolation of the platform to a range of biological targets. For example the previously established intramolecular metal-catalysed carbenoind chemistry could be employed for the function-driven discveory of novel fragments for a specific biological target. Scale up and isolation of the active fragments, could then be utilised as fragments for fragment elaboration with C-H functioanlsiation chemistry to improve the activity of the fragments (Figure 1.12).

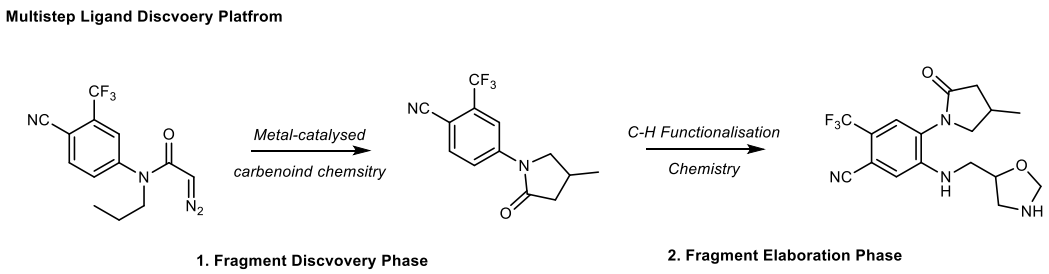

Figure 1.12 *Proposed multistep discovery platfrom that could be established with multiple synthetic strategies.*

A series of project objectives was outlined to evaluate the function-driven elaboration of fragments in activity-directed synthesis, which can ultimately be incpororated into a multistep function-driven platform. Hsp90 was chosen as the biological target to exemplify the fragment elaboration strategy with activity-directed synthesis.

Objective 1: Configure a range of C-H functionalisation reactions for application in plate-based microscale arrays (Section 1.4.1).

Objective 2: Establish a high-throughput assay and design, prepare and identify a series of Hsp90 fragment hits (Section 1.4.2).

Objective 3: Evaluate the value of C-H functionalisation and metal-catalysed carbenoid chemistry in the structure-blind elaboration of Hsp90 fragments (Section 1.4.3).

1.4.1 Objective 1: Configuration of C-H Functionalisation for Activity-Directed Synthesis

C-H functionalisation has the potential to synthetically grow along many C-H vectors of a fragment, allowing for the exploration of diverse chemical space. To evaluate C-H functionalisation for activity-directed synthesis, it was proposed that a range of C-H functionalisation literature reactions would be chosen, based on their mild reaction conditions (room temperature and air/moisture stable), reproduced in flask and the products isolated and characterised. To demonstrate the chosen reactions were amenable for plate-based reactions it was proposed that replication of the reactions, on microscale, in plate-based formats and comparison of the crude reaction LC-MS traces of flask and plate formats, would be performed to determine reaction reproducibility (Chapter 2.2). To broaden the range of chemistry, it was proposed that analysis of heating technology for parallel microscale arrays would be conducted by analysis of flask and plate-based reactions.

Given C-H functionalisations rely on a broad range of metal catalysts to activate C-H bonds, it was proposed a series of scavenging studies would be performed to ensure residual reaction components, such as metal catalysts and strong electrophiles, can be scavenged to prevent interference in the

biological assay. Ideally a range of C-H functionalisation reactions would be configured for parallel reaction arrays at room and elevated temperatures and an operationally simple workflow for scavenging metal catalysts and Michael acceptors be established.

1.4.2 Objective 2: Configuration of High-throughput Assay and Fragment Chemical Matter for Heat shock protein 90

The chosen biological target for evaluation of C-H functionalisation for fragment elaboration is Hsp90 (Heat shock protein 90), as it has been widely studied in various fragment-based drug discovery programmes and there are many reported fragments that looked well-suited to elaboration using C-H functionalisation chemistry (multiple directing groups).

It was proposed that a range of Hsp90 fragments, inspired by known ligands, that possess at least one potential directing group for C-H functionalisation, would be prepared and their biological activity assessed by generating dose response curves. For the biological assessment of the prepared fragments and screening of crude reaction mixtures, a high-throughput robust assay was required. The proposed assay for the project was a reported biochemical fluorescence anisotropy assay,[80] which required the expression of the protein, synthesis of the tracer and establishment of the control experiments.

It was proposed the assay would aid the selection of fragments to implement in the reaction arrays as well as ensuring the reaction array components do not interfere in the assay. Ideally a robust assay would be established which was suitable for identifying a series of Hsp90 fragment hits, that would serve as substrates for ADS, and enable biologically active reaction mixtures from ADS to be identified. It was envisaged the biologically active reaction mixtures would be a result of ligand-efficient synthetically elaborated fragments.

1.4.3 Objective 3: Implementation of Reaction Arrays

It was proposed the configuration of the chemistry and scavenging protocols in parallel plate-based format and establishment of the high-

throughput assay for assessing crude reaction mixtures would ensure a practical workflow for implementing the reaction arrays. It was proposed a range of reaction arrays based on different chemistry and elaboration strategies, C-H functionalisation and metal-catalysed chemistry, would be performed. Reactions would be performed by varying, fragment, substrate and catalyst combinations and crude reaction mixtures screened at low micromolar concentrations against Hsp90 for biological activity (Figure 1.13). The arrays would enable the value of each of the elaboration chemistries to be determined against Hsp90.

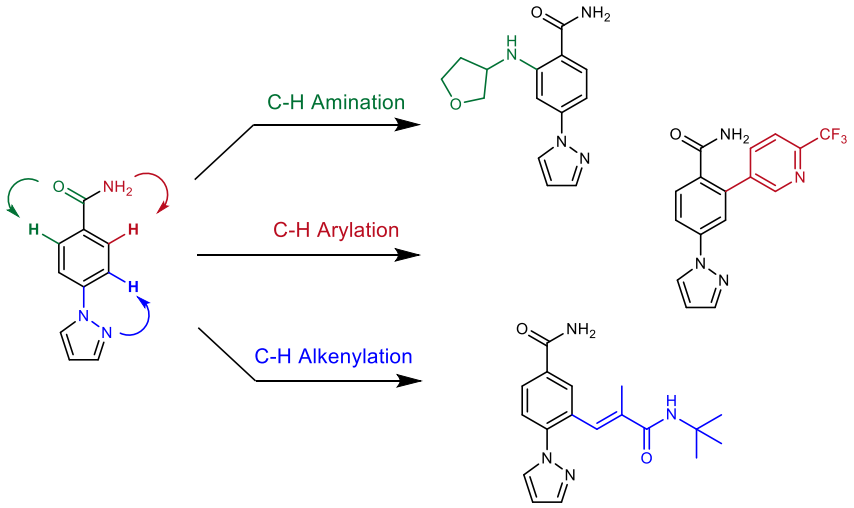

Figure 1.13 *Project overview: Example Hsp90 fragment that could be elaborated with various C-H functionalisation chemistries. Screening of the reaction mixtures would identify which C-H functionalisation strategy gave rise to bioactive mixtures.*

Chapter 2.
Evaluation of C-H Functionalisation Chemistry for Activity-Directed Synthesis

C-H functionalisation has been highlighted as a powerful tool for hit-to-lead studies,[44,81] due to its potential to synthetically elaborate a hit along any C-H vector of the molecule. The application of C-H functionalisation in ADS, has the potential to enable the structure-blind identification of productive vectors for fragment elaboration, contrasting starkly to conventional hit-to-lead studies. An overview of C-H functionalisation, including recent examples of functionalisations at sp^2- and sp^3-hybridised carbons is discussed. A range of C-H functionalisation transformations was evaluated for their implementation in plate-based arrays, by comparing reaction performance in flask- and various plate-based formats, followed by a post reaction work-up study to ensure crude reaction mixtures can be screened, without assay interference, against a biological target. The study enabled the identification of a portfolio of C-H functionalisation reactions for implementation in ADS, and the configuration and optimisation of a operationally simple ADS workflow.

2.1 Overview of C-H Functionalisation

The Carbon-Hydrogen bond is a generally unreactive bond (bond energies of C(sp^3)-H and C(sp^2)-H range from 370 to 460 kJ/mol) found in nearly all organic compounds.[82–84] The direct functionalisation of C-H bonds has emerged as powerful tool in synthetic chemistry as it provides the opportunity for new disconnections in complex molecules that were not previously possible. The field has applications in a wide range of sectors including polymers, agrochemicals, energy, natural products and pharmaceuticals.[82]

C-H functionalisation is the controlled activation and functionalisation of specific and remote C-H bonds in a molecule, generally in the presence of more reactive functional groups.[84] However, the inert nature of C-H bonds, and their ubiquitous nature in organic molecules, makes the selectivity and

reactivity of these bonds particularly challenging. The past few decades has seen the emergence of transition metal-catalysed C-H functionalisation, enabling the efficient construction of C-C and C-X (X = Heteroatom) bonds.[84]

Site selectivity can be controlled by the proximity of a C-H bond to a reactive metal centre, which is controlled by the use of directing groups within an organic molecule. Typically, coordination between heteroatoms in the directing group and the metal catalyst, bring the metal centre into close proximity to a C-H bond, which inserts into the C-H bond to create a carbon-metal bond (Figure 2.1).[84] This more reactive bond is then able to undergo a range of transformations with different reaction partners to give rise to new C-C and C-heteroatom bonds (Section 2.1.2). The advancement in mild C-H functionalisation reactions has enabled once latent C-H bonds to be seen as a reactive functional group in its own right, transforming synthetic strategies for chemists.[83,84]

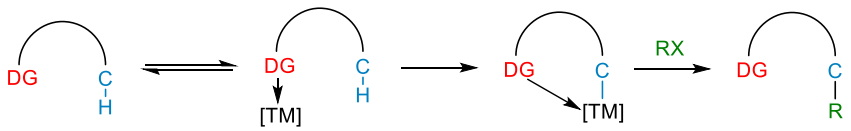

Figure 2.1 *Overview of C-H functionalisation: site selectivity is controlled by proximity of a C-H bond to directing group (DG), transition metal (TM) coordination and insertion and reaction with a substrate (RX).*

The recent emergence and advancements in C-H functionalisation via photoredox catalysis is seen as a complementary approach to transition metal-catalysed C-H functionalisation.[29] Photoredox catalysis has made the functionalisation of C(sp^3)-H bonds more accessible under mild reaction conditions and has also been highlighted as being of significant value in enabling new disconnections in synthetic strategies.[81]

2.1.1 The potential of C-H Functionalisation in Bioactive Small Molecule Discovery

C-H functionalisation has applications in a broad range chemical sectors, but has been highlighted and demonstrated as being of particular value in the

pharmaceutical industry. For instance, C-H functionalisation has been utilised in the synthesis of a range of medicinally relevant molecules[85] and in late-stage functionalisation of complex molecules.[86,87] For the pharmaceutical industry, late-stage functionalisation can facilitate the development of structure-activity relationships and the optimisation of potency and selectivity of lead compounds by reaction along C-H vectors unexplored by conventional synthetic strategies.[88]

In fragment-to-lead optimisation studies, structural information is key for making synthetic elaboration decisions, however the nature of the fragment-protein binding orientation can often mean there is disparity between the favoured growth vector and its synthetic accessibility. Often, fragment analogues containing functional handles for synthetic elaboration are required. This can result in a trade-off between the potential value and synthetic tractability of the elaborated fragment. C-H functionalisation and photoredox catalysis have been highlighted as a powerful tools in fragment-to-lead studies in fragment-based drug discovery (Figure 2.2).[31,44]

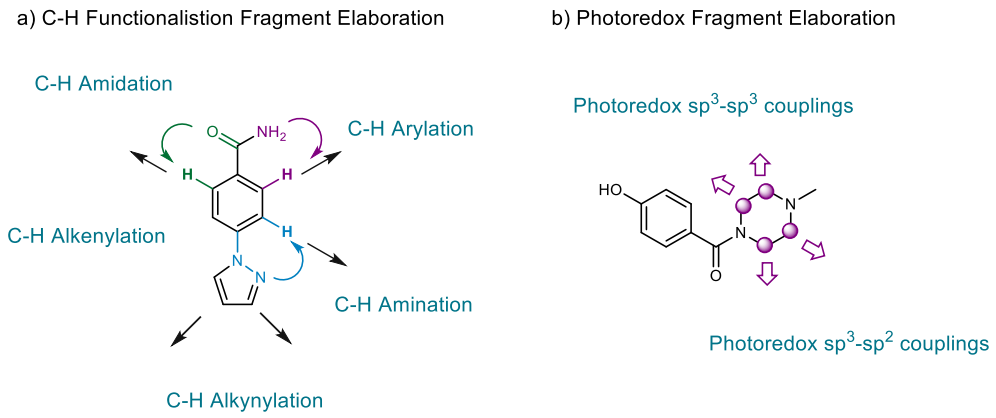

Figure 2.2 Potential for C-H functionalisation in fragment elaboration a) *Elaboration of Hsp90 fragments through transition-metal catalysed C-H Functionalisation b) Elaboration of Hsp90 fragments through photoredox catalysis.*

It was proposed that the application of C-H functionalisation in ADS would enable the structure-blind and function-driven elaboration of fragments. The range of potential C-H functionalisation chemistries for ADS is discussed (Section 2.1.2) and the evaluation and configuration of C-H functionalisation for ADS is described (Section 2.2).

2.1.2 The Scope of C-H Functionalisation Reactions

A vast range of C-H functionalisations reactions have been published over the last few decades, enabling a broad range of new synthetic connections to be made.[83,84] The use of directing groups and transition metals enables the selection and activation of a specific C-H bond, the most common of which is *ortho*-directed C(sp^2)-H functionalisations onto an aromatic ring (Figure 2.3 for selected examples). The use of directing groups has been widely studied, of which there are now a broad range; amides (Figure 2.3a), heteroaryls (Figure 2.3b), amines (Figure 2.3c), carboxylic acids (Figure 2.3d) as well as many others.[84] The range of C-H functionalisation types include, for example, introduction of alkyl, alkene and alkyne chains, amines, amides and aromatic rings, as well as much smaller groups, or even single atoms, such as hydroxyl groups and halogens, which are considered part of the late-stage functionalisation toolkit.[87] The choice of catalyst is often critical for the reaction progression, as well as the choice of additives such as base and oxidant.

There have also been numerous reported examples of directing C-H insertion to the *meta*- and *para*- positions of an aromatic rings, *via* the use of specifically designed (or transient) directing groups (Figure 2.3f).[89] The use of directing groups isn't always required, as the intrinsic reactivity of the substrate itself can control the position of functionalisation. For instance, the C-H alkenylation of pyrroles can be controlled by the choice of *N*-protecting group (Figure 2.3ei).[90] The *N*-Boc protected pyrrole **54** directs C-H insertion to the C2 position under electronic effects, whereas the *N*-TIPS protected pyrrole **55** directs insertion to the C3 position due to the steric bulk of the protecting group. Similarly, under palladium catalysis, C-H arylation of *N*-methylindole is directed to the C2 position (Figure 2.3eii).[91]

C-H functionalisation onto sp^3 hybridised carbons has also become common practice (Figure 2.3g).[92] Again, the choice of directing group and catalyst is crucial for reaction selectivity and a similarly broad range of transformations is possible. Strategies that enable the enantioselective reaction of C-H bonds are now emerging in the field, for example in the enantioselective C(sp^3)-H arylation of carboxylic acids (Figure 2.3g).[93]

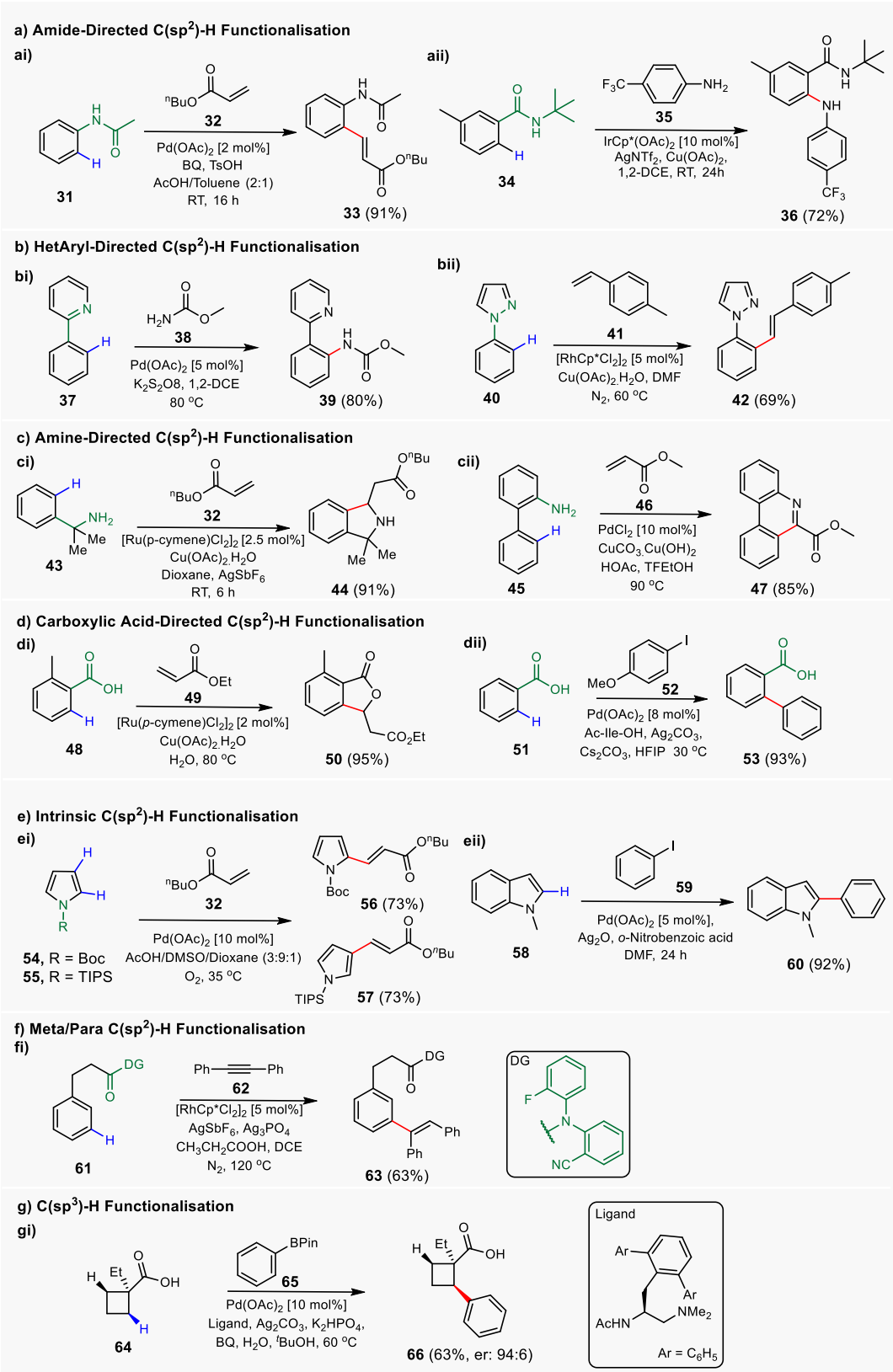

Figure 2.3 *C-H functionalisation chemistries:* ***a****) Amide-directed i) C-H alkenylation*[94] *ii) C-H amination*[95] ***b****) Heteroaryl-directed i) C-H amidation*[96] *ii) C-H alkenylation*[97] ***c****) Amine-directed i) C-H alkenylation*[98] *ii) C-H alkenylation*[99] ***d****) Carboxylic Acid-directed i) C-H alkenylation*[100] *ii) C-H arylation*[101] ***e****) Intrinsic C-H functionalisation i) C-H alkenylation*[90] *ii) C-H arylation*[91] ***f****) Meta C-H alkenylation*[102] ***g****) Enantioselective C(sp³)-H arylation*[93]

C-H functionalisation reactions typically proceed via a similar catalytic cycle (Figure 2.4). The first step requires activation of the substrate undergoing C-H functionalisation, in which the catalyst coordinates to the directing group, and inserts into a proximal C-H bond. The metal centre then coordinates and inserts into the reaction partner, allowing formation of a substrate carbon-reaction partner bond. The product is released, followed by oxidation of the catalyst to reform the active catalytic species. The example shown (outer blue circle) is the palladium catalysed *ortho* C-H alkenylation reaction into the acetamide **67** with *n*Butyl acrylate **32**.[94] The product **68** is released via a dehydropalladation and the catalyst is regenerated via oxidation with 1,4-benzoquinone (Figure 2.4).

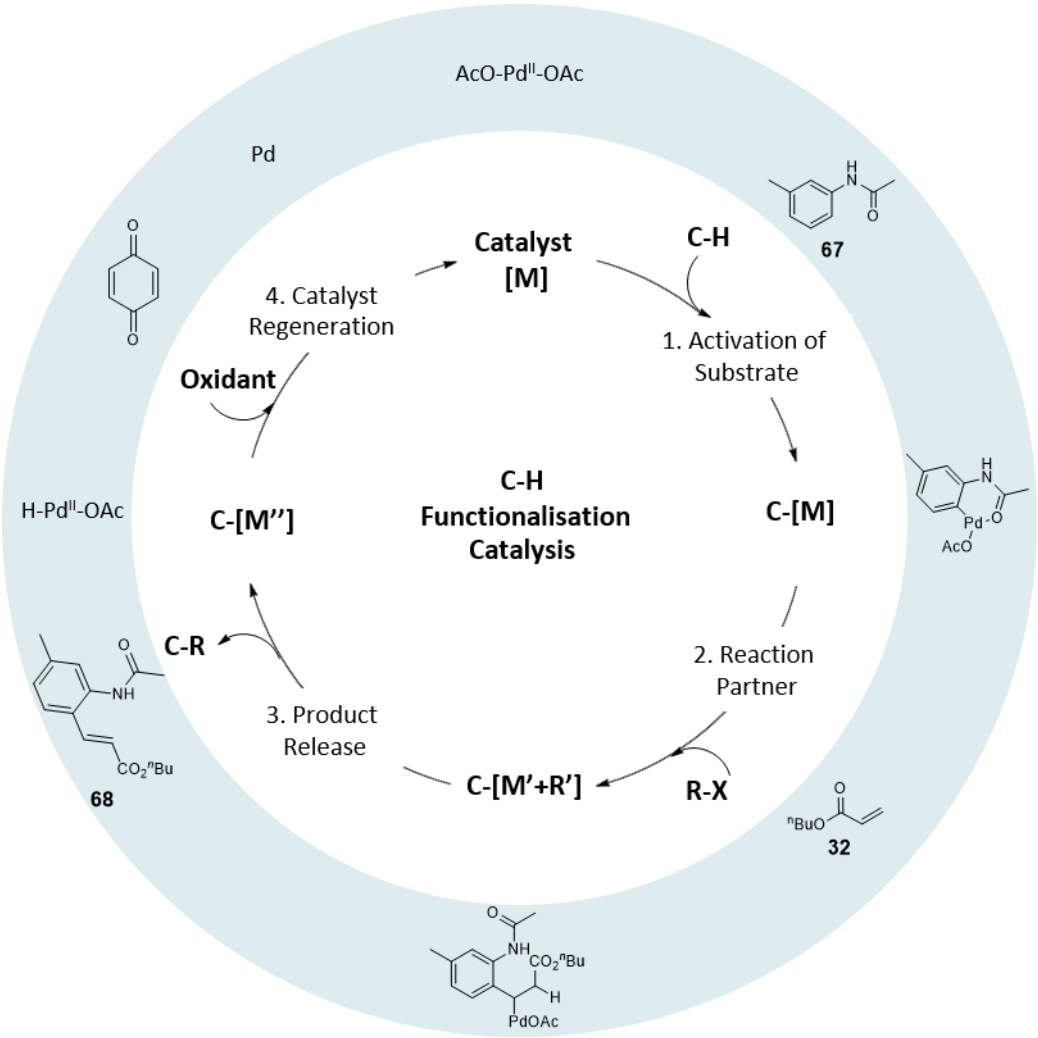

Figure 2.4 *General catalytic cycle for C-H functionalisation reactions with transition metal catalysts (centre).*[83] *Example (outer circle) palladium catalysed C-H alkenylation reaction in which substrate **67** is alkenylated ortho to the acetamide group with ^{n}butyl acrylate **32**.*[94]

2.1.3 Summary

C-H functionalisation has the potential to transform chemical strategies, and provides the opportunity for new disconnections, not previously possible, to be made. Mild C-H functionalisation reactions have become well established in recent years, through the development of a broad range of transition metal catalysts and directing groups. The direct functionalisation of C-H bonds has implications in a wide range of chemical industries, for instance in the discovery of bioactive small molecules, in particular hit-to-lead studies. C-H functionalisation applied in ADS has the potential to enable structure-blind and function-driven fragment elaboration.

2.2 Configuration of C-H Functionalisation Chemistry for Activity-Directed Synthesis

To enable the use of C-H functionalisation in activity-directed synthesis, a range of candidate C-H functionalisation reactions, that proceed under mild conditions, was identified (Section 2.2.1). As reactions in ADS are performed on microscale (typically 100 μL volume), in parallel-based format, at room temperature, under atmospheric conditions and without stirring, the C-H functionalisation reactions chosen must be amenable to these conditions. C-H functionalisation reactions often proceed under harsh conditions, with stoichiometric additives, high temperatures and with inert atmospheres, however there has been recent efforts within the field to identify milder C-H functionalisations reactions.[83]

A series of mild C-H alkenylations (Section 2.2.1.1), C-H aminations (Section 2.2.1.2) and C-H arylations (Section 2.2.1.3) was identified, and replicated as described in the literature on mmol scale in round-bottom flasks. LC-MS analysis of the crude reactions was performed followed by subsequent purification to characterise and identify the products. The reactions were then replicated under conditions representative of the ADS workflow (room temperature, air/moisture stable and without stirring) and prepared from stock solutions, in plate-based format. Comparison of flask- and plate-based crude reaction mixtures was used to identify C-H functionalisation reactions

amenable to ADS. The reactions were chosen to ensure a broad range of reaction type, directing groups and catalysts.

2.2.1 Evaluation of a Range of C-H Functionalisation Reaction Types for Parallel Microscale Reaction Arrays

2.2.1.1 Analysis of C-H Alkenylation Reactions

A broad range of C-H alkenylations have been reported which proceed under various catalytic systems and directing groups with a range of reaction partners (alkenes, acrylates acrylamides and alkynes).[83,84] The mild C-H alkenylations chosen for assessment in ADS (Table 2.1) were replicated in round-bottom flasks as reported in the literature (unless stated).

Reaction of *n*butyl acrylate **32** with substrate **31** (Entry 1, Table 2.1)[94] proceeded in much lower yield, 25%, compared to the reported literature yield, 72%. This was due to the reaction of **32** at both ortho positions of substrate **31**. The addition of a *meta*-methyl, **67**, resulted in the single C-H alkenylation to **68** in much higher yield, 55% (Entry 2, Table 2.1).[94] Both reactions proceed through coordination of the palladium catalyst to the acetamide directing group, followed by activation of the *ortho* C-H bond. Similarly, the -NH_2 of cumylamine **43** (Entry 3, Table 2.1)[98] directs C-H insertion to the *ortho* C-H under ruthenium catalysis. Following C-H functionalisation, the substrate undergoes cyclisation to form a five membered ring, due the electron withdrawing nature of substrate **44**. The reaction was performed under atmospheric conditions in 76% yield, compared to a literature yield of 91% which was performed under an inert atmosphere of nitrogen.

Finally reaction of *N*-Boc pyrrole **54** with *n*butyl acrylate **32** resulted in the C2 C-H functionalisation to **56** in 26% yield (Entry 4. Table 2.1)[90], compared to 72% reported in the literature. However, the literature procedure was modified to enable greater compatibility in ADS. In the literature, the reaction was performed under an atmosphere of O_2 at 35 ^{o}C, however in this instance the reaction was performed at room temperature with benzoquinone as the oxidant. Interestingly, protecting the pyrrole nitrogen with TIPS can enable C3, instead of C2, C-H functionalisation (see Section 2.1.2).

Entry	Substrate	Co-Substrate	Conditions	Product	Ref.
1	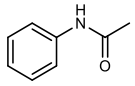 **31**	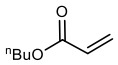 **32**	$Pd(OAc)_2$ [2 mol%] BQ, TsOH AcOH/Toluene (2:1) RT, 16 h **Yield: 25%** **Lit. Yield: 72%**	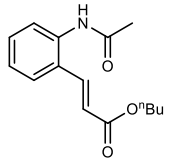 **33**	94
2	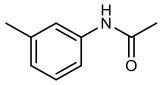 **67**		$Pd(OAc)_2$ [2 mol%] BQ, TsOH AcOH/Toluene (2:1) RT, 16 h **Yield: 55%** **Lit. Yield: 91%**	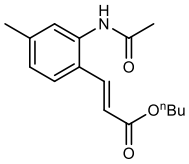 **68**	94
3*	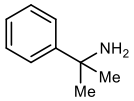 **43**		$[Ru(p\text{-cymene})Cl_2]_2$ [2.5 mol%] $Cu(OAc)_2.H_2O$ Dioxane, $AgSbF_6$ RT, 6 h **Yield: 76%** **Lit. Yield: 91%**	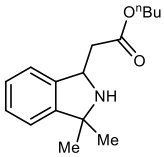 **44**	98
4**	 **54**		$Pd(OAc)_2$ [10 mol%], BQ, AcOH/DMSO/Dioxane (3:9:1) RT, 96 h **Yield 26%** **Lit. Yield: 72%**	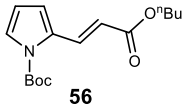 **56**	90

Table 2.1 *Exemplar C-H alkenylation reactions that were reproduced in flask (mmol scale) from the literature to identify reactions that proceed under mild conditions which could prove amenable to ADS microscale reaction array format. Deviation from literature procedures: *Performed under N_2 atmosphere in literature **Performed at 35 ^oC under O_2 atmosphere in the literature.*

With a range of mild C-H alkenylations identified, the reactions were replicated under ADS-conditions in plate-based format. Following reaction for 24 h, an LC-MS of the crude reaction mixture was collected, and comparison of the LC-MS trace of the crude reaction mixtures in flask and plate-based format was performed (Table 2.2). Similar LC-MS traces of flask and plate-based reactions demonstrated the reactions could be reproduced for ADS plated-based reaction arrays. The LC-MS traces for each of the three C-H alkenylation reactions replicated in flask and plates (Table 2.2) showed a similar product distribution and product masses with the same retention times. This demonstrated that the mild C-H alkenylation reactions were amenable for ADS and so these reactions were taken forward for their utilisation in activity-directed fragment elaboration.

		LC-MS Analysis	
Reaction	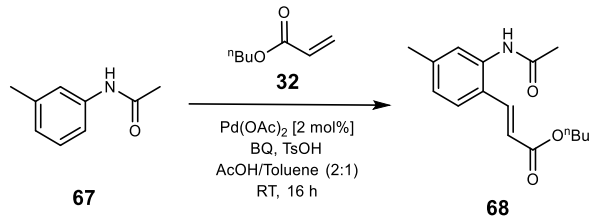	**Mass Found**	**Compound No.**
Flask	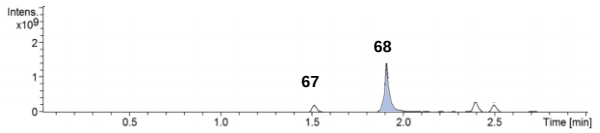	*MH*$^+$: 150.1 *MNa*$^+$: 298.1	**67** **68**
Plate	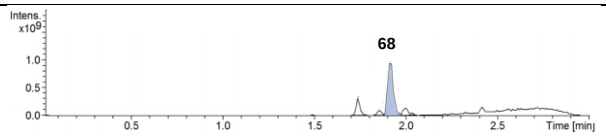	*MH*$^+$: 276.4	**68**
Reaction	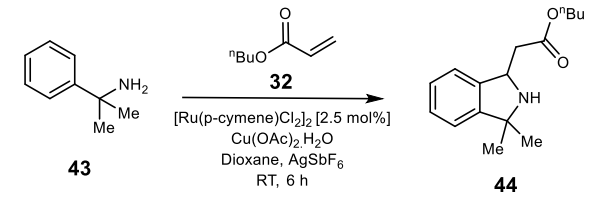	**Mass Found**	**Compound No.**
Flask	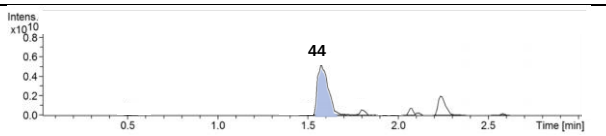	*MH*$^+$: 262.5	**44**
Plate	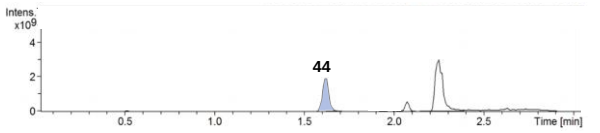	*MH*$^+$: 262.5	**44**
Reaction	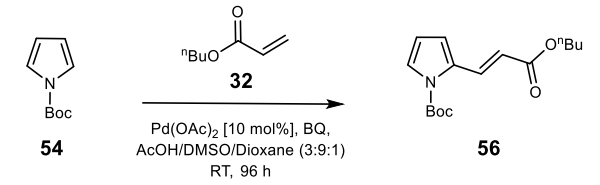	**Mass Found**	**Compound No.**
Flask	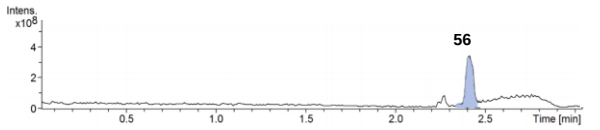	*MH*$^+$: 294.2	**56**
Plate	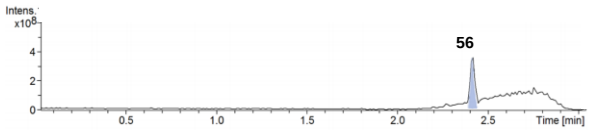	*MH*$^+$: 294.4	**56**

Table 2.2 *C-H alkenylation literature reactions reproduced in flask and plate-based formats. Plate-based reactions were repeated under ADS-array conditions and the crude plate reactions analysed against the crude flask reactions, by analysing LC-MS traces to determine their amenability in ADS. For the three C-H alkenylations replicated, comparable LC-MS traces demonstrated the successful transfer of reactions to plate-based format.*

2.2.1.2 Analysis of C-H Amination Reactions

C-H amination is the functionalisation of C-H bonds to form C-N bonds, of which there have been numerous reported examples.[103] The C-H aminations chosen for assessment in ADS (Table 2.3) were repeated in round-bottom flask, as described in the literature (unless stated).

Entry	Substrate	Co-Substrate	Conditions	Product	Ref.
1†	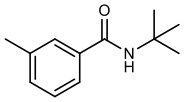 **69**	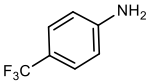 **35**	$IrCp^*(OAc)_2$ [10 mol%] $AgNTf_2$, $Cu(OAc)_2$, 1,2-DCE, RT, 24h **Yield: 58%** **Lit. Yield: 72%†**	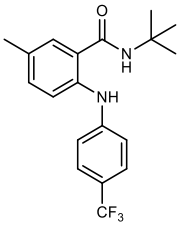 **70**	95
2††		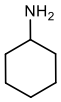 **71**	$[IrCp^*(Cl)_2]_2$ [5 mol%] $AgNTf_2$, $Cu(OAc)_2$, 1,2-DCE:HFIP (50:50) RT, 24 h **Yield: 38%** **Lit. Yield: 50%††**	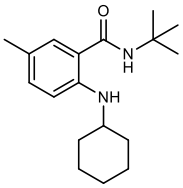 **72**	104
3	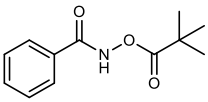 **73**	 **74**	$[RhCp^*Cl_2]_2$ [5 mol%] CsOAc, PivOH MeOH, RT, 16h **Yield: 61%** **Lit. Yield: 80%**	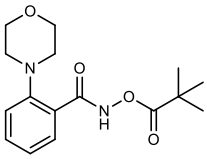 **75**	105

Table 2.3 *Exemplar C-H amination reactions that were reproduced in flask (mmol scale) from the literature to identify reactions that proceed under mild conditions which could prove amenable to ADS microscale reaction array format. Deviation from the literature:* † *No meta-methyl present on substrate* ***69*** *in the literature.* †† *No meta-methyl present on substrate* ***69*** *in the literature and reaction temperature dropped from 60 °C to room temperature.*

The iridium-catalysed *ortho* C-H amination of substrate **69** with *para*-(trifluoromethyl)aniline **35** gave product **70** in 58% yield, compared to the reported literature yield of 72% (Entry 1, Table 2.3).[95] However, substrate **69** incorporated a *meta*-methyl, to prevent C-H amination of both *ortho* positions, which was not present in the literature reaction. Similarly, reaction of **69** with cyclohexylamine **71** gave product **72** in 38% yield, compared to 50% in the literature (Entry 2.2, Table 2.3).[104] In this case the reaction was performed at

room temperature, compared to 60 ^{o}C in the literature, to ensure the reaction was compatible for ADS. Finally, the rhodium-catalysed *ortho* C-H amination of substrate **73** with *N*-chloroamine **74** gave product **75** in 61% yield (Entry 3, Table 2.3).[105] However, *N*-chloroamines would require synthesis for use as substrates in ADS due to their limited commercial availability.

C-H amination reactions one and three (Table 2.3) performed well in flask-format and were hence taken forward for study under ADS conditions in plate-based format. Similarly to the C-H alkenylations, LC-MS traces of the crude reaction mixtures, after 24 h, for each of the reactions in flask- and plate-based formats were compared to determine their compatibility in ADS (Table 2.4). As for the C-H alkenylations, the two C-H amination reactions produced similar LC-MS traces in both reaction formats, with similar product distributions and product retention times. Interestingly, in the cases of the C-H amination under iridium catalysis, the lack of stirring appeared to have minimal impact on product formation given the heterogenous nature of the reaction mixture. As reaction two (Table 2.3) proceeded in much lower yield than reported, due in part to the lower reaction temperature, heated reaction arrays were also explored for ADS (see Section 2.2.2). In this case similar LC-MS traces were also observed. As all three reactions performed well under ADS conditions they were taken forward for implementation in C-H functionalisation reaction arrays.

		LC-MS Analysis	
Reaction	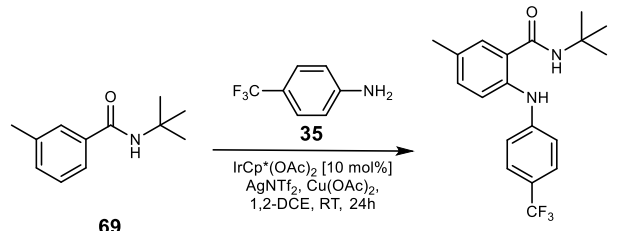	**Mass Found**	**Compound No.**
Flask	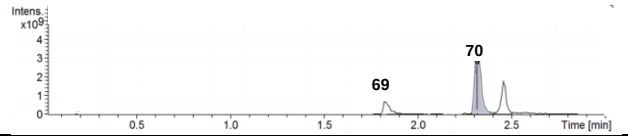	*MH*$^+$: 191.6 *MH*$^+$: 351.7	**69** **70**
Plate	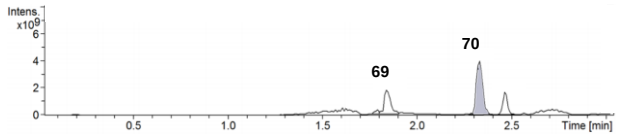	*MH*$^+$: 191.4 *MH*$^+$: 351.1	**69** **70**
Reaction	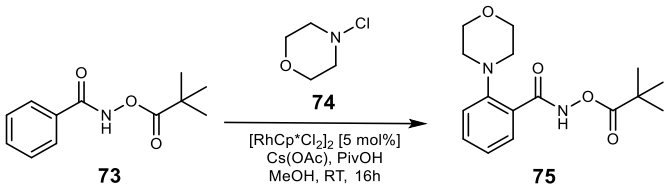	**LC-MS Analysis**	
		Mass Found	**Compound No.**
Flask	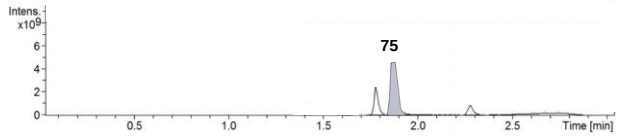	*MH*$^+$: 307.0	**75**
Plate	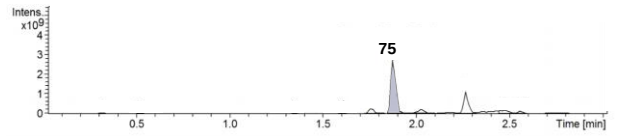	*MH*$^+$: 307.7	**75**

Table 2.4 *C-H amination literature reactions reproduced in flask and plate-based formats. Plate-based reactions were repeated under ADS-array conditions and the crude plate reactions analysed against the crude flask reactions by analysing LC-MS traces to determine their amenability in ADS. For the C-H aminations replicated, comparable LC-MS traces demonstrated the successful transfer of reactions to plate-based format.*

2.2.1.3 Analysis of C-H Arylation Reactions

Finally, a series of C-H arylations was identified and repeated in flask-based format as described in the literature (Table 2.5). C-H arylations is the replacement of a C-H bond with a C-aryl bond and would potentially prove valuable for fragment elaboration, as the hydrophobic nature of aromatic substituents would enable the elaborated fragment to fill the shape of a protein binding pocket through hydrophobic interactions. Any additional heteroatoms

would also have the potential to pick up additional hydrogen-bonding interactions, which are essential for increasing potency.[31]

The palladium-catalysed C-H arylation of substrate **76** with boronic acid **77** gave **78** in 75% yield (Entry 1, Table 2.5),[106] comparable to the literature yield of 85% (a small amount of product in which both ortho C-Hs were arylated was observed). The double C-H activation of acetamide **67** and xylene **79** produced **80** in 52% yield (Entry 2, Table 2.5).[107] The least sterically hindered position of xylene **79** is favoured for this transformation. C-H arylation of *N*-methylindole **58** with iodobenzene **59** produced **60** in 27%, much lower than the reported yield of 92% (Entry 3, Table 2.5).[91]

Entry	Substrate	Co-Substrate	Conditions	Product	Ref.
1	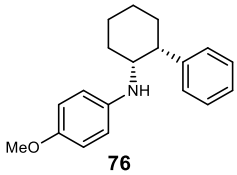 **76**	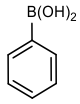 **77**	$Pd(OAc)_2$ [20 mol%], BQ $CH_2Cl_2/^iPrOH$ (50:50), RT, 24 h **Yield: 75%** **Lit. Yield: 85%**	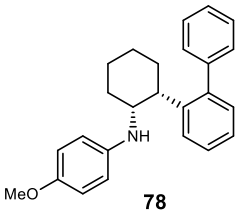 **78**	106
2	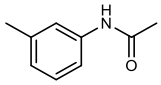 **67**	 **79**	$Pd(OAc)_2$ [10 mol%], $NH_4S_2O_8$, TFA RT, 24 h **Yield: 52%** **Lit. Yield: 82%**	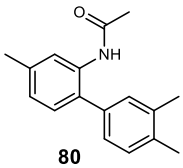 **80**	107
3	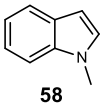 **58**	 **59**	$Pd(OAc)_2$ [5 mol%], Ag_2O, *o*-Nitrobenzoic acid, DMF, RT, 24 h **Yield: 27%** **Lit. Yield: 92%**	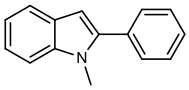 **60**	91

Table 2.5 *Exemplar C-H arylation reactions that were reproduced in flask (mmol scale) from the literature to identify reactions that proceed under mild conditions which could prove amenable to ADS microscale reaction array format.*

C-H arylations (Entries 1 and 2, Table 2.5) were replicated under ADS conditions in plate-based format. LC-MS traces for crude reaction mixtures in flask and plate-based formats were compared (Table 2.6). As for the C-H alkenylations and C-H aminations, similar LC-MS traces, with similar

production distribution and retention times demonstrated the compatibility of C-H arylations for ADS. Due to the poor yield of the C-H arylation of *N*-methylindole **60,** and limited substrate scope, it was decided not to take forward this reaction for ADS.

		LC-MS Analysis	
Reaction	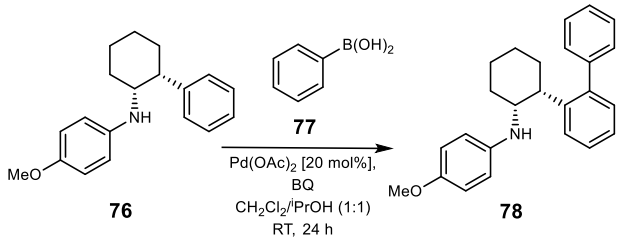	**Mass Found**	**Compound No.**
Flask	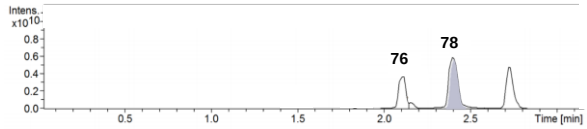	*MH*$^+$: 282.1 *MH*$^+$: *358.1*	**76** **78**
Plate	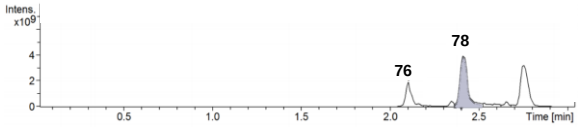	*MH*$^+$: 282.4 *MH*$^+$: *358.5*	**76** **78**
Reaction	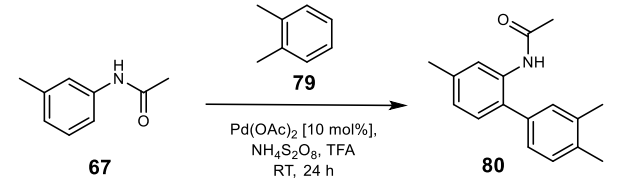	**LC-MS Analysis**	
		Mass Found	**Compound No.**
Flask	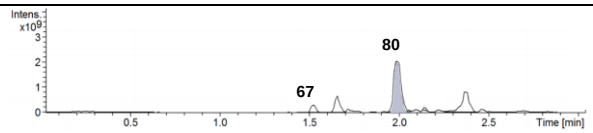	*MH*$^+$: 150.7 *MH*$^+$: 254.7	**67** **80**
Plate	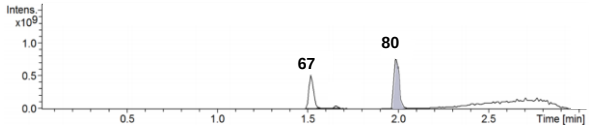	*MH*$^+$: 150.3 *MH*$^+$: 254.4	**67** **80**

Table 2.6 *C-H arylation literature reactions reproduced in flask and plate-based formats. Plate-based reactions were repeated under ADS-array conditions and the crude plate reactions analysed against the crude flask reactions by analysing LC-MS traces to determine their amenability in ADS. For the two C-H arylations replicated, comparable LC-MS traces demonstrated the successful transfer of reactions to plate-based format.*

2.2.2 Configuration of Parallel Heating Technology for C-H Functionalisation Arrays

To enable a broader range of chemistries, and potentially broader range of substrates, to be used in activity-directed synthesis, the options of heated and stirred reactions in parallel-based formats was investigated. Heating was investigated as examples already chosen (C-H amination with alkylamines, Entry 2 Table 2.4 and C-H alkenylation, Entry 4 Table 2.1) proceeded at elevated temperatures. The necessity for stirring in the reaction outcome was also investigated given the heterogenous nature of some of the reaction mixtures. A small range of reactions (Table 2.7) was investigated, by repeating the reactions in microvial format at room temperature and 60 ^{o}C both with and without stirring. As before, LC-MS traces of crude reaction mixtures were collected and compared to determine reaction progress. In all three cases, similar LC-MS traces under all reaction conditions demonstrated that stirring was not essential and that heated microscale reactions were possible in parallel format.

Reaction

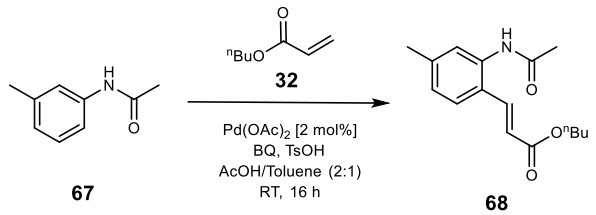

LC-MS Analysis		
a)	M_2H^+: 551.6	**68**
b)	M_2H^+: 551.6	**68**
c)	M_2H^+: 551.6	**68**
d)	M_2H^+: 551.6	**68**

	No Stirring	Stirring
RT	a) 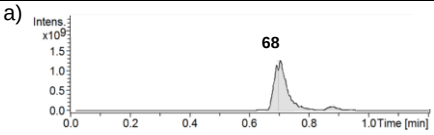	b) 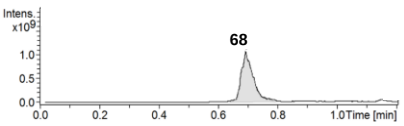
60 °C	c) 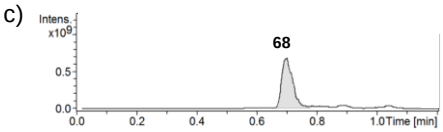	d) 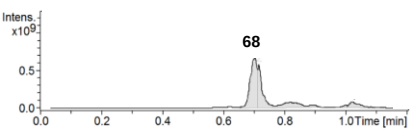

Reaction

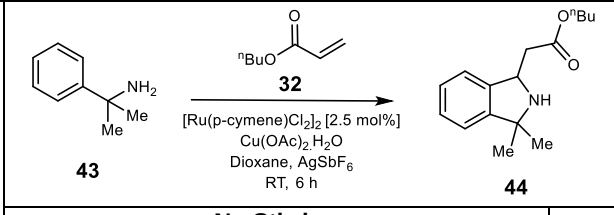

LC-MS Analysis		
a)	MH^+: 262.4	**44**
b)	MH^+: 262.4	**44**
c)	MH^+: 262.4	**44**
d)	MH^+: 262.4	**44**

	No Stirring	Stirring
RT	a) 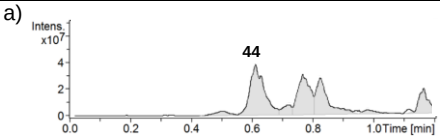	b) 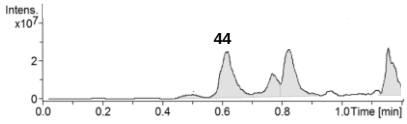
60 °C	c) 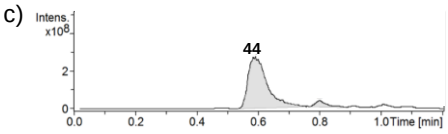	d) 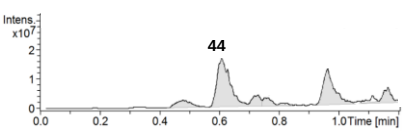

Reaction

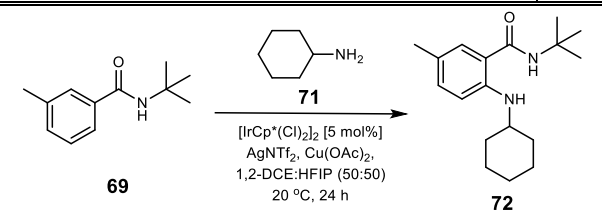

LC-MS Analysis		
a	MH^+: 289.5	**72**
b	MH^+: 289.5	**72**
c	MH^+: 289.5	**72**
d	MH^+: 289.5	**72**

	No Stirring	Stirring
RT	a) 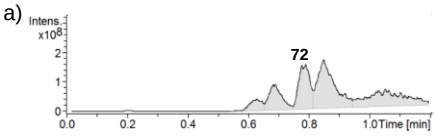	b) 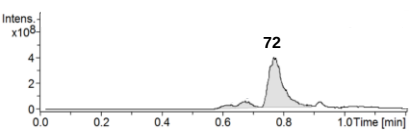
60 °C	c) 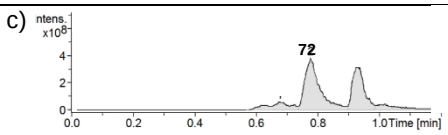	d) 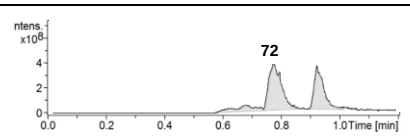

Table 2.7 *Evaluation of exemplar literature C-H Functionalisation reactions to determine importance of heating and stirring in reaction outcome by LC-MS.*

2.2.3 Summary

A selection of C-H functionalisation reactions (alkenylations, arylations and aminations) was chosen and successfully demonstrated as being applicable in plate-based microscale reaction arrays. It was determined that stirring was not essential for reaction progression and that heated reaction arrays could enable a broader range of chemistries and substrates scope used in ADS.

2.3 Post Reaction Work-up Procedures for C-H Functionalisation Chemistry in Reaction Arrays

To ensure crude reaction mixtures can be screened against the biological target of interest, without assay interference, it was proposed that incorporating a post reaction work-up procedure for parallel-based chemistry into the ADS workflow was needed. An operationally simple procedure for removing residual catalysts and Michael acceptors from crude reaction mixtures would ensure an efficient and streamlined workflow for ADS. For the proof-of-concept studies in ADS,[16,17] metal catalysts were scavenged form crude reaction mixtures using a QuadraPure Thiourea resin.

For C-H functionalisation a much broader range of catalysts are used, for example, from the configured chemistries (Section 2.2.1), palladium, iridium, rhodium and ruthenium as well as copper as an oxidant. The stoichiometric use of electrophiles is also prevalent in some of the chosen reactions; the use of benzoquinone as an oxidant and acrylates as reaction partners, which have the potential to undergo reaction with nucleophilic protein residues during the screening process. To ensure minimal assay interference, it was proposed that the use of a resin that could scavenge a broad range of metals and strong electrophiles from reaction mixtures was needed. A range of potential scavenger resins (Table 2.8) was used to investigate the potential to scavenge metals and electrophiles from crude reaction mixtures.

Quadrapure DET	Qaudrapure MPA	Quadrapure BzA
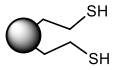	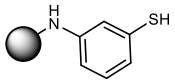	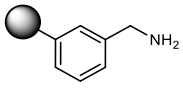
Macroporous Resin **Loading:** 1-2 mmol/g **Metals Scavenged†:** Cu, Fe, Pd, Rh	Macroporous Resin **Loading:** 1.5 mmol/g **Metals Scavenged†:** Ag, Au, Cd, Hg, Pb, Pt, Ru, Pd, Sn	Macroporous Resin **Stated Loading††:** 20 mg/g **Metals Scavenged†:** Co, Cu, Ni, Pd, Rh
Biotage MP-TNT	**Aminomethyl Polystyrene**	**QudraSil MP**
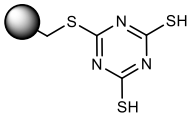		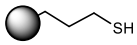
Macroporous Resin **Loading:** 0.66 mmol/g **Metals Scavenged†:** Pd and other heavy metals	Electrophile Scavenger **Loading:** 4.0 mmol/g **Metals Scavenged†:** -	Mesooporous Resin **Loading:** 1.2 mmol/g **Metals Scavenged†:** Cu, Ni, Pd, Rh, Ru, Pt, Ag

Table 2.8 *Functionalised resins that were investigated for their metal catalysts and electrophile scavenging capabilities. †Metals scavenged according to manufacturer's specification guidelines. †† Manufacturer's stated loaded presumed as 20 mg of benzylamine per 1 g of resin.*

2.3.1 Scavenging of Michael Acceptors

To establish the electrophile scavenging capabilities of the chosen resins (Table 2.8), a series of Michael acceptors with a range of electrophilicities was chosen (Figure 2.5). The aim was to identify the resin best able to scavenge the most electrophilic Michael acceptors, which would then be tested for its metal scavenging capabilities. Cinnamyl alcohol is a control substrate not expected to be scavenged, and substrates **68** and **70** are C-H functionalisation reaction products. Product **70** is not a Michael acceptor and not expected to be scavenged. The Quadrapure resins are macroporous and therefore non-swell resins, which are capable of scavenging in all organic solvents (see manufacturers guidelines). Deuterated chloroform was therefore selected for the scavenging study.

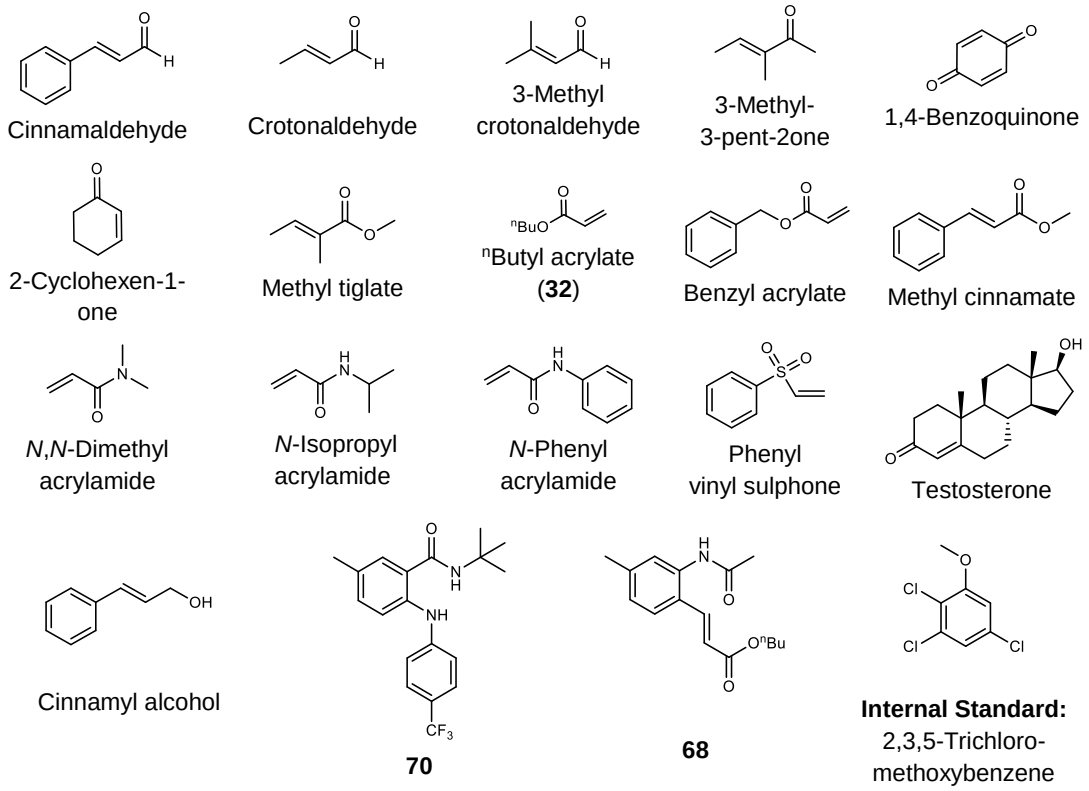

Figure 2.5 *Michael acceptors, with a broad range of electrophilicities, that were tested with a range of resins (Table 2.8) to determine which of the Michael acceptors could be scavenged with the resins. 2,3,5-trichloromethoxybenzene was the internal standard used in the NMR studies to quantify the amount of electrophile scavenged.*

A ^{1}H NMR spectroscopy (300 MHz) study was performed to determine the scavenging capabilities of the chosen resins with the range of Michael acceptors. Initially, a ^{1}H NMR spectrum for each of the Michael acceptors (0.03 mmol/mL of $CDCl_3$) was recorded with the addition of the internal standard 2,3,5-trichloro-methoxybenzene (0.03 mmol/mL). 2-3 eq. of each of the resins was then incubated with each of the Michael acceptors at room temperature for 24 h. After 24 h a second ^{1}H NMR spectrum was recorded. The peaks of the Michael acceptor before and after scavenging were set relative to the standard, and the difference in relative integrations between the two spectra was used to determine the amount of Michael acceptor scavenged (nearest 5%, Table 2.9). The Quadrapure DET and MPA resins were subsequently discontinued by the supplier and so results are not shown.

The results from the ^{1}H NMR data (Table 2.9) show that the Biotage MP-TMT and QuadraSil MP resins were only able to partially scavenge a small range of the Michael acceptors. The Aminomethyl PS and QuadraPure BzA

have a stronger correlation in their capability to scavenge more electrophilic Michael acceptors. They were both able to scavenge the majority of the α,β-unstaurated aldehydes and ketones with greater than 95% effectiveness (with exception of 3-methyl-3-pent-2-one). Quadrapure BzA was better able to scavenge less electrophilic Michael acceptors, compared to the aminomethyl PS resin, however left non-Michael acceptor substrates, such as cinnamyl alcohol and product **70** unscavenged. The Michael acceptor-containing product **68**, was left mostly unscavenged too (5%), which is ideal for the reaction arrays. The results demonstrated that Quadrapure BzA is able to remove highly electrophilic reaction substrates from reaction mixtures, but will not scavenge potential products formed in C-H functionalisation arrays, allowing the products to be screened in the biological assay. Quadrapure BzA was subsequently tested for its ability to scavenged metal catalysts from solution (Section 2.3.2).

Resin / **Michael Acceptor**	Biotage MP-TMT 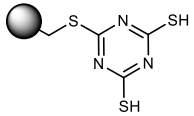 % of MA removed	QuadraSil MP  % of MA removed	Aminomethyl PS  % of MA removed	QuadraPure BzA 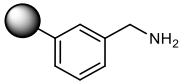 % of MA removed
Phenyl vinyl sulphone	25	10	75	>95
Cinnamaldehyde	<5	40	95	>95
Crotonaldehyde	25	70	>95	>95
3-Methyl crotonaldehyde	5	85	>95	>95
3-Methyl-3-pent-2-one	<5	50	<5	<5
1,4-Benzoqinone	95	85	>95	>95
2-Cyclohexen-1-one	50	>95	55	90
Benzyl acrylate	20	20	25	75
*n*Butyl acrylate, **32**	<5	5	<5	35
Methyl tiglate	25	30	25	25
Methyl cinnamate	<5	5	<5	<5
N-Phenylacrylamide	20	45	10	70
N-Isopropylacrylamide	<5	35	<5	<5
N,*N*-Dimethylacrylamide	30	55	15	20
Cinnamyl alcohol	5	55	<5	10
Testosterone	10	45	5	>95
70	<5	<5	<5	<5
68	<5	40	10	5

Table 2.9 *Scavenging capabilities of the resins against a range of Michael acceptors. Values shows the percentage of Michael acceptor scavenged as determined by ^{1}H NMR (300 MHz) spectroscopy, which were calculated to the nearest 5% by determining the difference in integrations of unscavenged scavenged mixtures relative to an internal standard (2,3,5-Trichloro-methoxybenzene).*

2.3.2 Scavenging of Metal Catalysts

Studies into the ability to scavenge metal catalysts from solution were conducted, to ensure catalysts could be removed from reaction mixtures to minimise any interference against the biological target in the assay. Stock solutions at the desired reaction array concentrations were prepared for each of the metal catalysts to be implemented in the reaction arrays (5 mM of $Pd(OAc)_2$, $[Ru(p\text{-Cymene})Cl_2]_2$, $[RhCP^*Cl_2]_2$ and $[IrCp^*Cl_2]_2$ and 50 mM of $Cu(OAc)_2$). 100 μL samples of the catalyst mixtures were scavenged with increasing amounts of the Quadrapure BzA resin (0 mg, 10 mg, 20 mg, 30 mg and 40 mg) for 24 hours. After 24 hours there was a visible reduction in colour (coloured → colourless) for all the metal catalyst solutions scavenged with the different amounts of resin, and a visible increase, of the catalyst colour on the Quadrapure BzA resin. However, subsequent Atomic Absorption Spectroscopy (AAS), to quantitatively measure the metal content of the unscavenged and scavenged catalyst solutions, proved difficult due to the small sample size (scale up to ensure enough sample (10 mL) for AAS studies would prove impractical).

To establish whether residual catalyst from the reaction mixtures interfered in the assay, scavenged reaction mixtures were screened as controls (see Appendix B) and there was no observed interference against the biological target. The Quadrapure BzA resin was shown to successfully scavenge strong electrophiles and metal catalysts from reaction mixtures, providing a simple and reliable post reaction work-up protocol to implement in the reaction arrays.

2.3.3 Evaluation of Scavenging Protocol for Crude C-H Functionalisation reaction mixtures

To further validate the QuadraPure BzA resin as a simple and efficient work-up procedure to implement in parallel plate-based reaction arrays, the resin was tested on an example literature reaction, (Entry 2, Table 2.1), which contained multiple electrophiles, from the starting material, additive and product, and the metal catalyst. The reaction was performed in 5 x 100 μL aliquots under ADS-conditions with 100 mM of substrate **67**, 200 mM of

substrate **32**, 50 mM benzoquinone and TsOH and 5 mM of $Pd(OAc)_2$ in $CDCl_3$. The reaction was left for 24 h, and a ^1H NMR (300 MHz) spectrum of one of the aliquots, including the internal standard 2,3,5-trichloro-methoxybenzene, was recorded. To each of the four remaining reaction aliquots, was added 10, 20, 30 and 40 mg of Quadrapure BzA resin respectively. The resin was left to incubate with the reaction mixture for 24 h, and then a ^1H NMR (300 MHz) of each of the aliquots was recorded, including the internal standard. The product mixture peaks were integrated relative to the standard peaks, and used to quantify the amount of each reaction component scavenged with the increasing amount of resin (^1H NMR (300 MHz) spectra for each aliquot after scavenging is shown in Figure 2.6).

In the presence of 10 mg of QuadraPure BzA resin (Figure 2.6b), >95% of the benzoquinone and 50% of the unreacted *n*butyl acrylate **32** were scavenged from the reaction mixture after 24 h. With 20 mg (Figure 2.6c) the amount of *n*butyl acrylate **32** scavenged increased to 90% and with 30 mg (Figure 2.6d) this amount increased to >95% as well a small amount (10%) of the reaction product **68**. When the amount of resin was increased to 40 mg, both the benzoquinone and *n*butyl acrylate were completely scavenged, with just 25% of the reaction product **68** scavenged (Figure 2.6e).

This demonstrated the ability of Quadrature BzA to scavenge highly electrophilic Michael acceptors, while leaving reaction products unscavenged. The resin was also demonstrated to successfully scavenge a range of metal catalysts used in C-H functionalisation to a level where no assay interference was observed (Chapter 4). The use of 30 mg of Quadrapure BzA as a parallel reaction array work-up procedure in C-H functionalisation reaction arrays, will provide an efficient step in the ADS work flow, prior to screening in the biological assay.

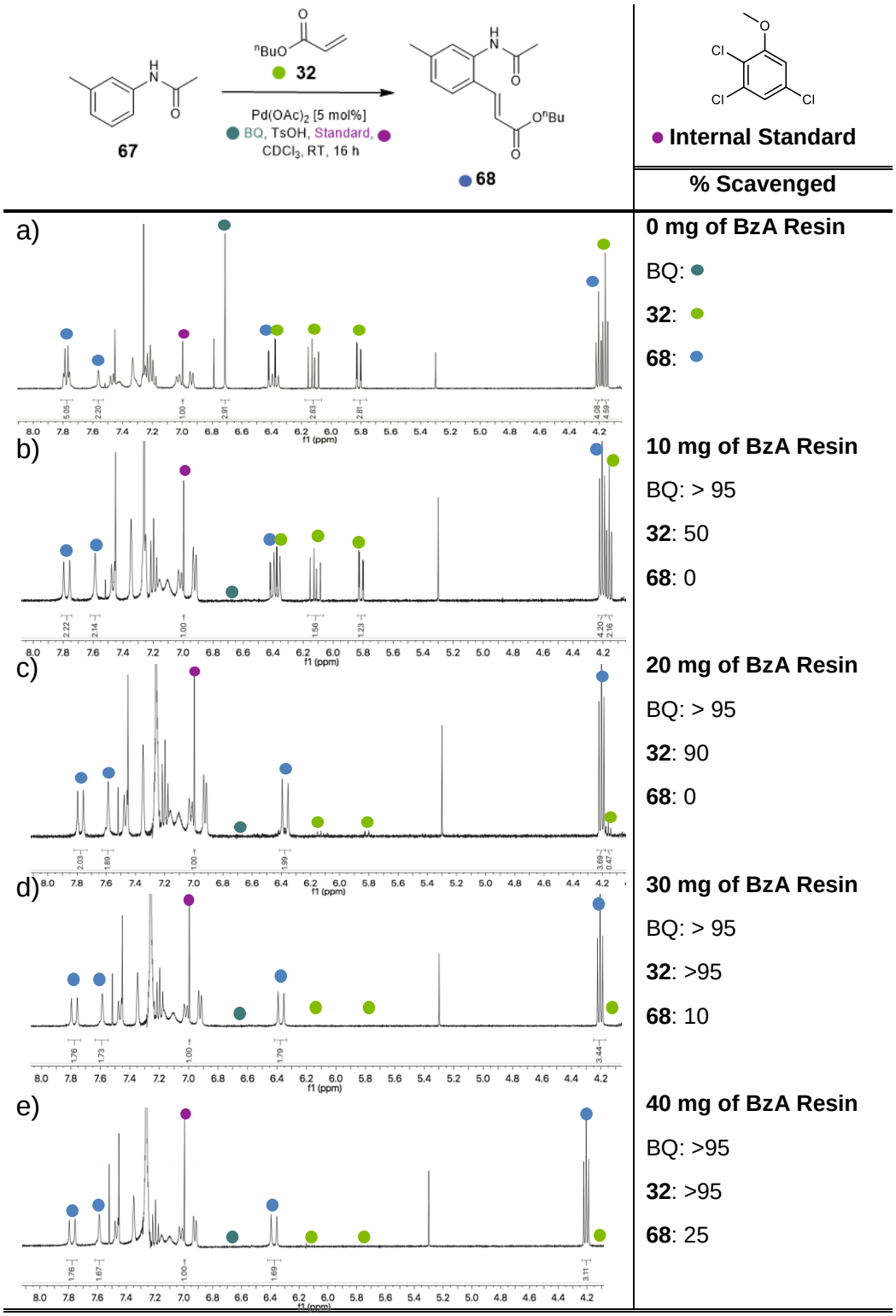

Figure 2.6 *Capability of Quadraupre BzA resin to scavenge an exemplar C-H alkenylation reaction (100 μL reactions with 100mM* ***67****, 200mM* ***32****, 50 mM BQ and TsOH and 5 mM Pd(OAc)₂). ¹H-NMR (300 MHz) spectra recorded A) before scavenging (reference spectrum) and after scavenging for 24 h with b) 10 mg of resin, c) 20 mg of resin, d) 30 mg of resin and e) 40 mg of resin.*

2.4 Summary

A vast range of C-H functionalisation reactions has been reported over the past few decades, which have the potential to transform synthetic strategies for chemists, by enabling new disconnections to be made. The ability to elaborate fragments along any C-H vector with C-H functionalisation chemistry has the potential to greatly enhance fragment-to-lead studies. It was proposed the use of C-H functionalisation in Activity-Directed Synthesis would enable fragment-to-lead studies to be conducted in a structure-blind and function-driven manner.

A range of reported C-H functionalisation reactions was repeated in flask and plate-based formats, to configure the chemistry for use in plate-based microscale reactions arrays. The study demonstrated that a range of reaction types (C-H alkenylations, aminations and arylations) could be reproduced in plates without stirring. Parallel heating technology for microscale reaction arrays was also established to enhance the range of chemistries and substrates used in ADS.

An efficient post reaction work-up procedure for parallel chemistry was established, with the use of 30 mg of Quadrapure BzA to scavenge metal catalysts and strong electrophiles. With the simple and efficient workflow for ADS established, C-H functionalisation reaction arrays can be performed under ADS conditions, scavenged, filtered and crude mixture screened against the biological target of interest.

The configuration of a range of mild C-H functionalisation chemistry at room and elevated temperatures in parallel-array format and the establishment of a operationally simple procedure for scavenging metal catalysts and Michael acceptors from crude reaction array mixtures has ensured a streamlined and efficient workflow. The established procedures can be exploited to potentially enable the structure-blind and function-driven identification of productive fragment elaboration vectors in ADS.

Chapter 3.
Configuration of a High-throughput Assay and Identification of Fragments for Hsp90

Hsp90 (Heat shock protein 90) is a molecular chaperone that has been linked to diseases such as Alzheimer's, cystic fibrosis and cancer, prompting the development of chemical inhibitors of the ATP-binding (*N*-terminal) domain of Hsp90.[108–110] Numerous chemical ligands have been reported from drug discovery programmes, many of which have been discovered *via* fragment-based workflows.[111–116] It was proposed the fragment and ligand chemical matter for Hsp90 would provide strong starting points for fragment elaboration strategies with C-H functionalisation chemistry in activity-directed synthesis. An overview of the biology, high-throughput assay and known chemical matter of Hsp90 is given. The design and synthesis of fragments which have the potential for elaboration with C-H functionalisation chemistry is discussed. A high-throughput fluorescence anisotropy assay for Hsp90 was established,[80] to screen and aid the selection of weakly binding fragments that could provide starting points for activity-directed fragment elaboration.

3.1 Biology of Hsp90

Hsp90 is a molecular chaperone that ensures eukaryotes maintain homeostasis under physiological changes, by maintaining the integrity of the cellular protein network (proteostasis).[110,117] Molecular chaperones are proteins that form reversible complexes with other protein substrates (clients), inducing the adoption of a client proteins active conformation. Hsp90 machinery is essential under stress conditions, such as an increase in temperature (heat shock)[118] and has also been found to play important roles under physiological conditions, for example, in the signalling of steroid hormone receptors.[119]

3.1.1 The Structure and Function of Hsp90

Hsp90 is a central component of eukaryotic cellular machinery and has hundreds of client proteins, which bind reversibly to Hsp90.[120] Hsp90 controls

the function and activity of its client proteins by facilitating protein folding, client-substrate binding and the assembly of multiprotein complexes (Figure 3.1 ai). Hsp90, through the binding to client proteins, is consequently involved in many cellular processes; DNA repair, cellular development, immune response and neurodegenerative disease.[110,120]

Hsp90 functions as a homodimer, in which each monomer consists of three highly conserved domains. The amino terminal domain (NTD), responsible for ATP binding,[121] the middle domain (MD), which is important for ATP hydrolysis and the binding of client proteins and the carboxy terminal domain (CTD) which is responsible for dimerisation (Figure 3.1 ai-iii).[122] The NTD and MD are connected by a flexible charged linker that helps mediate Hsp90 function.[123] Dimerisation of Hsp90 is essential for its *in vivo* function.[124,125] In the absence of ATP, Hsp90 adopts an open V-shaped conformation (Figure 3.1b).[126] ATP binding induces large conformational changes, which results in an NTD-closed state. For ATP hydrolysis to occur, the ATP-binding site of the NTD must interact with the MD. The NTD has low ATPase activity, K_d for ATP is approximately 400 μM, with a hydrolysis turnover in human Hsp90 of 0.1 min^{-1}.[121] Following ATP hydrolysis, ADP and inorganic phosphate (P_i) are released and Hsp90 readopts its open conformer (Figure 3.1b).

Hsp90 function is regulated by expression, post-translational modifications and interactions with co-chaperones (non-client proteins) and clients.[110,127] The expression of Hsp90 is induced by the stress-related transcription factor Heat-Shock Factor 1 (HSF1).[127,128] Hsp90, along with co-chaperone Hsp70, bind to HSF1 to keep it in its inactive state.[129] When co-chaperone proteins are needed for other functions and are unbale to bind to HSF1 to keep it in its inactive state, the expression of Hsp90 increases. Post-translational modifications, including phosphorylation, SUMOylation, acetylation and *S*-nitrosylation, modulate Hsp90 function, by altering the accessibility at binding sites.[130] Phosphorylation slows down the conformational cycle, affects client maturation and the interaction with co-chaperones.[131,132]

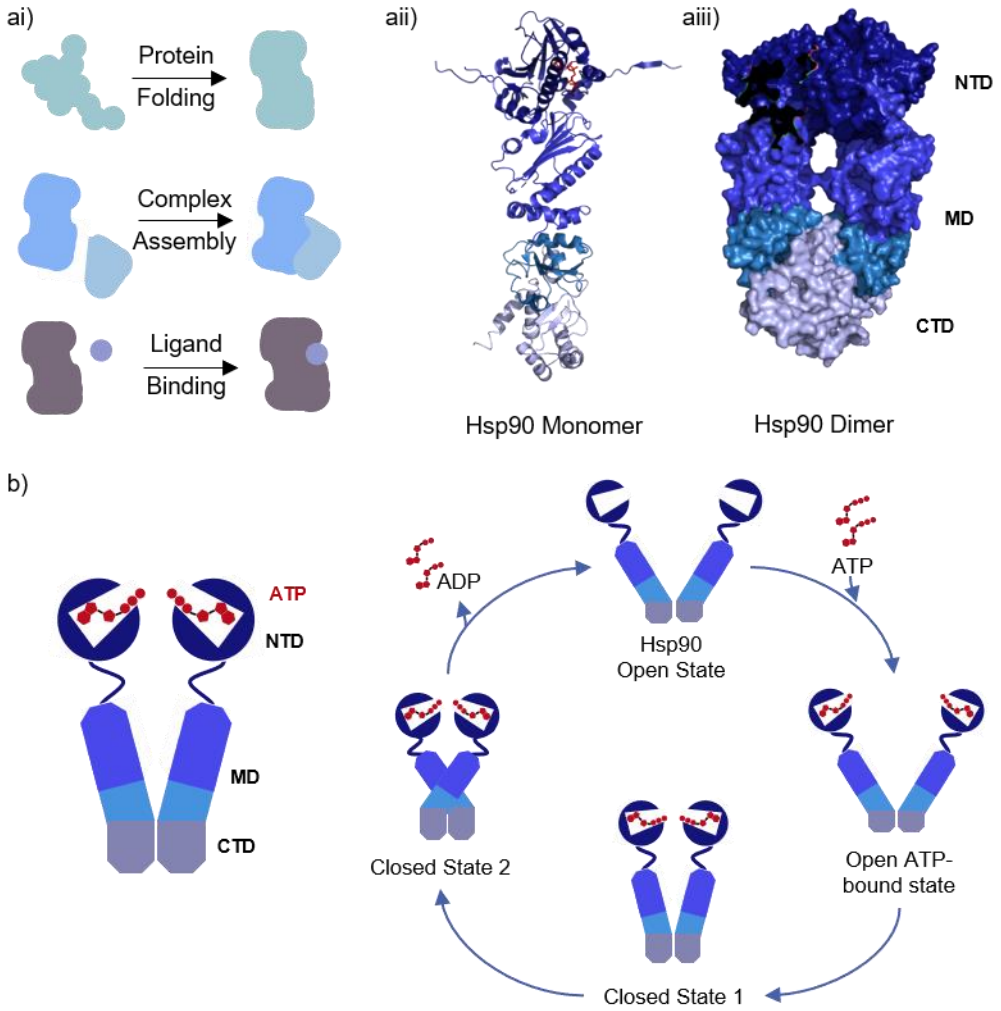

Figure 3.1 *Function and structure of Hsp90 (PDB ID: 2CG9, Saccharomyces cerevisiae)* ***ai****) Functions of Hsp90* ***aii****) Hsp90 Monomer with ATP (red) bound to the N-terminal domain (NTD)* ***ii****) Hsp90 dimer: NTD (dark blue) linked to middle domain (Large and small central blue sections) and C-terminal domain (CTD – Light purple).* ***b****) Conformation cycle of Hsp90.*[110]

Co-chaperones are non-client proteins that interact with chaperones and assist with the folding and activation of a chaperones client proteins.[110] Co-chaperones are the key regulators of Hsp90 and their binding sites have been identified in all three binding domains of Hsp90. Some co-chaperones are modulators of Hsp90s conformational cycle and others assist with client recruitment.[133] The co-chaperone p23, for example, binds to the NTD and MD of Hsp90 and inhibits ATPase activity and stabilises the closed state of Hsp90.[134]

Hsp90 has hundreds of client proteins, making it central to many cellular processes.[120] The identification of client binding sites is challenging, due to

the large size and dynamic nature of Hsp90-client complexes making crystallisation and NMR studies difficult. However, analysis of Hsp90-client complexes revealed 60% of the humane kinome and 30% of human E3 ubiquitin ligases associate with Hsp90.[135] Example client proteins include the tumour suppressor p53 which binds to all three domains of human Hsp90α[136] and the Alzheimer disease related protein tau, which has been shown to bind to a large surface between the NTD and MD of Hsp90β[137] (Hsp90α and Hsp90β are the two prominent functional isoforms found in the cytosol).

3.1.2 Heat Shock Protein 90 and Disease

Hsp90 has been implicated in various diseases and the role it plays in each disease varies.[110] Given Hsp90 is upregulated under changes to physiological conditions, it plays a key role in the survival of tumour cells which are under stress-conditions due to the presence of mutant proteins and rapid proliferation.[138] Indeed, increased levels of Hsp90 are found in tumour cells. Many of Hsp90s clients are involved in the progression of tumour growth, for example, tumour suppressor p53, telomerase and hypoxia-inducible factor 1α (HIF1α). Inhibition of Hsp90 disrupts multiple signalling cascades responsible for oncogenic progression. Given higher expression of Hsp90 in tumour cells, tumour cell Hsp90 has a higher affinity for chemical inhibitors than normal somatic cells.[139,140]

Other Hsp90 clients include the fibril- and plaque-forming protein amyloid-β (Aβ) and the hyperphosphorylated tau protein, which are implicated in Alzheimer's disease.[141] Inhibition of Hsp90 reduces the activity of kinases that phosphorylate tau, reducing aggregation.[142] Hsp90 has also been associated with diseases that include cystic fibrosis[143] and in viral[144] and protozoan[145] infections. The development of chemical inhibitors of Hsp90 offers an attractive potential to treat a wide range of diseases, due to its interaction and complexation with a large number of client proteins.

3.1.3 Chemical Inhibitors of the *N*-Terminal Domain of Heat Shock Protein 90

Chemical inhibition of the ATPase function of the NTD of Hsp90 is an attractive target in medicinal chemistry programmes, due to the many clients and subsequent related diseases of Hsp90. The development of chemical inhibitors of Hsp90 gained huge interest following the discovery that geldanamycin and radicicol were natural product inhibitors of Hsp90(NTD) (Figure 3.2a).[109,146]

Inhibition of Hsp90 with geldanamycin, a naturally occurring benzoquinone annamycin, isolated from *Streptomyces hygroscopicus*,[109] was shown to reduce cancer cell growth and depleted oncogenic proteins.[147] Despite its anticancer properties, geldanamycin failed to significantly progress through clinical trials due to its poor solubility and high toxicity. To address such issues with solubility and toxicity, various synthetic analogues have been reported which have subsequently entered clinical trials. 17-AGG (not shown), for example, is a geldanamycin analogue in which the 17-methoxy (benzoquinone methoxy) was replaced with an allylamino group, which entered phase I clinical trials; however, again failed to progress due to poor solubility.[109,148] Due to either poor solubility, toxicity or efficacy there are currently no synthetic analogues of geldanamycin undergoing clinical assessment.[109]

Radicicol is a macrocyclic lactone, isolated from *Monosporium bonorden*, which binds to Hsp90(NTD).[149] However, radicicol undergoes rapid metabolism *in vivo* and therefore shows no antitumor activitiy.[150] Several synthetic analogues have been developed, e.g. Onalespib[111,112] (AT13387) and NVP-AUY922[115,151] (Figure 3.2b), in which the resorcinol ring mimics the adenine ring of ATP, and is required for inhibition.[109] Indeed, the resorcinol ring is found in a wide range of chemical inhibitors and its binding mode is conserved in the crustal structures with Hsp90(NTD). NVP-AUY922 was discovered by Vernalis in a fragment-based discovery programme, which identified fragment **86** (Figure 3.4a, PDB: 2YE2) from a combination of fragment and *in silico* screening techniques.[115] Fragment **86** was subsequently confirmed as a hit through NMR experiments. Elaboration of **86**

(IC_{50}: 1 mM) through structure-guided design lead to the discovery of NVP-AUY922 which is nanomolar inhibitor (IC_{50}: 9 nM) of the Hsp90(NTD). NVP-AUY922 is currently undergoing clinical assessment for the treatment of stage IV non-small cell lung cancer.

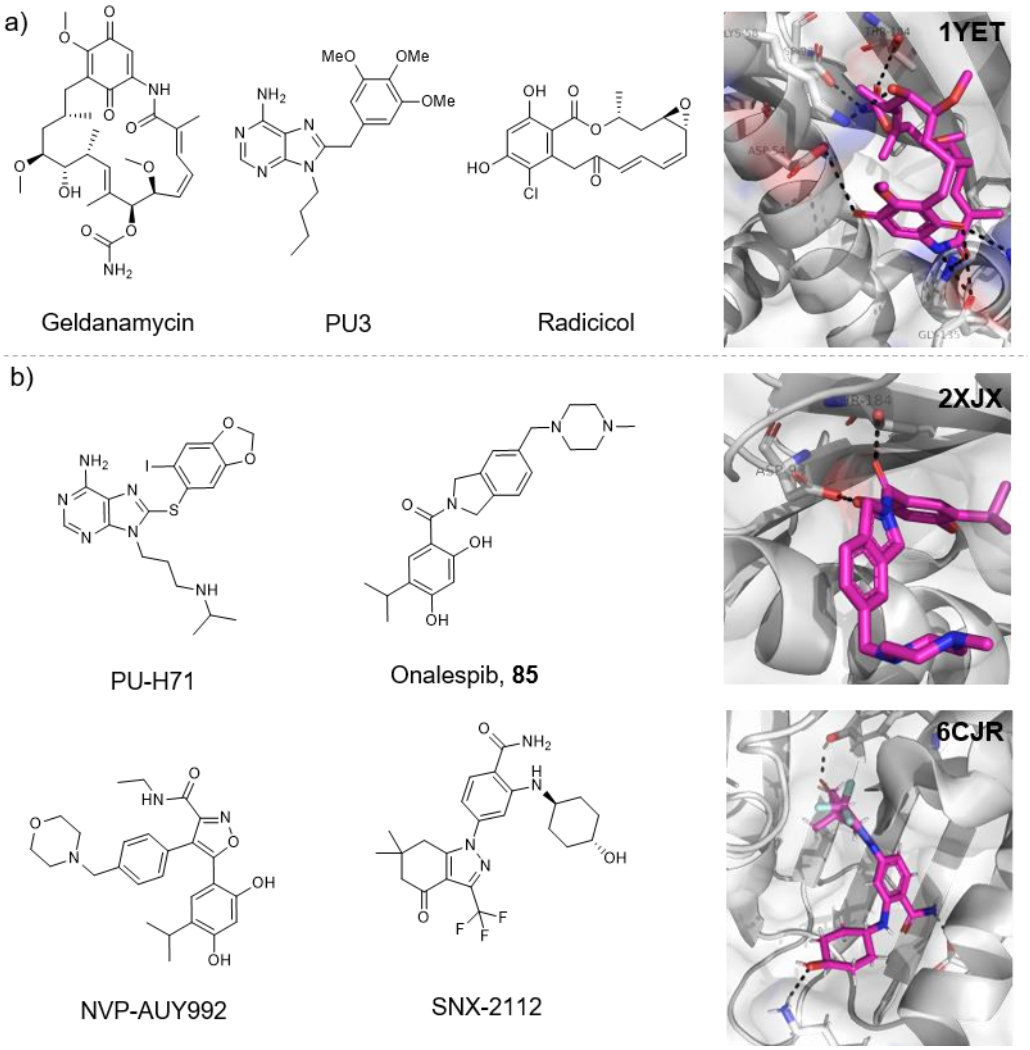

Figure 3.2 *Overview of Hsp90(NTD) inhibitors* ***a)*** *Natural product (inspired) inhibitors of Hsp90(NTD): Geldanamycin, Radicicol and PU3 have high affinity for Hsp90(NTD), however failed in clinical trials due to high toxicity. Geldanamycin bound to Hsp90(NTD) PDB: 1YET b) Synthetic inhibitors of Hsp90(NTD) PU-H71, Onalespib, NVP-AUY922 and SNX-2112. Onalespib bound to Hsp90(NTD), PDB: 2XJX and SNX-2112 bound to Hsp90(NTD), PDB: 6CJR.*

Onalespib **85** (Figure 3.2) was also discovered during a fragment-based discovery programme by Astex pharmaceuticals.[112] Fragment **81** (Figure 3.3 and Figure 3.4, PDB: 2XDL) was identified in a fragment screen using ligand-observed NMR. Fragment **81** was determined to have a

dissociation constant of 790 μM via isothermal calorimetry and was subjected to structure-guided optimisation, to yield **84** (K_d: 0.54 nM, LE: 0.57) as a lead compound (Figure 3.3). Subsequent optimisation identified clinical candidate Onalespib **85** (K_d: 0.71 nM, LE: 0.42),[111] which is currently undergoing clinical assessment against BRAF-mutant melanoma in combination with Dabrafenib and Trametinib.

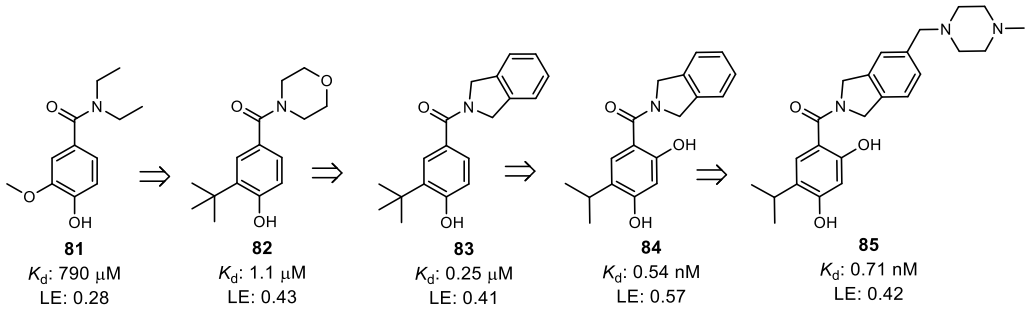

Figure 3.3 *Development of Onalespib **85** from fragment **81** in fragment-to-lead optimisation study by Astex pharmaceuticals.*[112]

Another class of chemical inhibitors include purine-based ligands, such as PU3 and PU-H71 (Figure 3.2), which were designed to mimic the binding mode of ADP to Hsp90.[152] PU-H71 is currently undergoing clinical assessment for the treatment of advanced malignancies and in combination with Nab-placlitaxel for the treatment of metastatic breast cancer. SNX-2112 (Figure 3.2) is a chemical inhibitor discovered be Serenex in a fragment-based approach,[111] in which the indazolone 2-aminobenzamide core mimics the ADP adenine core and is currently undergoing efficacy and safety assessment in combination with Ibrutinib.

3.2 Design and Synthesis of Hsp90 Fragments for Activity-Directed Synthesis

Hsp90 has been well studied as druggable target and there have been many chemical ligands (clinical candidates, lead-like ligands and fragments) which have been developed and reported. For this reason, along with the reported high-throughput fluorescence anisotropy assay (Section 3.3), it was proposed Hsp90 would make a tractable target for demonstrating C-H functionalisation as a potential methodology for elaborating fragments using

activity-directed synthesis. The fragments were designed to include at least one potential directing group for C-H functionalisation.

3.2.1 Design of Hsp90(NTD) Fragments for elaboration with C-H Functionalisation chemistry

For the evaluation of C-H functionalisation as a fragment elaboration strategy in activity-directed synthesis, a set of Hsp90 fragments was designed and then either purchased or synthesised to enable their biological evaluation and subsequent implementation in ADS. Fragments **81** and **86**-**92** have been reported as inhibitors (~10 μM – 5 mM affinities) of Hsp90 and have the potential to undergo C-H functionalisation reactions (Figure 3.4).[112,113,115,116] Assessment of the crystal structures of fragments **81**, **87**, **89** and **92**, revealed potentially productive C-H vectors within the fragments which would potentially be accessible synthetically due to their proximity to a directing group, e.g. C-H functionalisation *ortho* to the ketone directing group of fragment **87**. C-H functionalisation along the identified vectors has the potential to enhance the activity of the fragments by establishing new hydrogen-bonding and hydrophobic interactions with the target. A further 21 fragments (**93**-**97, 99, 101** and **103**-**116,** Figure 3.8) were designed based on these eight published fragments and through deconstruction of known Hsp90 ligands to identify new potential Hsp90 fragments. The rationale for the design of the 29 fragments is outlined below.

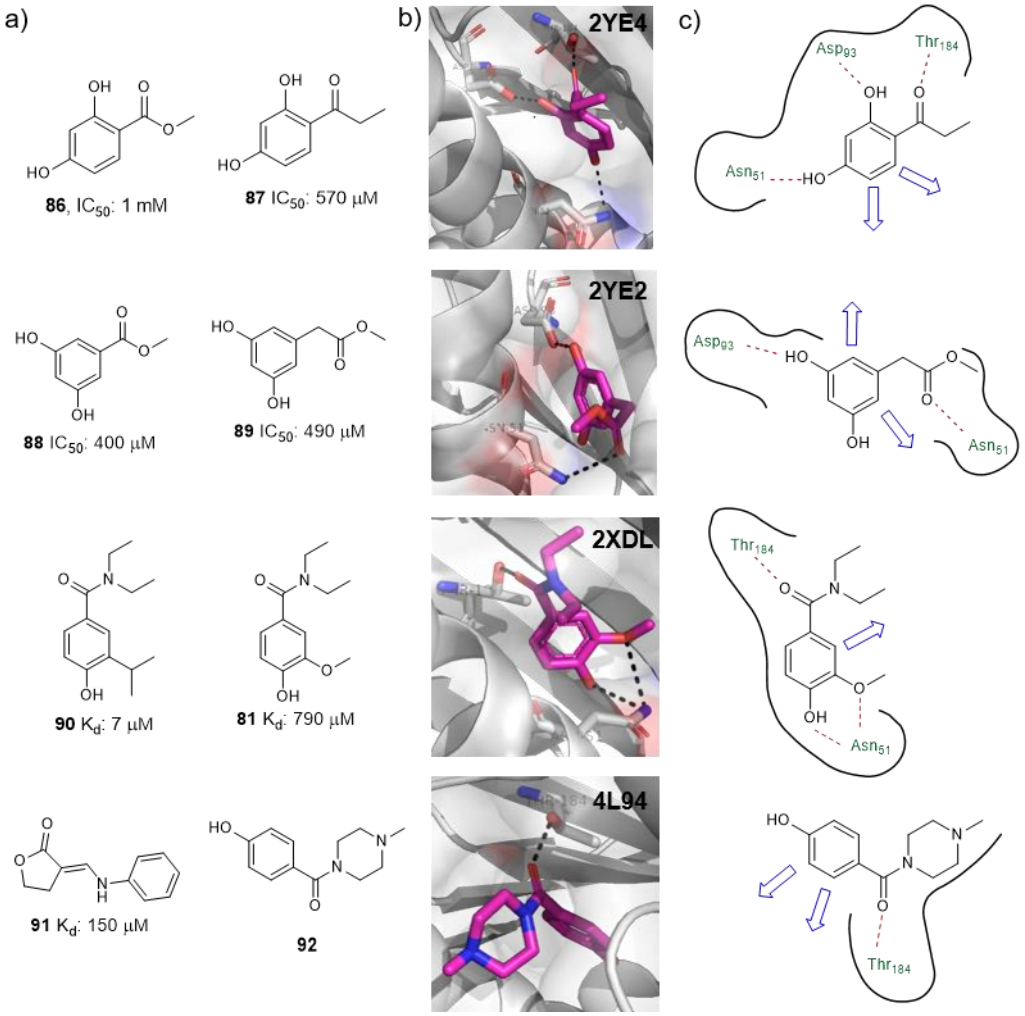

Figure 3.4 ***a)*** *Known Hsp90(NTD) fragments* ***81***, ***86-92*** *chosen for potential implementation in ADS based on their possibility to undergo C-H functionalisation elaboration.* ***b)*** *Crystal structures show fragments* ***87*** *(PDB: 2YE4),* ***89*** *(PDB: 2YE2),* ***81*** *(PDB: 2XDL) and* ***92*** *(PDB: 4L94, no reported affinity) bound to Hsp90(NTD).* ***c)*** *Potential synthetically tractable C-H vectors for elaboration of fragments* ***87***, ***89***, ***81*** *and* ***92*** *with C-H functionalisation chemistry (blue arrows indicate potential C-H functionalisation elaboration vectors).*[112,113,115,116]

Fragments **93-97** were designed based on published fragments **86**-**89** and **92** respectively, by removal of one of the hydroxyl groups from the aryl ring (Figure 3.5a). As discussed, the published fragments binding modes offer the potential to productively elaborate the fragments using C-H functionalisation chemistry (Figure 3.4). However, it was proposed hydroxy groups within phenol/resorcinol substrates may potentially dominate reactivity under C-H functionalisation conditions and, as discussed in chapter 2, substituents *meta* to a directing group can inhibit reaction at the *ortho*-

positions. Therefore, removal of one hydroxyl group may enable the fragments to maintain key hydrogen bonds to Hsp90 but enables greater synthetic accessibility, as well as the potential to select a series of phenol/resorcinol fragments with similar Hsp90(NTD) affinities.

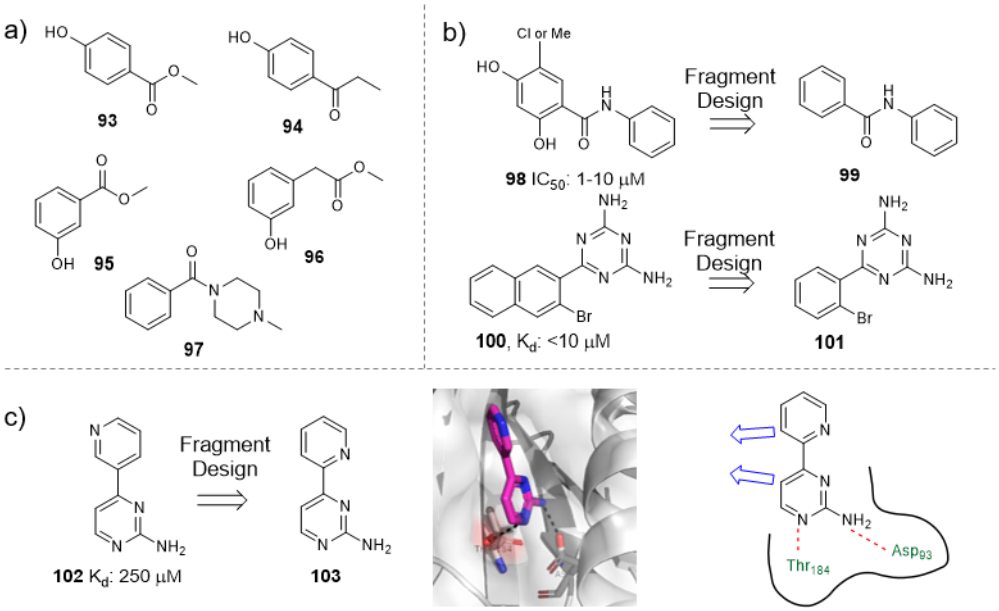

Figure 3.5 *Fragments **93-97, 99, 101** and **103** were designed from known Hsp90(NTD) fragments on the basis of their potential to undergo C-H Functionalisation in ADS (Blue arrow indicates potential C-H functionalisation elaboration vectors).*[112,113,115]

Fragments **99** and **101** were designed from reported fragments **98** and **100** respectively (Figure 3.5b).[113,115] Again, hydroxyl substituents of **98** were removed to give **100**, for reasons previously discussed, and was chosen due to the potential of the benzamide **100** to direct C-H functionalisation onto the *ortho*-positions of both aryl rings. The naphthalene ring of **100** was changed to a benzene ring to reduce the lipophilicity of the fragment and was chosen on the basis heteroaryl rings can direct C-H functionalisation onto the ortho position of an adjacent aryl ring. Finally, fragment **103** was designed from fragment **102** by moving the nitrogen of the pyridine ring one position on the ring, to enable both heteroaryl rings to direct C-H functionalisation onto the *ortho*-position of the adjacent aryl ring (Figure 3.5c).[112] Analysis of the crystal structure of **102** bound to Hsp90(NTD) shows the nitrogen of the pyridine does not make a hydrogen-bonding interaction and so moving it one position in the

ring was not expected to prove detrimental to binding but enable synthetic accessibility to both aryl rings with C-H functionalisation chemistry.

Fragments **104**-**110** (Figure 3.6) were designed from fragments **81** and **90** (Figure 3.6, which is an optimised fragment reported in the discovery of Onalespib).[112] The 4-hydroxy and 3-methoxy of **81** make key hydrogen bonding interactions with Hsp90(NTD) (Figure 3.4) however, the possibility of removing and/or swapping the 4-hydroxy to a methoxy was explored, again to minimise the potential of the hydroxyl to dominate reactivity under C-H functionalisation conditions. The amide group was also varied to include secondary and tertiary amides to enable this potential directing group to match to literature C-H functionalisation reactions (Chapter 2).

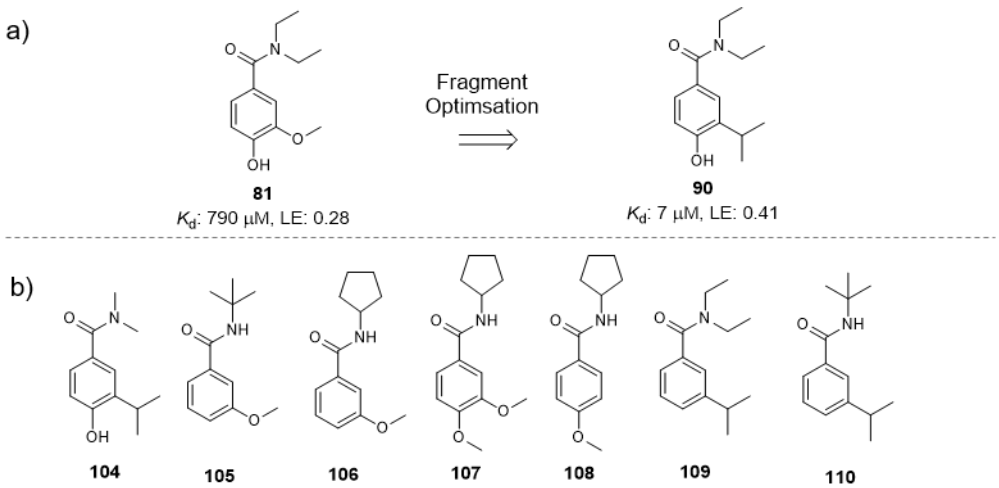

Figure 3.6 *Fragments **104**-**110** were designed by analysis of known Hsp90(NTD) fragments **81** and **90** on the basis of their potential to undergo C-H functionalisation in ADS.*[112]

Finally, a series of fragments was designed by deconstructing known Hsp90 ligands to identify core fragments which have the potential to undergo C-H functionalisation reactions. Deconstruction of AUY922-Lead and AUY922 itself revealed two potential fragments **111** and **112** which have the potential to undergo C-H functionalisation chemistry along vectors that look promising for productive fragment elaboration (Figure 3.7a). The fragment **112** contains and amide directing group which can direct C-H functionalisation onto the aryl

ring, and **111** contains a heteroaryl ring which can direct C-H functionalisation onto the adjacent ring.

Deconstruction of clinical candidate SNX-2112 revealed two core fragment structures, **113** and **114-116** which have the potential to undergo C-H functionalisation (Figure 3.7b). Both core fragments possess amide directing groups to direct *ortho* C-H functionalisation, with fragments **114**-**116** containing a heteroaryl to direct C-H functionalisation onto the adjacent aryl ring. Fragments **114-116** was deigned to incorporate primary and secondary amide directing groups to align with previously established C-H functionalisation reactions (Chapter 2).

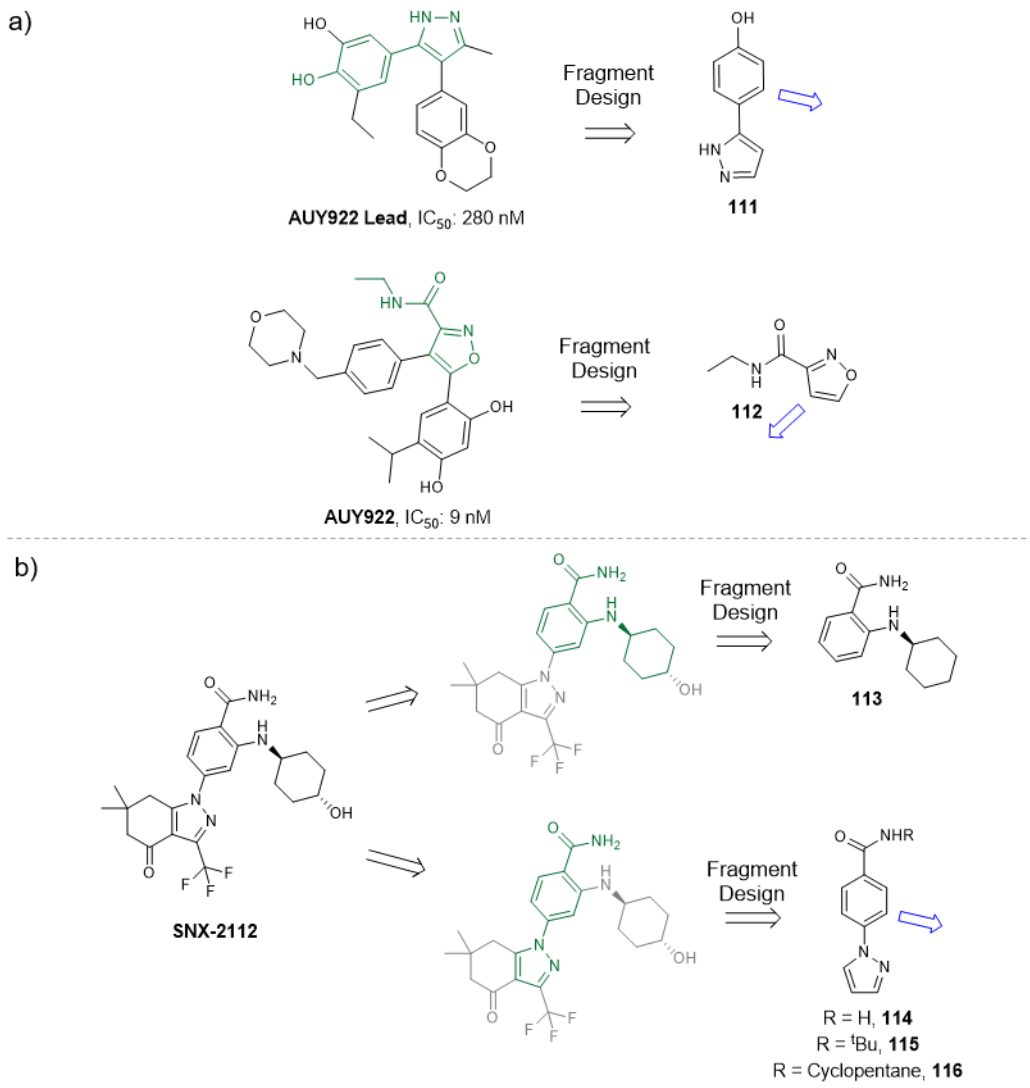

Figure 3.7 *Fragments **111**-**116** were designed by deconstructing known Hsp90(NTD) ligands on the basis of their potential to undergo C-H functionalisation in ADS (Blue arrow indicates potential C-H functionalisation elaboration vectors).*

3.2.2 Synthesis of Hsp90(NTD) Fragments

A total of 29 fragments (Figure 3.8) was designed, from known fragments and ligands of Hsp90(NTD), which have the potential (i.e. suitable directing groups) to undergo C-H functionalisation elaboration chemistry. Of the 29 fragments, fragments **81**, **86**-**89**, **92**-**96**, **99**, **103** and **111** were commercially available and hence purchased (green, Figure 3.8). The remaining 16 fragments required synthesis (red, Figure 3.8), and their syntheses are described below.

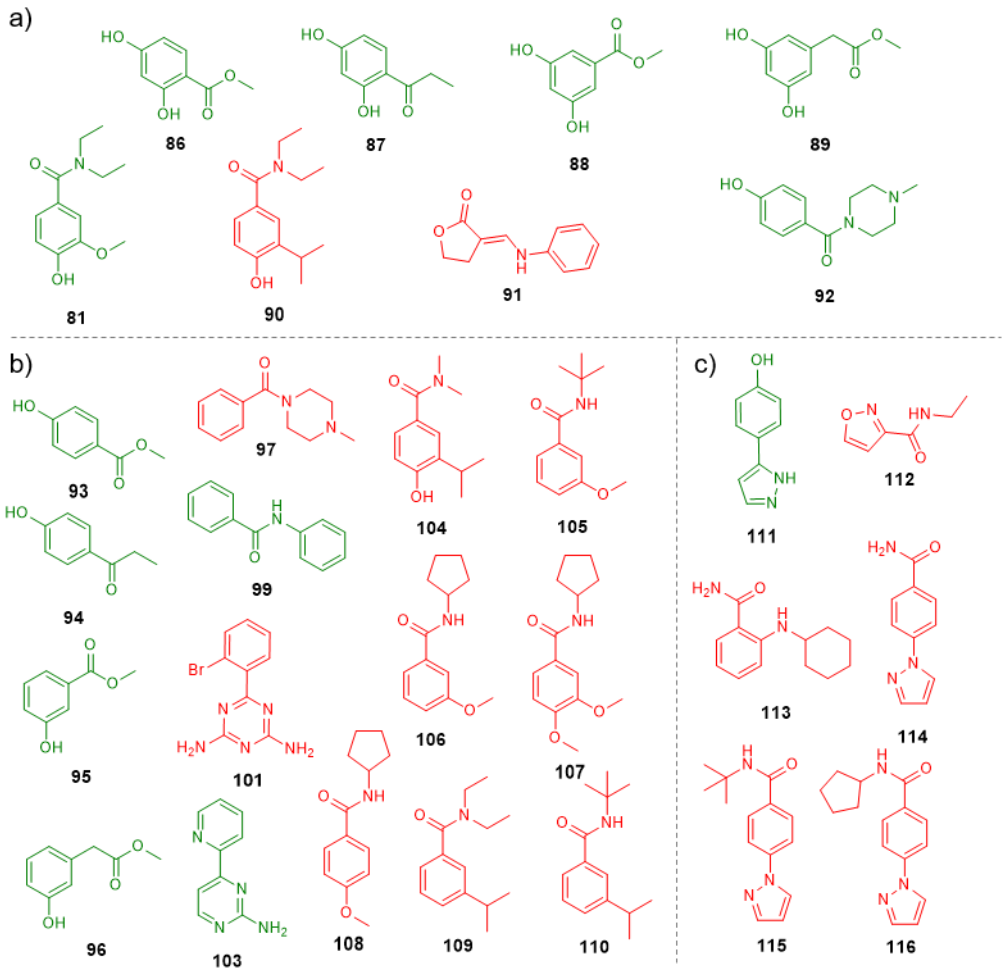

Figure 3.8 *Designed Hsp90(NTD) fragments for their potential to undergo synthetic elaboration in ADS using C-H functionalisation chemistry.* ***a****) Reported Hsp90(NTD) fragments from FBDD programmes.* ***b****) Fragments designed from reported fragments and have the potential to undergo C-H functionalisation elaboration.* ***c****) Fragments designed from reported ligands and have the potential to undergo C-H functionalisation elaboration. Design rationale is discussed in main text. Green fragments were commercially available and red fragments required synthesis (Section3.2.2).*

Fragments **90** and **104** were prepared via the same synthetic route in four steps, from commercially available 2-isopropylphenol **117** (Scheme 3.1). The phenol **117** was first protected as the triisopropyl silyl (TIPS) ether **118**, by reaction with TIPS-Cl in the presence of imidazole in good yield (74%). Subsequent bromination with *N*-bromosuccinimide resulted in the monobrominated silyl ether **119** after 3 h, also in good yield (81%). Bromination was electronically directed *para* to the oxygen substituent and *ortho*-bromination was not observed presumably due to the steric bulk of the silyl protecting group. The bromide **119** underwent lithium-halogen exchange upon treatment with butyl lithium. The resulting aryl-lithium species was subsequently trapped with the appropriate dialkyl carbomoyl chloride to yield **120** (40%) and **121** (44%). Deprotection of the silyl ether by treatment with KF afforded **104** in poor yield (12%) and **90** in modest yield (27%). Despite the modest yields, both fragments were readily accessible in four steps.

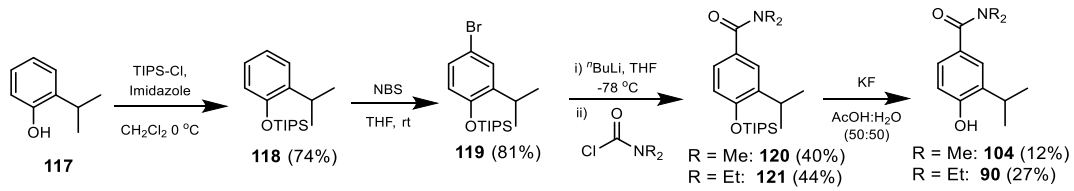

Scheme 3.1 *Synthesis of fragments **90** and **104** from 2-isopropylphenol **117.***

Fragment **91** was prepared via a known synthetic route in two steps (Scheme 3.2).[153] Condensation of γ-butyrolactone **122** with ethyl formate **123** in the presence of strong base (NaH) gave sodium salt **124** in very good yield (98%), which upon treatment with aniline hydrochloride in methanol produced the desired enaminolactone **91** in good yield (73%). As hypothesised in the reported methodology paper the use of polar solvent promotes formation of the *E*-isomer and ^{1}H and ^{13}C NMR data was identical to that previously reported. There was no observed correlation in the NOESY spectrum between the alkene C-H and the CH_2 at the 4-position of the oxolanone ring, supporting the formation of the *E*-isomer.

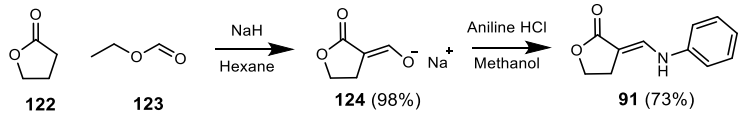

Scheme 3.2 *Synthesis of fragment **91** from γ-butyrolactone **122** and ethyl formate **123**.*[153]

Fragment **101** was prepared from a known literature procedure in a single step (Scheme 3.3).[154] Reaction of 2-bromobenzonitrile **125** with cyanoguanidine **126** in the presence of potassium hydroxide gave **101** (85%).

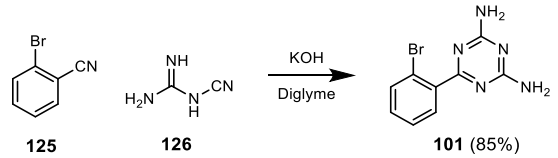

Scheme 3.3 *Synthesis of fragment **101** from 2-bromobenzonitrile and cyanoguanidine.*[154]

Fragment **113** was prepared via a two-step synthesis (Scheme 3.4). In the first step a palladium-catalysed Buchwald-Hartwig coupling of 2-bromobenoznitrile **125** with cyclohexylamine **71** gave **127** in 72% yield. The reaction proceeded under microwave irradiation with a dry and inert (N_2) atmosphere. Hydrolysis of the cyano group of **127** with potassium tertbutoxide and dry tert-butanol to the primary benzamide gave **113** in 58% yield (nucleophilic attack of the tertbutoxide into the nitrile and then addition of H_2O in the work up ensures hydrolysis to the primary amide).

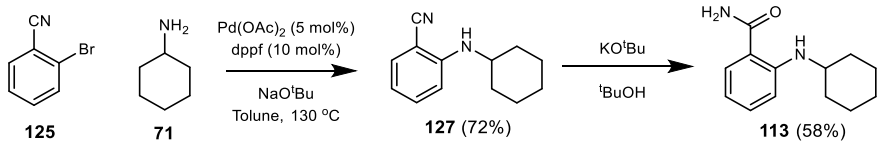

Scheme 3.4 *Synthesis of fragment **113**.*

Finally, fragments **97**, **105-110**, **112** and **114-116** were prepared via a series of amide coupling reactions from either the appropriate benzoic acids or benzoyl chlorides (Scheme 3.5). Benzamides were prepared from benzoic acids with two equivalents of amine in the presence of the coupling agent TBTU and DIPEA, with yields ranging from 48% to 89%. Fragments **114** and **97** were prepared from their benzoyl chlorides in 55% and 90% yields respectively.

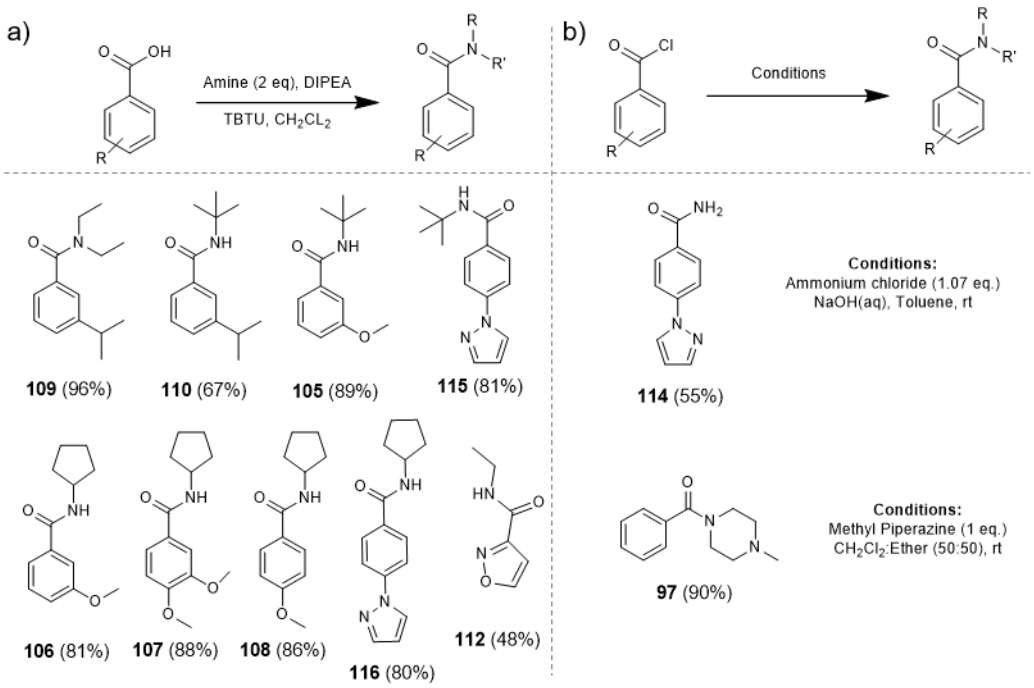

Scheme 3.5 *Synthesis of fragments **105-110**, **112**, **115** and **116** via amide coupling from the appropriate benzoic acids and synthesis of **97** and **114** via amide coupling from the appropriate benzoyl chlorides.*

A total of 29 fragments was successfully prepared or purchased, which were designed, from known fragments and ligands of Hsp90, to incorporate at least one potential directing group for C-H functionalisation chemistry. The fragments were subsequently screened to enable hits to be identified (Section 3.4).

3.3 Configuration of High-throughput Assay for Heat Shock Protein 90

3.3.1 Hsp90(NTD) Fluorescence Anisotropy Assay

Anisotropy is a molecular property that demonstrates the interaction of a fluorescent molecule (tracer) with plane polarised light.[155] The tracer is excited with light that is linearly polarised (Figure 3.7). The subsequent emitted polarised fluorescence is measured, at a given time, parallel and perpendicular to the plane of polarisation of the excitation light. The difference in intensities of the parallel and perpendicular emitted light arises from how quickly the tracer tumbles in solution, relative to the fluorescence lifetime of

the fluorophore. When the tracer molecule is free in solution, it tumbles very quickly and so when excited with plane polarised light, the emitted light is random with respect to the plane of polarisation (polarisation is small). When the tracer becomes tightly bound to a larger molecule e.g. its protein target, the rate the tracer tumbles is much slower and so when excited with plane-polarised light, the light emitted is also polarised (the observed polarisation is large), (Figure 3.9). Anisotropy can be used to determine the dissociation constant (K_d) of the fluorescent tracer, which in turn can be used to determine the affinity of unlabelled molecules using competition experiments.

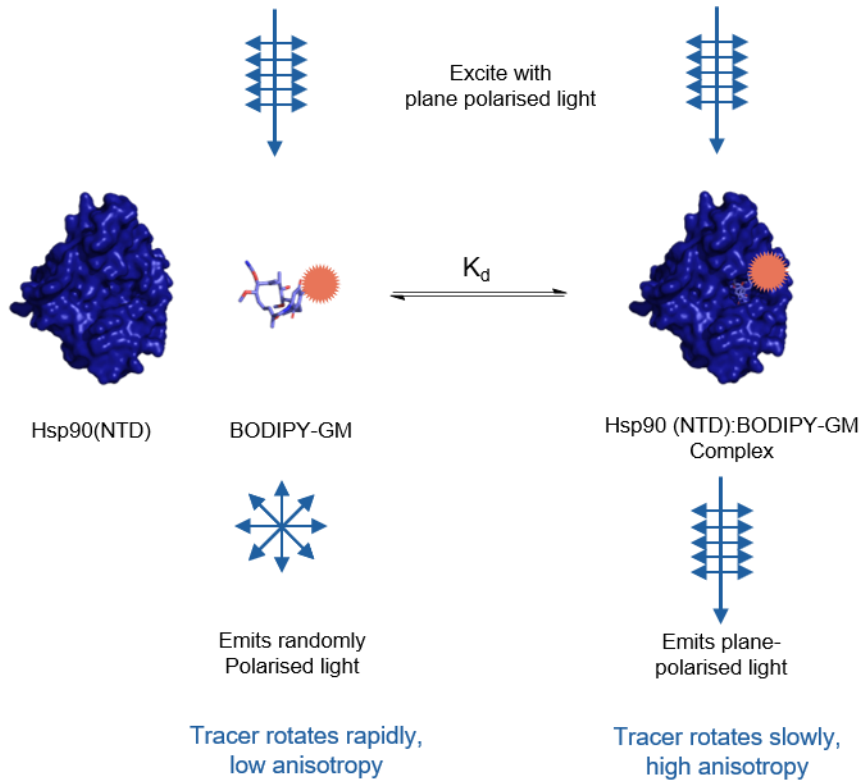

Figure 3.9 *Principles of fluorescence anisotropy assay used to determine the dissociation constants of labelled and unlabelled compounds for a protein (illustrated with Hsp90). The tracer is BODIPY-labelled geldanamycin. When the tracer is free in solution (not bound to Hsp90(NTD)) the observed polarisation is small, when the tracer is bound to Hsp90(NTD) the observed polarisation is large.*

3.3.2 Synthesis of Fluorescence Anisotropy Tracer: BODIPY-labelled Geldanamycin

The fluorescence anisotropy assay required the use of a fluorescently labelled ligand (tracer) in order to measure IC_{50} (and K_i) values of unlabelled compounds that interact with Hsp90(NTD). Established fluorescence polarisation (anisotropy) assays for Hsp90(NTD) report the use of geldanamycin labelled with a BODIPY fluorophore (BODIPY-GM) as the tracer.[80] BODIPY-GM **130** was prepared in a single step via Michael reaction of geldanamycin **128** with 4,4-difuoro-5,7-dimethyl-4-bora-3a,4a-diaza-*s*-indacene-3-propionylethylene-diamine hydrochloride **129** in the presence of diisopropylamine in excellent yield (86%).[156] DMSO stocks of the tracer were prepared, at a concentration of 190 μM, which was determined using the Beer-Lambert law from the measured absorbance and the fluorophore molecular extinction coefficient (79000 ± 6000 cm^{-1}). The K_d of the tracer for Hsp90(NTD) was subsequently determined as described in Section 3.3.4.

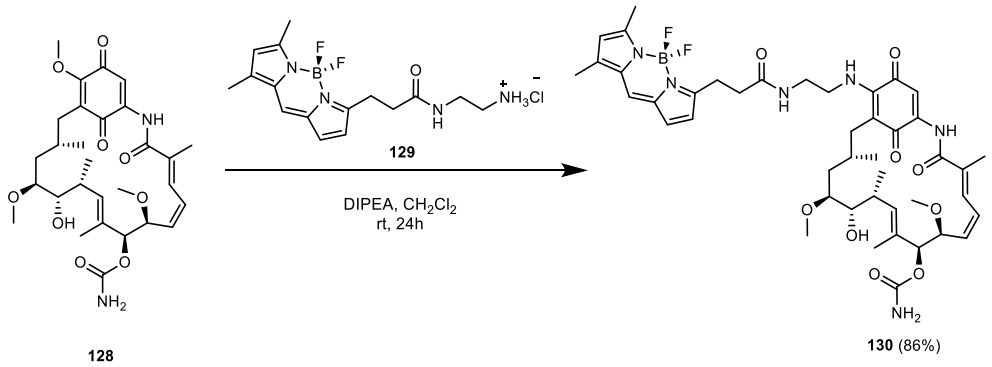

Scheme 3.6 *Synthesis of fluorescence anisotropy tracer, BODIPY-labelled Geldanamycin*

3.3.3 Hsp90(NTD) Protein Expression

The plasmid containing the gene for His_6-tagged *N*-terminal Hsp90, residues D9-E236, (His_6-Hsp90(NTD)) was transformed in *E. Coli* and cells were grown, harvested and purified (Ni-affinity and size-exclusion chromatography), as described (see experimental). The purified protein was stored in a sodium phosphate buffer (NaPi) and analysed by SDS PAGE

(Figure 3.10) and HRMS (expected mass from amino acid sequence: 27791 Da, HRMS found: 27791 Da) to confirm protein expression and purity.

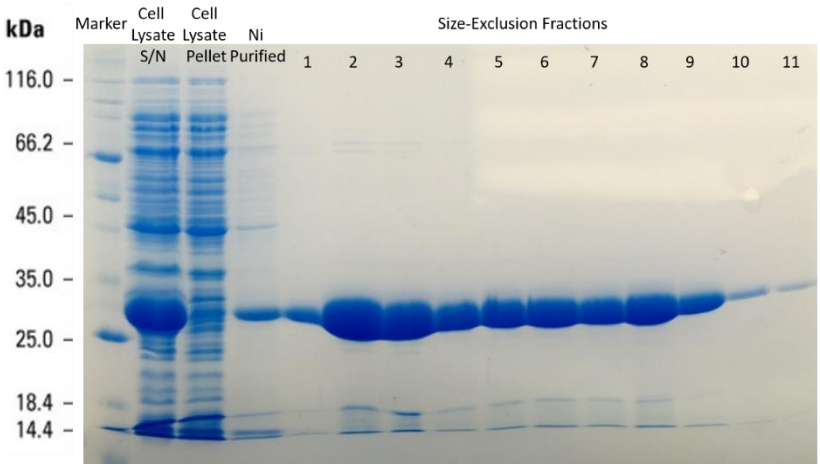

Figure 3.10 *SDS PAGE analysis for purification of Hsp90(NTD) by Ni-chromatography and size-exclusion chromatography. (S/N = supernatant, the cell lysate pellet was the centrifuged pellet after cells has been lysed and supernatant decanted).*

3.3.4 Configuration of Fluorescence Anisotropy Assay

Following successful protein expression and tracer synthesis, an initial set of experiments was performed to establish the optimal conditions under which to perform the assay for measuring both IC_{50} values of unlabelled ligands and for the screening of crude reaction mixtures from C-H functionalisation reaction arrays. The assay was adopted from previously reported fluorescence anisotropy assays for Hsp90(NTD).[80] The aim was to determine the limits of anisotropy (i.e. largest assay window: anisotropy of free and complexed tracer) by titrating protein (serial two-fold dilution) into fixed tracer (50 nM). The polarisation of emitted light was measured parallel and perpendicular to the plane of polarisation of the excited light, and an anisotropy value for each protein concentration was calculated. The plate was incubated at 4 ^{o}C and read at four time points, 0 h, 3 h, 4 h and 20 h. The anisotropy was plotted against protein concentration and the data fitted using a logistic fit (Figure 3.11). The limits of anisotropy were reached after approximately 4 h, however due to the slow and tight binding of geldanamycin (and BODIPY-GM), 20 h incubation was determined to give the best logistic fit with smallest error. The limits of anisotropy were determined to be r_{max} =

139 and r_{min} = -4 by fitting the data to a logistic fit (Equation 3, experimental 6.4).

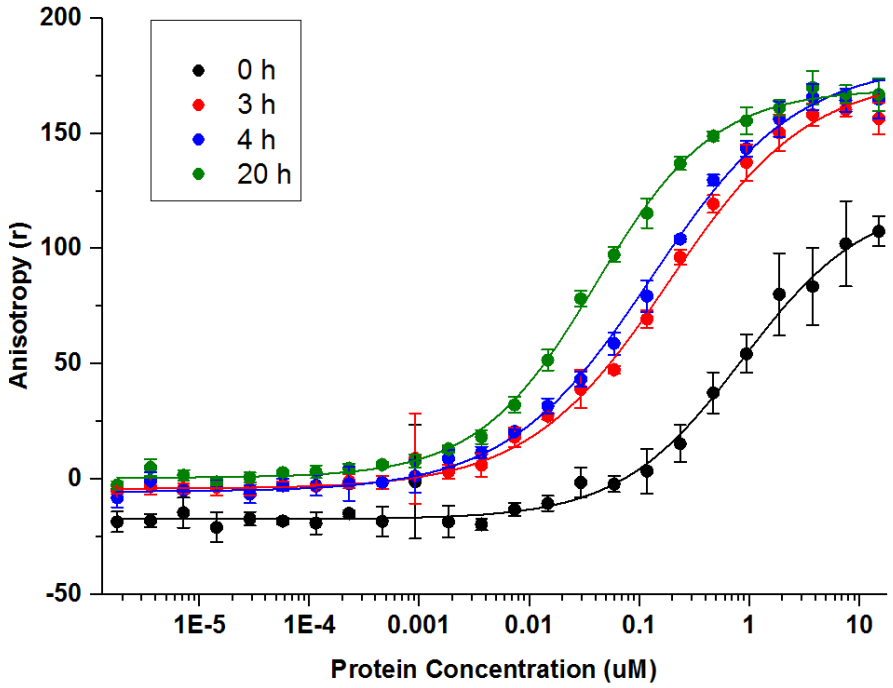

Figure 3.11 *The calculated anisotropy plotted against protein concentration in the presence of fixed amount of tracer (50 nM). The anisotropy was calculated at 0 h, 3 h, 4h and 20 h time points and the upper and lower anisotropy limits were determined to be r_{max} = 139 and r_{min} = -4 respectively.*

The total fluorescence for each protein concentration was calculated (Equation 2, experimental 6.4) to measure the change in quantum yield between the bound and free states (Figure 3.12c, λ = 2.39). The K_d of the tracer was determined by converting the measured anisotropy into the fraction of tracer bound (Equation 4, experimental 6.4) and then subsequently the amount of tracer bound, by multiplying the fraction bound by the concentration of the tracer (50 nM). The amount of tracer bound was plotted against the concentration of protein and the data fit to a non-linear least squares fitting algorithm (Figure 3.12d, Equation 5, experimental 6.4). The dissociation constant was determined to be K_d = 23.0 ± 3.3 nM (reported literature values range 6-30 nM).[80]

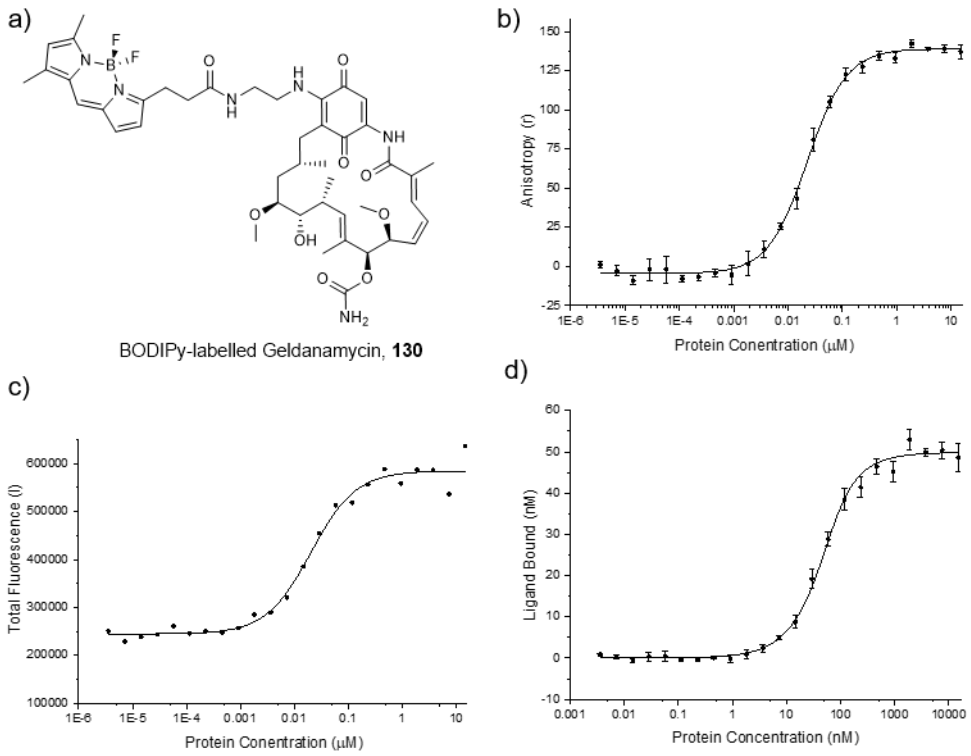

Figure 3.12 *Determination of limits of anisotropy and K_d of **a)** BODIPY-labelled geldanamycin **130**. **b)** Limits of anisotropy (upper r = 139, lower r = -4) determined from logistic fit of anisotropy vs protein concentration. IC_{50} of tracer: 22.6 ± 1.5 nM. **c)** Change in fluorescence (λ = 2.39) measured from total fluorescence vs protein concentration **d)** Determination of K_d from plotting the amount of tracer bound vs protein concentration, K_d of tracer: 23.0 ± 3.3 nM. See appendix D for calculations.*

To assess the ability of the assay to determine affinities of unlabelled compounds, a series of control experiments was performed with ligands which have reported IC_{50} values for their affinities to Hsp90(NTD). Dose response curves for geldanamycin, ATP and ADP were performed with fixed protein concentration (500 nM) and tracer concentration (50 nM). Plates were incubated at 4 ^{o}C for 20 h, and calculated anisotropy plotted against ligand concentration. The amount of tracer bound was then plotted against Log_{10}[competitor] and IC_{50} values were determined (Table 3.1 and Figure 3.13). The IC_{50} values are broadly in-line with reported literature values, however variation in values stems from the conditions of the assay used.

	Calculated IC_{50}	**Reported IC_{50}**
BODIPY-Geldanamycin	**K_d**: 23.0 ± 3.3 nM	**K_d:** 6-30 nM
Geldanamycin	*8.9 ± 1.7 μM*	*76.9 ± 2.5 nM*
ATP	145 ± 19 μM	100 ± 15 μM
ADP	54.8 ± 2.8 μM	20 ± 8 μM

Table 3.1 *Calculated and reported IC_{50} values for known Hsp90(NTD) inhibitors. K_d (not IC_{50}) shown for BODIPY-geldanamycin.*[80]

The IC_{50} values for ADP and ATP match those previously reported, however the IC_{50} for geldanamycin is two orders of magnitude higher than that reported from previous fluorescence anisotropy/polarisation assays (however, IC_{50} values were calculated from different protein and tracer concentrations). Geldanamycin is a slow Hsp90(NTD) binder[157] and notorious for poor solubility. Reports from various assays report geldanamycin with a broad range of IC_{50} values (0.3 – 1.2 μM) and can vary depending on the construct and length of Hsp90 used in the assay.[157–159] Given ATP and ADP behaved as previously reported and fragments **81** and **86**-**91** IC_{50}/K_d values matched those previously reported (see Table 3.2, fragments **81** and **86**-**90** affinities were also calculated from a fluorescence polarisation assay), the assay was deemed to be performing as expected.

a) Geldanamycin, IC_{50}: 8.9 ± 1.7 μM

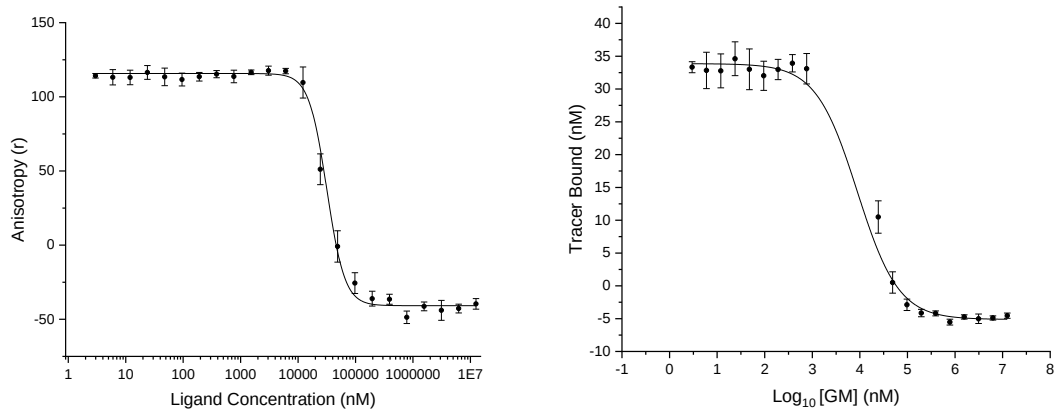

b) ATP, IC_{50}: 145 ± 19 μM

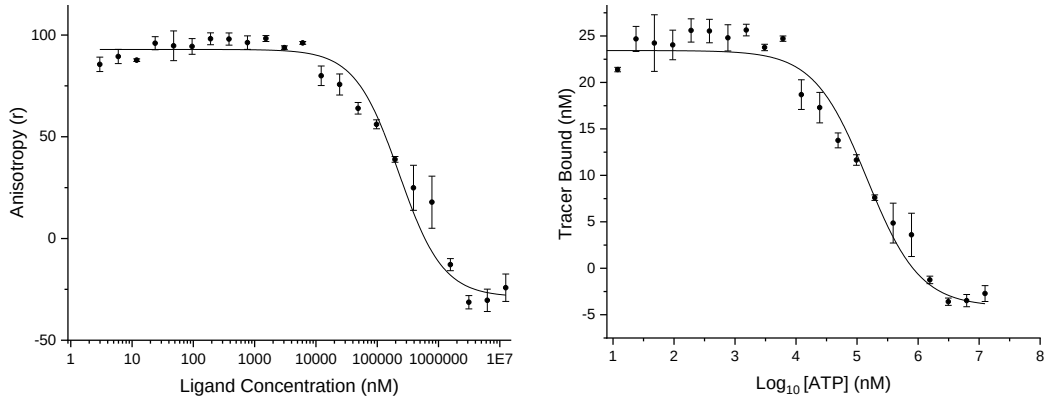

c) ADP, IC_{50}: 54.8 ± 2.8 μM

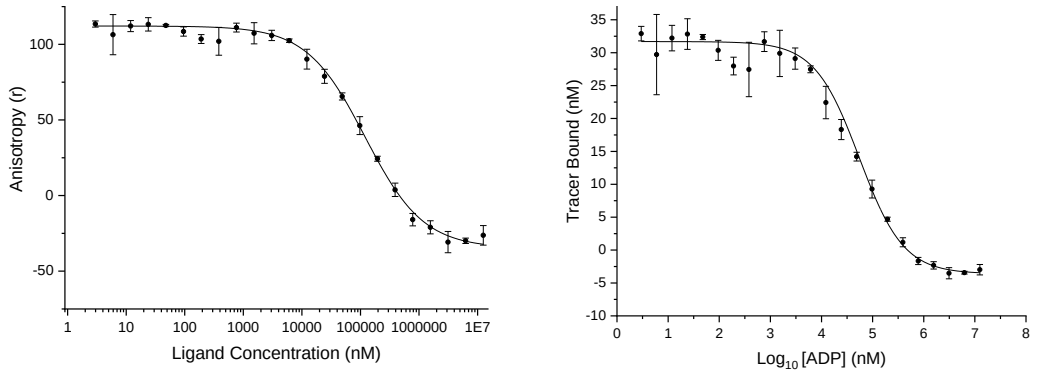

Figure 3.13 *Dose response curves for known Hsp90(NTD) inhibitors* ***a)*** *geldanamycin,* ***b)*** *ATP and* ***c)*** *ADP with anisotropy plotted against ligand concentration and tracer bound plotted against* Log_{10}*[Competitor] in order to calculate* IC_{50} *values. Competition assays were performed with 50 nM tracer, 500 nM Hsp90 and incubated at 4 °C for 20 h.*

3.4 Fragment Screen against Hsp90

To aid the selection of fragments implemented in C-H functionalisation reaction arrays in ADS, a screen of the prepared fragments (Section 3.3) was performed by generating dose response curves of each fragment at a range of fragment concentrations. At each concentration, fragment was incubated with 50 nM tracer and 500 nM Hsp90 at 4 ^{o}C for 20 h with a final DMSO concentration of 2%. The anisotropy at each fragment concentration was calculated, and a dose response curve (logistic fit) generated (Table 3.2). The anisotropy was converted to the amount of tracer bound (Equation 4, experimental 6.4) at each fragment concentration and plotted against $\log_{10}$[Ligand] and the data fit to a single site competition model (Table 3.2). The $\log IC_{50}$ was converted to an IC_{50} value for each fragment (Table 3.2), and, if required for comparison with reported affinities a K_i was calculated.

From the 29 prepared fragments, 15 had measurable biologically activity against Hsp90(NTD), in that they were shown to displace tracer. The eight reported fragments **81** and **86**-**92** showed affinity to Hsp90 with measurable IC_{50}s. IC_{50}/K_i values calculated for previously reported fragments **81** and **86**-**92** were broadly in line with the reported value (e.g. **86** IC_{50}: ~1.5 ± 0.2 mM (reported 1 mM), **81** K_i: ~850 ± 150 μM (reported K_d: 790 μM) and **90** K_i: ~17 ± 5 μM (reported K_d: 7 μM)). However, perhaps unsurprisingly, only seven of the remaining 21 designed fragments showed partial activity. However, designed fragments **99**, **101** and **104** did demonstrate activity of Hsp90(NTD) with a measurable IC_{50}'s of ~1.0 ± 0.2 mM, ~32 ± 11 μM and ~39 ± 13 μM respectively. **104** is comparable to the closely related and previously reported analogue **90**.

The 15 fragments which demonstrated (partial) activity with Hsp90(NTD) (Figure 3.14) can be placed into three clusters; previously reported fragments **81** and **86**-**92,** the designed fragments **99, 101** and **104** with measurable IC_{50}'s and the four designed fragments **106** and **114-116** which demonstrated partial activity and had no previous biological activity reported against Hsp90(NTD). Three key binding moieties were identified from the fragment hits; the resorcinol fragment, the para-hydroxy benzamide fragment and the para-pyrazoyl benzamide fragment (Figure 3.14). The remaining 14 fragments

demonstrated no biological activity against Hsp90(NTD). With the biological data for the fragment set, ten fragments were chosen for implementation in C-H functionalisation reaction arrays (Chapter 4).

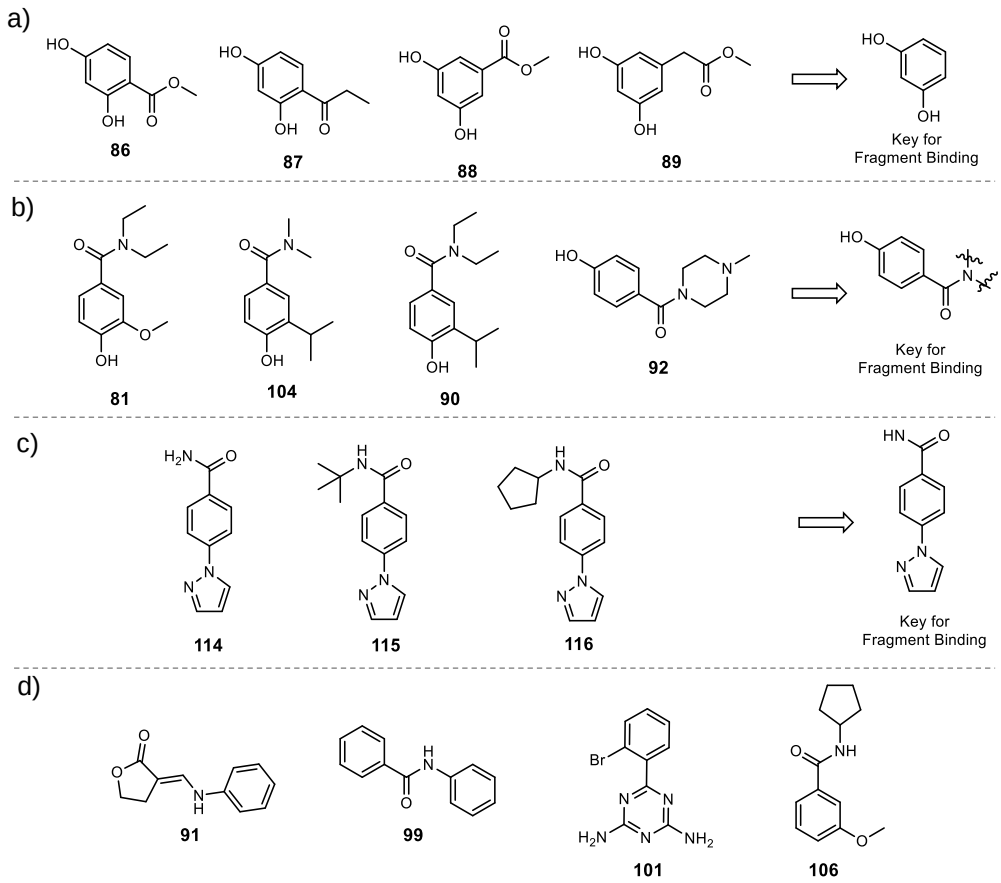

Figure 3.14 *Summary of fragment hits for Hsp90 a) Resorcinol key for fragment binding b) 4-acetamide-phenol key for fragment binding c) 4-pyrazoyl benzamide key for fragment binding d) Other fragment chemotypes*

Fragment	Dose response curves	
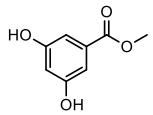 **88** **IC_{50}: ~1.7 ± 0.8 mM** Reported IC_{50}: 400 μM[115]	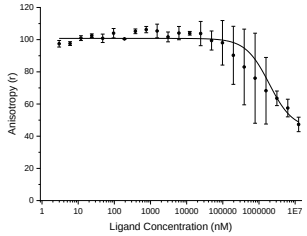	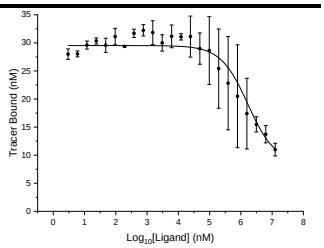
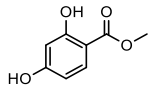 **86** **IC_{50}: ~1.5 ± 0.2 mM** Reported IC_{50}: 1 mM[115]	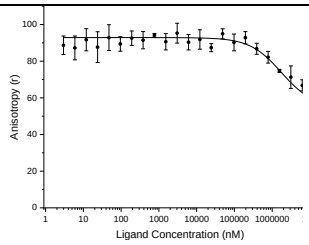	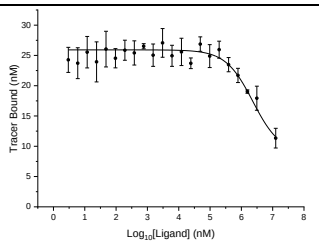
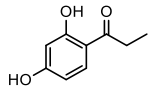 **87** **IC_{50}: > 5mM** Reported IC_{50}: 570 μM[115]	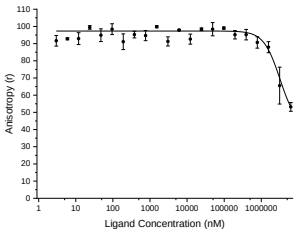	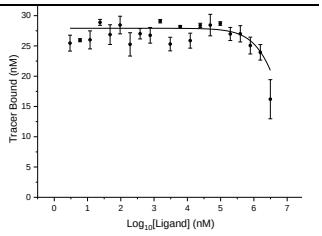
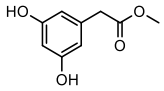 **89** **IC_{50}: ~1.0 ± 0.1 mM** Reported IC_{50}: 490 μM[115]	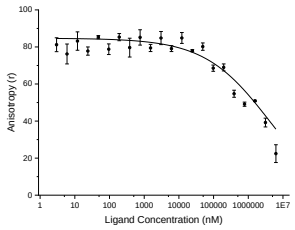	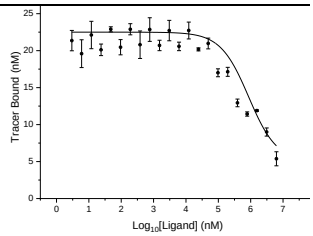
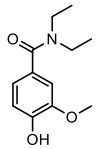 **81** **IC_{50}: >5 mM** **K_i: ~850 ± 150 μM** Reported K_d: 790 μM[112]	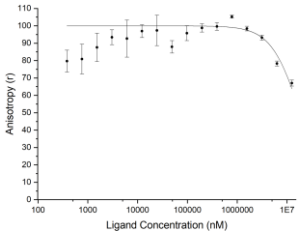	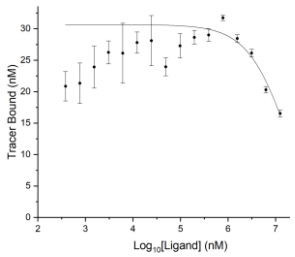
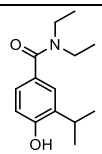 **90** **IC_{50}: 370 ± 90 μM** **Ki: ~17 ± 5 μM** Reported K_d: 7 μM[112]	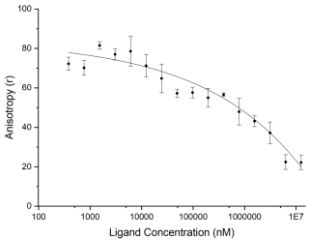	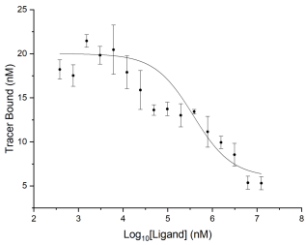

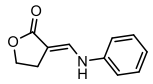 91 **IC_{50}: ~** Reported K_d: 150 μM[113]	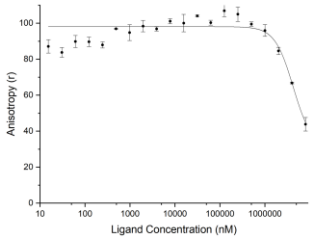 	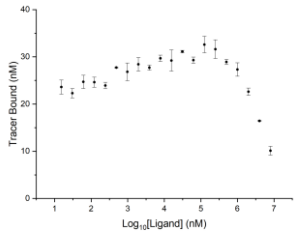
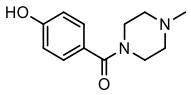 92 **IC_{50}: ~450 ± 140 μM**	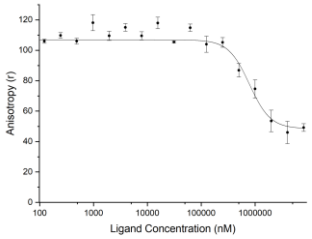 	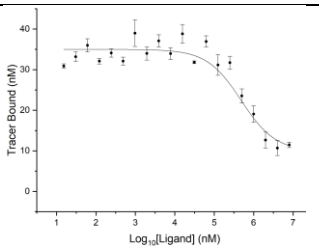
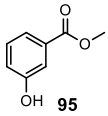 95 **IC_{50}: N/A (> 5mM)**	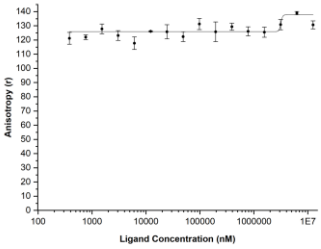 	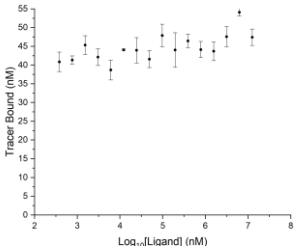
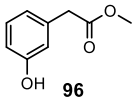 96 **IC_{50}: N/A (> 5mM)**	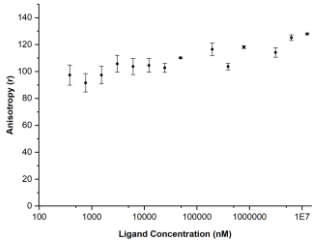 	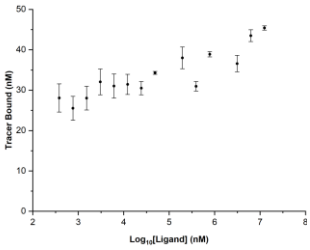
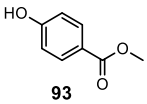 93 **IC_{50}: N/A (> 5mM)**	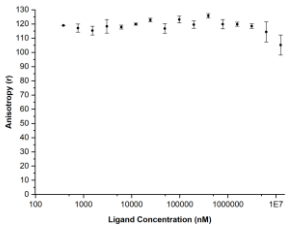 	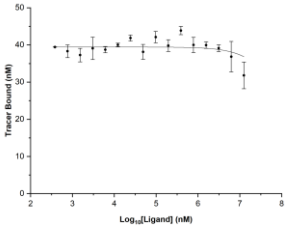
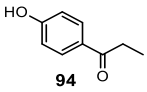 94 **IC_{50}: N/A (> 5mM)**	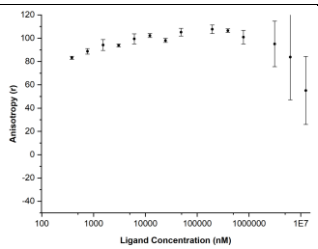 	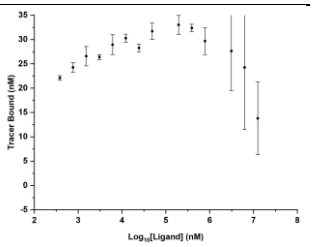
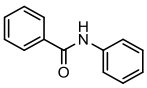 99 **IC_{50}: ~1.0 ± 0.2 mM**	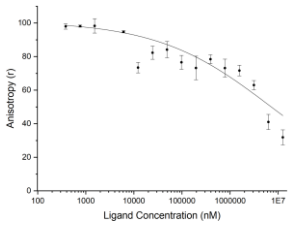 	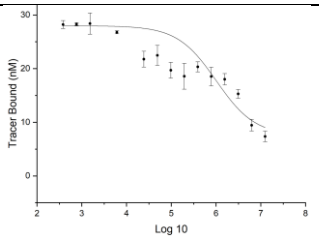

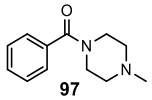 **97** **IC_{50}: N/A (> 5mM)**	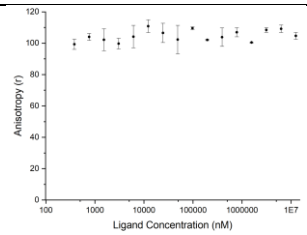	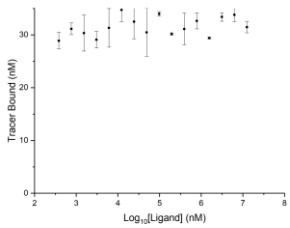
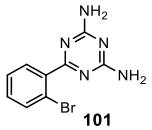 **101** **IC_{50}: ~32 ± 11 μM**	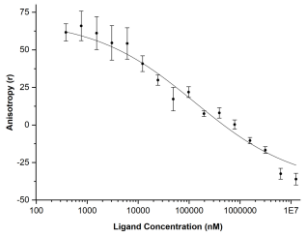	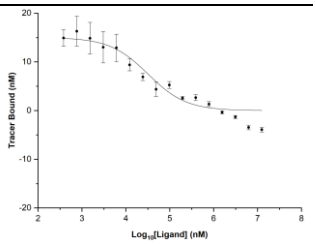
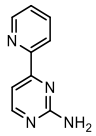 **103** **IC_{50}: N/A (> 5mM)**	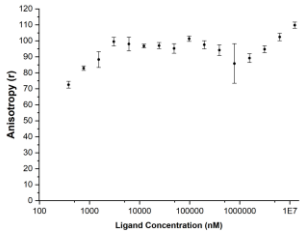	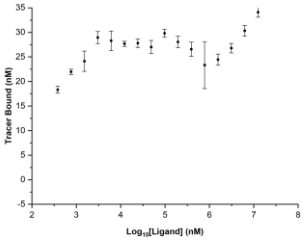
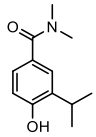 **104** **IC_{50}: ~39 ± 13 μM**	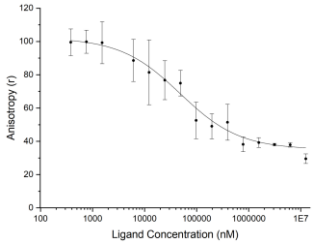	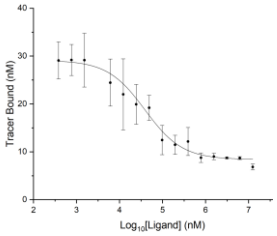
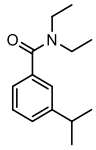 **109** **IC_{50}: N/A (> 5mM)**	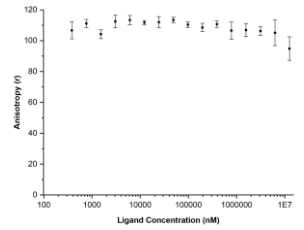	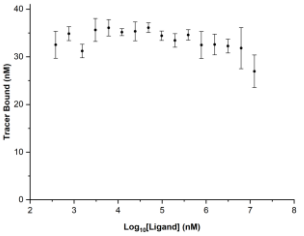
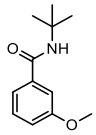 **105** **IC_{50}: N/A (>5 mM)**	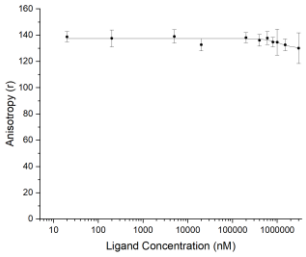	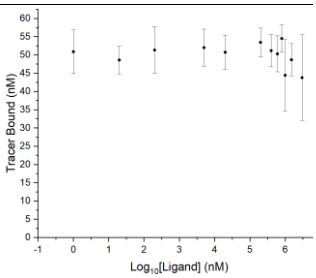
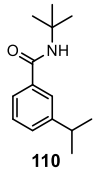 **110** **IC_{50}: N/A (>5 mM)**	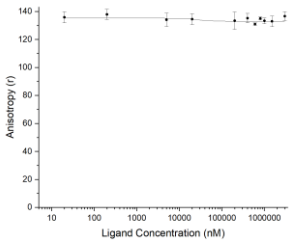	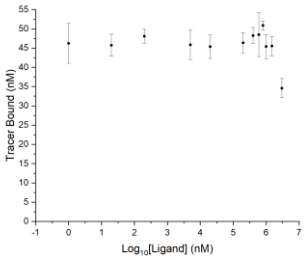

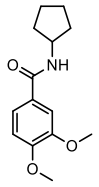 **107** **IC_{50}: N/A (>5 mM)**	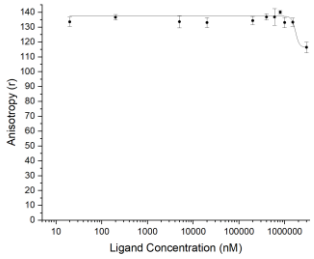	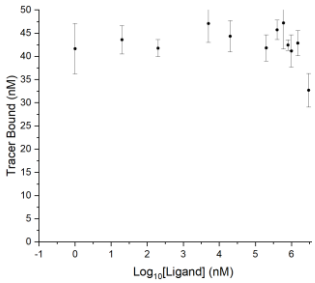
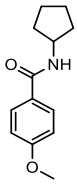 **108** **IC_{50}: N/A (>5 mM)**	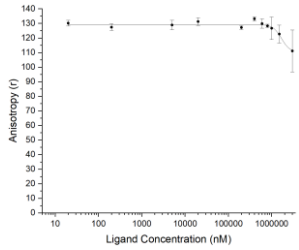	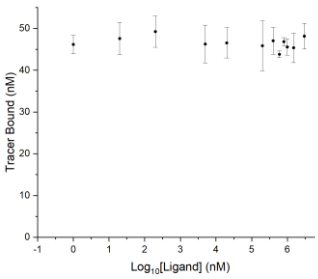
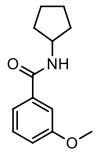 **106** **IC_{50}: N/A (>5 mM)**	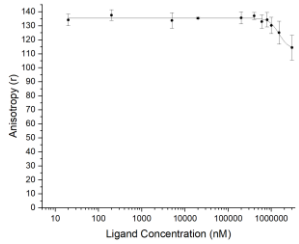	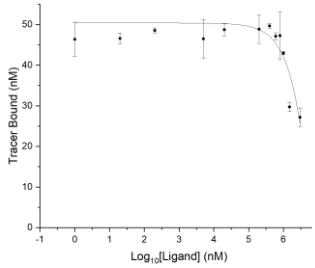
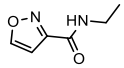 **112** **IC_{50}: N/A (>5 mM)**	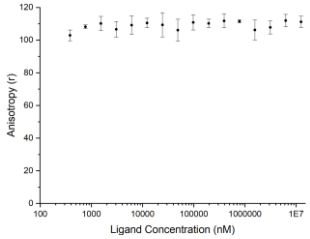	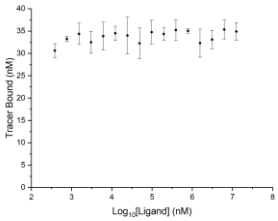
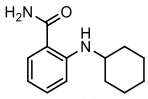 **113** **IC_{50}: N/A (>5 mM)**	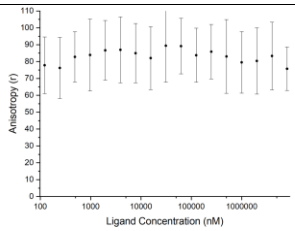	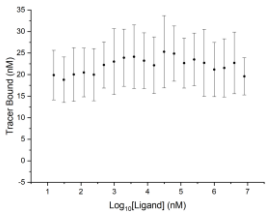
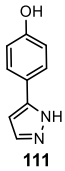 **111** **IC_{50}: N/A (>5 mM)**	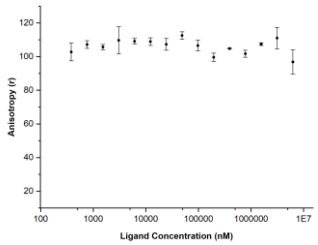	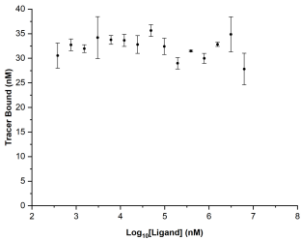
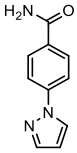 **114** **IC_{50}: N/A (>5 mM)**	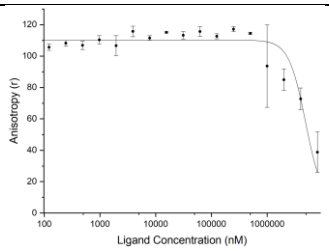	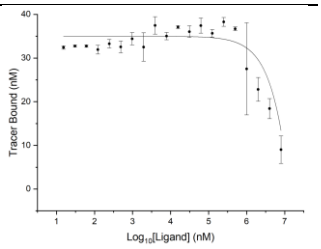

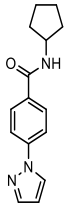 **116** **IC_{50}: N/A (>5 mM)**	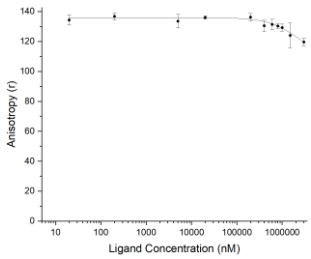	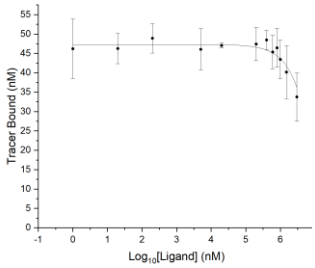
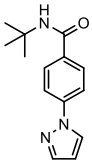 **115** **IC_{50}: N/A (>5 mM)**	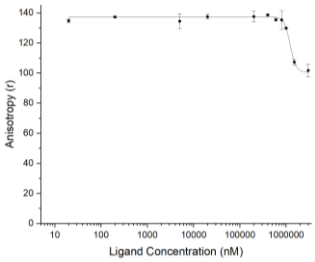	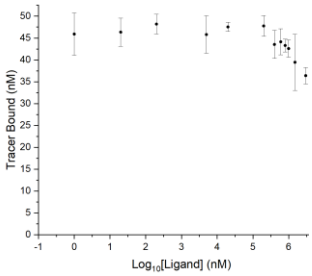

Table 3.2 *Fragment data generated from dose response curves to determine affinites of fragments for Hsp90(NTD).*

3.5 Summary

A series of Hsp90 fragments was designed and prepared based upon their potential to undergo productive C-H functionalisation reactions. Hsp90(NTD) was successfully expressed and purified and the tracer, BODIPY-GM, for the high-throughput fluorescence anisotropy assay synthesised. The controls experiments were performed to confirm the successful configuration of the assay, prior to the screening of the prepared fragment library. The establishment of the high-throughput assay will enable the rapid assessment of crude reaction array mixture for biological activity.

A range of fragments were identified as inhibitors of Hsp90(NTD), including novel fragments, all be it with modest biological activity, that had not previously been reported as Hsp90 inhibitors (Figure 3.14). The fragment data aided the selection of fragments with both biological activity and suitable directing groups for implementation in C-H functionalisation reaction arrays. With the assay and fragment hits established, reaction arrays using C-H functionalisation chemistry with Hsp90 fragments could be performed and assessed for biological activity, with the aim of identifying productive elaboration vectors of Hsp90 fragments.

Chapter 4.
Evaluation of Chemistries for the Structure-Blind and Function-Driven Elaboration of Hsp90 Fragments

Activity-directed synthesis has the potential to enable the structure-blind and function-driven elaboration of fragments, contrastingly starkly to conventional fragment-based ligand discovery, which is generally reliant on structural information to be successful. It was envisaged the use of C-H functionalisation and metal-catalysed carbenoid chemistry in activity-directed synthesis would potentially enable the identification of productive elaboration vectors of a fragment. A series of reaction arrays implementing both types of chemistry was performed, adopting different approaches for reaction array design, by varying the method for combining the reaction array components. It was envisaged the study would enable the identification of the more productive chemistry for structure-blind fragment elaboration and the more productive method for combining reaction components in the design of reaction arrays. The established high-throughput assay and LC-MS analysis of the crude reaction mixtures enabled the biologically activity and the success of the reactions to be rapidly assessed.

4.1 Preparation of Hsp90 Fragments for Implementation in Reaction Arrays

4.1.1 Acetate Protection of Phenol Fragments

Ten Hsp90 fragments (Section 4.2.1, Figure 4.2) were chosen from the set of 29 (Chapter 3) for implementation as substrates in reaction arrays, on the basis they demonstrated biological activity against Hsp90 and possessed at least one potential directing group for C-H functionalisation chemistry. The ten fragments were also chosen to possess a broad range of fragment chemotypes to maximise diversity in the reaction arrays. Of the ten chosen fragments, six were phenol fragments, which have the potential to dominate reactivity under the C-H functionalisation reaction conditions. It was envisaged acetyl protection of phenols would minimise reaction interference, and then the development of a simple deprotection strategy in parallel reaction array

format would reveal the phenol prior to screening in the assay. The six phenol fragments were protected by reaction in the presence of excess acetic anhydride and pyridine to give fragments **F1**, **F3**-**F6** and **F10** (Figure 4.1) in good yield (60-98%).

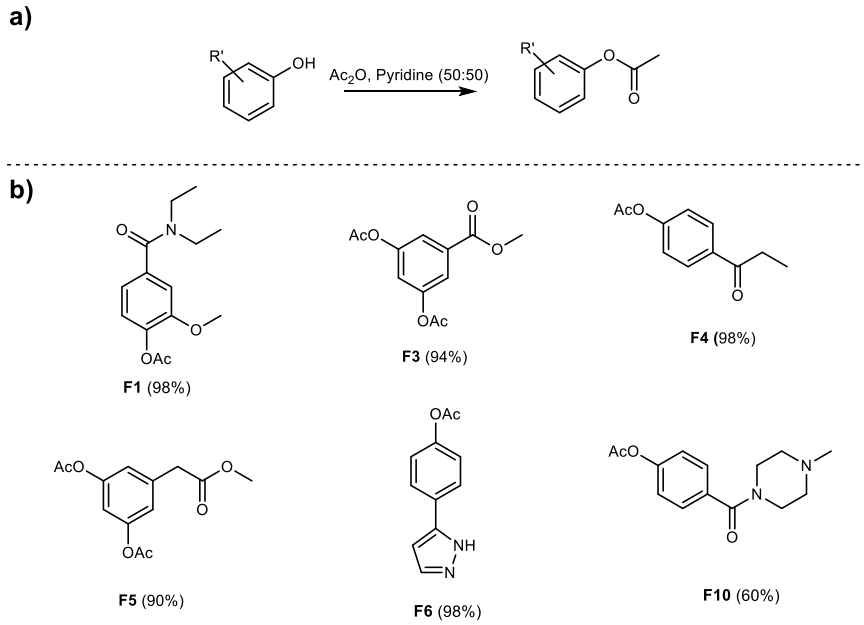

Figure 4.1 *Protection of phenol fragments. Acetate protection of phenol fragments in the presence of acetic anhydride and pyridine gave **F1**, **F3**-**F6** and **F10.***

4.1.2 Configuration of a Acetate Deprotection Strategy in Parallel-Format

As the phenol/resorcinol moiety is key for fragment binding (Chapter 3), the establishment of a simple to implement and mild acetate deprotection strategy was established. The use of methoxide, generated from methanol and sodium carbonate, was assessed as an acetate deprotection strategy for parallel reaction arrays (Table 4.1 and Appendix A). Firstly, an LC-MS and ^{1}H (300 MHz) NMR spectrum of the unprotected and protected fragments was collected to serve as reference spectra. The use of methoxide was tested in flask on ~mmol scale and the successfully deprotected fragment was isolated and characterised. The use of methoxide in the flask reactions successfully deprotected all the acetate-protected fragments, ^{1}H NMR (300 MHz) spectra and LC-MS data shown for unprotected fragment, protected fragment and fragment that had successfully been deprotected with methoxide in flask

(Table 4.1 and Appendix A), and was therefore assessed in parallel format in microscale reaction array format.

Each fragment (0.01 mmol) was added to a different microvial, followed by addition of a MeOH:THF (2:1 75 μL) solution and an aqueous sodium carbonate solution (25 μL, 470 mM). After 24 h the solvent was evaporated and the crude mixture analysed by LC-MS to reveal the successfully acetate-deprotected fragment in parallel format. The use of methoxide in parallel format was successful for all six acetate-protected fragments (Table 4.1 and Appendix A), and the deprotection conditions were subsequently determined to be mild enough not to cause interference in the high-throughput assay.

Finally, it was proposed the use of the Quadrature BzA resin would potentially enable the deprotection of the acetate-protected fragments. Each protected fragment (0.01 mmol) was added to a microvial in CH_2Cl_2 (100 μL) followed by addition of Quadrapure BzA (30 mg). After 24 h an LC-MS of each of the fragments was collected to reveal that the Quadrapure BzA resin could successfully deprotect all six fragments (Table 4.1 and Appendix A).

The deprotection study demonstrated acetate-protected phenol fragments could be readily deprotected under mild conditions with methoxide or the Quadrapure BzA resin in parallel reaction array format. Given the Quadrapure BzA has already been established for the scavenging of metal catalysts and Michael acceptors, it was chosen as the deprotection strategy to be implemented in the reaction array workflows. The use of a single strategy for the scavenging of metal catalysts and Michael acceptors and the acetate deprotection of fragments ensured a streamlined and efficient workflow for ADS.

90/F1	LC-MS Analysis	^{1}H NMR (300 MHz)
Unprotected Start (**90**)	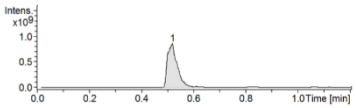 Mass Found $[MH]^+$: 224.4	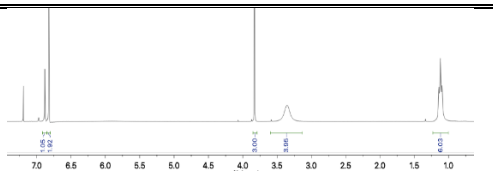
Protected (Purified **F1**)	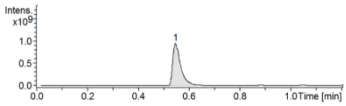 Mass Found $[MH]^+$: 266.4	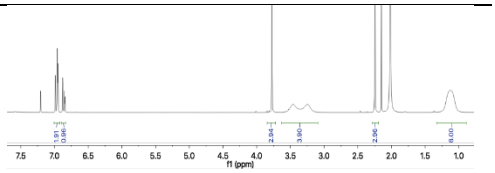
Deprotected (Purified **90**)	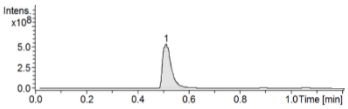 Mass Found $[MH]^+$: 224.3	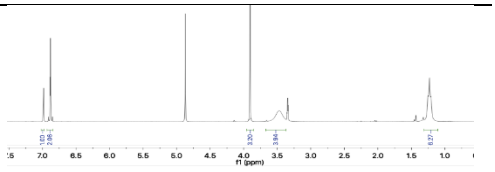
Deprotected in Plate (crude, **90**)	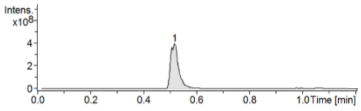 Mass Found $[MH]^+$: 224.4	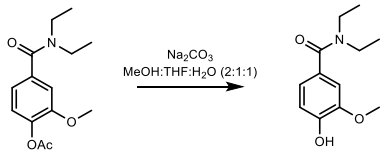
Deprotected in Plate (crude, **90**)	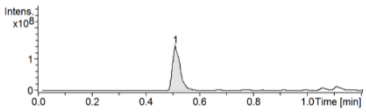 Mass Found $[MH]^+$: 224.4	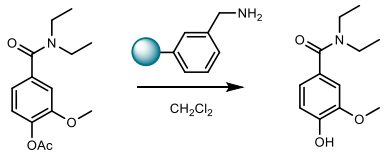

Table 4.1 LC-MS and ^{1}H NMR (300 MHz) for acetate protection and deprotection of phenol containing Hsp90 fragment **90**/**F1**. Protection was performed by reaction of phenol with acetic anhydride and pyridine and deprotection was performed with Na_2CO_3 in MeOH:THF:H2O (2:1:1) and LC-MS and ^{1}H NMR (300 MHz) data collected. Deprotection was performed in plates with MeOH:THF:H_2O (2:1:1) and with Quadrapure BzA resin (30 mg) and analysed by LC-MS. Calculated mass of unprotected and protected fragment **5**/**F1** $[MH]^+$: 224.3 and $[MH]^+$: 266.4 respectively.

4.2 C-H Functionalisation Reaction Arrays

A range of C-H functionalisation reaction arrays was performed to assess the chemistry as a structure-blind fragment elaboration strategy using activity-directed synthesis. Hsp90 fragments were combined with a diverse set of substrates, under a range of known C-H functionalisation catalytic systems, in a series of room temperature and heated (60 ^oC) reactions. Following reaction (48 h), crude reaction mixtures were scavenged

(Quadrapure BzA) and screened directly, without purification, for biological activity.

4.2.1 Room Temperature Reaction Arrays

4.2.1.1 Reaction Array Design

Room temperature C-H functionalisation reaction arrays were performed by combining Hsp90 fragments with a diverse set of substrates under a series of reported C-H functionalisation catalytic systems (Figure 4.2). As discussed, the ten fragments selected for implementation in ADS, for elaboration with C-H functionalisation chemistry, were chosen on the basis they demonstrated biologically activity with Hsp90 and possessed at least one directing group for C-H Functionalisation chemistry.

For implementation of C-H functionalisation chemistry in microscale reaction arrays, a diverse set of C-H functionalisation catalytic systems and substrates that can undergo the respective catalyst reaction type were selected. Eight catalyst systems, **C1**-**C8** (Figure 4.2) were chosen on the basis of their diverse range of possible reactions. Palladium catalysts **C1**-**C4** were chosen based upon their ability to undergo a range of C-H arylations and alkenylations; **C1** (C-H alkenylations),[160] **C2** (C-H arylations with aryl iodides),[101] **C3** (C-H alkenylations and C-H arylations with aryl boronic acids)[106] and **C4** (C-H alkenylations).[94] The rhodium catalyst **C5**[161] and the ruthenium catalyst **C6**[98] are both able to undergo C-H alkenylation and alkynylations and finally iridium catalysts **C7** and **C8** were chosen on the basis they can undergo C-H amination reactions with anilines[95] and alkyl amines[104] respectively.

Finally a set of 33 reaction substrates was chosen which were compatible for the C-H functionalisation reaction type of the chosen catalyst systems. Substrates were chosen from commercially available libraries (Sigma-Aldrich, Fluorochem, Fischer-Scientific and Alfer Asear) and were selected on their molecular properties as well as their potential to undergo at least one of the chosen C-H functionalisation reaction types. To aid the selection of substrates a Pipeline Pilot protocol was established (by Adam Nelson), which took databases of commercially available substrates and

filtered them for reaction substrate class (alkenes, alkynes, acrylates, acrylamides, aryl iodides/bromides, aryl boronic acids, anilines and alkyl amines). The filtered database was then filtered again by applying a molecular property filter to give a set of substrates, for each reaction substrate class, with less than 15 heavy atoms, less than three rotatable bonds and an AlogP of 0 ≤ 3. The sets of substrates were then filtered for price and maximised diversity to generate a final set of 33 substrates (**S1**-**S33**) for implementation in ADS (Figure 4.2).

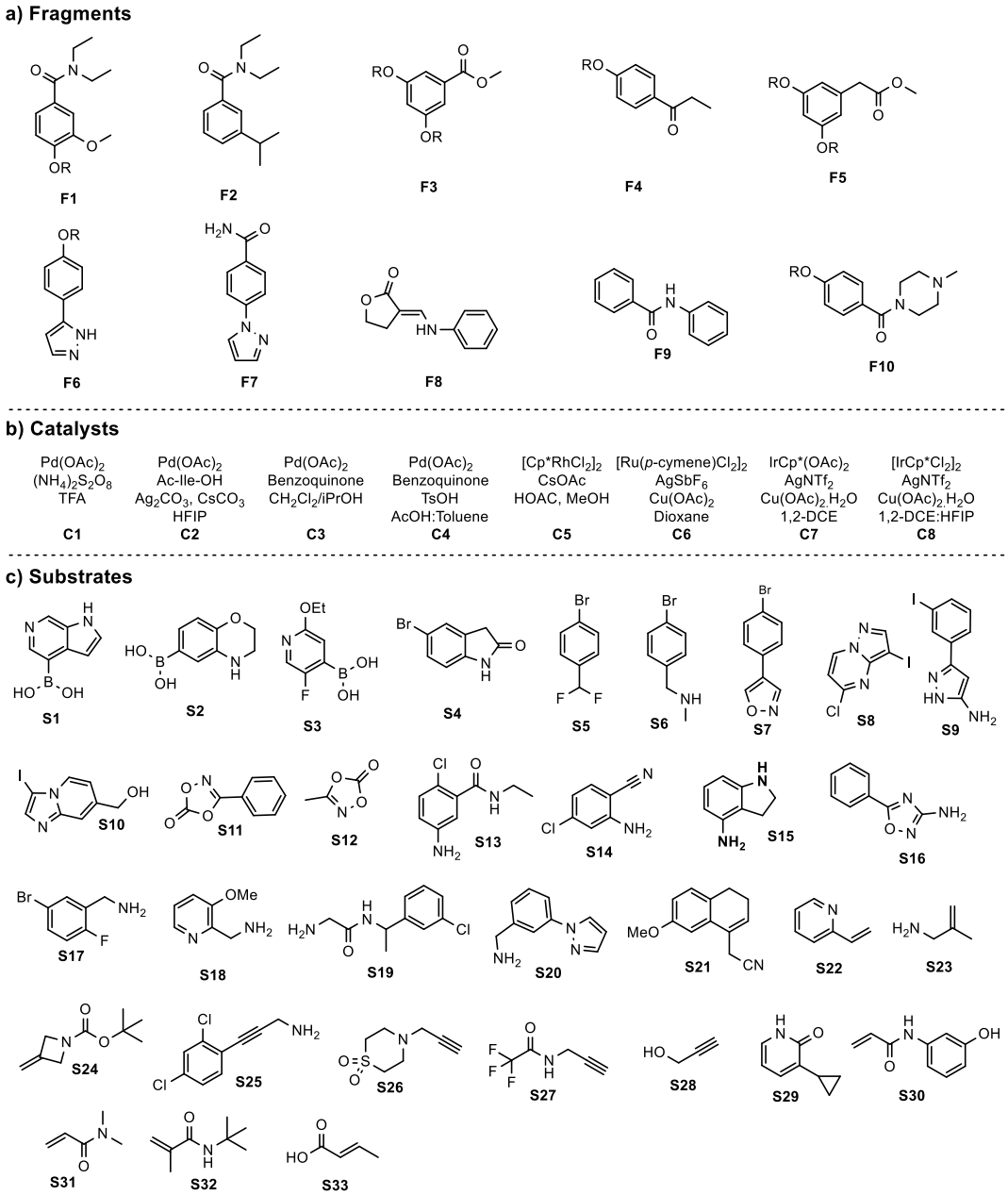

Figure 4.2 *Fragments (**F1**-**F10**) R=Ac, catalysts (**C1**-**C8**) and substrates (**S1**-**S33**) used in reaction arrays for potential elaboration of Hsp90 fragments with C-H functionalisation chemistry*

With the ten fragments, eight catalysts and 33 substrates selected, a total of 2640 reactions was in principle possible, enabling the rapid exploration of chemical space. However, it was proposed that not all 2640 possible reactions would prove productive and impractical to implement due to the unlikely reaction of some fragment, substrates and catalyst combinations. It was proposed a smaller subset of reactions would be performed to maximise reaction array efficiency, by matching two of the three reaction array components (in turn) based on literature precedent and then the paired components see a broad range of the third component. For instance, catalysts were matched to a substrate class (e.g. iridium catalysts matched with amines), which then see the full range of fragment chemotypes. For matching catalysts and substrates, each of the eight catalysts was paired with three substrates of the catalyst reaction type to give 24 catalyst-substrates pairs. Each catalyst-substrate pair then underwent reaction with all ten fragments to give 240 reaction combinations. This matching was similarly performed by pairing fragments and catalysts and pairing fragments and substrates to give a total of 720 reaction combinations (Figure 4.3).

Catalysts:	Substrates:	Cat-Sub Pairs:
C1	S29 S30 S32	3
C2	S5 S8 S9	3
C3	S1 S2 S3	3
C4	S29 S31 S33	3
C5	S24 S26 S27	3
C6	S23 S31 S33	3
C7	S17 S18 S19	3
C8	S13 S14 S15	3
		24

Catalyst-Substrate Pairs (X24) — Fragments (X10)

240 Reaction Combinations

Catalysts:	Fragments:	Cat-Frag Pairs:
C1	F1 F5	2
C2	F6 F8	2
C3	F7 F10	2
C4	F8 F9	2
C5	F2 F9	2
C6	F1 F7	2
C7	F3 F4	2
C8	F3 F4	2
		16

Catalyst-Fragment Pairs (X16) — Substrates (X15)

240 Reaction Combinations

Fragments:	Substrates:	Frag-Sub Pairs:
F1	S5 S27 S31	3
F2	S5 S6 S8	3
F3	S7 S24 S28	3
F4	S9 S26 S28	3
F5	S2 S8 S32	3
F6	S9 S23 S28	3
F7	S22 S23 S24	3
F8	S13 S14 S15	3
F9	S1 S15 S19	3
F10	S14 S26 S30	3
		30

Fragment-substrate Pairs (X30) — Catalysts (X8)

240 Reaction Combinations

720 from 2640 Possible Reactions

Figure 4.3 *Design of reaction array combinations by subsequently pairing fragments catalysts and substrates to give a diverse array of 720 reactions from a possible 2640.*

4.2.1.2 Reaction Array Execution

With the fragments, substrates and catalysts chosen, and the reaction array combinations designed, the reaction array itself was implemented. Fragments and substrates were prepared as stock solutions at 100 mM and 200 mM respectively (See component tables, Experimental 6.2.2 for solvent details). 100 μL of one of each was added to the vial of interest and the solvent allowed to evaporate. Catalyst system solutions were prepared at 5 mM in the appropriate catalyst reaction solvent (See component tables, Experimental 6.2.2 for additive concentrations and solvent systems) and 100 μL added to the vial of interest (Figure 4.4). Vials were capped and reactions left for 48 h, reaction solvent left to evaporate and reaction mixtures dissolved in CH_2Cl_2 (100 μL) followed by addition of Quadrapue BzA (30 mg) to scavenge for metal catalysts, Michael acceptors and for acetate deprotections. Reaction mixtures were capped and left to scavenge for 24 h, and the mixtures were then filtered, solvent allowed to evaporate to air followed by desiccation and finally crude reaction mixtures dissolved in DMSO (100 μL) to give a final total product concentration of 100 mM (with respect to fragment). Crude reaction mixtures were then screened against Hsp90 in the established high-throughput fluorescence anisotropy assay.

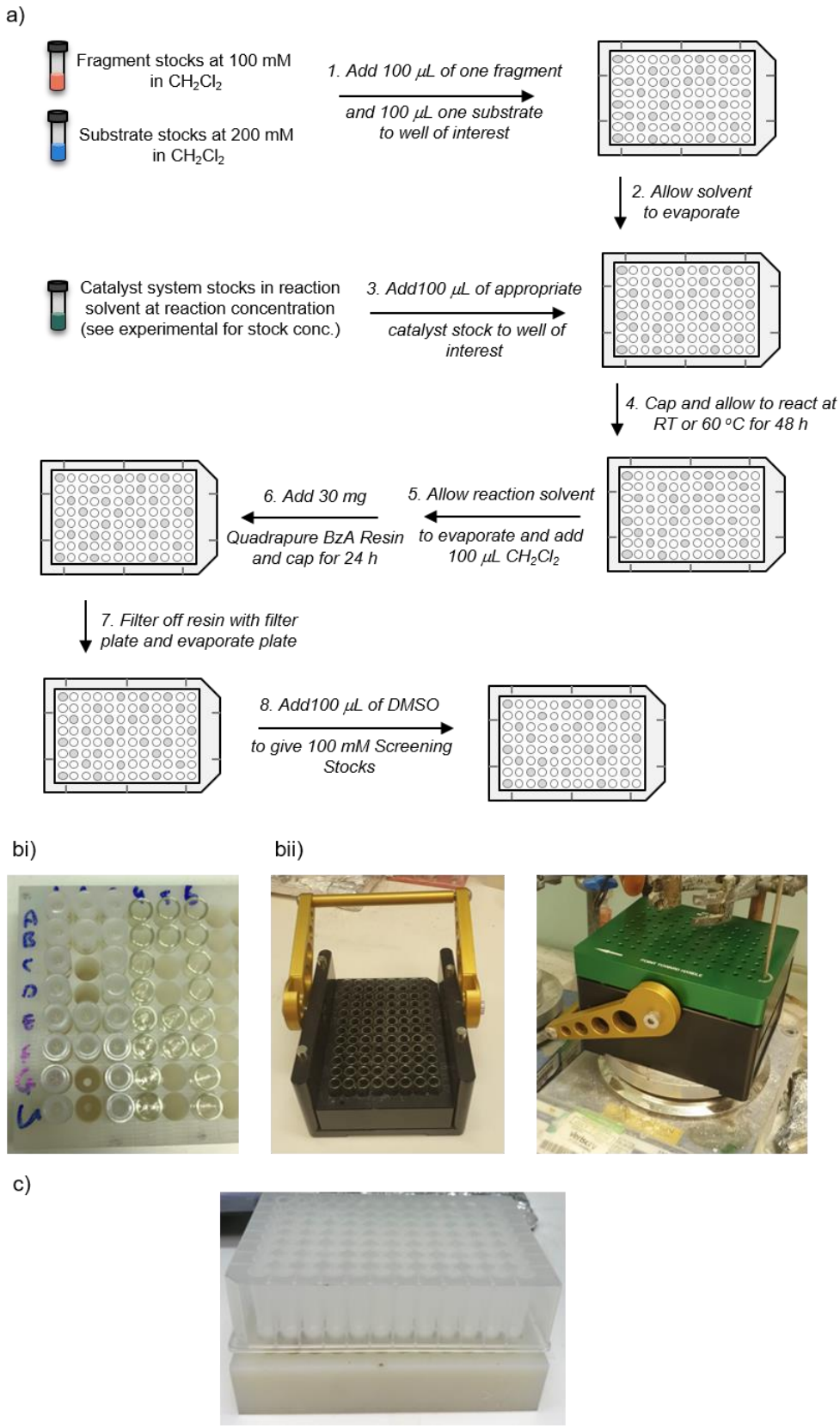

Figure 4.4 ***a)*** *Overview of ADS workflow* ***bi)*** *Room temperature reaction set up* ***bii)*** *unsealed and sealed elevated temperature set-up* ***c)*** *Filter plate for removing resin after scavenging*

4.2.1.3 Reaction Array Results

Following reaction array completion, crude reaction mixtures were screened against Hsp90 in the fluorescence anisotropy assay. The reaction mixtures were screened in triplicate. Controls of each of the reaction components in isolation were also performed, at the same concentration in which they were screened in the reaction mixtures, to enable the activity of the components to be observed (see Appendix B for component controls). Reaction array DMSO stocks (100 mM) were diluted into DMSO and then FA assay buffer to give stock solutions at 320 μM in 8:92 DMSO:Buffer (four times the final assay concentration). 5 μL of the DMSO:Buffer (8:92) reaction stocks was added to the assay plate followed by 5 μL of a 200 nM tracer stock solution followed finally by 10 μL of a 1 μM protein stock solution to give final concentration of tracer and protein of 50 nM and 500 nM respectively. The room temperature C-H functionalisation reaction arrays were screened at a total product concentration of 80 μM.

Each of the 720 C-H functionalisation reaction mixtures was screened at a total product concentration of 80 μM and the anisotropy data normalised relative to the positive control of 10 μM geldanamycin (100% activity) and negative control of 2% DMSO blank (0% activity). The data was displayed on polar charts with the negative control (0%) at the outer edge and the positive control (100%) at the centre. The room temperature C-H functionalisation reaction arrays were plotted on three charts for each of the component-pairing array designs; catalyst-substrate matching (Figure 4.5), catalyst-fragment matching (Figure 4.6) and fragment-substrate matching (Figure 4.7). For substrates **S15** and **S25** the activity of the isolated components was observed as 46% and 29% respectively in the control points (Appendix B).

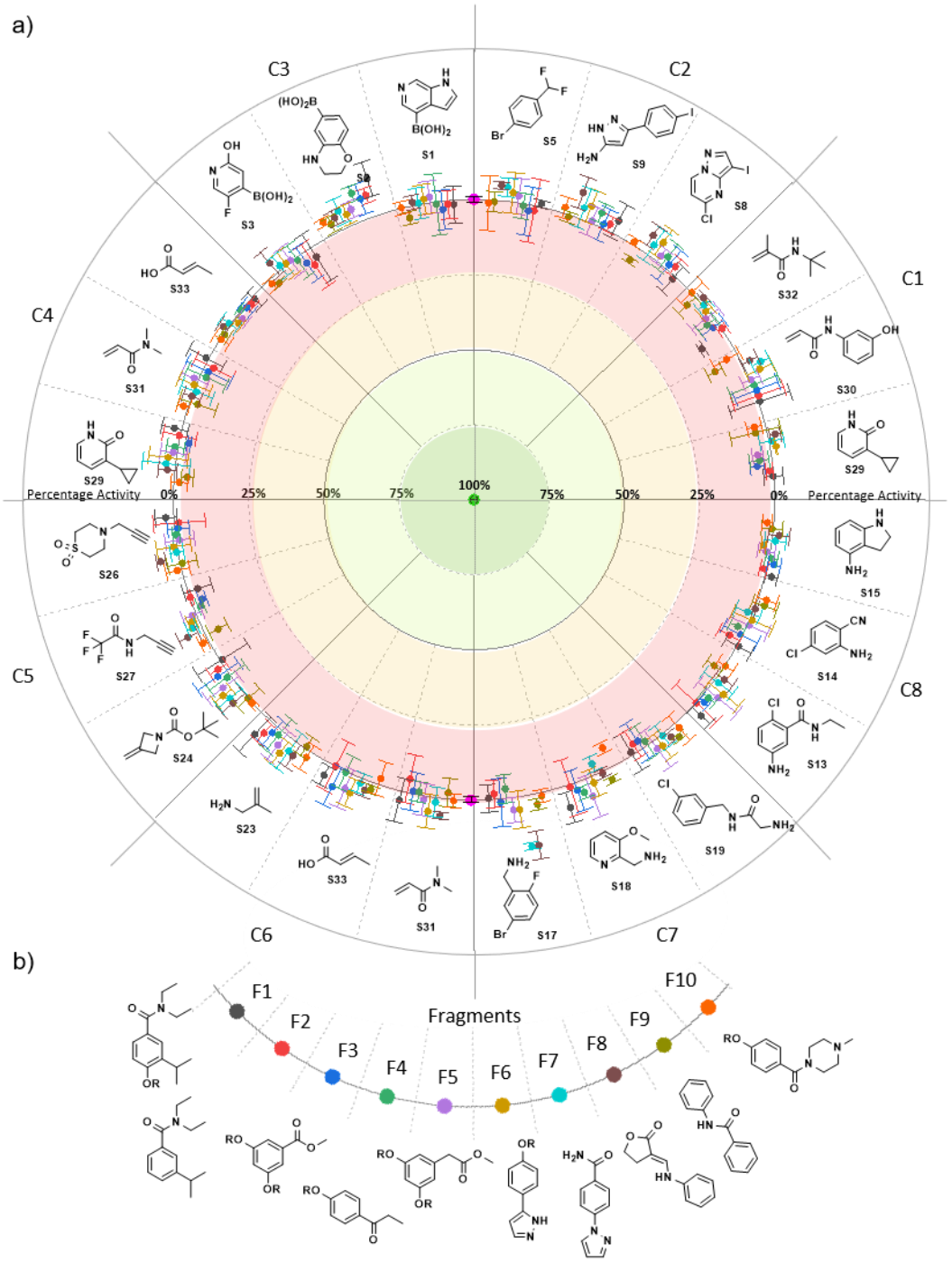

Figure 4.5 ***a)*** *Normalised bioactivity data against Hsp90 for the 240 C-H functionalisation reaction mixtures with matched catalyst-substrate pairings screened at 80 μM. The data was normalised relative to 10 μM Geldanamycin (green centre point, 100 %) and blank DMSO at the circumference (0%). No significant activity from the reaction mixtures was observed. Major sectors show the combinations of fragment and substrate under the eight catalyst systems (**C1**-**C8**). Each minor sector represents the ten fragments for each substrate reacted under each catalyst system (panel b).* ***b)*** *The ten Hsp90 fragments implemented in the arrays (R=Ac).See Appendix D for data processing.*

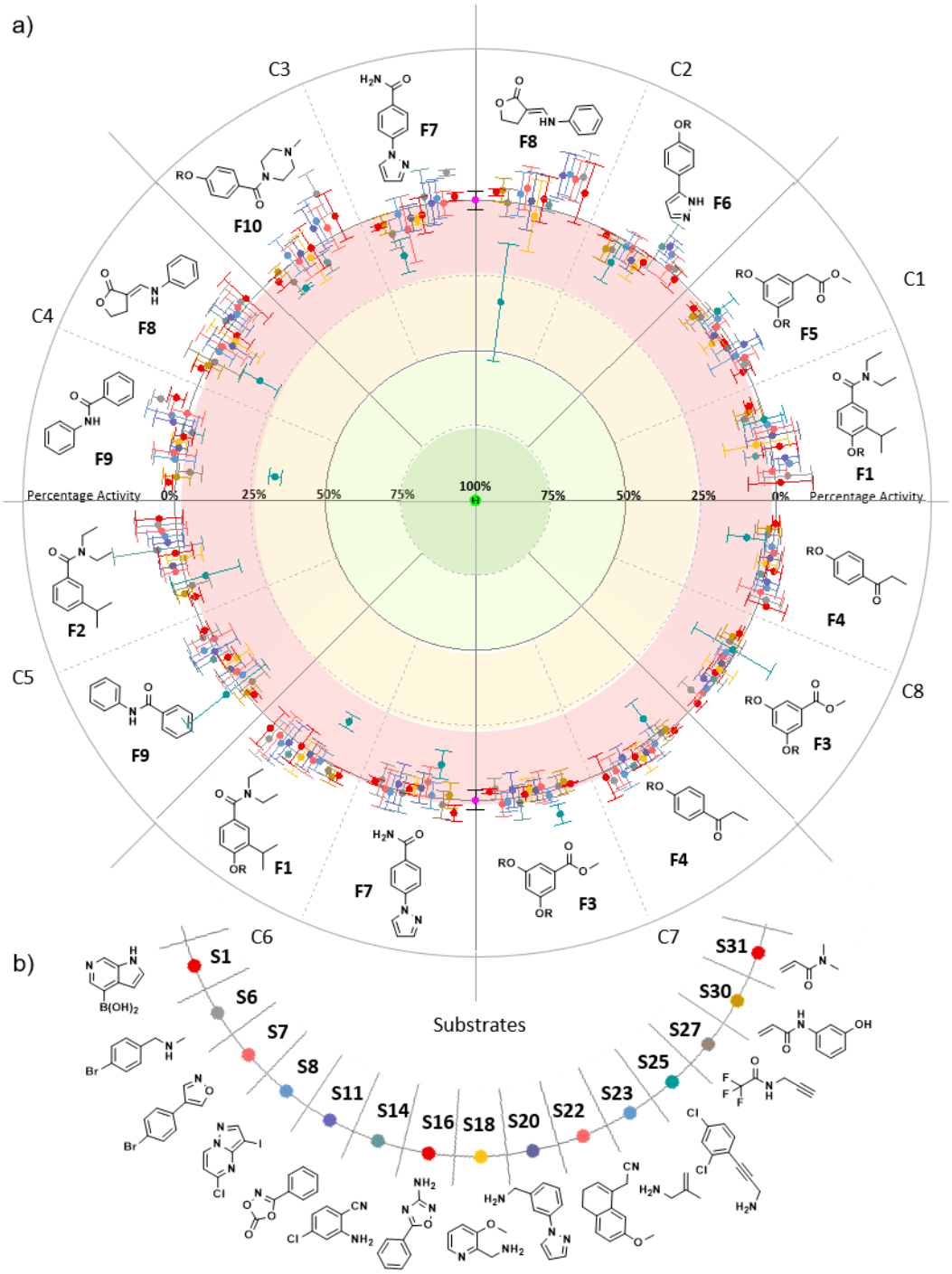

Figure 4.6 ***a)*** *Normalised bioactivity data against Hsp90 for the 240 C-H functionalisation reaction mixtures with matched catalyst-fragment pairings screened at 80 μM. The data was normalised relative to 10 μM Geldanamycin (green centre point, 100 %) and blank DMSO at the circumference (0%). No significant activity from the reaction mixtures was observed but the bioactivity from* ***S25*** *was observed. Major sectors show the combinations of catalyst and fragment under the eight catalyst systems (****C1****-****C8****). Each minor sector represents the 15 substrates for each fragment reacted under each catalyst system (panel b).* ***b)*** *The 15 substrates implemented in the arrays (R=Ac).*

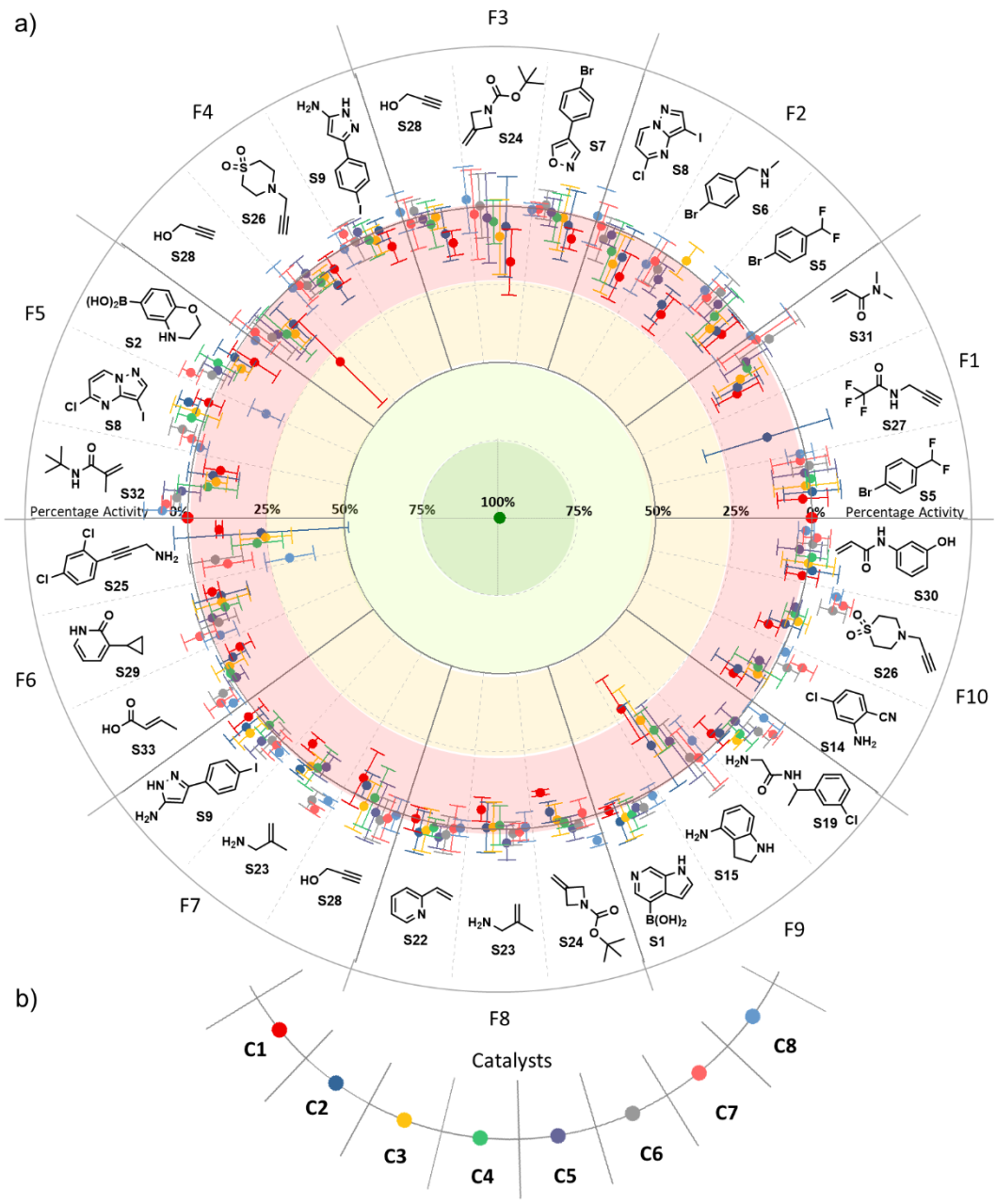

Figure 4.7 ***a)*** *Normalised bioactivity data against Hsp90 for the 240 C-H functionalisation reaction mixtures with matched fragment-substrate pairings screened at 80 μM. The data was normalised relative to 10 μM Geldanamycin (green centre point, 100 %) and blank DMSO at the circumference (0%). No significant activity from the reaction mixtures was observed but the activity from substrates* ***S15*** *and* ***S25*** *was observed. Major sectors show the combinations of fragment and substrate for each of the ten fragments (****F1-F10****). Each minor sector represents the eight catalyst systems for each combination of fragment and substrate (panel b).* ***b)*** *The eight catalyst systems implemented in the arrays (see component table, Experimental 6.2.2).*

From the bioactivity data of the 240 catalyst-substrate matched C-H functionalisation reactions screened at a total product concentration of 80 μM, there were no reaction mixtures with significant biological activity (Figure 4.5), that stemmed from productive reaction combinations, to design a subsequent round of ADS. For the catalyst-fragment matched array (Figure 4.6), increased bioactivity was only seen with substrate **S25** (~20% activity relative to geldanamycin at 10 μM) regardless of the fragment and catalyst combination. Given the activity of **S25** in the control points was observed at ~30%, it was deemed the activity from the reaction array mixtures stemmed from the activity of the substrate and not a product of the reaction arrays. Similarly for the fragment-substrate matched array (Figure 4.7), the increased bioactivity observed stemmed from the activity of substrates **S15** and **S25** and not from a product of the reaction array.

Unfortunately, from the 720 reactions performed, there were no active mixtures that could inform the design of a subsequent reaction array. At this stage it was not clear the reason for the lack of bioactivity from the reaction arrays, but it was proposed that the lack of activity stemmed from poorly performing/low yielding reactions. This was likely due the use of non-optimal combinations based on the literature precedent. While screening at higher concentrations was possible to enable detection of any low yielding products, it was probable that the activity of the fragments themselves would be observed, making identification of productive reaction mixtures difficult. It was therefore proposed, should any reaction have been low yielding, performing a reaction array at higher temperature, in the high-temperature set-up previously established, would potentially enable an increase in yield of products and thus enable detection in the assay.

4.2.2 Heated Reaction Arrays

4.2.2.1 Reaction Array Design and Execution

To determine whether poorly performing reactions were the reason for the lack bioactive reaction mixtures, a heated (60 ^{o}C) array of 130 C-H functionalisation reactions was performed using combinations of fragments, catalysts and substrates previously selected (Figure 4.2). It was envisaged

higher temperatures would increase reaction yields and enable any biologically active products to be identified In the assay. The catalysts **C2**, **C4**, **C6** and **C8** were chosen as they covered the reaction types (C-H arylation, C-H alkenylation and C-H aminations) established in parallel array format. Reactions combinations were selected based on catalyst-substrate literature precedent to potentially enable more productive reaction combinations. The catalyst-substrate pairs were then combined with five of the fragments under the four chosen catalyst systems.

Reactions arrays were implemented as described previously from stocks solutions of fragment, substrate and catalysts. For the heated array the reactions were heated to 60 ^{o}C in an Optiblock Parallel Synthesis Reaction Block sealed with PTFE-faced Silicone Septa Pads. Following reaction completion, reaction mixtures were similarly scavenged, evaporated and dissolved in 100 μL DMSO (total product concentration 100 mM).

4.2.2.2 Reaction Array Results

Reaction mixtures were similarly prepared as stock solutions in DMSO:Buffer (8:92) and screened in triplicate at a total product concentration of 100 μM, 50 nM of tracer and 500 nM of protein. The anisotropy data was normalised relative to the positive control of 10 μM geldanamycin (100% activity) and negative control of 2% DMSO blank (0% activity) and plotted on a polar chart (Figure 4.8). As for the room temperature array, none of the reaction mixtures showed significant biological activity against Hsp90 in the fluorescence anisotropy assay and therefore a second round of ADS could not be designed.

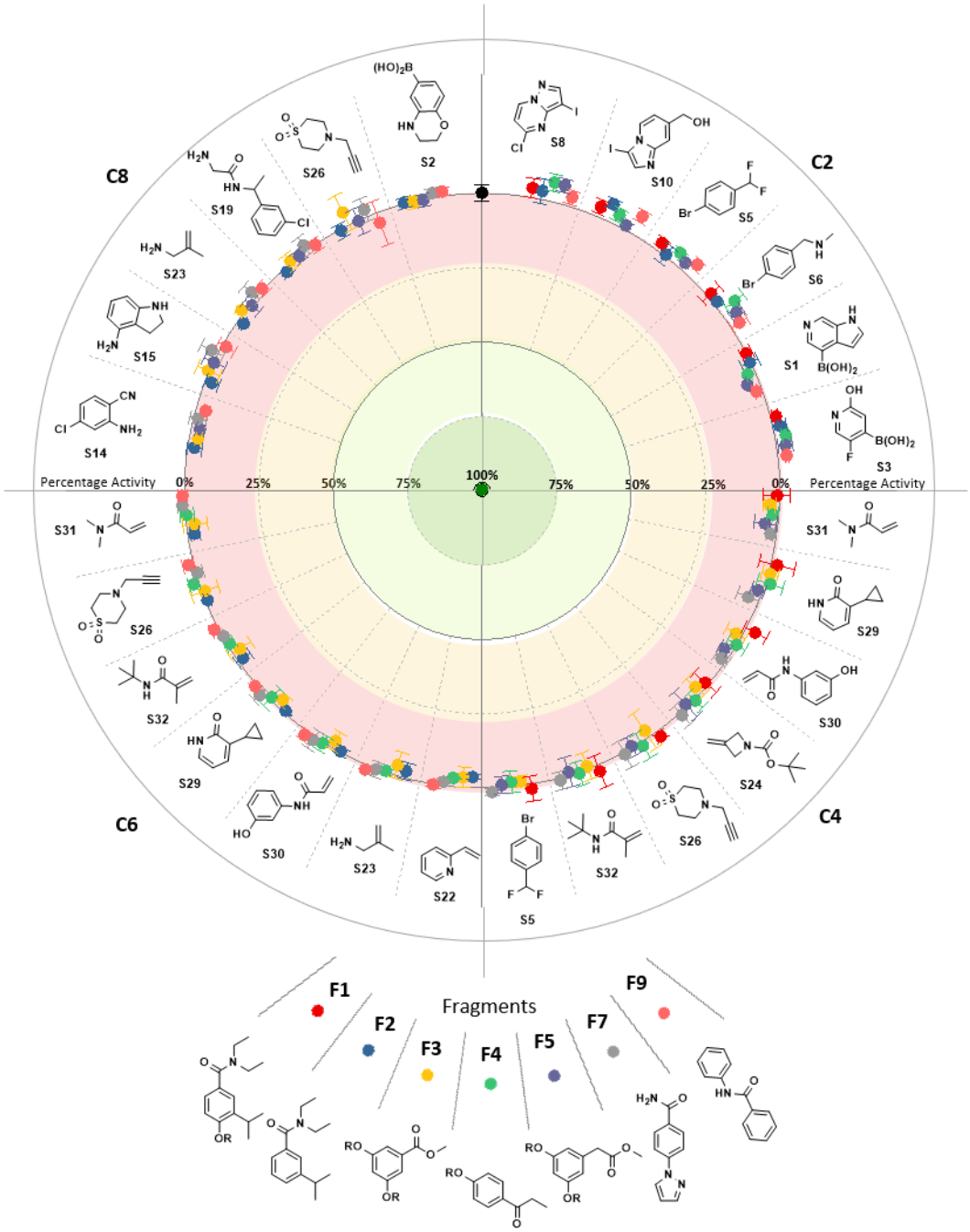

Figure 4.8 ***a)*** *Normalised bioactivity data against Hsp90 for the 130 C-H functionalisation reactions performed at 60 °C. The data was normalised relative to 10 μM Geldanamycin (green centre point, 100 %) and blank DMSO at the circumference (0%). No significant activity from the reaction mixtures was observed. Major sectors show the combinations of fragment and substrate under the four catalyst systems (**C2**, **C4**, **C6** and **C8**). Each minor sector represents five of fragments for each substrate reacted under each catalyst system (panel b).* ***b)*** *The seven Hsp90 fragments implemented in the arrays (R=Ac).*

4.2.3 Matched Chemistry Heated Reaction Arrays

Given that the crystal structures of the fragments bound to Hsp90 showed promising elaboration vectors accessible through C-H functionalisation chemistry, it is somewhat surprising that an active combination was not observed. It was probable the substrate scope of the reaction was not producing an active elaborated fragment and a wider array of reaction substrates required, or more simply the reactions themselves are not robust enough with the range of highly-functionalised substrates selected. It was therefore proposed to select a second set of fragments and substrates that are more closely aligned to the literature precedent to enable potentially productive elaboration vectors to be identified (Figure 4.9).

4.2.3.1 Reaction Array Design and Execution

From the fragments designed and prepared previously (Chapter 3), six fragments that had not been implemented in reaction arrays (**F11**-**F16**, Figure 4.9) were selected on the basis they contained a secondary amide (tert-Butyl or cyclopentylamine) as a potential directing group, which is a widely used in C-H functionalisations chemistry. These six fragments were chosen along with fragments **F7** and **F8** to give a set of eight fragments which did not possess the phenol fragment for Hsp90. While this has been shown as a key moiety for Hsp90 binding, the fragments selected all showed biological activity towards Hsp90 and would be more compatible for use in C-H functionalisations reactions.

For reaction array implementation, the eight fragments were reacted with five of the eight selected catalyst systems. The five catalyst systems had previously been established in parallel array format and were chosen to cover the range of C-H functionalisation reaction type. For each catalyst system, 64 reactions were performed with eight substrates (from a range of 37, **R1**-**R37**) that matched the catalyst reaction type to give a total of 320 reactions. The substrates were chosen from the Nelson chemical inventory on the basis they possessed the correct functional group for the reaction type of the catalyst system, and that the range of substrates for each substrate class was diverse. Reaction arrays were performed at 60 ^{o}C as previously described, scavenged,

evaporated and dissolved in 100 μL DMSO, to give a final total product concentration of 100 mM.

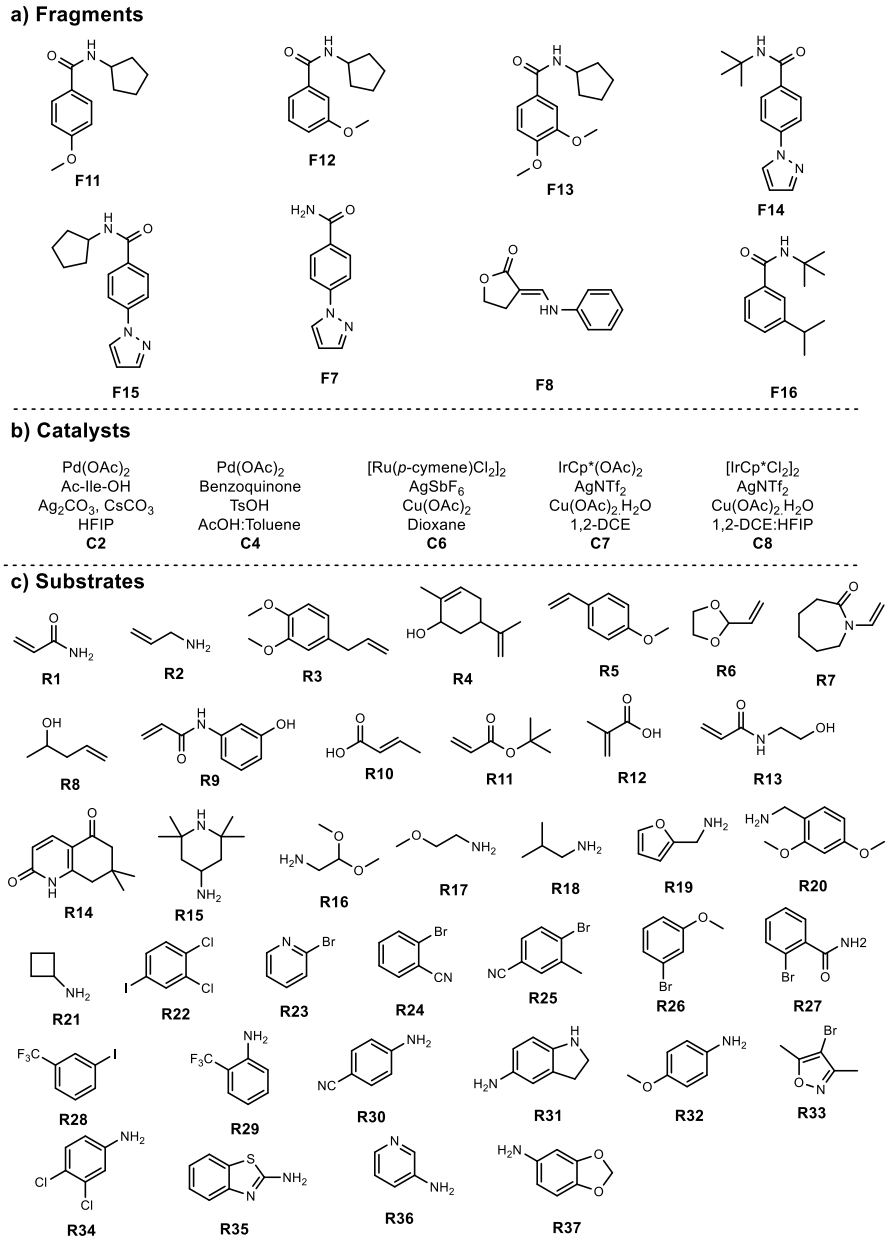

Figure 4.9 *Fragments catalysts and substrates implemented in reaction arrays for high temperature C-H functionalisation reaction arrays with literature-matched array design for elaboration of Hsp90 fragments.*

4.2.3.2 Reaction Array Results

Reaction mixtures were diluted in DMSO:Buffer (8:92), which were screened in the fluorescence anisotropy assay at a total product concentration of 100 μM, 50 nM of tracer and 500 nM of protein. The anisotropy data was normalised relative to 10 μM geldanamycin (100% activity) and 2% DSMO

blank (0% activity) and the normalised data plotted on a Polar Chart (Figure 4.10).

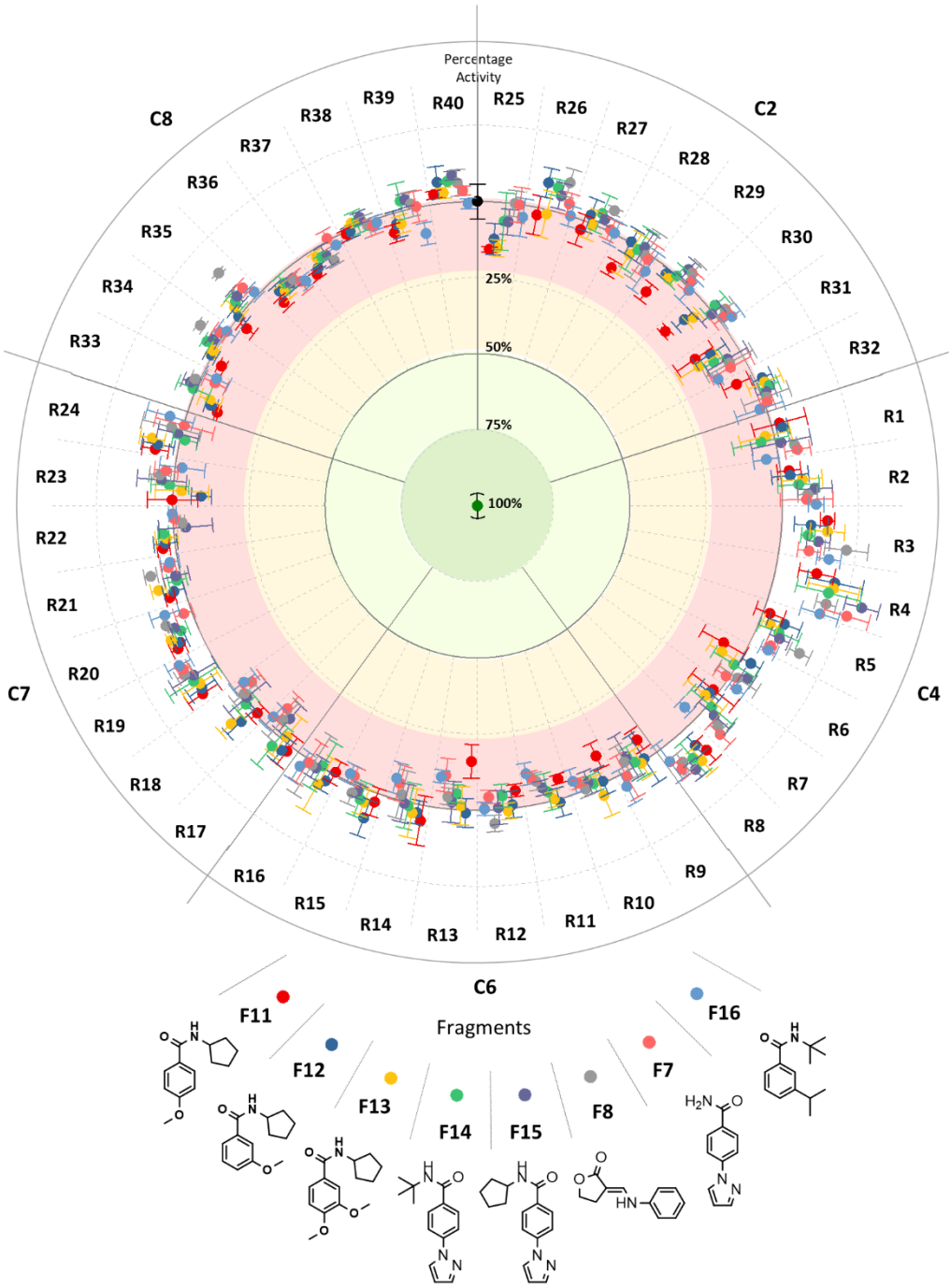

Figure 4.10 ***a)*** *Normalised bioactivity data against Hsp90 for the 320 C-H functionalisation reactions performed at 60 °C. The data was normalised relative to 10 μM Geldanamycin (green centre point, 100 %) and blank DMSO at the circumference (0%). No significant activity from the reaction mixtures was observed. Major sectors show the combinations of fragment and substrate under the five catalyst systems (**C2**, **C4**, **C6**, **C7** and **C8**). Each minor sector represents the eight fragments for each substrate reacted under each catalyst system (panel b).* ***b)*** *The eight Hsp90 fragments implemented in the arrays.*

Unfortunately, there were no reaction mixtures that were identified as being biologically active at a total product concentration of 100 μM and therefore a second round of ADS was not be designed. With 1170 C-H functionalisation reactions performed from combinations of 16 fragments, eight catalysts and 70 substrates, it was surprising that none of the reaction combinations produced biologically active mixtures. It was likely the reactions were performing systematically poorly with the choice of fragments and highly functionalised and polar substrates. Indeed, the systematic failure of highly-functionalised and polar substrates in similar reaction classes has been reported and that literature reaction methodology studies fail to identify a truly broad scope of substrates that would prove beneficial in medicinal chemistry workflows.[18,26,53] To determine whether it was indeed the poor reaction performance with the chosen fragments and substrates that was preventing discovery of bioactive reaction mixtures, an LC-MS study was performed to identify reactions that had successfully given products in the arrays.

4.2.4 Reaction Array Product Analysis

An LC-MS study of a random ~10% of the reactions was performed to determine the reaction performance of the C-H functionalisation reaction arrays. Identification of potential product masses from the reaction indicated formation of reaction products. Reaction array stocks (100 mM) were diluted into MeCN to give a final total product concentration of 5 mM and analysis of the reaction mixture was performed by LC-MS. LC-MS was performed with a positive and negative switching mode with a gradient elution H_2O and MeCN each plus 0.1% formic acid. The spectra were then analysed by searching for potential product masses of the bimolecular reaction (fragment + substrate) minus the mass of HX (X = H, Cl, Br, I or $B(OH)_2$.)

For the room temperature C-H functionalisation reaction arrays, 72 of the 720 reaction mixtures were analysed by LC-MS (Appendix C.1.1.1). From the 72 reactions analysed, only 8 reaction mixtures had masses corresponding to potential products as a result of a C-H functionalisation reaction indicating only ~10% of the reactions were successfully undergoing C-H functionalisation

reaction highlighting the poor performance of metal-catalysed reactions with highly-functionalised substrates.[18,53]

The reaction of fragment **F4** with boronic acid substrate **S1** under iridium catalysis **C8** was one example in which a mass of a potential product **P1** was identified (Figure 4.11), however, the iridium catalysed C-H arylation with aryl boronic acids has not been previously reported. Further analysis would be required to determine if the reaction had progressed to sufficiently progressed and indeed whether a novel transformation had been discovered.

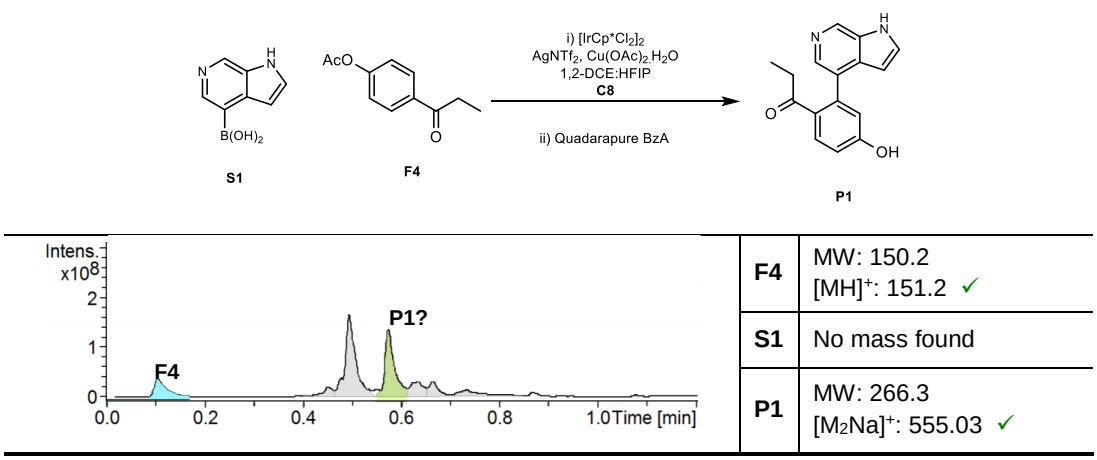

F4	MW: 150.2 $[MH]^+$: 151.2 ✓
S1	No mass found
P1	MW: 266.3 $[M_2Na]^+$: 555.03 ✓

Figure 4.11 *LCMS analysis of crude reaction mixture of fragment **F4** with boronic acid substrate **S1** under iridium catalysis **C8** identified an M_2Na product mass for potential product **P1** from the room temperature C-H functionalisation reaction arrays.*

Of the 72 reactions, 35 (~50%) still showed presence of fragment and/or substrate in the reaction mixture again suggesting that fragment and substrates were not going to completion, supporting the poor substrate scope of the reactions. It should also be noted that in the all cases in which fragment and products could be identified in reaction mixtures, it was the mass of the deprotected phenol fragment, supporting the capability of the Quadrapure BzA to readily perform acetate deprotections. In the cases in which fragment or product was not identified, subsequent analysis did not reveal any fragment/product masses which still remained acetate protected. Analysis of 20 of the 130 C-H functionalisation reactions performed at 60 ^{o}C showed only one reaction with a potential product mass, further supporting the poor substrate scope compatible with the reaction class.

Finally, from the LC-MS analysis of 30 of 320 matched-chemistry 60 ^{o}C C-H functionalisation reaction array, only four reactions with potential product masses were identified. Reaction of fragment **F11** with acrylamide substrate **R1** under ruthenium catalysis **C6** gave a potential product in the LC-MS, which is likely the result of a C-H alkenylation; a well reported transformation under ruthenium catalysis (Figure 4.12).[98]

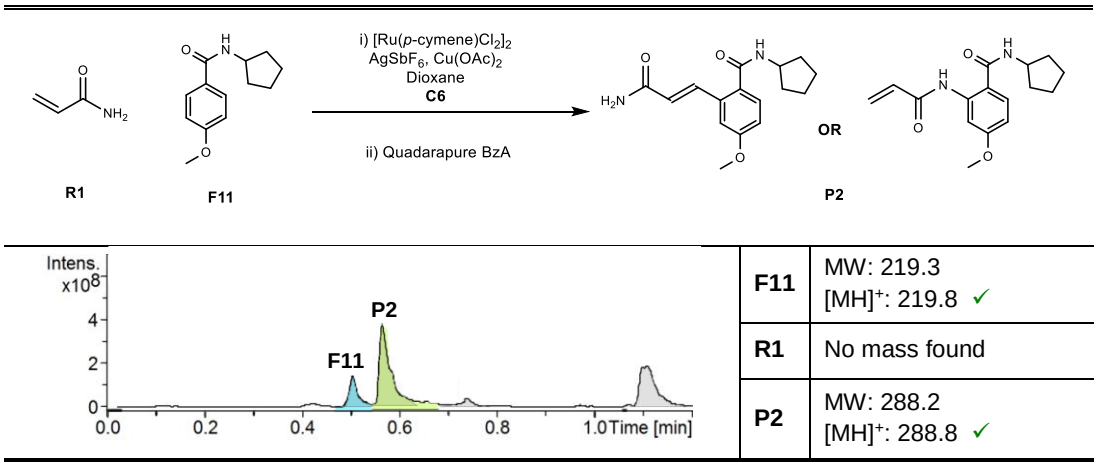

F11	MW: 219.3 $[MH]^+$: 219.8 ✓
R1	No mass found
P2	MW: 288.2 $[MH]^+$: 288.8 ✓

Figure 4.12 *LCMS analysis of crude reaction mixture of fragment **F11** with substrate **R1** under iridium catalysis **C6** identified an MH product mass for potential product **P2** from the 60 ^{o}C matched-chemistry C-H functionalisation reaction arrays.*

Of the 122 reactions analysed by LC-MS, only 13 mixtures gave potential products as a result of a C-H functionalisation reaction, highlighting the poor robustness of the reactions. It was therefore decided the use of C-H functionalisation chemistry, with substrates desirable in medicinal chemistry, was not compatible for ADS and that alternative chemistry explored as an elaboration strategy for Hsp90 fragments.

4.3 Metal-Catalysed Carbenoid Chemistry with α-Diazoamides Reaction Arrays

It was proposed that the use of metal-catalysed carbenoid chemistry with α-diazoamides would provide a more robust and reliable transformation for elaboration of Hsp90 fragments. Metal-catalysed carbenoid chemistry is able to undergo multiple possible reactions, e.g. C-H, O-H, N-H insertions and cyclopropanations (Chapter 1) and so has the potential to elaborate fragments in many possible approaches. Two approaches for the use of α-diazoamides were proposed; firstly to elaborate Hsp90 fragments with a diverse set of α-

diazoamides (prepared by Nelson group members via previously reported synthetic methods),[162,163] and secondly by preparing α-diazoamides bearing a Hsp90 fragment and reacting them with a range of co-substrates which can undergo at least one metal-catalysed carbenoid transformation.

4.3.1 Hsp90 Fragments with α-Diazoamides Reaction Array

For the reaction arrays for the elaboration of Hsp90 fragments with a diverse set of α-diazoamides, four fragments, two catalysts and 12 diazoamides were chosen to give a total of 96 possible reactions (Figure 4.13). The four fragments were chosen on the basis they could undergo at least one possible metal-catalysed carbenoid transformation; insertion into aromatic C-H, benzylic C-H, C-H next to oxygen or nitrogen, O-H insertion or a cyclopropanation. The twelve diazoamides were selected to give a diverse set possessing a range of aliphatic and aromatic substituents. The two catalysts were chosen based upon their potential to undergo different reaction modes (unpublished study by Adam Green, Adam Nelson and co-workers).

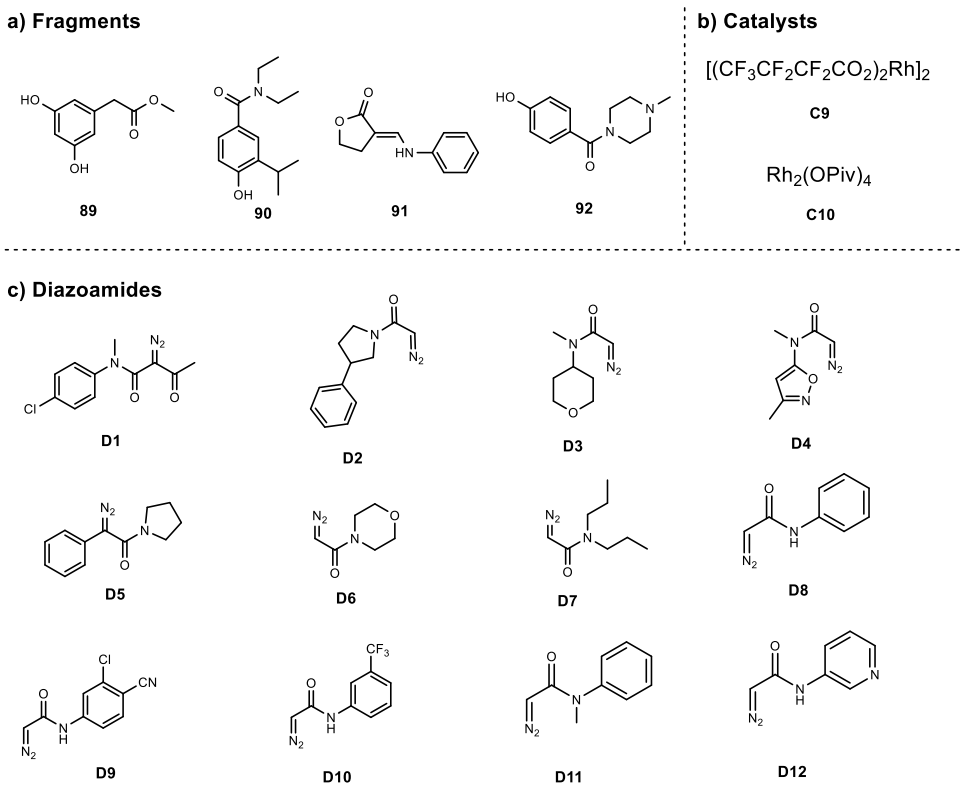

Figure 4.13 Fragments (**F5**, **F8**, **F10** and **F17**), α-diazoamides (**D1**-**D12**) and catalysts **C9** and **C10** used in reaction arrays for potential elaboration of Hsp90 fragments

All possible 96 reaction combinations were performed by preparing stocks of fragment in CH_2Cl_2 (200 mM), diazoamide in CH_2Cl_2 (200 mM) and catalyst in THF (12.5 mM). To the vial of interest was added one of each of fragment (50 μL) and catalyst (8 μL) and the solvent allowed to evaporate. Finally, was added one diazoamide (100 μL) and the vials capped to give a final reaction concentration of 100 mM fragment, 200 mM diazoamide and 1 mM catalyst. Following reaction completion, catalysts were scavenged using Quadrapure TU (30 mg) for 24 h, reaction mixtures filtered, evaporated and dissolved in DMSO (100 μL) to give a final total product concentration of 100 mM. Reaction stocks were diluted into DMSO:Buffer (8:92) to give stocks at four times the final assay concentrations (total product concentration: 400 μM), and then screened in triplicate at 100 μM in the fluorescence anisotropy assay. The anisotropy data was normalised relative to 10 μM geldanamycin (100% activity) and 2% DSMO blank (0% activity) and the normalised data plotted on a Polar Chart (Figure 4.14).

As for the C-H functionalisation reaction arrays, no significantly biologically active reaction mixtures were identified from the metal-catalysed carbenoid reaction array. There was slightly increased activity (~15%) for all mixtures, regardless of diazoamide and catalyst, with fragment **F17**. Given this fragment has a low micromolar IC_{50} for Hsp90, the activity observed stemmed from the activity of the fragment. Unfortunately on the basis of the activity data obtained, a second round of ADS could not be designed.

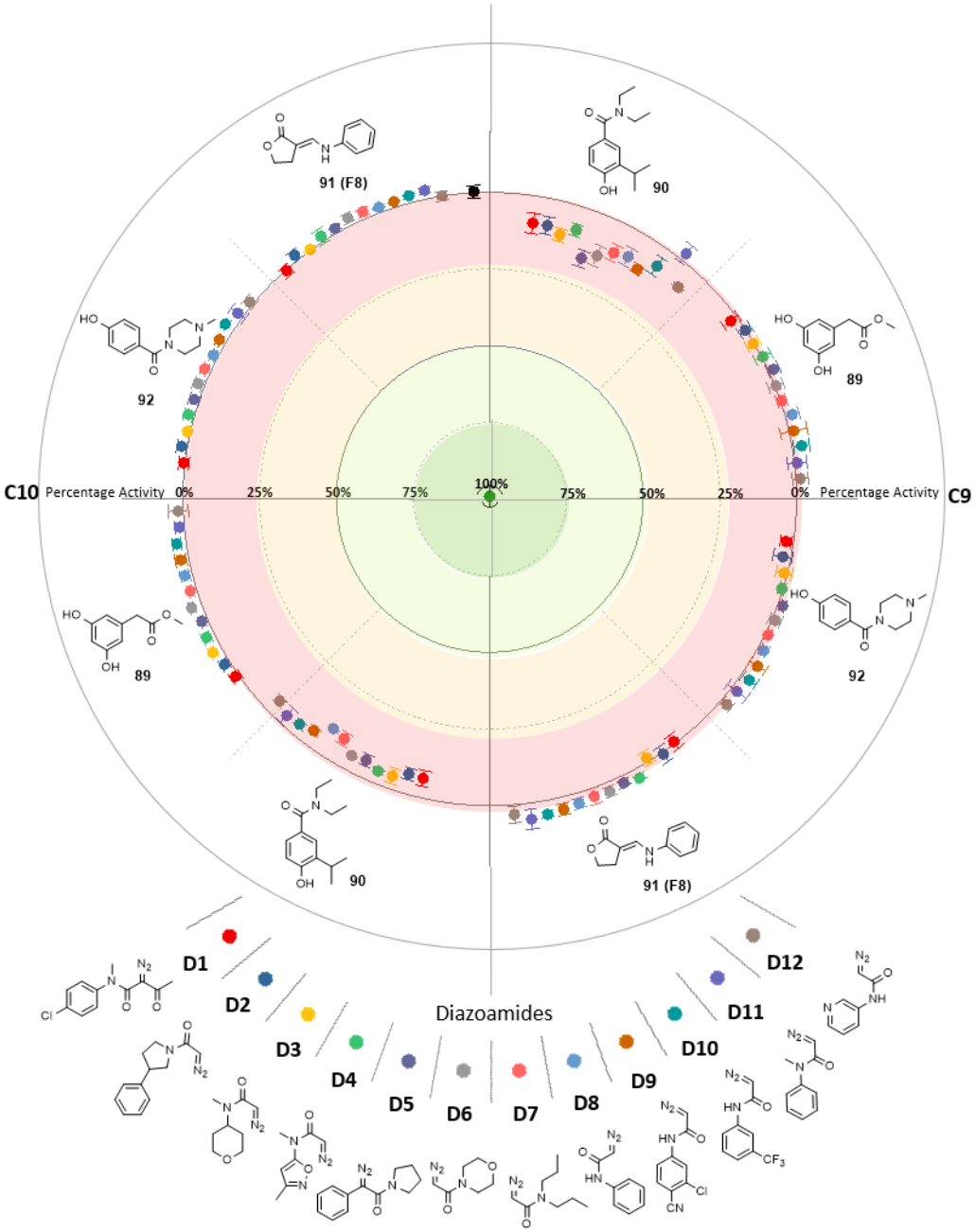

Figure 4.14 a) *Normalised bioactivity data against Hsp90 for the 96 metal-catalysed carbenoid reactions screened at 100 μM. The data was normalised relative to 10 μM Geldanamycin (green centre point, 100 %) and blank DMSO at the circumference (0%). No significant activity from the reaction mixtures was observed. Major sectors show the combinations of fragment and catalyst. Each minor sector represents the twelve diazoamides reacted with each combination of fragment and catalyst.* ***b)*** *The twelve α-diazoamides implemented in the arrays.*

4.3.2 α-Diazoamides-Fragments with Substrates Reaction Array

4.3.2.1 Reaction Array Design

The final array was the use of α-diazoamides bearing a Hsp90 fragment and performing reactions with a diverse set of co-substrates, in a similar approach to previous ADS studies.[16,17] Two α-diazoamides were selected along with two rhodium catalysts **C9** and **C10** and twenty diverse co-substrates, **CS1**-**CS20** (Figure 4.15). The two α-diazoamides **DF1** and **DF2** bearing the Hsp90 fragment, 2-isopropylphenol, required synthesis prior to the implementation in the reaction array (Scheme 4.1). The 20 co-substrates were chosen to give a diverse set and selected on the basis they possessed a functional group for potential reaction with an α-diazoamide (e.g. O-H and N-H insertions, C-H insertions next to O/N and cylcopropanations with unsaturated bonds). The two rhodium catalysts were chosen again based on their potential to undergo different reaction types (based on an unpublished study by Adam Green, Adam Nelson and co-workers).

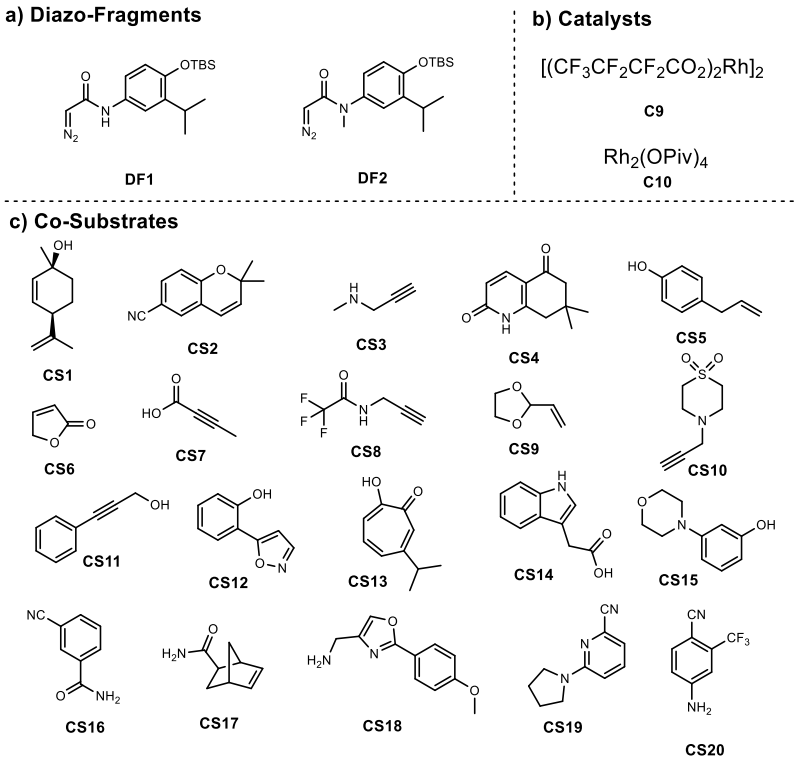

Figure 4.15 *Diazoamide-fragments (**DF1** and **DF2**), co-substrates (**CS1**-**CS20**) and catalysts **C9** and **C10** used in reaction arrays for potential elaboration of Hsp90 diazoamide-fragment*s

4.3.2.2 Synthesis of Hsp90 Fragment α-Diazoamides

The two α-diazoamides **DF1** and **DF2** for implementation in the reaction arrays incorporated the TBS protected 2-isopropylphenol moiety, which were prepared via known synthetic routes (Scheme 4.1).[162,163] The phenol fragments were TBS protected, as again they were envisaged as potentially dominating reactivity, due to the possibility of undergoing O-H insertions under metal-catalysed carbenoid chemistry. A parallel reaction array deprotection strategy was subsequently established to reveal the key phenol fragment for Hsp90 bioactivity prior to screening in the assay (Section 4.3.2.3).

The diazoamides were prepared from their respective amines, which were themselves synthesised in three and four steps from 2-isopropylphenol (Scheme 4.1). Firstly, nitration of 2-isopropylphenol **131** with HNO_3 and $ZnCl_2$ gave a mixture of the 4-mono, 6-mono and 4,6-dinitrated phenol which were separated via column chromatography to give the 4-nitro-2-isoproylphenol **132** in 57% yield. The phenol was readily protected as the tert-butyldimethylsilane **133** in 74% yield. Reduction of the nitro with H_2 and Pd/C yielded aniline **134** (78%) which could be methylated with $MeB(OH)_2$ and copper (II) acetate to give the methylaniline **135** (58% yield). A mixture of mono- and demethylated aniline was produced however separation was possible via chromatography using a slow elution gradient. Anilines **134** and **135** were then used to prepare the two a-diazoamides **DF1** and **DF2**. Firstly the toluenesulfonyl hydrazone chloride **136** was prepared from the corresponding acid by heating with thionyl chloride in toluene at 90 ^{o}C. The toluenesulfonyl hydrazone chloride **136** (used as crude material) was coupled with each aniline in the presence of DMA at 0 ^{o}C, which upon treatment with triethylamine gave diazoamides **DF1** and **DF2** in 50% and 79% yield respectively (Scheme 4.1b).

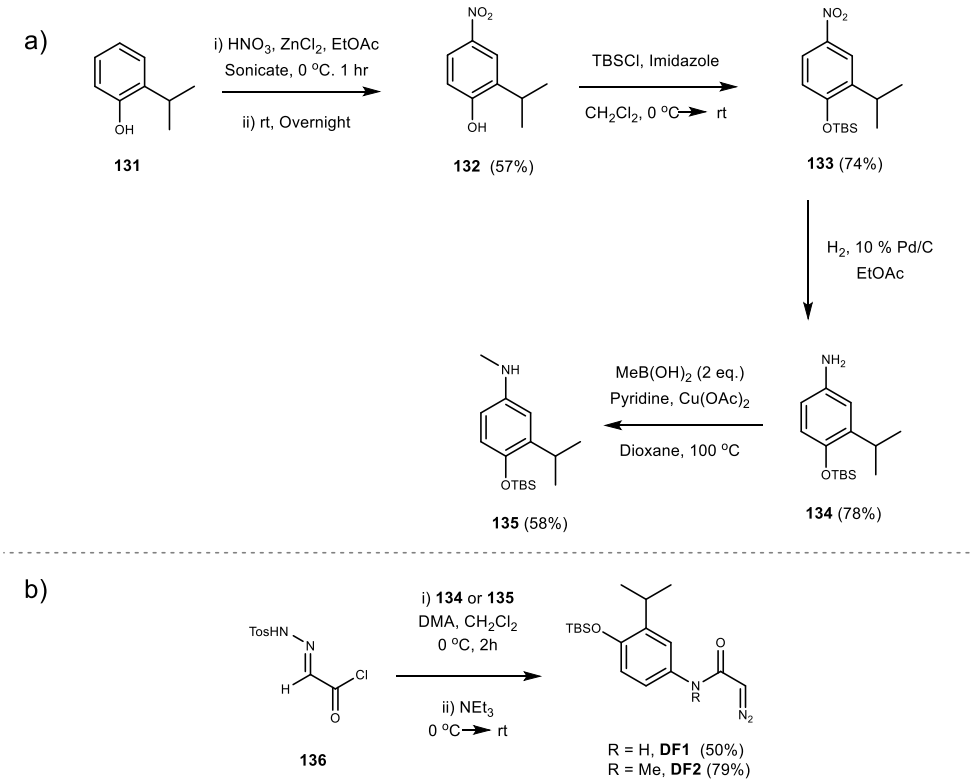

Scheme 4.1 *Synthesis of anilines **134** and **135** and α-diazoamides **DF1** and **DF2** for implementation in ADS reaction arrays.*

4.3.2.3 TBS Deprotection in Parallel Array Reaction Format

To enable reaction products to be screened as the deprotected phenol fragment, the key moiety for Hsp90 binding, a simple to implement and mild set of TBS deprotection conditions was established in parallel reaction array format. Substrate **137** was used as the model substrate for establishing the deprotection conditions (Figure 4.16).

The use of methoxide was assessed for its TBS deprotection capabilities; 0.01 mmol of substrate **137** was added to a microvial of interest followed 100 μL of a sodium methoxide (1.5 eq) solution in MeOD. The reaction was left for 6 h, diluted with 400 μL of MeOD to enable analysis of ^{1}H and ^{13}C NMR spectroscopy. A ^{1}H and ^{13}C NMR spectra of the initial protected substrate **137** and the reaction mixture was collected, to reveal the completely deprotected substrate **138** under the reaction conditions (Figure 4.16). There are no peaks corresponding to the protected substrate **137** (represented by blue circles in starting spectra) and there are new peaks corresponding to the

formation of **138** (green circles). LC-MS analysis also showed the mass of the TBS deprotected substrate **138**.

The use of methoxide (1.5 eq) in MeOH enabled the simple to implement deprotection of TBS-protected phenol fragments in microscale reaction arrays. An efficient workflow for performing reaction arrays was established; reactions are prepared and left to react for 24 h, reaction solvent evaporated and TBS-protected phenols deprotected with a solution of methoxide (1.5 eq) in methanol (100 μL) for 6h and then the metal catalysts scavenged with Quadrapure TU (30 mg) resin.

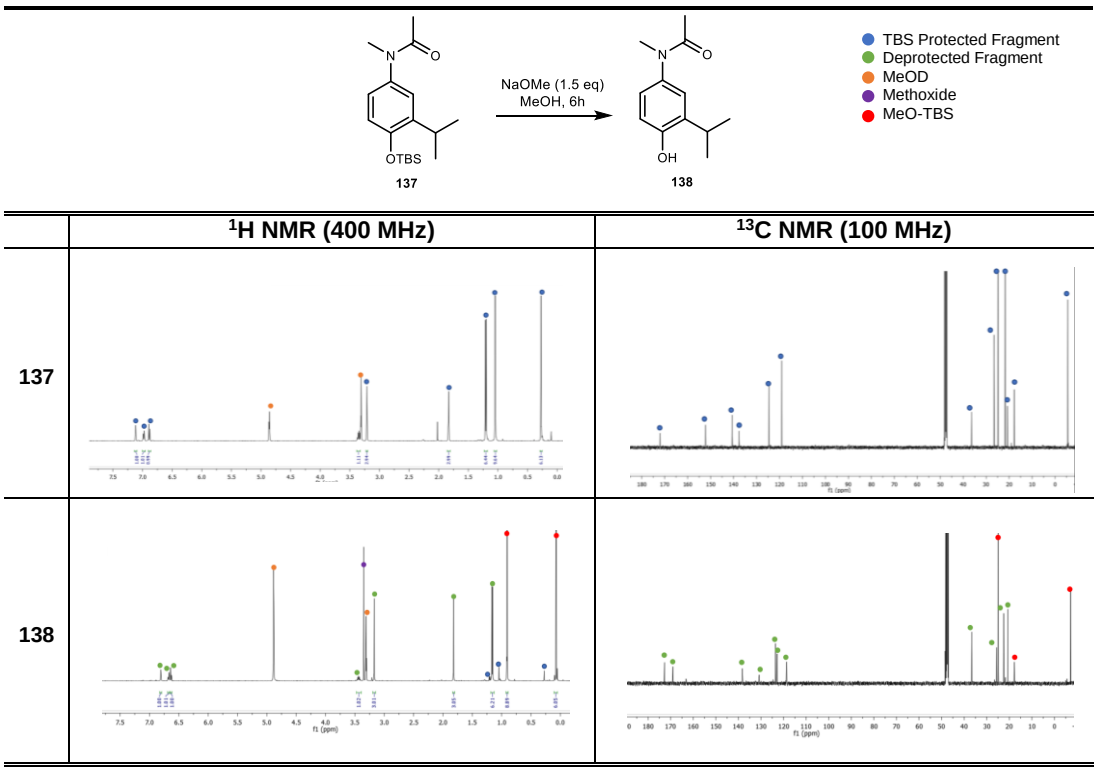

Figure 4.16 *^{1}H and ^{13}C NMR spectroscopy study showed the use of sodium methoxide (1.5 eq) in MeOH could readily as deprotection strategy for TBS-protected fragments in parallel reaction array format.*

4.3.2.4 Reaction Array Execution and Results

With the two a-diazoamides bearing the Hsp90 fragment successfully prepared and the 20 co-substrates **CS1**-**CS20** and the two catalysts **C9** and **C10** chosen, the 80 possible reactions were performed. Diazoamides and co-substrate stocks were prepared in CH_2Cl_2 at 100 mM and 200 mM respectively

and catalysts in THF at 12.5 mM. To a vial of interest was added one co-substrate (100 μL) and catalyst (8 μL) and the solvent allowed to evaporate. Finally, to each vial was added one diazoamide (100 μL) to give a final concentration of 100 mM diazoamide, 200 mM co-substrate and 1 mM of catalyst. Reactions were left for 24 h and then the solvent evaporated. Deprotections were performed with sodium methoxide (1.5 eq) in methanol (100 μL) for 6h, methanol evaporated, mixtures dissolved in CH_2Cl_2 (100 μL) and metal catalysts scavenged with Qudrapure TU (30 mg) for 24 h, reaction mixtures filtered and solvent evaporated. Reaction mixtures were dissolved in DMSO (100 μL) to give a final product concentration of 100 mM. Reaction mixtures were prepared in DMSO:Buffer (8:92) at four times the assay concentration (400 μM), and screened at a total product concentration 100 μM (final DMSO concentration 2%) in the fluorescence anisotropy assay. The anisotropy data was normalised relative to 10 μM Geldanamycin and plotted on a polar chart (Figure 4.17).

The bioactivity data from the final reaction array (Figure 4.17) unfortunately did not reveal any reaction mixtures with significant biological activity and therefore a subsequent round of ADS could not be designed. Given the success of the approach against the androgen receptor in previous ADS studies,[16,17] it was somewhat surprising that there were no biologically active reaction mixtures. As for the C-H functionalisation reaction arrays, an LC-MS study was performed to determine the success of the reactions in the array.

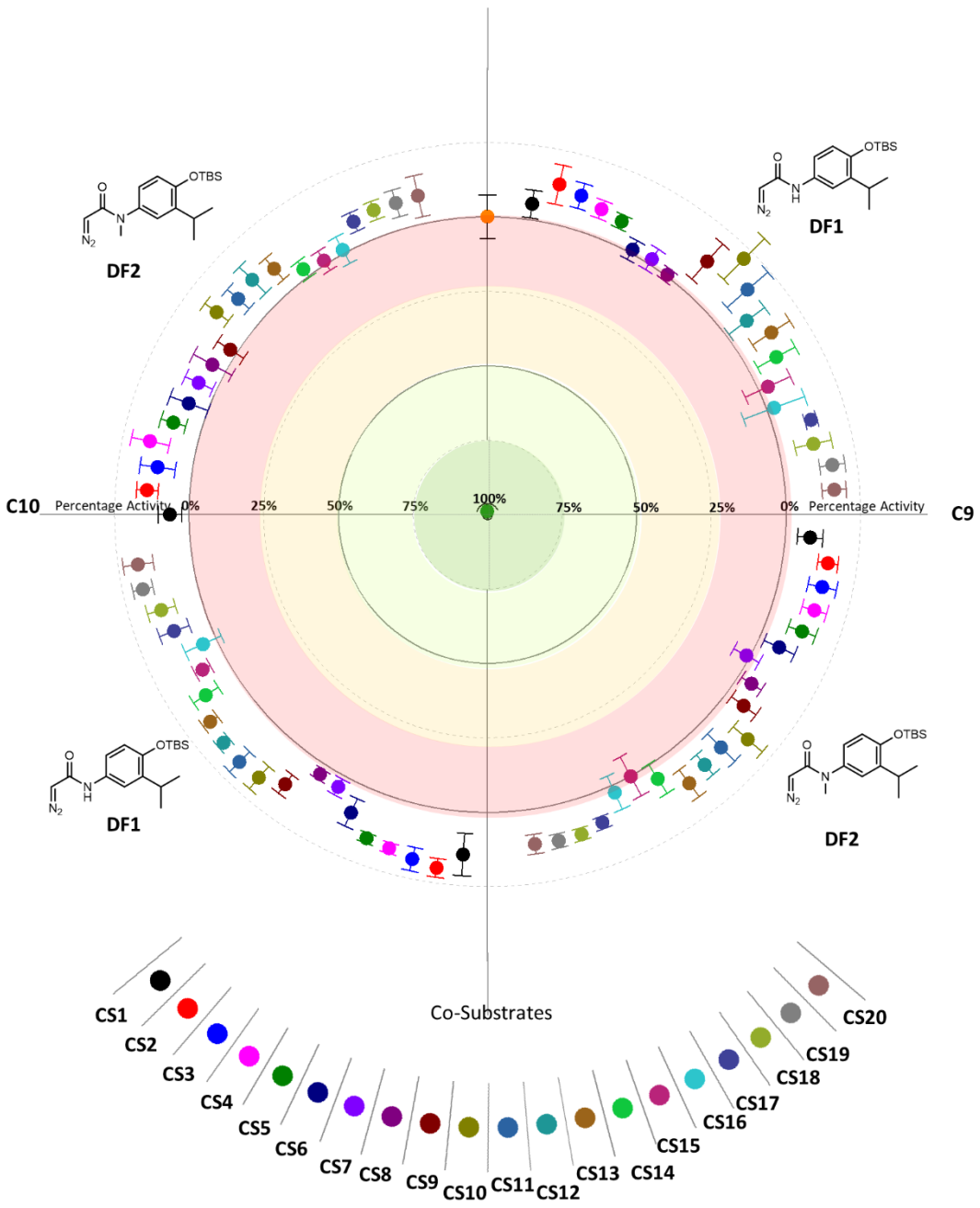

Figure 4.17 a) *Normalised bioactivity data against Hsp90 for the 80 metal-catalysed carbenoid reactions screened at 100 μM. The data was normalised relative to 10 μM Geldanamycin (green centre point, 100 %) and blank DMSO at the circumference (0%). No significant activity from the reaction mixtures was observed.* ***b)*** *The twenty co-substrates implemented in the arrays.*

4.3.3 Metal-catalysed Carbenoid Reaction Array Product Analysis

From the two reaction arrays with the metal-catalysed carbenoid chemistry, a total of 176 reactions was performed. A total of 20 reactions, from the two approaches, were analysed by LC-MS to determine the success rate of the reactions. From the LC-MS, the mass of the biomolecular reaction minus the mass of nitrogen would indicate the successful formation of products in the reaction. For the reactions of fragment and the diverse α-diazoamides, just two of the ten reactions gave masses corresponding to possible products, both of which used catalyst **C9**.

From the arrays which implemented α-diazoamides bearing Hsp90 fragments and the diverse co-substrates, again just two of the products gave masses for potential products. In this case both reaction products were observed with diazoamide **DF1** and catalyst **C10**. The reaction of diazoamide-fragment **DF1** with co-substrate **CS13** the $Rh_2(OPiv)_4$ **C10** catalyst gave two potential product masses in the LC-MS analysis, which could be a result of a cyclopropanation or O-H insertion reaction (Figure 4.18). Both products would have identical masses and in this case the same mass was identified in peaks with different retention times (0.58 and 0.60 min). This suggests more than one possible product was being formed in the reaction, highlighting the unpredictable nature of the metal-catalysed carbenoid chemistry.

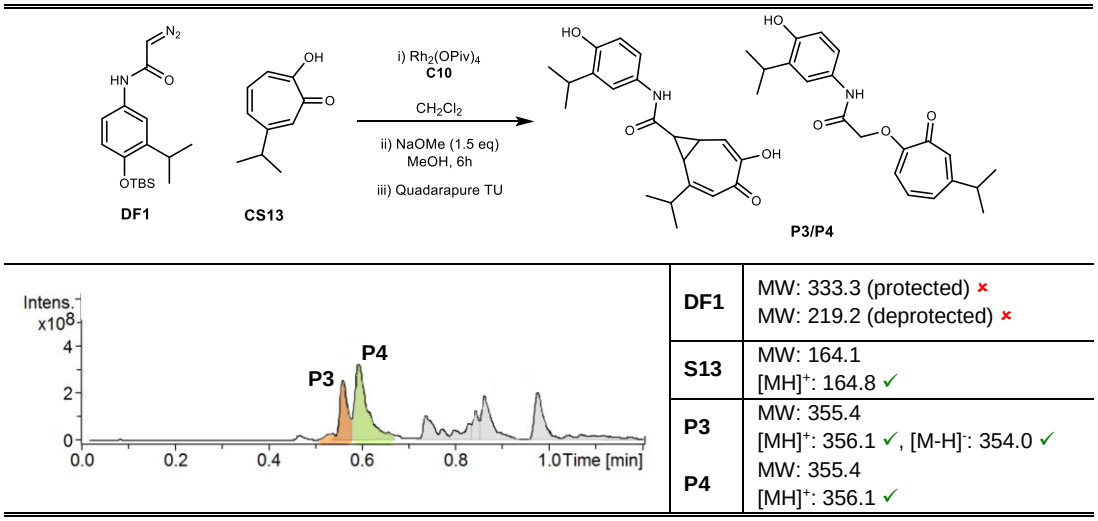

Figure 4.18 *LCMS analysis of crude reaction mixture of diazo-fragment **DF1** with co-substrate **CS13** under rhodium catalysis **C10** identified two [MH]+ product mass for hypothesised products **P3** and **P4** from the metal-catalysed carbenoid reaction arrays.*

However, due to the low success rate of reactions in the array, it was likely the poorly performing reactions were the reason for no biologically active mixtures from the arrays. The lack of bioactivity in the reactions that were successful in giving products, was potentially due to low yield and therefore not identified in the assay at the screening concentration or simply the product itself was simply not biologically active. To enable greater conversion to products with the diazoamide-fragments and co-substrates, a broader range of catalysts and solvents could be used in future studies.

4.4 Summary

It was proposed the use of C-H functionalisation and metal-catalysed carbenoid chemistry implemented in ADS would potentially enable the elaboration of Hsp90 fragments to discover ligands with increased biologically activity. A total of 1170 C-H functionalisation reactions was performed in a series of room temperature and 60 ^{o}C reaction arrays as well as 176 metal-catalysed carbenoid reactions. In all cases, none of the reaction mixtures demonstrated significant biological activity to design a subsequent round for ADS. Around 10% of all the reactions performed were analysed by LC-MS to determine the success rate of the reactions. Roughly 10% of the C-H functionalisation reactions performed showed masses for possible products, and ~20% for the metal-catalysed carbenoid reactions. The poor conversion of substrates to products in the arrays was likely the reason for no biologically active mixtures being observed. This study demonstrated the poor substrate scope, in particular highly-functionalised and polar substrates, in modern methodology studies, and is further evidence that a truly reliable and robust set of transformations is required for the discovery of biologically active ligands in medicinal chemistry workflows (see Chapter 5 for discussion).

Chapter 5.
Summary, Conclusions and Future Work

5.1 Summary

Fragments are attractive starting points in drug discovery workflows and are typically subjected to structure-guided fragment elaboration cycles to develop them into leads.[46,47,49,114] However, the synthetic elaboration of fragments can be challenging due to the poor accessibility of potentially productive elaboration vectors imposed by the limitations of the established medicinal chemistry toolkit.[18,44,81] To enable the structure-blind and function-driven elaboration of fragments using ADS, a series of new tools and protocols for ADS was established.

ADS is a function-driven molecular discovery approach, which borrows concepts associated from the evolution of biosynthetic pathways found in nature.[16,17] ADS aims to maximise the diversity of hits that can seed discovery programmes, by implementing chemical reactions that are currently underutilised in discovery programmes. To assess the potential of the structure-blind and function-driven elaboration of fragments using ADS, the reported study incorporated two key aspects; firstly, the development of underpinning tools for implementation in ADS (section 5.1.1) and secondly, the value of these established tools for function-driven fragment elaboration was assessed in the context of Hsp90 (Section 5.1.2).

5.1.1 Configuration and Optimisation of a Streamlined Workflow for Activity-Directed Synthesis

To maximise the diversity of hits discovered *via* activity-directed synthesis, the chemical toolkit for ADS was expanded. C-H functionalisation was chosen for its potential to synthetically elaborate multiple C-H vectors of a fragment. An optimised workflow for ADS was then established for the function-driven fragment elaboration using either directed C-H functionalisation reactions or metal-catalysed carbenoid chemistry.

A series of reported C-H functionalisation reactions, which covered a broad range of reaction types, was configured for implementation in parallel microscale reaction arrays at room and elevated (60 ^{o}C) temperatures. The literature reactions were assessed under conditions that would be amenable to ADS. In particular, the reactions were prepared from stock solutions and performed in microvials in parallel array format under atmospheric conditions without the requirement of agitation. LC-MS analysis of the crude reaction mixtures enabled the reactions that were successfully translated into ADS-format to be identified.

To minimise potential assay interference from residual components of the reaction mixtures, such as metal catalysts and Michael acceptors, a scavenging protocol was established for the post reaction work-up of crude reaction mixtures. The use of Quadrapure BzA resin was successfully demonstrated as an efficient approach for removing metal catalysts and highly electrophilic Michael acceptors form crude reaction mixtures prior to biological screening. The resin was later also demonstrated to enable the deprotection of acetate-protected phenol fragments. The use of the Quadrapure BzA resin enabled an efficient post reaction work-up procedure that was simple to implement in parallel array format to be configured, ensuring a streamlined workflow for ADS.

Hsp90 was identified as a tractable target to validate C-H functionalisation chemistry as a fragment elaboration strategy using ADS. Fragment-based discovery had previously been applied in the successful discovery of ATP-competitive ligands for Hsp90. The previously reported fluorescence anisotropy assay for Hsp90 was adapted to enable the development of a high-throughput assay that enabled biologically active fragments and reaction array mixtures to be identified. The NTD of Hsp90 was successfully expressed and characterised by SDS-page and HRMS. BODIPY-labelled geldanamycin was readily synthesised from geldanamycin and was used as the tracer for the fluorescence anisotropy assay. The assay performance was evaluated by performing a series of control experiments with geldanamycin, ATP and ADP.

A series of 29 Hsp90 fragments was designed, by analysing known fragments and ligands, and successfully prepared. The fragments were designed to incorporate as least one potential C-H functionalisation directing group. The fragments were screened in dose response to generate IC_{50} values, which enabled the selection of a subset of fragments for implementation in the reaction arrays. The design, synthesis and screening of the small fragment library enabled the discovery of novel analogues of previously reported Hsp90 fragments, which were subsequently used as substrates in activity-directed synthesis. 15 of the 29 fragments had measurable biological activity against Hsp90, seven of which have not been previously reported as fragments for Hsp90.

The phenol containing fragments were acetate-protected, to minimise reaction interference, for implementation in the C-H functionalisation reaction arrays. The acetate protecting group could be readily removed with the Quadrapure BzA resin in parallel array format. A set of α-diazoamides which incorporated a key Hsp90 fragment was also synthesised, to enable the value of the metal-catalysed carbenoid chemistry to be assessed.

The value of the configured chemistry and established scavenging and deprotection protocols was assessed by implementing them in a series of reaction arrays. The synthesised Hsp90 fragments served as the substrates for ADS and the developed fluorescence anisotropy assay, along with the use of LC-MS, was used to assess the biological activity and success rate of the crude reaction mixtures (Section 5.1.2).

5.1.2 Reaction Array Implementation and Results for Hsp90

A series of reaction arrays was performed implementing both the C-H functionalisation and metal-catalysed carbenoid chemistry. The value of the chemistries for the structure-blind and function-driven elaboration of Hsp90 fragments was explored. The established protocols (Section 5.1.2) enabled reaction arrays to be performed efficiently on microscale in parallel reaction array format, metal catalysts and Michael acceptors to be scavenged, fragment protecting groups to be removed, and the biological activity and

reaction success rate be determined by using the established high-throughput assay and LC-MS.

A total of 1346 reactions was performed using the C-H functionalisation and metal-catalysed carbenoid chemistry in a series of reaction arrays (Table 5.1). The reaction arrays were also assessed to identify the optimal method for designing reaction combinations. For the arrays that harnessed C-H functionalisation chemistry, a total of 1170 reactions was performed at room and at elevated temperatures (60 ^{o}C) and the method for designing reaction combinations was also assessed. For the metal-catalysed carbenoid chemistry, all combinations of reaction components were assessed in both of the arrays performed. The carbenoid arrays were designed and implemented in two approaches; by reaction of Hsp90 fragments with a diverse set of α-diazoamides and by reaction of α-diazoamides bearing an Hsp90 core fragment with a diverse set of co-substrates.

Chemistry Implemented	Reaction Array Temperature	Total Number of Possible Combinations	Array Design	Number of Reactions Performed
C-H Functionalisation	rt	2640	**Matched**: Fragment-Substrate Pairs	240
			Matched: Fragment-Catalyst Pairs	240
			Matched: Catalyst-Substrate Pairs	240
	rt	924	**Matched**: Catalyst-Substrate Pairs	130
	60 ^{o}C	1480	**Matched**: Catalyst-Substrate Pairs	320
Metal-Catalysed Carbenoid	rt	96	**Exhaustive:** Fragments + diazoamides	96
	rt	80	**Exhaustive**: Diazoamide-fragments + co-substrates	80

Table 5.1 *Summary of reaction arrays implemented in activity-directed synthesis to assess C-H functionalisation chemistry and metal-catalysed carbenoid chemistry as function-driven fragment elaboration strategies.*

From the bioactivity data of the screened array mixtures using both sets of chemistry, there were no productive reaction combinations that informed the design of a subsequent array. Observed bioactivity from the reaction mixtures stemmed from unreacted reaction components with low levels of bioactivity. This provided evidence that hits from the workflow would have been identified provided reaction combinations had been productive.

To determine the lack of hits from the reaction mixtures an LC-MS study was performed to assess the success rate of the reactions in the arrays. 10% of the reaction mixtures from the C-H functionalisation and metal-catalysed carbenoid reaction mixtures were analysed, which revealed poorly performing reactions. Reaction mixtures were analysed by searching for potential product masses and roughly 10% of those analysed had masses of potential intermolecular products. The poorly performing reactions in the arrays was

likely a key contributing factor for the lack of biologically active mixtures, provided successful reactions would have indeed led to products with increased bioactivity.

5.2 Discussion and Conclusions

The interest in C-H functionalisation chemistry from the synthetic community has grown rapidly over the last few decades,[82–84] with multiple C-H functionalisation methodology papers reported on a weekly basis. Synthetic methodology papers typically report the substrate scope of the transformation, by varying the positions, sterics and electronics of the various R groups on each of the reaction partners, under the optimal reaction conditions.[53] The substrate scope is typically accompanied by a practical application of the transformation, to demonstrate the potential of the transformation and drive the uptake of the transformation in molecular discovery. Indeed, C-H functionalisation chemistry is often highlighted for its potential to revolutionise molecular discovery by enabling access to disconnections of a target molecule that were not previously possible.[85–87,164,165]

Given the unprecedented era for new synthetic methodologies, the slow uptake of these methodologies in medicinal chemistry workflows for the discovery of novel bioactive molecules is remarkable.[18,53] Indeed, the range of chemical reactions implemented in medicinal chemistry workflows has remained roughly constant (although very slowly increasing) for the last 30 years.[20] This is due, in part, to the requirement for reliable and robust synthetic transformations implemented in discovery workflows to maximise productivity. While new synthetic methodologies report a broad substrate scope under idealised reaction conditions, they often fail to validate the chemistry with highly-functionalised and polar substrates, which are often required for the preparation of drug-like compounds.[18,26,53] Drug molecules typically contain amines, *N*-heterocycles and unprotected polar groups.[18] Indeed, such reactions with highly-functionalised substrates systematically fail under the model reaction conditions, leading to logP drift, in which the final synthesised library of molecular compounds is typically more lipophilic than the initially deigned library.[27]

The poor performance of synthetic methodologies with highly-functionalised substrates has led to the development and implementation of high-throughput nano/microscale reaction optimisation into medicinal chemistry workflows.[60] Exemplar studies have seen the reaction optimisation of palladium cross-couplings (C-C, C-O, C-N and C-S) with highly-functionalised substrates in batch[57] and flow-based[58] systems. Multiple reaction parameters were explored, such as catalyst, base, reagent stoichiometry and catalyst loading, to enable a broader scope of substrates to be used, enabling a greater number of compounds to be successfully prepared thus increasing the value of the specific reaction class. This is highlighted in the nanoscale synthesis and affinity ranking of CHK1 inhibitors, in which under a single reaction condition (per reaction class) just 158 of 384 target compounds were successfully prepared.[68] By exploring four sets of reactions conditions (per reaction class) 345 of the 384 target compounds were prepared. For reactions to be successful with highly-functionalised substrates, a range of catalyst systems and reaction conditions typically need to be investigated for each combination of substrate.

Studies have also been performed that enable sufficiently robust reactions that are fit for purpose to be identified. Robustness screens allow the functional group tolerance of a reaction to be assessed by the use of additives under the standard reaction conditions.[53] Reporting a robustness screen alongside the publication of new synthetic methodologies can enable sufficiently robust transformation to be identified and adopted. It is clear from the ADS study with C-H functionalisation chemistry, significant optimisation of reaction conditions for each combination of substrate would be required. For future or novel synthetic transformations to be adopted and harnessed in the discovery of novel bioactive small molecules within in such discovery platforms, the chemical methodology itself must robust and be tolerant to a broad range of functional groups.

5.3 Outlook for Future Activity-Directed Syntheses

While the reaction arrays themselves failed to deliver reaction mixtures with significant biological activity that would have enabled the discovery of

new bioactive ligands against Hsp90, the study lead to a series of positive outcomes which could prove useful for future studies. Firstly, an optimised workflow for performing high-throughput parallel reaction arrays was established. The adoption of microvials has enabled parallel reactions to be performed at room and elevated temperatures, demonstrated by the successful replication of literature C-H functionalisation reactions in microscale format. The use of scavenger resins, in particular Quadrapure BzA, can be used for the parallel removal of metal catalysts and Michael acceptors from reaction mixtures. The study also demonstrated that if protection of polar groups is required to minimise potential reaction interference, the deprotection in parallel can readily be performed. The optimised workflow could be readily transferred for alternative reaction classes in activity-directed synthesis, which can be used in the discovery of novel bioactive small molecules against a range of biological targets.

The discovery of novel ligands of Hsp90 through ADS proved challenging, however a series of novel analogues of previously reported fragments was identified from the fragment screen. The high-throughput assay was readily established and enabled the identification of bioactivity, all be it from the unreacted reaction components, from crude reaction mixtures.

To enable Hsp90 ligands to be discovered in activity-directed synthesis, alternative chemistry could be implemented, such as the use of photoredox chemistry. The use of photoredox-mediated C-H functionalisation for fragment elaboration has been reported in high-throughput format.[31] The study demonstrated the cross dehydrogenative heteroarylation of cyclic amines. As a strategy for the discovery of novel ligands of Hsp90, a fragment screen of heteroarenes could be performed (heteroarenes could potentially mimic the binding mode of the ADP/ATP core) to identify novel Hsp90 fragments which can then be coupled in high-throughput to a broad range of cyclic amines, which upon screening in the assay, enable the identification of productive reaction combinations (Figure 5.1).

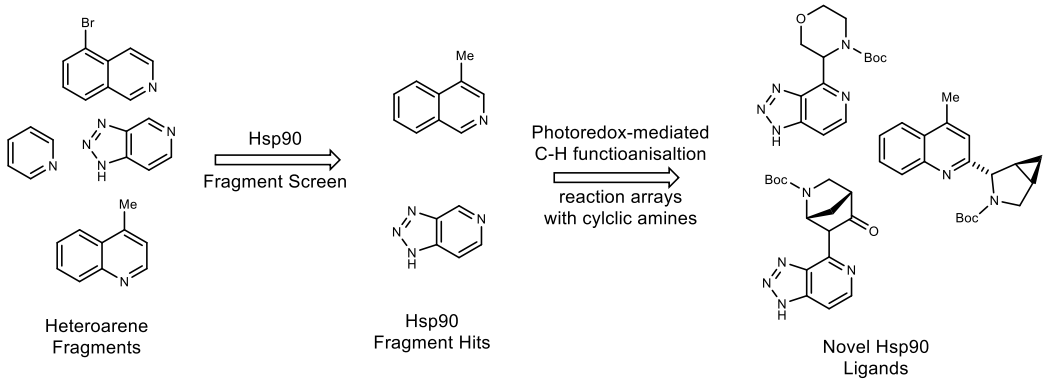

Figure 5.1 *Potential future study implementing photoredox C-H functionalisation of heteroarenes with cyclic amines for Hsp90 ligand discovery in activity-directed synthesis.*

Chapter 6.
Experimental

6.1 General Information and Instrumentation

Commercially available starting materials were obtained from Sigma−Aldrich, Acros, Fluorochem, Alfa Aesar, Fisher Scientific, Enamine BB (EU), SLS (Scientific Laboratory Supplies) and Insight Biotechnology. All non-aqueous reactions were performed under a nitrogen atmosphere unless otherwise stated. Water-sensitive reactions were performed in anhydrous solvents in oven-dried glassware and cooled under nitrogen before use. Anhydrous dichloromethane (DCM), anhydrous tetrahydrofuran (THF), anhydrous toluene, anhydrous diethyl ether, anhydrous ethanol, anhydrous methanol and anhydrous acetonitrile were obtained from a PureSolv MD5 Purification System. Anhydrous dimethyl sulfoxide (DMSO), anhydrous 1,2-dichloroethane, anhydrous dimethylformamide (DMF) and anhydrous 1,4-dioxane were obtained from SureSeal bottles from Sigma−Aldrich. All other solvents used were of chromatography or analytical grade. Petrol refers to petroleum spirit (b.p. 40–60 °C) and ether refers to diethyl ether. Solvents were removed under reduced pressure using a Büchi rotary evaporator and Vacuubrand PC2201 Vario diaphragm pump.

Thin layer chromatography (TLC) was performed using aluminium backed silica (Merck silica gel 60 F254) plates obtained from Merck. Ultraviolet light (λ_{max} = 254 nm) and $KMnO_4$ were used for visualization. Flash column chromatography was performed using silica gel 60 (35-70 µm particles) supplied by Merck. Infrared spectra were recorded using a Bruker Alpha-P ATR FR-IR Spectrometer. Absorptions are reported in wavenumbers (cm^{-1}).

Analytical LCMS was performed using two systems. An Agilent 1200 series LC system comprising a Bruker HCT Ultra ion trap mass spectrometer, a high vacuum degasser, a binary pump, a high performance autosampler and a micro well plate autosampler, an autosampler thermostat, a thermostated column compartment and a diode array detector. The system used a Phenomenex Luna C18 50 x 2 mm 5 micron column with two solvent systems:

MeCN/H_2O + 0.1% formic acid or MeCN/H_2O. Secondly, an Ultimate3000 HPLC instrument with a Bruker Amazon Speed MS Detector with electrospray ionization. The system ran with a positive and negative switching mode and UV diode array detector using a Phenomenex Kinetex C18 column (2.6 micron, 2.1x50mm) and gradient elution H_2O and MeCN each plus 0.1% formic acid. Accurate mass spectrometry was performed using electrospray ionisation on a Bruker MaXis Impact spectrometer.

Proton (^{1}H) and carbon (^{13}C) NMR data was collected on Bruker 300, 400, 500 or 500-CP(cryoprobe) MHz spectrometers using an internal deuterium lock. Data was collected at 300 K unless otherwise stated. Chemical shifts (δ) are given in parts per million (ppm) and referenced to the residual solvent peak. Coupling constants (*J*) are reported in Hertz (Hz) and splitting patterns are reported in an abbreviated manner: app. (apparent), s (singlet), d (doublet), t (triplet), q (quartet), sext. (sextet), hept. (heptet), m (multiplet) and br (broad). NMR data was reported in the format: ppm (number of protons, splitting pattern, coupling constant (Hz), proton ID). Assignment of signals was aided by the use of DEPT 135, COSY, HMQC, HMBC and NOESY.

6.2 Chemistry

6.2.1 General Procedures

General Procedure (A) for Evaluation of Reported C-H Functionalisation Microscale Reactions in parallel format

Reactions were performed using 0.75 mL borosilicate glass vials (8 x 30 mm, Chemglass #CV-7000-0830). Substrates refers to the reactant bearing the directing group for C-H functionalisation and co-substrate refers to the functionalisation reaction partner. Substrates and co-substrates stocks were prepared in CH_2Cl_2 at 100 mM and 200 mM respectively and 100 μL of one of each was added to the vial of interest and the solvent allowed to evaporate. Catalyst-system stock solutions were prepared at 5 mM, with respect to catalyst, in the appropriate solvent system with reaction additives prepared in the same ratio to catalyst as reported (Table 6.3). 100 μL of the catalyst-system solution was added to the vial of interest, to give final concentration of

substrate, co-substrate and catalyst of 100 mM, 200 mM and 5 mM respectively and the reactions sealed and allowed to react at rt for 24 h. Reaction mixtures were analysed via LC-MS, by preparing 5 mM stock solutions in MeCN.

General Procedure (B) for Evaluation of Heated Parallel Microscale Reactions

Reactions were performed sealed using 0.75 mL borosilicate glass vials (8 x 30 mm, Chemglass #CV-7000-0830) and sealed using an OptiBlock Parallel Synthesis Reaction Block (Chemglass #OP-5000-01) and PTFE-Faced Silicone Septa Pads (Chemglass #OP-5000-60). Substrates and co-substrates stocks were prepared in CH_2Cl_2 at 100 mM and 200 mM respectively and 100 μL of one of each was added to the vial of interest and the solvent allowed to evaporate. Catalyst-system stock solutions were prepared at 5 mM, with respect to catalyst, in the appropriate solvent system with reaction additives prepared in the same ratio to catalyst as reported (Table 6.3). 100 μL of the catalyst-system solution was added to the vial of interest, to give final concentration of substrate, co-substrate and catalysts of 100 mM, 200 mM and 5 mM respectively and the reactions sealed and heated at 60 ^{o}C for 24 h. Reaction mixtures were analysed via LC-MS by preparing 5 mM stock solutions in MeCN.

General Procedure (C) for Michael Acceptor Scavenging Screen

The scavenging capabilities of the functionalised solid-support resins was determined by performing a screen on a model set of Michael acceptors with varying electrophilicities. A stock solution of the corresponding Michael acceptor (0.15 mmol) and an internal standard, 2,4,5-trichloro-methoxybenzene (0.15 mmol) in $CDCl_3$ (5 mL) was prepared and aliquoted (5 x 1 mL, 0.03 mmol of Michael acceptor and 0.03 mmol of standard per 1 mL). The ^{1}H NMR spectrum of one aliquot was recorded to serve as the unscavenged reference spectrum. To the remaining four aliquots was added one of the functionalised resins (2-3 eq. depending on resin loading) and left

to scavenge for 24 h. The reaction mixtures were filtered and a ^{1}H NMR spectrum of the filtrate recorded. The peaks for the Michael acceptor in the unscavenged and scavenged were integrated relative to the internal standard to determine the amount of Michael acceptor scavenged from solution.

General Procedure (D) for Metal Catalyst Scavenging Screen

The metal scavenging capabilities of the Quadrapure BzA solid-supported resin was assessed by performing a screen against a range of metal catalysts. 5mM stock solutions of each of the appropriate metal catalysts (see Section 3.1.3.2) were prepared, 2.5 moles in 500 µL of CH_2Cl_2, and aliquoted (5 x 100 µL). To each solution was added increasing amounts of the Quadrapure BzA resin (0 mg, 10 mg, 20 mg, 30 mg and 40 mg) and left to scavenge for 24 h. Reaction solutions were filtered, washed with CH_2Cl_2 (5 x 100 µL), left to evaporate overnight and then desiccated for a further 24 h. Scavenged mixtures were screened in the biological assay to determine the effect of residual metal catalysts in the assay.

General Procedure (E) for Literature Reaction Scavenging

The scavenging capabilities of the Quadrapure BzA solid-supported resin was tested on a model C-H functionalisation reaction as followed. A solution of *n*Butyl acrylate (14.3 µL, 100 mM), 3-methylacetanilide (15.0 mg, 100 mM), 1,4-benzoquinone (5.50 mg, 50.0 mM), *para*-toluenesulphonic acid (9.50 mg, 50.0 mM), $Pd(OAc)_2$ (1.10 mg, 5.00 mM) and 2,4,5-trichloro-methoxybenzene (4.20 mg, 20.0 mM) in $CDCl_3$ (986 µL) was left to react at rt for 24 h. Aliquots (5 x 100 µL) were taken and to each was added increasing amounts of Quadrapure BzA (0 mg, 10 mg, 20 mg, 30 mg or 40 mg) and left to scavenge for 48 h at rt. The aliquoted reaction mixtures were each filtered, washed with $CDCl_3$ (5 x 100 µL) and the samples analysed by ^{1}H NMR (300 MHz) spectroscopy.

General Procedure (F) for Amide Couplings

To a solution of benzoic acid, DIPEA (2.00 eq.), TBTU (2.00 eq.) in CH_2Cl_2 (10 mL/mmol) was added amine (2.00 eq.) and the reaction mixture stirred at rt overnight. The reaction mixture was diluted with H_2O (10 mL/mmol), extracted with CH_2Cl_2 (3 x 10 mL) washed with brine (3 x 10 mL), dried ($MgSO_4$) and concentrated under reduced pressure. The crude residue was purified using column chromatography.

General Procedure (G) for Acetylation of Phenols

A solution of phenol (1.00 eq.) in Ac_2O (26.0 eq.) and pyridine (31.0 eq.) was stirred at rt for 18 h. The reaction mixture was evaporated under reduced pressure by addition of toluene (3X). The crude mixture was dissolved in CH_2Cl_2: 10% (w/v) copper (II) sulphate solution (50:50) and stirred for 10 min. The aqueous layer was extracted with CH_2Cl_2, dried ($MgSO_4$) and concentrated to give the acetate protected phenol.

General Procedure (H) for Deacetylation of Phenols

To a stirred solution of acetate protected phenol (0.2 mmol) in MeOH:THF (2:1, 1.5 mL), was added a solution of sodium carbonate (25 mg) in H_2O (0.5 mL) and stirred overnight. The reaction mixture was concentrated under reduced pressure and the residue partitioned between EtOAc and H_2O, the organics washed with brine, dried ($MgSO_4$) and concentrated under reduced pressure to yield the deprotected phenol.

General Procedure (I) for Deacetylation of Phenols in Parallel Arrays

To a vial charged with acetate protected phenol (0.01 mmol) was added MeOH:THF (2:1, 75.0 μL), followed by addition of sodium carbonate solution (25.0 μL, 470 mM). The reaction mixture was left for 24 h, left open to the air to evaporate for 24 h and then desiccated for 24 h. Subsequent analysis by LC-MS and ^{1}H NMR (300 MHz) spectroscopy revealed the deprotected phenol.

General Procedure (J) for Deacetylation of Phenols in Parallel Arrays

To a vial charged with acetate protected phenol (0.01 mmol) in chloroform (100 μL) was added Quadrapure BzA resin (30.0 mg) and the solution left for 24 h. Subsequent analysis by LC-MS and ^{1}H NMR (300 MHz) spectroscopy revealed the deprotected phenol.

General Procedure (K) for LCMS Analysis of Crude Reaction Arrays Mixtures

Crude reaction array mixtures (100 mM in DMSO) were analysed by LC-MS by preparing 5 mM stocks in MeCN (100 μL) and ran with a positive and negative switching mode and UV diode array detector using a Phenomenex Kinetex C18 column (2.6 micron, 2.1x50mm) and gradient elution H_2O and MeCN each plus 0.1% formic acid. Reactions were analysed for conversion to products by searching for the bimolecular reaction mass minus the mass of H-X (X = H, Cl, Br, I or $B(OH)_2$).

6.2.2 Implementation of Reaction Arrays

6.2.2.1 C-H Functionalisation Reaction Arrays

Reaction arrays were performed in 0.75 mL borosilicate glass vials (8 x 30 mm, Chemglass #CV-7000-0830) in 96-vial (12 x 8) array format and sealed with PTFE snap plugs. Fragments, substrates and catalyst stock solutions were prepared as shown in Tables 6.1**,** 6.2 and 6.3 respectively. To each vial was added one fragment (100 μL) and one substrate (100 μL) and the solvent allowed to evaporate. Catalyst-system stock solutions (100 μL) were added to the vial of interest and capped, to give a final reaction concentration of 100 mM fragment, 200 mM substrate and 5 mM of catalyst (see Table 6.3 for additive concentrations) and reactions left at rt for 48 h. After 48 h the reaction solvent was allowed to evaporate open to air for 24 h, CH_2Cl_2 (200 μL) was added along with Quadrapure BzA resin (30.0 mg), reaction mixtures capped and left to scavenge for 24 h. Reaction mixtures were filtered, washed with CH_2Cl_2 (3 x 100 μL), CH_2Cl_2 evaporated open to air followed by desiccation

and finally reaction mixtures dissolved in DMSO (100 μL) to give a final total product concentration (with respect to fragment) of 100 mM.

For heated reaction arrays, stock components and reactions were prepared and performed identically as described, except the reactions were sealed using an OptiBlock Parallel Synthesis Reaction Block (Chemglass # OP-5000-01) and PTFE-Faced Silicone Septa Pads (Chemglass #OP-5000-60) and heated to 60 °C, scavenged, filtered and dissolved in DMSO (100 μL) to give a final total product concentration (with respect to fragment) of 100 mM.

Reaction Array Components Implemented in Room Temperature Array and Heated Array 1:

Fragments (Set 1) (Prepared in CH_2Cl_2)

Fragment	MW	Stock Conc. (mM)	Fragment	MW	Stock Conc. (mM)
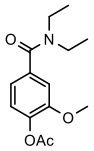 **F1**	265.1	100	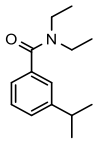 **F2**	219.2	100
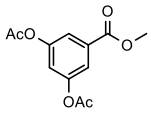 **F3**	257.0	100	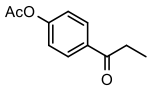 **F4**	192.1	100
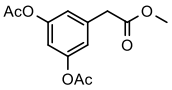 **F5**	266.1	100	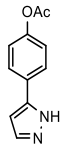 **F6**	202.1	100
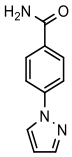 **F7**	187.1	100	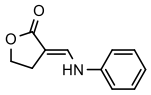 **F8**	189.1	100
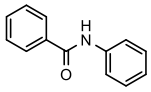 **F9**	197.1	100	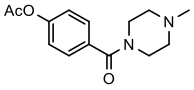 **F10**	262.1	100

Table 6.1 *Fragment stock concentrations prepared in CH_2Cl_2 implemented in ADS reaction arrays*

Substrates (Set 1)

Substrate	MW	Stock Conc. (mM)	Solvent	Substrate	MW	Stock Conc. (mM)	Solvent
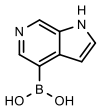 **S1**	162.0	200	MeOH	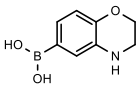 **S2**	179.0	200	MeOH
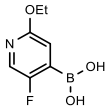 **S3**	185.0	200	MeOH	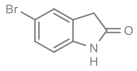 **S4**	212.1	200	Insoluble*
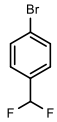 **S5**	207.0	200	Acetone	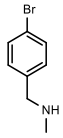 **S6**	200.1	200	Acetone
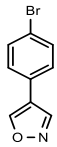 **S7**	224.1	200	Acetone	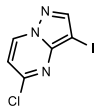 **S8**	279.5	200	CH_2Cl_2
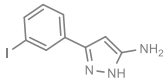 **S9**	285.1	200	Insoluble*	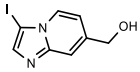 **S10**	274.1	200	CH_2Cl_2
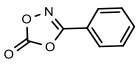 **S11**	163.1	200	Acetone	 **S12**	101.1	-	Not Prepared†
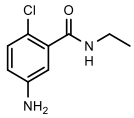 **S13**	198.7	200	CH_2Cl_2	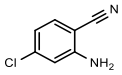 **S14**	152.6	200	Acetone
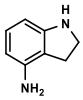 **S15**	134.2	200	Acetone	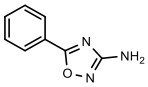 **S16**	161.2	200	Acetone
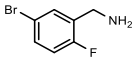 **S17**	204.0	200	CH_2Cl_2	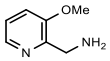 **S18**	138.2	200	Acetone
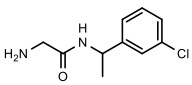 **S19**	212.1	200	Acetone	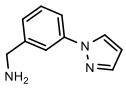 **S20**	173.2	200	Acetone
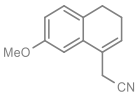 **S21**	199.3	200	Insoluble*	 **S22**	105.1	200	Acetone
 **S23**	71.1	200	Acetone	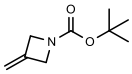 **S24**	169.2	200	Acetone
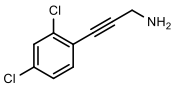 **S25**	200.1	200	CH_2Cl_2	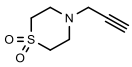 **S26**	173.2	200	Acetone

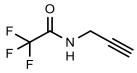 **S27**	151.1	200	Acetone	 **S28**	56.1	200	Acetone
 **S29**	135.2	200	Acetone	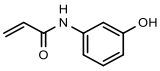 **S30**	163.2	200	Acetone
 **S31**	99.1	200	Acetone	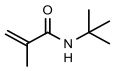 **S32**	141.1	200	Acetone
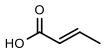 **S33**	86.1	200	Acetone				

Table 6.2 *Substrate stock concentrations prepared in MeOH, Acetone or CH_2Cl_2 implemented in ADS reaction arrays (*Insoluble in CH_2Cl_2, Acetone, MeOH, MeCN, Toluene, EtOAc, DCE, Ether and Pentane, † Volatile)*

Catalysts

Catalyst System	Component	MW	Stock Conc. (mM)	Solvent
C1[160]	$Pd(OAc)_2$ $(NH_4)_2S_2O_8$	224.5 228.2	5 200	TFA
C2[101]	$Pd(OAc)_2$ Ac-Ile-OH Ag_2CO_3 $CsCO_3$	224.5 173.2 275.7 325.8	5 5 50 50	HFIP
C3[106]	$Pd(OAc)_2$ Benzoquinone	224.5 108.1	5 200	CH_2Cl_2:^{i}PrOH (50:50)
C4[94]	$Pd(OAc)_2$ Benzoquinone TsOH	224.5 108.1 172.2	5 100 50	AcOH:Toluene (2:1)
C5[161]	$[Cp^*RhCl_2]_2$ CsOAc HOAc	618.1 192.0 60.1	5 25 120	MeOH
C6[98]	$[Ru(p\text{-cymene})Cl_2]_2$ $AgSbF_6$ $Cu(OAc)_2.H_2O$	612.4 343.6 181.6	5 200 200	Dioxane
C7[95]	$IrCp^*(OAc)_2$ $AgNTf_2$ $Cu(OAc)_2.H_2O$	446.0 338.0 181.6	5 200 50	1,2-DCE
C8[104]	$[Cp^*IrCl_2]_2$ $AgNTf_2$ $Cu(OAc)_2.H_2O$	796.7 388.0 181.6	5 200 50	1,2-DCE:HFIP (50-:50)

Table 6.3 *Catalyst system stock concentrations prepared in reaction solvent implemented in ADS reaction arrays*

Reaction Array Components Implemented in Chemistry-Targeted Heated Array 2 (Fragments **F7** and **F8** were prepared and used as described previously along with fragments **F11**-**F16**, Catalyst systems **C2**, **C4**, **C6**, **C7** and **C8** which were matched with substrates (**R1**-**R37**) below based on literature reactions):

Fragments (Set 2) (Prepared in CH_2Cl_2)

Fragment	MW	Stock Conc. (mM)	Fragment	MW	Stock Conc. (mM)
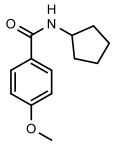 **F11**	219.3	100	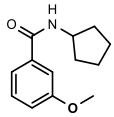 **F12**	219.3	100
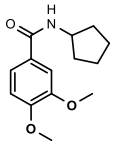 **F13**	249.3	100	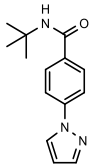 **F14**	243.3	100
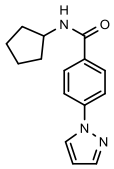 **F15**	255.3	100	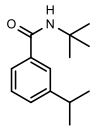 **F16**	219.3	100
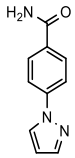 **F7**	187.1	100	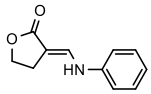 **F8**	189.1	100

Table 6.4 *Fragment stock concentrations prepared in CH_2Cl_2 implemented in ADS heated reaction arrays at 60 ºC*

Substrates (Set 2)

Substrate	MW	Stock Conc. (mM)	Solvent	Substrate	MW	Stock Conc. (mM)	Solvent
Substrates for C4							
 **R1**	71.1	200	CH_2Cl_2	 **R2**	57.1	200	CH_2Cl_2
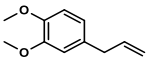 **R3**	178.2	200	CH_2Cl_2	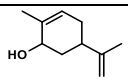 **R4**	152.2	200	CH_2Cl_2
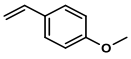 **R5**	134.2	200	CH_2Cl_2	 **R6**	100.1	200	CH_2Cl_2
 **R7**	139.2	200	CH_2Cl_2	 **R8**	86.1	200	CH_2Cl_2
Substrates for C6							
 **R1**	71.1	200	CH_2Cl_2	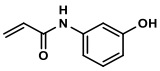 **R9**	163.2	200	CH_2Cl_2
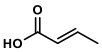 **R10**	86.1	200	CH_2Cl_2	 **R7**	139.2	200	CH_2Cl_2

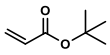 **R11**	128.2	200	CH_2Cl_2	 **R12**	86.1	200	CH_2Cl_2
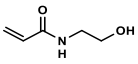 **R13**	115.1	200	CH_2Cl_2	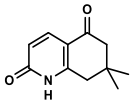 **R14**	119.2	200	CH_2Cl_2
Substrates for C7							
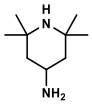 **R15**	156.3	200	CH_2Cl_2	 **R2**	57.1	200	CH_2Cl_2
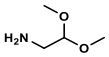 **R16**	105.1	200	CH_2Cl_2	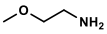 **R17**	75,1	200	CH_2Cl_2
 **R18**	73.1	200	CH_2Cl_2	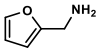 **R19**	91.1	200	CH_2Cl_2
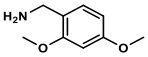 **R20**	167.2	200	CH_2Cl_2	 **R21**	71.1	200	CH_2Cl_2
Substrates for C2							
 **R22**	272.9	200	CH_2Cl_2	 **R23**	158.0	200	CH_2Cl_2
 **R24**	182.2	200	CH_2Cl_2	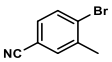 **R25**	196.1	200	CH_2Cl_2
 **R26**	187.0	200	CH_2Cl_2	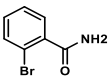 **R27**	200.0	200	CH_2Cl_2
 **R28**	176.0	200	CH_2Cl_2	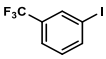 **R29**	272.0	200	CH_2Cl_2
Substrates for C8							
 **R30**	161.1	200	CH_2Cl_2	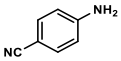 **R31**	118.1	200	CH_2Cl_2
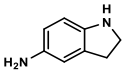 **R32**	134.2	200	CH_2Cl_2	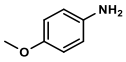 **R33**	123.2	200	CH_2Cl_2
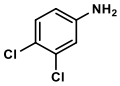 **R34**	162.0	200	CH_2Cl_2	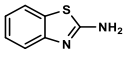 **R35**	150.2	200	CH_2Cl_2
 **R36**	94.1	200	CH_2Cl_2	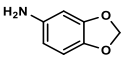 **R37**	137.1	200	CH_2Cl_2

Table 6.5 *Substrates (**R1**-**R37**) prepared at the final reaction concentration for implementation in ADS reaction arrays. Substrates were matched to their respective catalysts based on known literature reactions.*

6.2.2.2 Fragment and α-Diazoamide Reaction Arrays

Reaction arrays for the proposed elaboration of fragments with α-diazoamides under rhodium catalysis were performed by preparing fragment and diazoamide stocks at 200 mM in CH_2Cl_2 and catalysts stocks at 12.5 mM in THF. To the reaction vial of interest was added one fragment (50.0 μL) and catalyst (8.00 μL) and the solvent allowed to evaporate. Finally one diazoamide was added (100 μL) to each reaction vial to give a final concentration of fragment (100 mM), α-diazoamide (200 mM) and catalyst (1.00 mM). Reaction vials were capped and left for 24 h at rt, followed by addition of Quadrapure TU (30.0 mg) to each vial and reaction mixtures left to scavenge at rt for 24 h. Reaction mixtures were filtered, solvent allowed to evaporate open to air followed by desiccation and reaction mixtures dissolved in DMSO (100 μL) to give a final total product concentration (with respect to fragment) of 100 mM.

Fragments (Set 3) (Prepared in CH_2Cl_2)

Fragment	MW	Stock Conc. (mM)	Fragment	MW	Stock Conc. (mM)
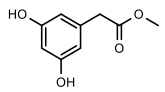 **89**	182.2	200	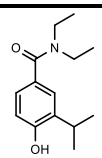 **90**	235.3	200
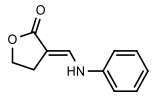 **91**	189.2	200	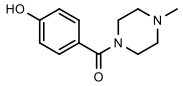 **92**	220.3	200

Table 6.6 *Fragment stock concentrations prepared in CH_2Cl_2 implemented in ADS metal-catalysed carbenoid reaction arrays.*

Rhodium Catalysts (Prepared in THF)

Catalyst	MW	Stock Conc. (mM)	Catalyst	MW	Stock Conc. (mM)
$[(CF_3CF_2CF_2CO_2)_2Rh]_2$ **C9**	1057.9	12.5	$Rh_2(OPiv)_4$ **C10**	610.3	12.5

Table 6.7 *Catalysts stock concentrations prepared in CH_2Cl_2 implemented in ADS metal-catalysed carbenoid reaction arrays*

α-Diazoamide Substrates (Prepared in CH_2Cl_2 From Nelson library, prepared by Nelson group members)

α-Diazoamide	MW	Stock Conc. (mM)	α-Diazoamide	MW	Stock Conc. (mM)
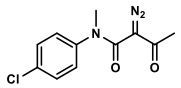 **D1**	251.7	200	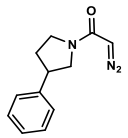 **D2**	215.3	200
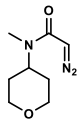 **D3**	183.2	200	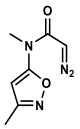 **D4**	180.2	200
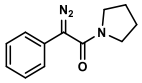 **D5**	215.3	200	 **D6**	155.2	200
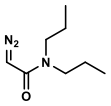 **D7**	169.2	200	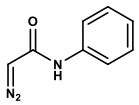 **D8**	161.2	200
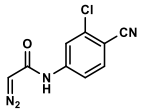 **D9**	220.6	200	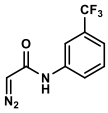 **D10**	229.2	200
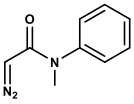 **D11**	175.2	200	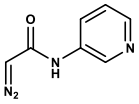 **D12**	162.2	200

Table 6.8 *α-Diazoamide substrates stock concentrations prepared in CH_2Cl_2 implemented in ADS metal-catalysed carbenoid reaction arrays.*

6.2.2.3 α-Diazoamide-Fragment and Co-Substrate Reaction Arrays

Reaction arrays for the proposed elaboration of α-diazoamides bearing an Hsp90 motif with a range of co-substrates under rhodium catalysis were performed by preparing α-diazoamide and co-substrate stocks at 100 mM and 200 mM in CH_2Cl_2 respectively and catalysts stocks at 12.5 mM in THF. To the reaction vial of interest was added one co-substrate (100 μL) and catalyst (8.00 μL) and the solvent allowed to evaporate. Finally one α-diazoamide fragment was added (100 μL) to each reaction vial to give a final concentration α-diazoamide fragment (100 mM), co-substrate (200 mM) and catalyst (1.00 mM). Reaction vials were capped and left for 24 h at rt, followed by addition of Quadrapure TU (30.0 mg) to each vial and reaction mixtures left to scavenge at rt for 24 h. Reaction mixtures were filtered, solvent allowed to evaporate open to air followed by desiccation and reaction mixtures dissolved

in DMSO (100 μL) to give a final total product concentration (with respect to fragment) of 100 mM.

α-Diazoamide fragments prepared in CH_2Cl_2

α-Diazoamide Fragment	MW	Stock Conc. (mM)	α-Diazoamide Fragment	MW	Stock Conc. (mM)
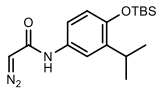 **DF1**	333.5	100	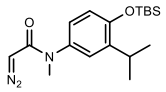 **DF1**	347.5	100

Table 6.9 *α-Diazoamide fragments stock concentrations prepared in CH_2Cl_2 implemented in ADS metal-catalysed carbenoid reaction arrays*

Co-Substrates prepared in CH_2Cl_2

Co-Substrate	MW	Stock Conc. (mM)	Co-Substrate	MW	Stock Conc. (mM)
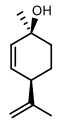 **CS1**	152.1	200	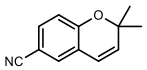 **CS2**	185.1	200
 **CS3**	69.1	200	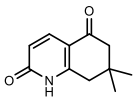 **CS4**	191.1	200
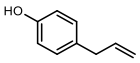 **CS5**	134.2	200	 **CS6**	84.02	200
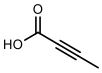 **CS7**	84.02	200	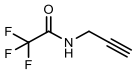 **CS8**	151.0	200
 **CS9**	100.1	200	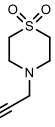 **CS10**	173.1	200
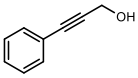 **CS11**	132.1	200	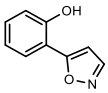 **CS12**	161.1	200
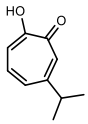 **CS13**	164.1	200	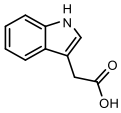 **CS14**	175.2	200
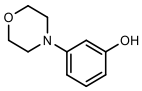 **CS15**	179.2	200	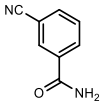 **CS16**	146.1	200
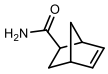 **CS17**	137.1	200	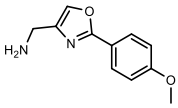 **CS18**	204.1	200

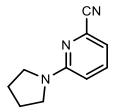 CS19	173.1	200	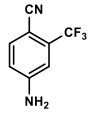 CS20	186.1	200

Table 6.10 *Co-substrate stock concentrations prepared in CH_2Cl_2 implemented in ADS metal-catalysed carbenoid reaction arrays*

6.2.3 Compound Data

Butyl (2E)-3-(2-acetamido-4-methylphenyl)prop-2-enoate, 68

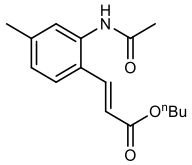

68

*n*Butyl acrylate (0.42 mL, 3.00 mmol) in toluene (2.25 mL) was added at rt to a suspension of 3-methylacetanilide (448 mg, 3.00 mmol), $Pd(OAc)_2$ (15.0 mg, 0.06 mmol), benzoquinone (324 mg, 3.00 mmol) and *p*-toluene sulfonic acid monohydrate (286 mg, 3.00 mmol) in acetic acid (4.5 mL) and the mixture stirred at rt overnight. After 16 h the reaction mixture was diluted with diethyl ether (15 mL) and neutralised with aqueous NaOH solution (2.0 M). The aqueous phase was extracted with diethyl ether (3 × 15 mL) and the combined organic phases washed with water (3 × 15 mL), dried ($MgSO_4$), and concentrated under reduced pressure to give the crude product which was purified by flash column chromatography eluting with 50:50 petroleum ether-ethyl acetate to give the enoate **68**[94] (452 mg, 55%) as a colourless solid, R_f = 0.31 (50:50, Petroleum ether−ethyl acetate); δ_H (500 MHz; $CDCl_3$) 7.84 (1H d, *J* 15.8, 3-H), 7.65 (1H, s, phenyl 3-H), 7.53 (1H, d, *J* 8.0, phenyl 6-H), 7.21 (1H, br s, NH) 7.09 (d, *J* 8.0, phenyl 5-H), 6.44 (1H, d, *J* 15.8, 2-H), 4.27 (2H, t, *J* 6.7, butyl 1-H_2), 2.43 (3H, s, acetamide-H_3), 2.30 (3H, s, methylphenyl-H_3), 1.75 (2H, p, *J* 6.7, butyl 2-H_2), 1.50 (2H, h, *J* 7.4, butyl 3-H_2) and 1.03 (3H, t, *J* 7.4, butyl 4-H_3); δ_C (125 MHz; $CDCl_3$) 168.7, 167.0, 141.5, 139.0, 135.7, 127.0, 125.7, 125.1, 124.8, 119.6, 64.6, 30.8, 24.2, 21.5, 19.2 and 13.7; ν_{max}/cm^{-1} (film) 3269, 2957, 2931, 2871, 1709, 1657, 1626, 1570 and 1534; HRMS Found MH^+: 276.1601. ($C_{16}H_{21}NO_3$ requires *MH,* 276.1600).

Butyl 2-(3,3-dimethyl-2,3-dihydro-*1H*-isoindol-1-yl)acetate, 44

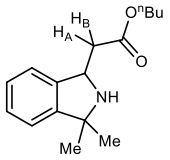

44

Cumylamine (68.0 mg, 0.5 mmol) and *n*butyl acrylate (128 mg, 1.0 mmol) were added at rt to a suspension of [Ru(*p*-cymene)Cl_2]$_2$ (15.0 mg, 0.025 mmol), silver hexafluoroantimonate (35.0 mg, 0.10 mmol) and copper (II) acetate monohydrate (200 mg, 1.00 mmol) in dioxane (3 mL). The mixture was stirred for 6 h under nitrogen atmosphere at rt. The mixture was diluted with saturated aqueous sodium bicarbonate solution (40 mL) containing ethylenediamine (1 mL) and then extracted with ethyl acetate (2 × 40 mL). The combined organic layers were dried (Na_2SO_4) and concentrated under reduced pressure to give the crude product which was purified by flash column chromatography, eluting with 50:50 hexane-ethyl acetate to give the acetate **44**[98] (37.0 mg, 28%) as a colourless viscous oil, R_f = 0.21 (50:50, hexane−ethyl acetate); δ_H (500 MHz; $CDCl_3$) 7.26-7.20 (2H, m, isoindolyl 6-H and 7-H), 7.16-7.11 (2H, m, isoindolyl 5-H and 8-H), 4.83 (1H, dd, *J* 8.9 and 4.2, isoindolyl 1-H), 4.16-4.08 (2H, m, butyl 1-H_2), 2.88 (1H, dd, *J* 16.0 and 4.2, acetate 2-H_A), 2.60 (1H, dd, *J* 15.9 and 8.9, acetate 2-H_B), 2.23 (1H, br s, NH), 1.65-1.57 (2H, m, butyl 2-H_2), 1.48 (3H, s, Me), 1.42-1.33 (2H, m, butyl 3-H_2), 1.38 (3H, s, Me) and 0.93 (3H, t, *J* 7.4, butyl 4-H_3); δ_C (125 MHz; $CDCl_3$) 172.3, 149.7, 141.8, 127.5, 126.9, 121.9, 121.3, 64.5, 62.9, 57.4, 41.8, 30.7, 29.9, 19.2 and 13.7; v_{max}/cm^{-1} (film) 2960, 2933, 2872, 1728, 1667 and 1606; HRMS Found MH^+: 262.1809. ($C_{16}H_{23}NO_2$ requires *MH* 262.1808).

The reaction was repeated as stated but under atmospheric conditions to yield the crude product which was purified by flash chromatography, eluting with 50:50 hexane-ethyl acetate to give the acetate **44** (100 mg, 76%) as a colourless viscous oil with spectroscopically identical data to that obtained previously.

tert-Butyl 2-[(1E)-3-butoxy-3-oxoprop-1-en-1-yl]-1H-pyrrole-1-carboxylate, 56

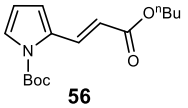

56

$Pd(OAc)_2$ (48.0 mg, 0.20 mmol), *n*butyl acrylate (286 µL, 2.00 mmol), *N*-boc pyrrole (670 µL, 4.00 mmol), and benzoquinone (218 mg, 2.00 mmol) were added to a mixture of acetic acid/dioxane/DMSO (3:9:1, 10 mL) in a round-bottom flask and stirred at rt under atmospheric conditions for 96 h. The reaction mixture was diluted with diethyl ether (50 mL), water (20 mL) and filtered through a plug of celite and the organic phase dried ($MgSO_4$) and concentrated under reduced pressure to yield the crude product which was purified using flash column chromatography eluting with 75:25, hexane−diethyl ether to yield the carboxylate **56**[90] as a colourless oil (150 mg, 26%), R_f = 0.25 (75:25 hexane−diethyl ether); δ_H (500 MHz; $CDCl_3$) 8.27 (1H, d, *J* 15.9, propenyl 1-H), 7.39 (1H, d, *J* 3.5, pyrrole 5-H), 6.69 (1H, d, *J* 3.5, pyrrole 3-H), 6.21 (1H, d, *J* 15.9, propenyl 2-H), 6.21 (1H, t, *J* 3.5, pyrrole 3-H), 4.18 (2H, t, *J* 7.0, Butyl 1-H_2), 1.66 (3H, quin, *J* 7.0, butyl 2-H_2), 1.62 (s, 9H, tert-butyl H_9), 1.42 (sext, *J* 7.4, butyl 3-H_2) and 0.95 (3H, t, *J* 7.4, butyl 4-H_3); δ_C (125 MHz; $CDCl_3$) 167.2, 149.0, 134.9, 131.1, 124.8, 116.6, 114.8, 111.4, 84.9, 64.2, 30.8, 28.0, 19.2 and 13.7; ν_{max}/cm^{-1} (film) 2963, 2876, 1742, 1701 and 1624; HRMS Found MH^+: 294.1703. ($C_{16}H_{23}NO_4$ requires *MH,* 294.1705).

Iridium pentamethylcyclopentadienyl diacetate

$[IrCp^*(OAc)]_2$

A suspension of $[IrCp^*Cl_2]_2$ (50.0 mg, 0.06 mmol) and AgOAc (45.0 mg, 0.27 mmol) in dry toluene (2.5 mL) was stirred at rt under an atmosphere of argon for 3h. The yellow solution was filtered from a residue of silver chloride and excess silver acetate and the filtrate was evaporated under reduced pressure to give $IrCp^*(OAc)_2$ as an orange powder (45 mg, 80%), δ_H (500 MHz; $CDCl_3$) 1.93 (6H, s, acetate-H_3) and 1.57 (15H, s, Cp*-methyl).[95]

***N*-tert-Butyl-5-methyl-2-{[4-(trifluoromethyl)phenyl]amino}benzamide, 70**

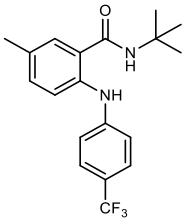

70

N-tert-Butyl-3-methylbenzamide (38.2 mg, 0.20 mmol), 4-(trifluoromethyl)aniline (32.0 mg, 0.20 mmol), IrCp*$(OAc)_2$ (10.0 mg, 0.02 mmol), Silver(I) Bis(trifluoromethanesulfonyl)imide (232 mg, 0.60 mmol) and copper (II) acetate monohydrate (20.0 mg, 0.10 mmol) were added to a round-bottom flask at rt. 1,2-Dichloroethane (0.66 mL) was added and the mixture stirred under atmospheric conditions at rt for 24 h. The reaction was then filtered through a pad of celite, diluted with CH_2Cl_2 (10 mL) and a saturated solution of NH_4OH (10 mL). The aqueous layer was extracted with CH_2Cl_2 (3 x 10 mL), the combined organic layers were dried ($MgSO_4$), filtered and concentrated under reduced pressure. The resulting crude residue was purified using flash column chromatography eluting with 50:50 hexane−EtOAc to yield benzamide **70**[95] as a pale yellow oil (41.0 mg, 58%), *R*f = 0.32 (50:50 hexane−EtOAc); δ_H (500 MHz; $CDCl_3$) 9.00 (1H, br s, NH), 7.41 (2H, d, *J* 8.5, phenyl 2'-H and 6'-H), 7.28 (1H, d, *J* 8.5, phenyl 4-H), 7.13 (1H, s, phenyl 6-H), 7.08 (3H, m, phenyl 3-H, 3'-H and 5'-H), 5.91 (1H, br NH), 2.25 (3H, s, methyl), 1.38 (9H, s, tert-Butyl); $\delta_{C,}$ (125 MHz; $CDCl_3$) 168.8, 145.9, 140.2, 132.3, 129.7, 128.0, 126.5 (q, *J* 3.7), 122.4 (q, *J* 270.1), 122.2 (q, *J 32.5)*, 117.9, 117.2, 29.7, 28.9 and 20.6; v_{max}/cm^{-1} (film); 3446, 3326, 1644 and 1588; HRMS Found MH^+: 351.1675 ($C_{19}H_{21}F_3N_2O$ requires *MH,* 351.1684).

***N*-(pivaloyloxy)benzamide, 73**

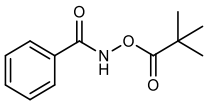

73

Benzylhydroxamic acid (1.00 g, 7.30 mmol), pivaloyl chloride (0.87 mL, 7.30 mmol), triethylamine (0.87 mL, 7.30 mmol) in THF (40 mL) were stirred at rt

for 16 h. The reaction mixture was diluted with EtOAc (50 mL) and washed with HCl (1N 50 mL), water (2 × 50 mL) and brine (50 mL), the organic layer dried ($MgSO_4$) and concentrated under reduced pressure. The crude product was crystallised from Et_2O-pentane to give a colourless microcrystalline powder, *N*-(pivaloyloxy)benzamide **73** (1.40 g, 87%); δ_H (500 MHz, $CDCl_3$), 9.30 (1H, br s, NH), 7.81 (2H, d, *J* 8.0, 2-H and 6-H), 7.54 (1H, t, *J* 8.0, 4-H), 7.42 (1H, t, *J* 8.0, 3-H and 5-H), 1.35 (9H, s, tert-butyl H_9); $\delta_{C,}$ (125 MHz, $CDCl_3$) δ 177.1, 166.8, 132.6, 130.9, 128.8, 127.5, 38.5 and 27.0; v_{max}/cm^{-1} (film) 3205, 2976, 1778, 1660 and 1581; HRMS Found MNa^+: 244.0943 ($C_{12}H_{15}NO_3Na$ requires *MNa, 244.0950*).

[2-(morpholin-4-yl)phenyl]formamido 2,2-dimethylpropanoate, 75

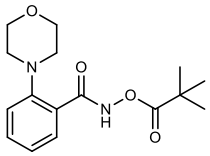

75

$[RhCp^*Cl_2]_2$ (15.5 mg, 0.02 mmol), CsOAc (191 mg, 1.00 mmol), *N*-pivaloyloxybenzamide **73** (112 mg, 0.50 mmol) and PivOH (24.0 mg, 0.03 mmol) was added to a dried round-bottom flask and flushed with nitrogen. Dry MeOH (2.5 mL) was added followed by addition of *N*-chloromorpholine (125 mg, 1.00 mmol) and the solution was stirred at rt under an atmosphere of nitrogen for 16 h. The reaction mixture was diluted with EtOAc (2 mL), filtered through silica, washed with EtOAc (3 x 5 mL) and filtrate evaporated under reduced pressure. The resulting residue was purified by flash column chromatography eluting with 85:15 pentane−ethyl acetate to yield propanoate **75**[105] (104 mg, 68%) as a colourless solid; *R*f = 0.23 (85:15 pentane−ethyl acetate); $\delta_{H,}$ (500 MHz, CDCl3) 8.11 (1 H, dd, *J* 7.8 and 1.7, phenyl 3-H), 7.46 (1 H, ddd, *J* 8.2, 7.3 and 1.7, phenyl H_5), 7.30 – 7.23 (2 H, m, phenyl 4-H and 6-H), 3.92–3.80 (4 H, m, morpholine 2-H_2 and 6-H_2), 3.03–2.88 (4H, m, morpholine 3-H_2 and 5-H_2) and 1.31 (9 H, s, *tert*-butyl); $\delta_{C,}$ (100 MHz, $CDCl_3$) 176.2, 164.1, 150.7, 133.1, 131.6, 126.8, 126.4, 121.9, 67.1, 53.8, 38.5 and 27.2; v_{max}/cm^{-1} (film) 2975, 2852, 1772, 1681 and 1598; HRMS Found MH^+: 307.1659 ($C_{16}H_{22}N_2O_4$ requires *MH*, 307.1658).

The reaction was repeated as stated at rt under an atmospheric conditions to yield the crude product which was purified by flash chromatography, eluting with 50:50 hexane-ethyl acetate to give the propanoate **75** (94.0 mg, 61%) with spectroscopically identical data to that obtained previously.

4-methoxy-*N*-(2-phenylcyclohexyl)aniline, 76

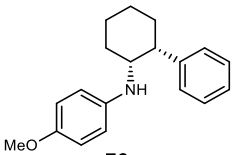

76

2-phenylcyclohexanone (500 mg, 2.90 mmol), *p*-methoxyaniline (354 mg, 2.90 mmol) and acetic acid (173 µL, 2.88 mmol) were stirred in 1,2-dichloroethane (15 mL) for 1 h at rt. Sodium triacetoxyborohydride (0.92g, 4.32 mmol) was added and the solution stirred for 18h at rt. Saturated aqueous sodium bicarbonate solution (20 mL) was added and the organic phase was dried ($MgSO_4$) and concentrated under reduced pressure to yield the crude product which was purified by flash column chromatography using 95:5, petroleum ether−ethyl acetate to give the aniline **76** (339 mg, 42%) as a pale yellow oil, R_f = 0.44 (95:5 Petroleum Ether−EtOAc); δ_H (500 MHz; $CDCl_3$) 7.28-7.22 (4H, m, aniline 2-H, 3-H, 5-H and 6-H), 7.17-7.13 (1H, m, phenyl 4-H), 6.67-6.62 (2H, m, phenyl 2-H and 6-H), 6.39-6.32 (2H, m, phenyl 3-H and 5-H), 3.70 (1H, m, cyclohexyl 1-H), 3.65 (3H, s, methoxy-H_3), 3.37 (1H, br s, NH), 2.96 (1H, dt, *J* 12.2 and 3.6, cyclohexyl 2-H), 2.10-2.04 (1H, m, cyclohexyl-H), 1.97-1.85 (2H, m, cyclohexyl-H_2), 1.86-1.78 (1H, m, cyclohexyl-H) and 1.63-1.50 (3H, m, cyclohexyl-H_3); δ_C (125 MHz; $CDCl_3$) 151.9, 144.2, 142.4, 128.4, 127.8, 126.3, 115.1, 114.8, 55.9, 54.9, 46.5, 30.4, 26.1, 25.9 and 20.5; ν_{max}/cm^{-1} (film) 3412, 2932, 2857 and 1617 and 1602; HRMS Found MH^+: 282.1857. ($C_{19}H_{23}NO$ requires *MH,* 282.1858).

4-methoxy-*N*-[2-(2-phenylphenyl)cyclohexyl]aniline, 78

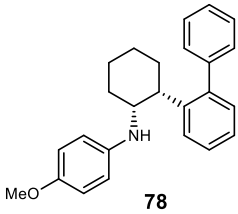

78

$Pd(OAc)_2$ (9.00 mg, 0.04 mmol), benzoquinone (43.2 mg, 0.40 mmol), phenylboronic acid (49.0 mg, 0.40 mmol) and CH_2Cl_2 (1.5 mL) were added at rt to a flask, followed by a solution of aniline 76 (57.0 mg, 0.20 mmol) in isopropanol (0.3 mL). The mixture was stirred at rt for 24 h and then diluted with CH_2Cl_2 (15 mL), washed with saturated aqueous sodium bicarbonate solution (3 x 20 mL), the combined aqueous layers extracted with CH_2Cl_2 (3 x 20 mL) and the combined organic layers were dried ($MgSO_4$) and then concentrated under reduced pressure to give the crude product which was purified by flash column chromatography eluting with 99:1 petroleum ether-ethyl acetate to give the aniline **78**[106] (51.0 mg, 76%) as a pale yellow oil, R_f = 0.31 (50:50 petroleum ether−ethyl acetate); δ_H (500 MHz; $CDCl_3$) 7.43-7.36 (4H, m, phenyl-H_4), 7.31-7.26 (1H, m, phenyl-H), 7.24-7.15 (4H, m, phenyl-H_4), 7.11 (1H, td, *J* 7.4 and 1.3, phenyl-H), 6.57-6.51 (2H, m, phenyl-H_2), 6.20-6.13 (2H, m, phenyl-H_2), 3.61 (3H, s, methyl), 3.35 (1H, br s, NH), 3.25 (1H, d, *J* 3.3, cyclohexyl 1-H), 3.08 (1H, dt, *J* 12.8 and 3.3, cyclohexyl 2-H), 1.92-1.81 (1H, m, cyclohexyl-H), 1.80-1.69 (2H, m, cyclohexyl-H_2), 1.66-1.57 (1H, m, cyclohexyl-H), 1.43-1.34 (2H, m, cyclohexyl-H_2), 1.28-1.16 (1H, m, cyclohexyl-H) and 1.12-1.00 (1H, m, cyclohexyl-H); δ_C (125 MHz; $CDCl_3$) 151.7, 142.6, 141.4, 137.1, 136.3, 132.7, 130.2, 129.3, 128.6, 128.1, 127.4, 126.8, 125.8, 114.9, 55.8, 53.5, 42.5, 30.6, 26.2, 26.1 and 20.1; ν_{max}/cm^{-1} (film) 3408, 3058, 3025, 2929, 2855, 1600 and 1510; HRMS Found MH^+: 358.2182. ($C_{25}H_{27}NO$ requires *MH,* 358.2171).

***N*-[2-(3,4-dimethylphenyl)-5-methylphenyl]acetamide, 80**

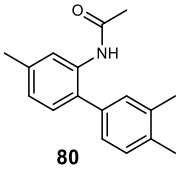

80

Ammonium persulfate (228 mg, 1.00 mmol), 3-methyl acetanilide (75.6 mg, 0.50 mmol) and $Pd(OAc)_2$ (11.6 mg, 0.05 mmol) was added to a round-bottom flask at rt. TFA (0.74 mL, 10.0 mmol) and *o*-xylene (1.22 mL, 10.0 mmol) were added and the reaction mixture stirred at rt for 24 h. The mixture was then diluted with CH_2Cl_2 (10 mL), filtered through a celite pad and washed with CH_2Cl_2 (10 mL). The filtrate was concentrated under reduced pressure and the resulting crude product purified by flash column chromatography eluting with 2:1 petroleum ether−EtOAc to give the acetamide **80**[107] as a yellow oil (60.0 mg, 52%), R_f = 0.32 (2:1 petroleum ether−EtOAc); δ_H (500 MHz; $CDCl_3$) 8.10 (1H, br s, NH), 7.27-7.18 (2H, m, phenyl-H_2), 7.14-7.07 (3H, m, phenyl-H_3), 6.97 (1H, d, *J* 7.7, phenyl 5-H), 2.40 (3H, s, acetamide-methyl), 2.33 (3H, s, methyl), 2.32 (3H, s, methyl), 2.02 (3H, s, methyl); δ_C (125 MHz; $CDCl_3$) 168.2, 138.1, 137.4, 136.2, 135.7, 134.6, 130.6, 130.2, 129.9, 129.4, 126.6, 125.1, 122.0, 24.7, 21.5, 19.9 and 19.5; v_{max}/cm^{-1} (film) 3415, 3293, 2864, 1681 and 1620; HRMS Found MH^+: 254.1544. ($C_{17}H_{19}NO$ requires *MH,* 254.1545).

1-methyl-2-phenyl-1H-indole, 60

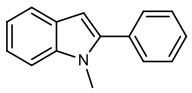

60

$Pd(OAc)_2$ (11.2 mg, 0.05 mmol), Ag_2O (174 mg, 0.75 mmol), 2-nitrobenzoic acid (251 mg, 1.50 mmol), iodobenzene (224 µL, 2.00 mmol) and *N*-methylindole (128 µL 1.00 mmol) were added to a round-bottom flask at rt. Anhydrous DMF (2 mL) was added and the reaction mixture stirred at rt under atmospheric conditions for 24 h. The reaction mixture was filtered through a plug of silica and then concentrated under reduced pressure and the resulting crude product was purified using flash column chromatography eluting with 98:2 hexane−EtOAc to yield the indole **60**[91] as a colourless, amorphous solid (57.0 mg, 27%), R_f = 0.32 (98:2 hexane−EtOAc); δ_H (500 MHz; $CDCl_3$) 7.68 (1H, d, *J* 7.9, 7-H), 7.59-7.52 (2H, m, phenyl 2-H and 6-H), 7.51 (2H, t, *J* 8.0, phenyl 3-H and 5-H), 7.48-7.40 (1H, m, 6-H), 7.40 (1H, d, *J* 8.0, 8-H), 7.30 (1H, td, *J* 7.2 and 1.1, 4-H), 7.19 (1H, td, *J* 8.0 and 1.1, 5-H), 6.61 (1H, s, 3-H) and 3.78 (3H, s, methyl); δ_C (125 MHz; $CDCl_3$) 141.6,

138.4, 132.9, 129.4, 128.5, 128.0, 127.9, 121.7, 120.5, 119.9, 109.7, 101.7 and 31.2; ν_{max}/cm^{-1} (film) 3054, 2918 and 1601; HRMS Found MH$^+$: 208.1119. ($C_{15}H_{13}N$ requires *MH,* 208.1126).

***N-tert*-Butyl-2-(cyclohexylamino)-5-methylbenzamide, 72**

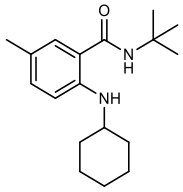

72

N-tert-Butyl-3-methylbenzamide (38.2 mg, 0.20 mmol), cyclohexylamine (19.8 mg, 0.20 mmol), $[IrCp^*Cl_2]_2$ (8.00 mg, 0.01 mmol), Silver(I) Bis(trifluoromethanesulfonyl)imide (232 mg, 0.60 mmol), copper (II) acetate monohydrate (20.0 mg, 0.10 mmol) were added to a round-bottom flask. A solution of 1,2-dichloroethane and hexafluoroisopropanol (50:50, 0.66 mL) was added and the reaction heated under atmospheric conditions at 60 ^oC overnight. The reaction was then filtered through a pad of celite, diluted with CH_2Cl_2 (10 mL) and a saturated solution of NH_4OH (10 mL). The aqueous layer was extracted with CH_2Cl_2 (3 x 10 mL), the combined organic layers dried ($MgSO_4$), filtered and concentrated under reduced pressure. The resulting crude residue was purified using flash column chromatography eluting with 50:50 hexane−ethyl acetate to yield benzamide **72**[104] as a pale yellow oil**,** (28.0 mg, 49%), *R*f = 0.6 (50:50 hexane−EtOAc); δ_H (300 MHz; $CDCl_3$) 7.08-7.01 (2H, m, phenyl 4-H and 6-H), 6.62 (1H, d, *J* 8.2, phenyl 3-H), 5.88 (1H, br s, NH), 3.27 (1H, m, cyclohexyl 1-H), 2.22 (3H, s, methyl), 2.02 (2H, m, cyclohexyl 2-H_A and 6-H_A), 1.75 (2H, m, cyclohexyl 2-H_B and 6-H_B), 1.45 (9H, s, *tert*-butyl) and 1.41-1.20 (6H, m, cyclohexyl 3-H_2, 4-H_2 and 5-H_2); δ_C; (100 MHz, $CDCl_3$) δ 169.6, 146.2, 132.8, 127.8, 123.4, 117.4, 112.7, 51.4, 33.1, 29.0, 26.0, 25.0 and 20.3, ν_{max}/cm^{-1} (film); 3442, 3346, 2931, 2856, 1644, 1608 and 1577, HRMS Found MH$^+$: 289.2293 ($C_{18}H_{28}N_2O$ requires *MH,* 289.2280).

The reaction was repeated as stated at rt to yield the crude product which was purified by flash chromatography, eluting with 50:50 hexane-ethyl

acetate to give the benzamide **72** (22.0 mg, 38%) with spectroscopically identical data to that obtained previously.

Tris(propan-2-yl)(2-(propan-2-yl)phenoxy)silane, 118

118

To a solution of 2-isopropylphenol (3.00 g, 22.0 mmol) and triisopropylsliane chloride (6 mL, 27.0 mmol) in dry CH_2Cl_2 (30 mL) at 0 ^oC was added imidazole (3.70 g, 55.0 mmol) and the solution stirred at 0 ^oC for 18 h. The reaction mixture was quenched with H_2O (20 mL), extracted with EtOAc (3 x 15 mL) and the combined organic layers washed with brine (3 x 20 mL), dried ($MgSO_4$) and concentrated under reduced pressure. The resulting colourless oil was purified using flash column chromatography eluting with hexane to yield silane **118** (4.70 g, 74%). *R*f = 0.56 (hexane); $\delta_{H,}$ (400 MHz, $CDCl_3$) 7.07 (1H, dd, *J* 7.7 and 1.8, 6-H), 6.89 (1H, td, *J* 7.7 and 1.8, 5-H), 6.77 (1H, td, *J* 7.7 and 1.3, 4-H), 6.64 (1H, dd, *J* 7.7 and 1.3, 3-H), 3.25 (1H, hept, *J* 6.9, propan-2-yl 2-H), 1.24-1.14 (3H, m, *tris*-propan-2-yl 2-H_3), 1.08 (6H, d, *J* 6.9, propan-2-yl 1-H_3 and 3-H_3) and 0.99 (18H, d, *J* 7.4, *tris*-propan-2-yl 1-H_9 and 3-H_9); $\delta_{C,}$ (100 MHz, $CDCl_3$) 152.3, 141.0, 129.3, 128.9, 119.4, 113.1, 26.9, 22.6, 18.1 and 13.1; ν_{max}/cm^{-1} (film) 3031, 2893, 1598 and 1580; HRMS (no mass found on positive or negative mode).

4-Bromo-2-(propan-2-yl)phenoxytris(propan-2-yl)silane, 119

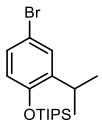

119

To a solution of silane **118** (3.00 g, 10.0 mmol) in THF (25 mL) was added *N*-bromosuccinimide (1.80 g, 10.0 mmol) and the reaction solution was stirred at rt for 6 h. The reaction mixture was washed with saturated aqueous sodium thiosulphate solution (3 x 20 mL), the combined aqueous layers extracted with EtOAc (3 x 20 mL), the combined organic layers washed with brine (3 x 20 mL), dried ($MgSO_4$) and concentrated under reduced pressure to yield crude silane **119** as a pale yellow oil (3.00 g, 81%), *R*f = 0.59

(hexane); $\delta_{H,}$ (400 MHz, $CDCl_3$) 7.14-7.13 (1H, m, 3-H), 6.99 (1H, d, *J* 8.5, 5-H), 6.51 (1H, d, *J* 8.5, 6-H), 3.19 (1H, h, *J* 6.9, propan-2-yl 2-H), 1.24-1.11 (3H, m, *tris*-propan-2-yl 2-H_3), 1.06 (6H, d, *J* 6.9, propan-2-yl 1-H_3 and 3-H_3) and 0.98 (18H, d, *J* 7.4, *tris*-propan-2-yl 1-H_9 and 3-H_9); $\delta_{C,}$ (100 MHz, CDCl3) 152.3, 141.0, 129.3, 128.9, 119.4, 113.1, 26.9, 22.6, 18.1 and 13.1; v_{max}/cm^{-1} (film): 2944, 2865, 1777 and 1706.

_N_,_N_-Dimethyl-3-(propan-2-yl)-4-{[tris(propan-2-yl)silyl]oxy}benzamide, 120

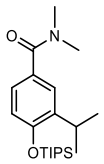

120

To a solution of silane **119** (1.00 g, 2.70 mmol) in THF (20 mL) under an atmosphere of nitrogen at -78 ^oC was added dropwise *n*BuLi (1.40 M in hexanes, 2.5 mL, 3.50 mmol) and stirred for 3 h. Dimethyl carbamoyl chloride (750 μL, 8.10 mmol) was added at the reaction mixture allowed to warm to rt and stirred for 24 h. The reaction mixture was quenched with H_2O (20 mL), extracted with EtOAc (3 x 15 mL) and organics washed with saturated aqueous sodium bicarbonate (3 x 15 mL), brine (3 x 15 mL), dried ($MgSO_4$) and concentrated under reduced pressure. The residue was purified by column chromatography eluting with hexane–EtOAc (80:20) to yield the benzamide **120** (0.40 g, 40%) as a colourless solid, *R*f = 0.14 (hexane–EtOAc, 80:20); δ_H (400 MHz, $CDCl_3$); 7.16 (1H, d, *J* 2.3, 2-H), 7.00 (1H, dd, *J* 8.2 and 2.3, 6-H), 6.58 (1H, d, *J* 8.2, 5-H), 3.19 (1H, hept, *J* 6.9, propan-2-yl 2-H_1), 3.00 (6H, br s, dimethyl H_6), 1.18 (3H, hept, *J* 7.4, *tris*-propn-2-yl 2-H_3) 1.10 (6H, d, *J* 6.9, propan-2-yl 1-H_3 and 3-H_3) and 1.00 (18H, d, *J* 7.4, *tris*-propan-2-yl 1-H_9 and 3-H_9); δ_C (100 MHz, $CDCl_3$); 172.0, 155.8, 135.0, 127.9, 126.4, 126.0, 116.0, 44.5, 26.9, 22.6, 18.0 and 14.1; v_{max}/cm^{-1} (film); 3160, 2940, 2916, 2879, 1725, 1610 and 1589; HRMS Found MH^+: 364.3675 ($C_{21}H_{38}NO_2Si$ *requires MH*, 364.2672).

_N_,_N_-Diethyl-3-(propan-2-yl)-4-{[tris(propan-2-yl)silyl]oxy}benzamide, 121

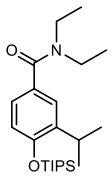

121

To a solution of silane **119** (1.00 g, 2.70 mmol) in THF (20 mL) under an atmosphere of nitrogen at -78 ^{o}C was added dropwise *n*BuLi (1.40 M in hexanes, 2.5 mL, 3.5 mmol) and stirred for 3 h. Diethyl carbamoyl chloride (1.0 mL, 8.10 mmol) was added at the reaction mixture allowed to warm to rt and stirred for 24 h. The reaction mixture was quenched with H_2O (20 mL), extracted with EtOAc (3 x 15 mL) and organics washed with saturated aqueous sodium bicarbonate (3 x 15 mL), brine (3 x 15 mL), dried ($MgSO_4$) and concentrated under reduced pressure. The residue was purified by column chromatography eluting with hexane–EtOAc (80:20) to yield the benzamide **121** (0.47 g, 44%) as a colourless solid, *R*f = 0.16 (hexane–EtOAc, 80:20); δ_H (400 MHz, $CDCl_3$) 7.14 (1H, d, *J* 2.2, 2-H), 6.96 (1H, dd, *J* 8.2 and 2.2, 6-H), 6.51 (1H, d, *J* 8.2, 5-H), 3.32 (4H, very br d *(rotameric)* ethyl CH_2), 3.18 (1H, h, *J* 6.9, propan-2-yl 2-H_1), 1.56 (3H, br s, ethyl CH_3), 1.18 (3H, hept, *J* 7.6, *tris*-propan-2-yl 2-H_3), 1.16 (6H, d, *J* 6.9, propan-2-yl 1-H_3 and 3-H_3), 1.14 (3H br s, ethyl CH_3) and 0.99 (18H, d, *J* 7.6, *tris*-propan-2-yl 1-H_9 and 3-H_9); δ_C (100 MHz, $CDCl_3$) 179.6, 155.9, 134.0, 127.6, 125.2, 125.1, 116.4, 42.3, 26.8, 22.1, 18.0, 15.5 and 13.8; v_{max}/cm^{-1} (film); 3060, 2981, 2972, 1625 and 1580; HRMS Found MH^+: 392.2980 ($C_{23}H_{42}NO_2Si$ *requires MH*, 392.2985).

4-hydroxy-_N,N_-dimethyl-3-(propan-2-yl)benzamide, 104

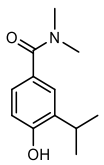

104

Benzamide **120** (0.40 g, 1.10 mmol) was dissolved in TFA:H_2O (50:50, 10 mL), potassium fluoride (174 mg, 3.30 mmol) added and heated to 80 ^{o}C overnight. The reaction mixture was diluted with H_2O (10 mL), extracted with

EtOAc (3 x 10 mL) and organics washed with saturated aqueous sodium bicarbonate (3 x 10 mL), brine (3 x 10 mL), dried ($MgSO_4$) and concentrated under reduced pressure. The resiude was purified by column chromatography eluting with hexane–EtOAc (50:50) to yield the benzamide **104** (28.0 mg, 12%) as a colourless solid, *R*f = 0.10 (hexane–EtOAc, 50:50); δ_H (400 MHz, $CDCl_3$) 7.18 (1H, d, *J* 2.2, 2-H), 6.97 (1H, dd, *J* 8.2 and 2.2, 6-H), 6.53 (1H, d, *J* 8.2, 5-H), 3.16 (1H, hept, *J* 6.9, propanyl 2-H_1), 2.99 (6H, br s dimethyl) and 1.12 (6H, d, *J* 6.9 propanyl H_6); δ_C (100 MHz, $CDCl_3$) 172.8, 155.3, 134.6, 127.0, 126.1, 125.9, 115.0, 26.8 and 22.4; v_{max}/cm^{-1} (film) 3118, 2960, 2928, 1726, 1613 and 1600; HRMS Found MH^+: 208.1332 ($C_{12}H_{18}NO_2$ *requires MH*, 208.1338).

***N,N*-diethyl-4-hydroxy-3-(propan-2-yl)benzamide, 90**

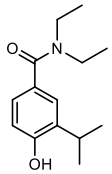

90

Benzamide **121** (0.40 g, 1.00 mmol) was dissolved in TFA:H_2O (50:50, 10 mL), potassium fluoride (174 mg, 3.30 mmol) added and heated to 80 ^oC overnight. The reaction mixture was diluted with H_2O (10 mL), extracted with EtOAc (3 x 10 mL) and organics washed with saturated aqueous sodium bicarbonate (3 x 10 mL), brine (3 x 10 mL), dried ($MgSO_4$) and concentrated under reduced pressure. The residue was purified by column chromatography eluting with hexane–EtOAc (50:50) to yield the benzamide **90** (65.0 mg, 27%) as a colourless solid, *R*f = 0.24 (hexane–EtOAc 50:50); δ_H (500 MHz, $CDCl_3$); 7.12 (1H, d, *J* 2.1, 2-H), 6.93 (1H, dd, *J* 8.1 and 2.1, 6-H), 6.52 (1H, d, *J* 8.1, 5-H), 3.34 (4H, very br d *(rotameric)* ethyl CH_2), 3.16 (1H, h, *J* 6.9, propanyl 2-H_1), 1.57 (3H, br s, ethyl CH_3), 1.14 (6H, d, *J* 6.9, propanyl 1-H_6) and 1.14 (3H, br s, ethyl CH_3); δ_C (75 MHz, DMSO-d_6); 170.5, 155.2, 133.8, 127.7, 125.0, 124.5, 114.4, 41.3, 26.2, 22.3 and 15.6; v_{max}/cm^{-1} (film); 3062, 2980, 2948, 1610 and 1594; HRMS Found MH^+: 236.1650 ($C_{14}H_{22}NO_2$ *requires MH*, 236.1651).

Sodium [(1*E*)-2-oxocyclopentylidene]methanolate, 124

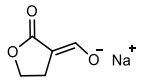

124

To a suspension of NaH (60% in mineral oil, 1.20 g, 0.03 mol) in hexane (20 mL) was added dropwise a mixture of ethyl formate (2.40 mL, 0.03 mmol) and γ-butyrolactone (2.20 mL, 0.03 mmol). After addition of 10% of the mixture, ethanol absolute (1 mL) was added to initiate the reaction, followed by the dropwisde addition of the remaining mixture. The mixture was refluxed for 2 h and the resulting precipitate filtered and washed with cold hexane (3 x 10 mL) and dried to give the methanolate **124**[153] (4.00 g, 99%) as a colouress amorphous solid. $\delta_{H,}$ (400 MHz, MeOH-d_4) 8.56 (1H, m, methanolate H_1), 4.24 (2 H, dd, *J* 8.4 and 7.6, oxocyclopentyl 3-H_2) and 2.81 (2 H, dd, *J* 8.4 and 7.6, oxocyclopentyl 4-H_2); $\delta_{C,}$ (100 MHz, DMSO-d_6) 175.7, 173.5, 167.3, 63.4 and 26.1; v_{max}/cm^{-1} (film); 3300, 2937, 2855, 1708 and 1561; HRMS Found M$^+$: 136.0497 ($C_5H_5NaO_3$ *requires M*, 136.0136).

(*3E*)-3-[(phenylamino)methylidene]oxolan-2-one, 91

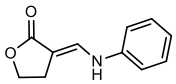

91

To a solution of sodium salt **124** (2.00 g, 15.0 mmol) in methanol (50 mL), was added aniline hydrochloride (4.00 g, 31.0 mmol) and the mixture refluxed overnight. The reaction mixture was concentrated under reduced pressure, diluted with H_2O (30 mL), the combined organics extracted with CH_2Cl_2 (3 x 10 mL), organics washed with HCl (3 x 10 mL), saturated aqueous sodium bicarbonate (3 x 10 mL) and brine (3 x 10 mL). The organics were concentrated under reduced pressure and crude product purified by flash column chromatography eluting with hexane–EtOAc (50:50) to yield oxolanone **91**[153] (2.60 g, 73%) as a colourless solid, *R*f = 0.2; δ_H (400 MHz, DMSO-d_6) 9.04 (1H, d, *J* 13.0, NH), 7.66 (1H, dt, *J* 13.0 and 2.3, methylidene 2-H_1), 7.29 (2H, apparent t *J* 7.7, phenyl 3-H and 5-H), 7.16 (2H, d, *J* 7.7, phenyl 2-H and 6-H), 6.95 (1H, tq, *J* 7.7 and 1.0, phenyl 4-H_1), 4.30 (2H, t, *J* 7.8, oxolanone 5-H_2) and 2.88 (2H, td, *J* 7.8 and

2.3, oxolanone 4-H_2), δ_C (75 MHz, DMSO-d_6) 172.9, 141.6, 134.8, 129.4, 121.6, 115.1, 95.5, 64.6, and 24.7; v_{max}/cm^{-1} (film); 3277, 2978, 1722, 1622 and 1600; HRMS Found MNa^+: 262.0680 ($C_{11}H_{11}NO_2Na$ *requires MNa*, 262.0688)

6-(2-bromophenyl)-1,3,5-triazine-2,4-diamine, 101

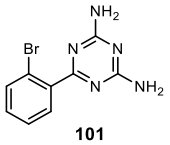

101

2-Bromobenzonitrile (3.70 g, 20.0 mmol), dycyanodiamide (2.50 g, 30.0 mmol) and potassium hydroxide (0.20 g, 3.60 mmol) were stirred in diethylene glycol dimethyl ether (37 mL) at 100 ^oC for 8 h. Additonal dycanodiamide (1.25 g, 0.15 mmol) was added and stirred at 100 ^oC for a further 8 h. The mixture was cooled to rt, diluted with water (20 mL) and the resulting precipitate collected by filtration and washed with cold water (3 x 10 mL) to afford the diamine **101**[154] (4.50 g, 85%); $\delta_{H,}$ (400 MHz, DMSO-d_6) 7.66 (1H, dt, *J* 7.9 and 1.1, 3-H), 7.47 (1 H, dd, *J* 7.6 and 1.9, 6-H), 7.43 (1H, dt, *J* 7.6 and 1.1, 5-H), 7.33 (1H, d, *J* 7.9 and 1.9, 4-H), 6.84 (4H, br s, NH); $\delta_{C,}$ (100 MHz, DMSO) δ 173.7, 167.4, 140.4, 133.2, 130.7, 130.5, 127.8 and 120.5; v_{max}/cm^{-1} (film) 3515, 3401, 3116, 1630 and 1537. HRMS Found MH^+: 266.0029 ($C_9H_8BrN_5$ *requires MH,* 266.0041).

2-(cyclohexylamino)benzonitrile, 127

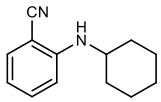

127

To a microwave vial was added 2-bromobenzonitrile (1.00 g, 5.50 mmol), $Pd(OAc)_2$ (62.0 mg, 0.03 mmol), dppf (300 mg, 0.55 mmol) and NaO^{t}Bu (1.60 g, 16.5 mmol). The vial was degassed and flushed with nitrogen. To a separate crimped vial was added cyclohexylamine (1.90 mL, 16.5 mmol), which was degassed, flushed with nitrogen followed by addition of toluene (5 mL) and the solution transferred to the microwave vial, followed by addition of toulene (10 mL). The reaction mixture was heated under

microwave irradiation to 130 ºC for 1.5 h. The reaction mixture was diluted with toluene (10 mL), partitioned with H_2O (3 x 10 mL), aqueous layers extracted with EtOAc (3 x 10 mL), combined organics washed with saturated aqueous sodium bicarbonate solution (3 x 10 mL), brine (3 x 10 mL), dried ($MgSO_4$) and concentrated under reduced pressure. The crude residue was purified using flash column chromatography eluting with hexane–EtOAc (90:10), to yield the benzonitrile **127** (800 mg, 72%) as a pale brown oil, *R*f = 0.40 (hexane–EtOAc 90:10); δ_H (300 MHz, $CDCl_3$) 7.42 – 7.31 (2H, m, 6-H and 4-H), 6.68 (1H, d, *J* 8.5, 3-H), 6.63 (1H, td, *J* 7.5 and 1.0 5-H), 4.46 (1H, d, *J* 7.3, NH), 3.37 (1H, ddq, *J* 10.4, 7.3 and 4.0, cychlohexyl 1-H), 2.12 – 1.95 (2H, m, cylohexyl 2-H_A and 6-H_A), 1.82 (2H, dt, *J* 12.4 and 4.0 cyclohexyl 2-H_B and 6-H_B), 1.75 – 1.63 (1H, m, cylohexyl 4-H), 1.48 – 1.16 (5H, m, cyclohexyl 3-H_2, 4-H and 5-H_2); δ_C (75 MHz, Chloroform-*d*) 149.4, 134.1, 132.9, 118.1, 115.9, 111.0, 95.5, 51.4, 33.0, 25.6 and 24.8; ν_{max}/cm^{-1} (film); 3404. 2930, 2854, 2229, 1709, 1604 and 1576; HRMS Found MNa^+: 223.1205 ($C_{13}H_{16}N_2Na$ *requires MNa*, 223.1211).

2-(cyclohexylamino)benzamide, 113

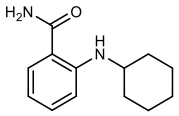

113

To an oven-dried dry flask charged with benzonitrile **127** (500 mg, 2.50 mmol) and potassium tert-butoxide (842 mg, 7.50 mmol) was added dry tert-butanol (10 mL). The reaction mixture was stirred under an atmosphere of nitrogen at 100 ºC overnight. The reaction mixture was cooled to rt, quenched with H_2O (10 mL), organics washed with brine (3 x 10 mL), dried ($MgSO_4$) and concentrated under reduced pressure. The crude material was purified using flash column chromatography eluting with hexane–EtOAc (70:30) to yield the benzamide **113** (270 mg, 50%); *R*f = 0.30 (hexane–EtOAc 70:30); δ_H (300 MHz, $CDCl_3$), 7.78 (1H, s, NH), 7.29 (1H, dd, *J* 8.0 and 1.1, 6-H), 7.25 – 7.16 (1H, m 4-H), 6.64 (1H, d, *J* 8.0 3-H), 6.44 (1H, ddd, *J* 8.0, 7.0 and 1.1 5-H), 5.58 (2H, br s, NH_2), 3.28 (1H, br s, cyclohexyl 1-H), 1.93 (2H, dd, *J* 10.2 and 4.0, cyclohexyl 2-H_A and 6-H_B), 1.81 – 1.49

(4H, m, cyclohexyl 2-H_B, 3-H, 5-H and 6-H_B) and 1.42 – 1.13 (4H, m, cyclohexyl, 3-H, 4-H_2 and 5-H); δ_C (75 MHz, $CDCl_3$) 212.2, 172.2, 160.4, 133.7–132.5 (m), 128.5, 113.7, 112.3, 50.6, 32.8, 25.9 and 24.7; v_{max}/cm^{-1} (film); 3453, 3347, 3168, 2931, 2855, 1632 and 1612; HRMS Found MH^+: 219.1497 ($C_{13}H_{19}N_2O$ *requires MH*, 219.1497).

***N,N*-Diethyl-3-(propan-2-yl)benzamide, 109**

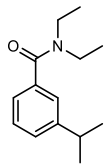

109

To a solution of 3-isopropylbenzoic acid (1.00 g, 6.00 mmol), DIPEA (5.2 mL, 30.0 mmol), TBTU (4.50 g, 14.0 mmol) in CH_2Cl_2 (20 mL) was added diethylamine (6.20 mL, 60.0 mmol), and the reaction mixture stirred at rt overnight. The reaction mixture was diluted with H_2O (15 mL), extracted with pentane (3 x 10 mL) washed with brine (3 x 10 mL), dired ($MgSO_4$) and concentrated under reduced pressure. The crude residue was purified using column chromatography eluting with pentane–EtOAc (80:20) to yield the benzamide **109** as a yellow oil (1.20 g, 96%) ; *R*f = 0.25 (pentane–EtOAc 80:20); δ_H (300 MHz, $CDCl_3$) 7.24 – 7.12 (3H, m, phenyl H_3), 7.07 (1H, dt, *J* 7.1 and 1.6, phenyl H), 3.30 (4H, very br d, *(rotameric)* ethyl CH_2), 2.82 (1H, h, *J* 6.9, propanyl 2-H_1), 1.16 (6H, d, *J* 6.9 propanyl H_6), 1.16 (3H, very br s, *(rotameric)* ethyl CH_3), and 1.06 (3H, very br s, *(rotameric)* ethyl CH_3); δ_C (75 MHz, $CDCl_3$); 171.7, 149.1, 137.3, 128.3, 127.2, 124.3, 123.6, 43.2, 39.2, 34.0, 23.9, 14.2 and 12.9; v_{max}/cm^{-1} (film); 2962, 2933, 2873, 1628 and 1583; HRMS Found MNa^+: 242.1546 ($C_{14}H_{21}NONa$ *requires MNa*, 242.1421).

***N*-tert-butyl-3-(propan-2-yl)benzamide, 110**

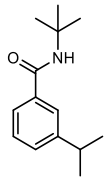

110

According to general procedure F, 3-isopropylbenzoic acid (0.50 g, 3.00 mmol) and tert-butylamine (630 μL, 6.00 mmol) gave a crude material which was purified using column chromatography using hexane–EtOAc (80:20) to yield the benzamide **110** as a white solid (438 mg, 67%); *R*f = 0.30 (hexane–EtOAc 80:20); δ_H (300 MHz, $CDCl_3$) 7.58 – 7.54 (1H, m, 6-H), 7.39 (1H, app. ddd, *J* 4.5, 3.8 and 2.1, 2-H), 7.30 – 7.22 (2H, m, 4-H and 5-H), 2.88 (1H, hept, propanyl 2-H_1), 1.41 (9H, s, tert-butyl H_9) and 1.20 (6H, d, *J* 7.0, propanyl 1-H_3 and 3-H_3); δ_C (100 MHz, $CDCl_3$) 167.2, 149.4, 136.0, 129.3, 128.4, 125.2, 123.8, 51.6, 34.2, 28.9 and 23.9; ν_{max}/cm^{-1} (film); 3295, 2970, 1655, 1586, 1514 and 1487; HRMS Found MH$^+$: 220.1645 ($C_{14}H_{22}NO$ *requires MH*, 220.1696).

_N_-tert-butyl-3-methoxybenzamide, 105

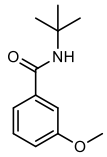

105

According to general procedure F, 3-methoxybenzoic acid (0.50 g, 3.30 mmol) and tert-butylamine (693 μL, 6.60 mmol) gave a crude material which was purified using column chromatography eluting with hexane–EtOAc (80:20) to yield the benzamide **105** as a white solid (609 mg, 89%); *R*f = 0.40 (hexane–EtOAc 80:20); δ_H (300 MHz, $CDCl_3$) 7.26 (1H, app. t, *J* 2.0, 6-H), 7.23 (1H, app. t, *J* 8.0, 5-H), 7.14 (1H, app dt, *J* 6.5 and 1.0, 2-H), 6.94 (1H, ddd, *J* 8.0, 2.6 and 1.0, 4-H), 3.78 (3H, s, methoxy H_3) and 1.40 (9H, s, tert-butyl H_9); δ_C (100 MHz, $CDCl_3$) 166.7, 159.8, 137.4, 129.4, 118.4, 117.3, 112.1, 55.4, 51.6 and 28.9; ν_{max}/cm^{-1} (film); 3298, 3010, 2971, 1636, 1587, 1530 and 1488; HRMS Found MH$^+$: 208.1275 ($C_{12}H_{18}NO_2$ r*equires MH,* 208.1288).

***N*-tert-butyl-4-(1H-pyrazol-1-yl)benzamide, 115**

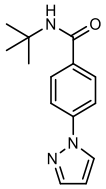

115

According to general procedure F, 4-(pyrazol-1-yl)benzoic acid (0.50 g, 2.70 mmol) and tert-butylamine (560 μL, 5.40 mmol) gave a crude material which was purified using column chromatography eluting with hexane–EtOAc (70:30) to yield the benzamide **115** as a white solid (527 mg, 81%); *R*f = 0.20 (hexane–EtOAc 70:30); δ_H (300 MHz, $CDCl_3$) 7.91 (1H, d, *J* 2.4, pyrazol-1-yl 5-H), 7.78 – 7.65 (5H, m, 2-H, 3-H, 5-H, 6-H and pyrazol-1-yl 3-H), 6.45 – 6.41 (1H, m, pyrazol-1-yl 4-H), 5.88 (1H, br s, NH) and 1.42 (9H, s, tert-butyl H_9); δ_C (100 MHz, $CDCl_3$) 165.9, 142.0, 141.7, 133.6, 128.2, 126.8, 118.5, 108.3, 51.8 and 28.9; v_{max}/cm^{-1} (film); 3312, 2969, 1654, 1609, 1586, 1590 and 1500; HRMS Found MH^+: 244.1384 ($C_{14}H_{18}N_3O$ r*equires MH,* 244.1440).

***N*-cyclopentyl-3-methoxybenzamide, 106**

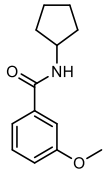

106

According to general procedure F, 3-methoxybenzoic acid (0.50 g, 3.30 mmol) and cyclopentylamine (652 μL, 6.60 mmol) gave a crude material which was purified using column chromatography eluting with hexane–EtOAc (70:30) to yield the benzamide **106** as a white solid (583 mg, 81%); *R*f = 0.26 (hexane–EtOAc 70:30); δ_H (400 MHz, $CDCl_3$) 7.27 (1H, app dd, *J* 2.5 and 1.7, 6-H), 7.23 (1H, app t, *J* 5.9, 2-H), 7.19 – 7.15 (1H, m, 5-H), 6.95 (1H, ddd, *J* 8.2, 2.6 and 1.0, 4-H), 4.52 – 4.20 (1H, m, cyclopentyl 1-H), 2.20 – 1.87 (2H, m, cyclopentyl 2-H and 5-H), 1.82 – 1.56 (4H, m, cyclopentyl 2-H, 3-H, 4-H and 5-H) and 1.50 – 1.28 (2H, m, cyclopentyl 3-H and 4-H); δ_C (100 MHz, $CDCl_3$) 167.0, 159.8, 136.5, 129.5, 118.5, 117.4, 112.3, 55.5, 51.8, 33.3 and 23.8; v_{max}/cm^{-1} (film); 3245, 3073, 2957, 2869, 2828, 1631,

1602. 1586 and 1536; HRMS Found MH^+: 220.1354 ($C_{13}H_{18}NO_2$ r*equires MH,* 220.1338).

N-cyclopentyl-3,4-dimethoxybenzamide, 107

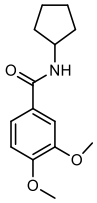

107

According to general procedure F, 3,4-dimethoxybenzoic acid (0.50 g, 2.80 mmol) and cyclopentylamine (543 μL, 5.50 mmol) gave a crude material which was purified using column chromatography eluting with hexane–EtOAc (50:50) to yield the benzamide **107** as a white solid (604 mg, 88%); *R*f = 0.10 (hexane–EtOAc 50:50); δ_H (300 MHz, $CDCl_3$) 7.35 (1H, d, *J* 2.0, 2-H), 7.15 (1H, dd, *J* 8.3 and 2.0, 6-H), 6.77 (1H, d, *J* 8.3, 5-H), 5.93 (1H, br s, NH), 4.39 – 4.24 (1H, m, cyclopentyl 1-H), 3.86 (3H, s, 4-methoxy), 3.84 (3H, s, 3-methoxy), 2.09 – 1.96 (2H, m, cyclopentyl 2-H and 5-H), 1.71 – 1.52 (4H, m, cyclopentyl 2-H, 3-H, 4-H and 5-H) and 1.51 – 1.34 (2H, m, cyclopentyl 3-H and 4-H); δ_C (100 MHz, $CDCl_3$) 166.8, 151.5, 148.9, 127.6, 119.2, 110.7, 110.2, 56.0, 51.7, 33.2 and 23.9; ν_{max}/cm^{-1} (film);3313, 2960, 2870, 2839, 1629, 1603, 1583, 1541 and 1502; HRMS Found MH^+: 250.1437 ($C_{14}H_{20}NO_3$ r*equires MH,* 250.1438).

***N*-cyclopentyl-4-methoxybenzamide, 108**

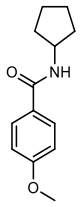

108

According to general procedure F, 4-methoxybenzoic acid (0.50 g, 3.30 mmol) and cyclopentylamine (652 μL, 6.60 mmol) gave a crude material which was purified using column chromatography eluting with hexane–EtOAc (70:30) to yield the benzamide **108** as a white solid (625 mg, 86%); *R*f = 0.25 (hexane–EtOAc 70:30); δ_H (400 MHz, $CDCl_3$) 7.67 – 7.61 (2H, m,

2-H and 6-H), 6.88 – 6.80 (2H, m, 3-H and 5-H), 4.37 – 4.27 (1H, m, cyclopentyl 1-H), 3.77 (3H, s, methoxy H), 2.08 – 1.93 (2H, m, cyclopentyl 2-H and 5-H), 1.81 – 1.52 (4H, m, cyclopentyl 2-H, 3-H, 4-H and 5-H) and 1.48 – 1.33 (2H, m, cyclopentyl 3-H and 4-H); δ_C (100 MHz, $CDCl_3$) 166.7, 162.0, 128.6, 127.3, 113.7, 55.4, 51.6, 33.3 and 23.8; ν_{max}/cm^{-1} (film); 3291, 2962, 2869, 1645, 1607, 1577, 1531 and 1496; HRMS Found MH^+:220.1283 ($C_{13}H_{18}NO_2$ r*equires MH,* 220.1288).

_N_-cyclopentyl-4-(1H-pyrazol-1-yl)benzamide, 116

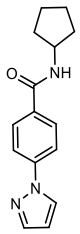

116

According to general procedure F, 4-(pyrazol-1-yl)benzoic acid (0.50 g, 2.70 mmol) and cyclopentylamine (525 μL, 5.40 mmol) gave a crude material which was purified using column chromatography eluting with hexane–EtOAc (70:30) to yield the benzamide **116** as a white solid (527 mg, 81%); *R*f = 0.20 (hexane–EtOAc 70:30); δ_H (300 MHz, $CDCl_3$) 7.91 (1H, d, *J* 2.5, pyrazol-1-yl 5-H_1), 7.81 – 7.75 (2H, m, 2-H and 6-H), 7.74 – 7.66 (3H, m, 3-H, 5-H and pyrazol-1-yl 3-H), 6.67 – 6.26 (1H, m, pyrazol-1-yl 4-H), 5.97 (1H, br s, NH), 4.76 – 4.02 (1H, m, cyclopentyl 1-H), 2.13 – 1.96 (2H, m, cyclopentyl 2-H and 5-H), 1.77 – 1.54 (4H, m, cyclopentyl 2-H, 3-H, 4-H and 5-H) and 1.50 – 1.36 (2H, m, cyclopentyl 3-H and 4-H); δ_C (100 MHz, $CDCl_3$) 166.2, 142.2, 141.7, 132.6, 128.3, 126.8, 118.6, 108.3, 51.8, 33.3 and 23.9; ν_{max}/cm^{-1} (film); 2961, 1650, 1601, 1520 and 1500; HRMS Found MH^+: 256.1375 ($C_{15}H_{18}N_3O$ r*equires MH, 2*56.1400).

_N_-ethyl-1,2-oxazole-3-carboxamide, 112

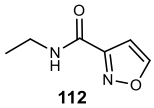

112

A solution of isoxazole-3-carboxylic acid (1.00 g, 8.50 mmol), TBTU (6.00 g, 18.0 mmol) and DIPEA (3.10 mL, 18.0 mmol) in CH_2Cl_2 (20 mL) was

stirred at rt for 1 h. Ethylamine hydrochloride was added (4.50 g, 44.0 mmol), and the reaction mixture stirred at rt overnight. The reaction mixture was diluted with H_2O (15 mL), extracted with EtOAc (3 x 10 mL) washed with a saturated sodium bicarbonate solution (3 x 10 mL), brine (3 x 10 mL), dired ($MgSO_4$) and concentrated under reduced pressure. The crude residue was purified using column chromatography eluting with hexane–EtOAc (50:50) to yield the oxazole **112** as a yellow solid (0.60 g, 48 %); *R*f = 0.46 (hexane–EtOAc 50:50); δ_H (400 MHz, $CDCl_3$) 8.48 (1H, d, *J* 1.7 5-H), 6.84 (1H, d, *J* 1.7 4-H), 3.51 (2H, q, *J* 7.3 ethyl CH_2) and 1.27 (3H, t, *J* 7.3, ethyl CH_3);δ_C (100 MHz, $CDCl_3$) 159.7, 158.5, 157.9, 104.4, 34.5 and 14.7; ν_{max}/cm^{-1} (film); 3157, 3124, 2981, 1789, 1676 and 1654; HRMS Found MNa^+: 163.0475 ($C_6H_8N_2O_2Na$ *requires MNa*, 163.0483).

4-(1H-pyrazol-1-yl)benzamide, 114

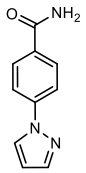

114

A solution of ammonium chloride (0.28 g, 1.07 mmol) in distilled water (4 mL) was covered with a thin layer of toluene (3 mL) and cooled to 0 ^oC. A solution of NaOH (0.42 g, 2.2 mmol) in distilled water (3 mL) was added directly to the aqueous layer followed by a solution of 4-(1H-pyrazol-1-yl)benzyl chloride (1.0 g, 4.85 mmol) in toluene (20 mL). The biphasic mixture was stirred overnight at rt and then cooled to 0 ^oC and the resulting precipitate was filtered, washed with cold water (3 x 20 mL) and toluene (3 x 20 mL) to yield the benzamide **114** as a colourless solid (491 mg, 55%); $\delta_{H,}$ (400 MHz, DMSO-d_6) 8.60 (1H, d, *J* 2.2, pyrazol-1-yl 3-H), 8.01 (2H, d, *J* 8.6, phenyl 2-H and 6-H), 7.94 (2H, d, *J* 8.6, phenyl 3-H and 5-H), 7.80 (1H, d, *J* 2.2, pyrazol-1-yl 5-H), 7.40 (1H, *br* s, NH) and 6.59 (1H, t, *J* 2.2, pyrazol-1-yl 4-H); $\delta_{C,}$ (100 MHz, DMSO) 167.5, 142.0, 132.1, 129.5, 128.5, 118.1 and 108.8; ν_{max}/cm^{-1} (film): 3414, 3156, 3107, 1752 and 1654; HRMS Found MH^+: 188.0816 ($C_{10}H_9N_3O$ *requires MH*,188.0824).

1-benzoyl-4-methylpiperazine, 97

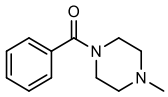

97

To a solution of methyl piperazine (925 µL, 8.00 mmol) in 50:50 CH_2Cl_2-ether (10 mL) was added dropwise a solution of benzoyl chloride (923 µL, 8.00 mmol) in CH_2Cl_2-ether (2 mL) and stirred overnight at rt. The resulting precipitate was filtered, washed with cold ether (2 x 10 mL) to yield the piperazine **97** a colourless amorphous solid (1.47 g, 90%), $\delta_{H,}$ (400 MHz, DMSO-d_6) 7.57–7.37 (5H, m, phenyl H_5), 3.39 (4H, appearing as v. broad m, piperazine 2-H_2 and 6-H_2), 3.19 (4H, s appearing as v. broad m, piperazine 3-H_2 and 5-H_2), 2.75 (3H, s, methyl); $\delta_{C,}$ (100 MHz, DMSO) 169.7, 135.2, 130.5, 129.0, 127.6, 52.4, 49.7 and 42.5; v_{max}/cm^{-1} (film): 3340, 2954 1625 and1575; HRMS Found MH^+: 205.1337 ($C_{12}H_{16}N_2O$ *requires MH,* 205.1341).

BODIPY-labeled Geldanamycin, 130

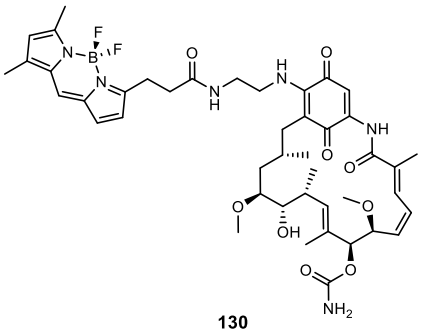

130

A solution of BODIPY FL EDA (2.50 mg, 0.07 mmol), Geldanamycin (8.00 mg, 0.014 mmol) and DIPEA (7.50 µL, 0.042 mmol) in CH_2Cl_2 was stirred at rt for 24 h. The mixture was was purified by column chromatography eluting with 75:25 CH_2Cl_2-acetone to yield GM-BODIPY **130**[156] (5.00 mg 86%). *R*f = 0.38 (75:25 CH_2Cl_2-acetone); δ_H (500 MHz, $CDCl_3$) 9.13 (1H, s), 7.20 (1H, s), 7.05 (1H, s), 6.95 (1H, d, *J* 11.7), 6.83 (1H, d, *J* 4.1), 6.62-6.54 (2H, m), 6.25 (1H, d, *J* 4.1), 6.13 (1H, s), 5.91 (1H, d, *J* 9.5), 5.86 (1H, t, *J* 10.5), 5.18 (1H, s), 4.76 (2H, *br* NH), 4.31 (2H, d, *J* 9.9), 3.65-3.41 (5H, m), 3.35 (3H, s), 3.27 (3H, s), 3.25 (2H, d, *J* 7.3), 2.73 (3H, dtd, *J* 14.5, 7.1 and 2.1), 2.55 (3H, s), 2.30 (1H, dd, *J* 14.0 and 10.7), 2.25 (3H, s), 2.03 (2H, s), 1.80 (3H, d, *J* 1.3), 1.78 (2H, t, *J* 3.8), 1.73-1.65 (1H, m), 1.00 (3H, d, *J* 6.9), 0.94 (3H,

d, *J* 6.7); $\delta_{C,}$ (100 MHz, DMSO-d_6) 183.9, 180.3, 173.1, 168.3, 156.2, 156.0, 145.6, 140.8, 135.8, 135.0, 133.9, 132.7, 128.1, 126.6, 123.9, 120.7, 117.3, 109.0, 81.8, 81.5, 81.3, 72.6, 69.5, 57.1, 56.7, 53.8, 53.4, 46.9, 39.2, 35.6, 35.0, 34.2, 32.3, 31.7, 29.7, 29.3, 24.7, 22.8, 15.0, 12.8, 12.6, 12.3, 11.4 and 1.0; ν_{max}/cm^{-1} (film); 3456, 2249 and 1620; HRMS Found MNa$^+$: 885.4149 ($C_{44}H_{57}BF_2N_6O_9$ *requires MNa,* 885.4156). Data consistent with literature.[156]

4-(1H-pyrazol-5-yl)phenyl acetate, F6

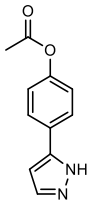

F6

General Procedure A yielded acetate F6 as a pale yellow oil (0.22 g, 98%); δ_H (300 MHz, $CDCl_3$) 8.21 (1H, d, *J* 2.8, pyrazolyl 4-H), 7.82 (2H, dt, *J* 8.7 and 2.0, 2-H and 6-H), 7.11 (2H, dt, *J* 8.7 and 2.0, 3-H and 5-H), 6.67 (1H, d, *J* 2.8, pyrazolyl 5-H) and 2.25 (3H, s, OAc); δ_C (100 MHz, CD_3OD) 169.7, 157.2, 150.5, 126.9, 126.4, 121.8, 115.5 and 19.5; ν_{max}/cm^{-1} (film); 3150, 2918, 1739 and 1606; HRMS Found MH$^+$: 203.0823 ($C_{11}H_{11}N_2O_2$ *requires MH*, 203.0821)

4-(Diethylcarbamoyl)-2-methoxyphenyl acetate, F1

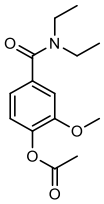

F1

General Procedure A yielded acetate **F1** as a pale yellow oil (0.60 g, 98%); δ_H (300 MHz, $CDCl_3$) 6.97 (1H, d, *J* 8.1, 6-H), 6.95 (1H, d, *J* 1.9, 3-H), 6.86 (1H, dd, *J* 8.1 and 1.9, 5-H), 3.77 (3H, s, methoxy), 3.35 (4H, very br d *(rotameric)* ethyl CH_2), 2.25 (3H, s, OAc) and 1.28 – 0.97 (6H, m, ethyl CH_3); δ_C (75 MHz, $CDCl_3$) 170.7, 168.8, 151.2, 140.4, 135.5, 122.7, 118.5, 111.1,

56.0, 43.4, 39.5 and 20.6; v_{max}/cm^{-1} (film); 2980, 2254, 1762, 1713 and 1617; HRMS Found MH^+: 266.1418 ($C_{14}H_{20}NO_4$ *requires MH*, 266.1392)

4-(4-methylpiperazine-1-carbonyl)phenyl acetate, F10

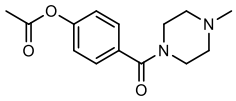

F10

General Procedure A yielded acetate **F10** as a pale yellow oil (39.0 mg, 6%); δ_H (300 MHz, $CDCl_3$) 7.38 (2H, d, *J* 8.6, 2-H AND 6-H), 7.08 (2H, d, *J* 8.6, 3-H and 5-H), 3.78 (4H, br s piperazine 2-H_2 and 6-H_2), 2.76 (4H, s, piperazine 3-H_2 and 5-H_2), 2.49 (3H, s, OAc) and 2.25 (3H, s, *N*-Me). δ_C (100 MHz, $CDCl_3$) 169.1, 158.5, 129.4, 128.6, 121.8, 115.4, 54.0, 44.9, 44.6 and 21.1; v_{max}/cm^{-1} (film); 2929, 2798, 1754, 1713 and 1607; HRMS Found MH^+: 263.1398 ($C_{14}H_{19}N_2O_3$ *requires MH*, 263.1396).

4-propanoylphenyl acetate, F4

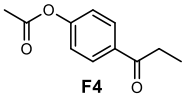

F4

General Procedure A yielded acetate **F4** as a pale yellow oil (0.70 g, 98%); δ_H (300 MHz, $CDCl_3$) 7.93 (2H, d, *J* 8.8, 2-H and 6-H), 7.12 (2H, d, *J* 8.8, 3-H and 5-H), 2.92 (2H, q, *J* 7.2, propanoyl 2-H_2), 2.26 (3H, s, OAc) and 1.16 (3H, t, *J* 7.2, propanoyl 3-H_2); δ_C (100 MHz, CD_3OD) 171.7, 169.1, 146.4, 129.3, 123.5, 121.6, 31.2, 19.5 and 7.1; v_{max}/cm^{-1} (film); 2979, 1753, 2939, 1680 and 1592.

Methyl 2-[3,5-bis(acetyloxy)phenyl]acetate, F5

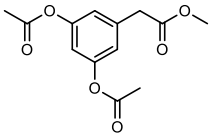

F5

General Procedure A yielded acetate **F5** as a pale yellow oil (0.66 g, 90%); δ_H (300 MHz, $CDCl_3$) 6.87 (2H, d, *J* 2.1, phenyl 2-H_1 and 6-H_1), 6.79 (1H, t, *J* 2.1, phenyl 4-H_1), 3.62 (3H, s, methoxy), 3.54 (2H, s, acetate 2-H_2) and

2.20 (6H, s, OAc); δ_C (75 MHz, CD_3OD) 172.9, 170.6, 152.5, 137.9, 121.1, 115.4, 52.5, 41.0 and 20.8; v_{max}/cm^{-1} (film); 2955, 1765. 1733, 1616 and 1593; HRMS Found MNa^+: 289.0699 ($C_{13}H_{14}O_6Na$ *requires MNa* 289.0688).

Methyl 3,5-bis(acetyloxy)benzoate, F3

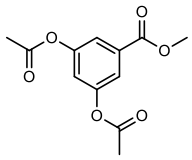

F3

General Procedure A yielded acetate **F3** as a pale yellow oil (0.70 g, 94%); δ_H (300 MHz, $CDCl_3$), 7.59 (2H, d, *J* 2.2, 2-H and 6-H), 7.07 (1H, t, *J* 2.2, 4-H), 3.84 (3H, s, methoxy) and 2.23 (6H, s, OAc); δ_C (75 MHz, CD_3OD), 172.9, 170.6, 152.5, 137.9, 121.1, 115.4, 52.5 and 41.0; v_{max}/cm^{-1} (film); 3082, 2963, 1767, 1713 and 1590; HRMS Found MNa^+: 275.0549 ($C_{12}H_{12}O_6Na$ *requires MNa* 275.0531)

3-phenyl-5H-1,4,2-dioxazol-5-one, S12

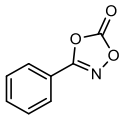

S12

To a stirred solution of benzohydroxamic acid (0.50 g, 3.70 mmol) in CH_2Cl_2 (40 mL) was added carbonyldiamidazole (0.60 g, 3.70 mmol) and the reaction stirred at rt for 0.5 h. The reaction was quenched with HCl (1N, 20 mL), extracted with CH_2Cl_2 (3 x 20 mL), dried ($MgSO_4$) and concentrated under reduced pressure to afford the dioxazolone **S12** as a white solid (0.55 g); *R*f = 0.5 (hexane–EtOAc 90:10); δ_H (400 MHz, $CDCl_3$) 7.92 – 7.85 (2H, m, 2-H and 6-H), 7.72 – 7.64 (1H, m, 4-H) and 7.62 – 7.53 (2H, m, 3-H and 5-H); δ_C (100 MHz, $CDCl_3$) 1635, 153.8, 133.8, 129.4, 126.6 and 120.2; v_{max}/cm^{-1} (film); 2980, 1893, 1862, 1616 and 1590

4-Nitro-2-(propan-2-yl)phenol, 132

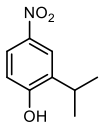

132

According to a modified procedure,[166] 70% HNO_3 (2.5 mL) was added to a solution of 2-isopropylphenol (5.00 g, 37.0 mmol) in EtOAc (25 mL) at 0 ºC. $ZnCl_2$ (5.00 g, 37.0 mmol) was added and the mixture sonicated at rt for 1 h and then stirred at rt overnight. The reaction mixture was diluted with H_2O (25 mL) and the organics washed with H_2O (3 x 20 mL), saturated aqueous sodium bicarbonate solution (3 x 20 mL) and brine (3 x 20 mL), dried ($MgSO_4$) and concentrated under reduced pressure. The crude orange oil was purified using flash column chromatography eluting with a gradient of hexane–EtOAc (95:5 to 0:100) to yield the phenol **132** as a bright yellow oil (3.50 g, 57%); *R*f = 0.19 (hexane–EtOAc 80:20); δ_H (400 MHz, $CDCl_3$) 8.05 (1H, d, *J* 2.8, 3-H), 7.92 (1H, dd, *J* 8.8 and 2.8, 5-H), 6.79 (1H, d, *J* 8.8, 6-H), 3.21 (1H, hept, *J* 6.9, propan-2-yl 2-H) and 1.21 (6H, d, *J* 6.9, propan-2-yl 1-H_3 and 3-H_3); δ_C (100 MHz, $CDCl_3$) 159.7, 142.0, 136.4, 123.7, 123.4, 115.7, 27.5 and 22.6; ν_{max}/cm^{-1} (film); 3204, 2967, 2872, 1607, 1541 and1452**;** LC-MS Found MH^+:182.2 ($C_9H_{12}NO_3$ *requires MH*, 182.1).

Tert-butyldimethyl[4-nitro-2-(propan-2-yl)phenoxy]silane, 133

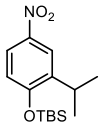

133

To a solution of tert-butyldimethylsilyl chloride (2.90 g, 19/0 mmol) and imidazole (1.30 g, 19.0 mmol) in CH_2Cl_2 (50 mL) was added 4-Nitro-2-(propan-2-yl)phenol **132** (3.50 g, 19.0 mmol) and the reaction stirred at rt overnight. The reaction mixture was diluted with H_2O (25 mL), the aqueous extracted with CH_2Cl_2 (3 x 20 mL) and the combined organics washed with saturated aqueous sodium bicarbonate solution (3 x 20 mL) and brine (3 x 20 mL), dried ($MgSO_4$) and concentrated under reduced pressure. The crude product was purified using flash column chromatography eluting with hexane–EtOAc (80:20) to yield the silane **133** as an orange oil (4.10 g,

74%); *R*f = 0.5 (hexane–EtOAc 80:20); δ_H (400 MHz, $CDCl_3$) 8.11 (1H, d, *J* 2.8, 3-H), 7.98 (1H, dd, *J* 8.9 and 2.8, 5-H), 6.82 (1H, d, *J* 8.9, 6-H), 3.31 (1H, hept, *J* 6.9, propan-2-yl 2-H), 1.23 (6H, d, *J* 6.9, propan-2-yl 1-H_3 and 3-H_3), 1.03 (9H, s, tert-butyl H_9) and 0.30 (6H, s, dimethyl H_6); δ_C (101 MHz, $CDCl_3$) 158.8, 141.9, 140.3, 122.8, 122.6, 117.9, 26.9, 25.7, 22.5, 18.3 and -4.1; ν_{max}/cm^{-1} (film); 2960, 2931, 2860, 1608, 1584,1514 and 1486; HRMS Found MH^+: 296.1688 ($C_{15}H_{26}NO_3Si$ *requires MH*, 296.1682).

4-[(Tert-butyldimethylsilyl)oxy]-3-(propan-2-yl)aniline, 134

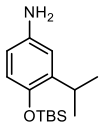

134

To a solution of tert-butyldimethyl[4-nitro-2-(propan-2-yl)phenoxy]silane **133** (2.00 g, 6.80 mmol) in EtOAc (75 mL) was added 10% Pd/C (2.00 g). The flask was flushed with nitrogen and then repeatedly evacuated and flushed with hydrogen and the reaction left to stir under a hydrogen atmosphere at rt overnight. The reaction flask was purged with nitrogen and filtered through a short plug of celite and the celite washed with EtOAc (3 x 15 mL). The filtrate was concentrated under reduced pressure and the crude product purified using flash column chromatography eluting with hexane–EtOAc (70:30) to yield the aniline **134** as an orange-brown oil (1.40 g, 78%); *R*f = 0.15 (hexane–EtOAc 70:30); δ_H (400 MHz, $CDCl_3$) 6.40 (1H, d, *J* 8.4, 5-H), 6.39 (1H, d, *J* 2.9, 2-H), 6.22 (1H, dd, *J* 8.4 and 2.9, 6-H), 3.19 (2H, br s, NH_2), 3.06 (1H, hept, *J* 6.9, propan-2-yl 2-H), 0.97 (6H, d, *J* 6.9, propan-2-yl 1-H_3 and 3-H_3), 0.82 (9H, s, tert-butyl, H_9) and 0.00 (6H, s, dimethyl H_6); δ_C (100 MHz, $CDCl_3$) 145.5, 140.0, 139.8, 118.9, 113.8, 113.2, 26.6, 26.2, 22.9, 18.3 and -4.2; ν_{max}/cm^{-1} (film); 3385, 2966, 2972, 1612, 1588, 1520 and 1492; HRMS Found M_2Na^+: 553.3414 ($C_{30}H_{54}N_2O_2Si_2Na$ *requires* M_2Na, 553.3622).

4-[(Tert-butyldimethylsilyl)oxy]-*N*-methyl-3-(propan-2-yl)aniline, 135

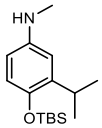

135

By modification of an existing procedure,[167] copper acetate (1.80 g, 9.80 mmol) was added to a solution of 4-[(Tert-butyldimethylsilyl)oxy]-3-(propan-2-yl)aniline **134** (1.00 g, 3.80 mmol) and pyridine (1.00 mL, 13.3 mmol) in dioxane (50 mL) and the reaction mixture stirred at rt for 0.25 h. To the reaction mixture was added methyl boronic acid (0.50 g, 8.30 mmol) and the reaction mixture heated to 100 ^{o}C for 3 h. The reaction mixture was filtered through celite, concentrated under reduced pressure, diluted with EtOAc (30 mL), washed with H_2O (3 x 10 mL), saturated aqueous sodium bicarbonate solution (3 x 10 mL) and brine (3 x 10 mL), dried ($MgSO_4$) and concentrated under reduced pressure. The crude product was purified using flash column chromatography eluting with a gradient of hexane–EtOAc (100:0 to 50:50) to give the aniline **135** as an orange-brown solid (0.56 g, 53%); *R*f = 0.4 (hexane–EtOAc 80:20); δ_H (400 MHz, $CDCl_3$) 6.65 (1H, d, *J* 8.5, 5-H1), 6.51 (1H, d, *J* 2.9, 2-H), 6.35 (1H, dd, *J* 8.5 and 2.9, 6-H), 3.41 (1H, s, br NH H_1), 3.26 (1H, hept, *J* 6.9, propan-2yl 2-H_1), 2.80 (3H, s, Methyl H_3), 1.18 (6H, d, *J* 6.9, propan-2-yl 1-H_3 and 3-H_3), 1.01 (9H, s, tert-butyl H_9) and 0.19 (6H, s dimethyl H_6); δ_C (100 MHz, $CDCl_3$) 144.8, 143.8, 139.7, 118.9, 111.3, 109.9, 31.6, 26.7, 25.9, 22.9, 18.3 and -4.2; ν_{max}/cm^{-1} (film); 2960, 2930, 2859, 1612, 1588 and 1499; HRMS Found MH^+:280.2043 ($C_{16}H_{30}NOSi$ *requires MH*, 280.2097).

***N*-{4-[(Tert-butyldimethylsilyl)oxy]-3-(propan-2-yl)phenyl}-2-diazoacetamide, DF1**

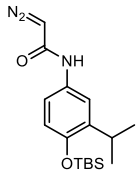

DF1

p-Toluenesulfonylhydrazone acid chloride (700 mg, 2.70 mmol) was dissolved in CH_2Cl_2 (10 mL), flushed with nitrogen and cooled to 0 °C. A solution of aniline **134** (500 mg, 1.90 mmol) in CH_2Cl_2 (5 mL) and dimethylaniline (350 μL, 2.70 mmol) were slowly added and the reaction mixture stirred for 2 h before dropwise addition of triethylamine (1.20 mL, 8.10 mmol). The reaction mixture was allowed to return to rt and the resulting red solution stirred for a further 0.5 h. The reaction mixture was washed with 10% (w/v) aqueous citric acid solution (3 x 10 mL), the combined organics dried (Na_2SO_4) and concentrated under reduced pressure. The crude product was purified using flash column chromatography eluting with pentane–ether (50:50) to yield the diazoacetamide **DF1** as a yellow solid (333 mg, 50%); *R*f = 0.20 (Pentane–ether 50:50); δ_H (500 MHz, Acetone-d_6) 8.72 (1H, br s, NH), 7.42 (1H, d, *J* 2.6, 2-H), 7.37 (1H, dd, *J* 8.6 and 2.6, 6-H), 6.77 (2H, d, *J* 8.6, 5-H), 5.36 (1H, s, diazoacetamide 2-H), 3.33 (1H, hep, *J* 6.9, propan-2-yl 2-H), 1.18 (6H, d, *J* 6.9 propan-2-yl 1-H_3 and 3-H_3), 1.04 (9H, s, tert-butyl H_9) and 0.25 (6H, s, dimethyl H_6); δ_C (125 MHz, Acetone-d_6) 164.1, 149.2, 139.8, 134.7, 119.3, 118.4, 118.3, 48.4, 27.5, 26.3, 23.3, 19.0 and -3.9; v_{max}/cm^{-1} (film); 3279, 3085, 2959, 2929, 2886, 2858, 2101, 1622, 1602, 1550, 1490 and 1471; HRMS Found MH^+: 334.1949 ($C_{17}H_{28}N_3O_2Si$ *requires MH*, 334.1951).

***N*-{4-[(tert-butyldimethylsilyl)oxy]-3-(propan-2-yl)phenyl}-2-diazo-*N*-methylacetamide, DF2**

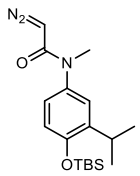

DF2

p-Toluenesulfonylhydrazone acid chloride (700 mg, 2.70 mmol) was dissolved in CH_2Cl_2 (10 mL), flushed with nitrogen and cooled to 0 °C. A solution of aniline **135** (500 mg, 1.80 mmol) in CH_2Cl_2 (5 mL) and dimethylaniline (350 μL, 2.70 mmol) were slowly added and the reaction mixture stirred for 2 h before dropwise addition of triethylamine (1.20 mL, 8.10 mmol). The reaction mixture was allowed to return to rt and the resulting red solution stirred for a further 0.5 h. The reaction mixture was washed with 10% (w/v) aqueous citric acid solution (3 x 10 mL), the combined organics dried (Na_2SO_4) and concentrated under reduced pressure. The crude product was purified using column chromatography eluting with pentane–ether (80:20) to yield the diazoacetamide **DF2** as a yellow solid (500 mg, 79%); *R*f = 0.40 (Pentane–ether 80:20); δ_H (500 MHz, Acetone-d_6) 7.15 (1H, d, *J* 2.7, 2-H), 7.00 (1H, dd, *J* 8.5 and 2.7, 6-H), 6.91 (1H, d, *J* 8.5, 5-H), 4.77 (1H, s, diazoacetamide 2-H), 3.35 (1H, hept, *J* 6.9, propan-2-yl 2-H), 3.21 (3H, s, methyl H_3), 1.21 (6H, d, *J* 6.9, propan-2-yl 1-H_3 and 3-H_3), 1.05 (9H, s, tert-butyl H_9) and 0.29 (6H, s, dimethyl H_6); δ_C (125 MHz, Acetone-d_6) 166.0, 153.0, 141.3, 137.8, 126.4, 126.4, 120.0, 47.3, 37.4, 27.7, 26.3, 23.2, 19.0 and -3.9; ν_{max}/cm^{-1} (film); 3280, 3085, 2959, 2930, 2859, 2101, 1622, 1602, 1549 and 1491; HRMS Found MH^+: 348.2112 ($C_{18}H_{30}N_3O_2Si$ *requires MH*, 348.2107).

6.3 Biology

6.3.1 Protein Expression

6.3.1.1 Cell Lines, Media and Buffers

Bacterial Strains and Plasmids:

***E. coli* DH5α cells**: – For plasmid Cloning

***E. coli* BL21 (DE3):** – For Protein Production

pET-28a (Kan^r) plasmid: contains the His_6-Hsp90-NTD(D9-E236) gene.

Media:

Luria-Bertani Broth – 25 g/L

For 100 mL of Luria-Bertani broth (25 g/L) 2.50 g of Luria-Bertani medium was added to dH_2O (100 mL) and autoclaved (20 min, 121 °C) and stored at rt.

Kanamycin 1000x stock – 25 mg/mL

For 5 mL 1000X Kanamycin, 125 mg of Kanamycin was added to dH_2O (5 mL), sterile filtered (0.22 µM syringe filter) and stored at -20 °C (1 mL aliquots).

Isopropyl β-d-1-thiogalactopyranoside (IPTG) 1000x stock – 238 mg/mL

For 3 mL 1000X IPTG, 714 mg of IPTG was added to dH_2O (3 mL) sterile filtered (0.22 µM syringe filter) and stored at -20 °C (1 mL aliquots).

Luria-Bertani Agar with Kanamycin (25 µg/mL) Plates

For 400 mL Luria Bertani/Agar solution containing 25 g/L LB and 15 g/L Agar, 10 g Luria Bertani medium and 6 g Agar was added to dH_2O (400 mL) and autoclaved (20 min, 121 °C). Once the solution had reached 50 °C, 1000x Kanamycin (400 µL) was added and the solution poured into plates (25 mL/plate). The plates were left to harden at rt and stored at 4 °C.

Buffers:

Buffer A (40 mM HEPES, pH 8, 300 mM NaCl, 5 mM DTT)

For 2000 mL of Buffer A, 1M HEPES (80 mL), 4M NaCl (150 mL) and 1M DTT (10 mL) was added to dH_2O (1600 mL), adjusted to pH 8, volumed to 2000 mL by addition of dH_2O, filter sterilised and stored at 4 °C.

Buffer B (40 mM HEPES, pH 8, 300 mM NaCl, 5 mM DTT, 1M Imidazole)

For 300 mL of Buffer B, Imidazole (20.4 g) was added to Buffer A (300 mL), filter sterilised and stored at 4 °C.

Wash Buffer B1 (40 mM HEPES, pH 8, 300 mM NaCl, 5 mM DTT, 10 mM Imidazole)

For 300 mL Buffer B1, mix Buffer A (297 mL) and Buffer B (3 mL) and store at 4 °C.

Wash Buffer B2 (40 mM HEPES, pH 8, 300 mM NaCl, 5 mM DTT, 20 mM imidazole)

For 300 mL Buffer B2, mix Buffer A (294 mL) and Buffer B (6 mL) and store at 4 °C.

Elution Buffer B3 (40 mM HEPES, pH 8, 300 mM NaCl, 5 mM DTT, 250 mM Imidazole)

For 300 mL Buffer B3, mix Buffer A (225 mL) and Buffer B (75 mL) and store at 4 °C.

Storage Buffer (20 mM, pH 7.5)

For 200 mL NaP_i Buffer (20 mM) add 0.5 M Na_2HPO_4 to dH_2O (192 mL) and adjust pH 7.5 with 0.5 M NaH_2PO_4.

Fluorescence Anisotropy (FA) HEPES Buffer (pH 7.3)

To dH_2O was added 20 mM HEPES (pH 7.3), 50 mM KCl, 5mM $MgCl_2$, 20mM Na_2MoO_4, 0.01% Np40 (Tergitol) followed by fresh addition before use of 0.1 mg/mL Bovine Gamma Globulin (BGG) and 2mM 1,4-Dithiothreitol (DTT).

4XSB Buffer (SDS-Gel)

For 1 mL of 4XSB buffer add 4xlaemelli (900 µL) to 2-mercaptoethanol (100 µL) and stored at 4 °C.

6.3.1.2 Transformations for Plasmid Stocks and Sequencing

pET-28a (Kan^r) plasmid containing His_6-Hsp90-NTD(D9-E236) (2 µL) was transformed into an aliquot of DH5α cells (25-50 µL) by incubating the plasmid with the cells on ice for 30 min. The transformation mixture was subjected to a heat shock (42 °C) for 45 sec. Luria-Bertani Media (500 µL) was added to the transformation mixture and then incubated for 1 h (37 °C, 250 rpm). The mixture was centrifuged (3000 rpm, 2 min), the supernatant discarded, the pellet re-suspended and then plated onto LB Agar with kanamycin (25 µg/mL). The plates were incubated (37 °C) overnight (maximum of 16 h). A single colony was picked from the plate and incubated in LB media (5 mL) containing Kanamycin (5 µL, 30 °C, 250 rpm) overnight. The plasmid was then isolated and purified using a PureLink® Quick Plasmid Miniprep Kit as described in the manufacturer's instructions. Plasmid stocks were stored at –20 °C.

6.3.1.3 Protein Expression

For protein expression transformations were carried out as above into BL21 (DE3) *E. coli* cells. Following incubation overnight, a single colony was picked from the plate and incubated in Luria-Bertani media (5 mL) containing kanamycin (5 µL) for *ca.* 4 h or until the optical density (OD) at 600 nm had reached ~1.00 (37 °C, 250 rpm). This starter culture (2 mL) was transferred into pre-warmed Luria-Bertani media (50 mL, starting OD_{600} ~ 0.1) and incubated *ca.* 2 h or until the optical OD_{600} ~1.00 (37 °C, 250 rpm). The culture mixture was then transferred to pre-warmed Luria-Bertani media (450 mL,

starting OD_{600} ~ 0.1) and incubated *ca.* 2 h or until the optical OD_{600} ~1.00 (37 °C, 250 rpm). Protein expression was induced by adding 1 mM IPTG (500 µL of IPTG 1000X stock per 500 mL of culture) and incubated overnight (20 °C, 250 rpm). Cells were harvested by centrifugation (5000 rpm, 20 min, 4 °C), the supernatant discarded, the pellet re-suspended in buffer A (35 mL) and stored at -80 °C.

6.3.1.4 Cell Lysis

The bacterial pellet was removed from the -80 °C and allowed to thaw to rt. and inverted slowly to allow gentle mixing. Lysozyme (20 mg/mL) and one protease inhibitor P8849 tablet (Roche complete EDTA free) dissolved in buffer A (1 mL) was added to the thawed pellet. The pellet was incubated on ice for 0.5 h. The pellet was then sonicated (6 sec. on/6 sec. off × 10 cycles) at 4 °C. The sonicated pellet was centrifuged (20,000 rpm, 20 min, 4 °C). The supernatant was sterile filtered (0.45 µm syringe filter) and kept on ice ready for purification.

6.3.1.5 Purification of His_6-Hsp90-NTD(D9-E236)

The cell lysate containing His_6-Hsp90-NTD(D9-E236) was loaded onto a Ni-packed column (GE Healthcare Life Sciences) using buffer A (10 mL), washed with buffer B1 (10 mL) and buffer B2 (10 mL), and protein eluted with buffer B3 (20 mL). Following elution the fractions containing His_6-Hsp90-NTD(D9-E236) were collected and combined and then dialysed against NaP_i buffer (pH 7.3) overnight at 4 °C. Protein purification was analysed by SDS PAGE and by HRMS.

6.4 Fluorescence Anisotropy Assay

6.4.1 Measurement of Anisotropy

Fluorescence Anisotropy measurements were carried out on an Envision™ 2013 multilabel plate reader (PerkinElmer) using the following optics:

	Manufacturer's Description	Wavelength (nm)	Bandwidth (nm)
Dichromoic Mirror	FITC FP D505 Single Mirror	505	
Excitation Filter	FITC FP 485	485	14
Emission Filter 1:	FITC FP P-pol 535	535	40
Emission Filter 2:	FITC FP S-pol 535	535	40

Assays were performed using black 384 well plates (Corning #4514 or #3676). The reading protocol was optimised (instrument gain, read height) using the instrument software to ensure that the detector was not saturated. 150 flashes were used per measurement.

The anisotropy (*r*) was calcuated using equation 1.

$$r = 1000 \times \frac{s - gp}{s + g2p} \quad \boldsymbol{Equation\ 1}$$

The total fluorescence intensity (I) was calculated using equation 2.

$$I = S + g2p \quad \boldsymbol{Equation\ 2}$$

Where s in the intensity of light emitted with the same polarisation as the excitation light, p is the light emitted with perpendicular polarisation to the excitation light, g is the grating factor which accounts for the responsiveness of an instrument to light with differing polarisations. In these assays this was set to 0.91 as part of the optimisation process.

Blank corrections were performed by subtracting the average of the appropriate blank in the s and p channels prior to calculations of the anisotropy.

The BODIPY-labelled Geldanamycin was stored as stock solutions at 190 μM in DMSO at – 20 °C. All stock solutions were kept on ice at all times.

6.4.2 Determination of Limits of Anisotropy

To rows A-F, wells 1-24 was added 10 μL of FA buffer. 10 μL of a protein stock solution (60 μM, 4x final concentration) was added to well 1 in each of the rows A-F, and the contents of the well agitated with a pipette. Following addition and agitation 10 μL of the contents of well 1 in rows A-F was transferred to well 2, agitated, then 10 μL transferred to well 3. The process was repeated across the entire series to well 23 across rows A-F, where after agitation 10 μL was removed and discarded. 10 μL of 100 nM BODIPY-Geldanamycin (final concentration 50 nM) was added to all well in rows A, C and E and 10 μL of FA buffer added to all wells in rows B, D, and F to serve as blanks. Plates were incubated at 4 °C for 20 h (optimal incubation time) and the anisotropy of each well was measured and the average intensities measured in the wells containing no tracer (rows B, D and F) were used to provide a blank correction for each protein concentration. The anisotropy was plotted against protein concentration with the standard deviation of the replicates used as the error. The data was fitted to a logistic function (equation 3) to find the lower and upper limits of the anisotropy r_{max}, r_{min} which reflect the anisotropy of the tracer when in the unbound and bound state state respectively.

$$r = \frac{r_{min} - r_{max}}{1 + (x/x_0)^p} + r_{max} \quad \textbf{Equation 3}$$

Average values were calculated to be r_{max} = 139 r_{min} = - 4 and these values were used throughout subsequent assays. This data was also used to calculate the change in quantum yield between the bound and free states of the assay by checking for any variation in total intensity over the course of the titration ($\lambda = 2.39$).

6.4.3 Determination of the Dissociation Constant of the Fluorescent Tracer

A serial dilution by a ½ of protein (stock concentration 60 μM, 4x final concentration) across a series, rows A-F, well 1-24 was performed as described above, followed by addition of 10 μL of tracer (100 nM, final concentration 50 nM) to wells 1-24 in rows A, C and E and 10 μL of buffer to wells 1-24 in rows B, D and F to serve as blanks. The anisotropy in each well was calculated and converted to the fraction of tracer bound using equation 4 and finally into the amount of tracer bound by multiplying by the total concentration of tracer in the well of interest (50 nM).

$$\frac{L_B}{L_T} = \left[\frac{\lambda(r_{max} - r)}{(r - r_{\min})} + 1\right]^{-1} \quad \textbf{\textit{Equation 4}}$$

The data was plotted and fitted to equation 5 using a non-linear least squares fitting algorithm in Originpro to determine the K_d of the tracer for the protein. The error in K_d was obtained from the fitting error within the procedure.

$$L_B = \frac{(L_T + P_T + K_d) - \sqrt{(L_T + P_T + K_d)^2 - 4L_T P_T}}{2} \quad \textbf{\textit{Equation 5}}$$

L_B is the concentration of fluorescent tracer bound to protein, L_T is the total tracer concentration, P_T is the total concentration of protein.

6.4.4 Competition Experiments to Determine the Dissociation Constant of Unlabelled Ligands

Dissociation constants for unlabelled control ligands; geldanamycin, ATP and ADP, and all subsequent unlabelled ligands were determined as described. Stocks of unlabelled ligand were prepared in DMSO (500 mM) and diluted in FA buffer (50 mM) prior to addition to the assay plate. 10 μL of buffer was added to wells 1-24 in rows A-D. 10 μL of unlabelled ligand was added to well 1 in each of the four rows and diluted by ½ across the entire series. 5 μL of tracer (200 nM) was added to all wells in rows A-C and 5 μL of buffer to all well in row D. Finally, 5 μL of protein (2 μM) was added to all wells in rows A-D. The plates were incubated at 4 ^{o}C for 20 h and the anisotropy for all wells

measured and calculated by subtracting the intensities of the s and p channels in the blank wells from the well of interest. The anisotropy in each well was converted into the fraction of tracer bound using equation 4, and finally into the amount of tracer bound by multiplying by the final tracer concentration (50 nM). The bound amount was plotted against the $\log_{10}$ of the competitor concentration and the data fitted to a single site competition model (Equation 6) in OriginPro. The error in IC_{50} was taken from the fitting error of the data.

$$L_B = Min + \frac{(Max - Min)}{1 + 10^{(x - LogIC_{50})}} \quad \boldsymbol{Equation\ 6}$$

Where *x* is the Log_{10} of the unlabelled ligand concentration. Max and Min are the upper and lower asymptotes of the curve.

The IC_{50} values were then converted into K_i of the competitor ligand by combination with K_d of the protein using the method of Nicolovska-Coleska.[168]

As the error in the final K_i involves components from the error in the measurement of the K_d of the tracer and the IC_{50} of the inhibitor, the error was assessed using simulation. A series of simulations were run with a simulated value of K_d and IC_{50} generated around the observed mean, the probability of the value occurring was based upon a normal distribution with standard deviation equal to the fitting error of each value. The simulated value was then propagated to give a simulated Ki. 2000 simulations were performed with the final error estimated from the standard deviation of the simulated results.

6.4.5 Fragment Screen

Fragment stocks were prepared in DMSO at 500 mM and subsequently diluted to 50 mM in FA buffer prior to addition to the assay plate. Screening of individual compounds was performed in triplicate, with a single blank recorded for each concentration of ligand. 10 μL of FA buffer was added to wells 1-24 across four rows of the plate. To the first well in each row was added 10 μL of 50 mM fragment (4X stock) and was diluted by ½ across each well in the row to well 23, where after the final addition and agitation 10 μL was removed and discarded. To all wells in three rows was added 5 uL of tracer (200 nM, 4X stock) and to all wells in the fourth row was added 5 uL of FA buffer (serves

as blank). Finally, to all wells in all four rows was added 5 μL of protein (2 μM, 4X stock). The plates were incubated at 4 ^{o}C for 20 h, and the anisotropy measured for each well in the series.

6.4.6 Screening Crude Reaction Array Mixtures

Crude reaction mixtures were stored as 100 mM DMSO stocks and were diluted accordingly into DMSO and then DMSO:Buffer (8:92) at four times the final assay concentration prior to addition into the assay plate. Reaction array mixtures were screened in triplicate and with a single blank (no tracer) as a control. 5 μL of the reaction array mixtures in DMSO:Buffer (8:92) were added to the well of interest followed by 5 μL of a 200 nM tracer solution (5 μL of buffer for the blank). Finally 10 μL of a 1 μM protein stock solution was added to all wells to give a final concentration of 50 nM tracer and 500 nM protein. The final DMSO concentration in all wells was 2%. Assay plates were incubated at 4 ^{o}C for 20 h. The anisotropy in each well was calculated and the anisotropy data normalised relative to the positive (10 μM geldanamycin) and negative (2% DMSO) controls.

List of References

1 X. S. Zheng, T. F. Chan and H. H. Zhou, *Chem. Biol.*, 2004, **11**, 609–618.

2 U. Rix and G. Superti-Furga, *Nat. Chem. Biol.*, 2009, **5**, 616–624.

3 M. Aitken, M. Kleinrock, J. Lyle, D. Nass and L. Caskey, *Medicines Use and Spending Shifts: A Review of the Use of Medicines in the U.S. in 2014*, New Jersey, 2015.

4 A. M. Edwards, R. Isserlin, G. D. Bader, S. V. Frye, T. M. Willson and F. H. Yu, *Nature*, 2011, **470**, 163–165.

5 S. M. Paul, D. S. Mytelka, C. T. Dunwiddie, C. C. Persinger, B. H. Munos, S. R. Lindborg and A. L. Schacht, *Nat. Rev. Drug Discov.*, 2010, **9**, 203–214.

6 B. Munos, *Nat. Rev. Drug Discov.*, 2009, **8**, 959–968.

7 D. E. Scott, A. R. Bayly, C. Abell and J. Skidmore, *Nat. Rev. Drug Discov.*, 2016, **15**, 533–550.

8 C. A. Lipinski, *Drug Discov. Today Technol.*, 2004, **1**, 337–341.

9 P. G. Polishchuk, T. I. Madzhidov and A. Varnek, *J. Comput. Aided. Mol. Des.*, 2013, **27**, 675–679.

10 A. H. Lipkus, Q. Yuan, K. A. Lucas, S. A. Funk, W. F. Bartelt 3rd, R. J. Schenck, A. J. Trippe and C. A. S. Registry, *J. Org. Chem.*, 2008, **73**, 4443–4451.

11 S. R. Langdon, N. Brown and J. Blagg, *J. Chem. Inf. Model.*, 2011, **51**, 2174–2185.

12 R. D. Taylor, M. MacCoss and A. D. G. Lawson, *J. Med. Chem.*, 2014, **57**, 5845–5859.

13 D. G. Brown and J. Boström, *J. Med. Chem.*, 2018, **61**, 9442–9468.

14 R. MacArron, M. N. Banks, D. Bojanic, D. J. Burns, D. A. Cirovic, T. Garyantes, D. V. S. Green, R. P. Hertzberg, W. P. Janzen, J. W. Paslay, U. Schopfer and G. S. Sittampalam, *Nat. Rev. Drug Discov.*, 2011, **10**, 188–195.

15 J. P. Hughes, S. Rees, S. B. Kalindjian and K. L. Philpott, *Br. J. Pharmacol.*, 2011, **162**, 1239–1249.

16 G. Karageorgis, S. Warriner and A. Nelson, *Nat. Chem.*, 2014, **6**, 872–876.

17 G. Karageorgis, M. Dow, A. Aimon, S. Warriner and A. Nelson, *Angew. Chemie, Int. Ed. English*, 2015, **54**, 13538–13544.

18 D. C. Blakemore, L. Castro, I. Churcher, D. C. Rees, A. W. Thomas, D. M. Wilson and A. Wood, *Nat. Chem.*, 2018, **10**, 383–394.

19 J. Boström, D. G. Brown, R. J. Young and G. M. Keserü, *Nat. Rev. Drug Discov.*, 2018, **17**, 709–727.

20 D. G. Brown and J. Bostrom, *J. Med. Chem.*, 2016, **59**, 4443–4458.

21 S. D. Roughley and A. M. Jordan, *J. Med. Chem.*, 2011, **54**, 3451–3479.

22 T. W. J. Cooper, I. B. Campbell and S. J. F. MacDonald, *Angew. Chemie - Int. Ed.*, 2010, **49**, 8082–8091.

23 W. P. Walters, J. Green, J. R. Weiss and M. A. Murcko, *J. Med. Chem.*, 2011, **54**, 6405–6416.

24 N. Schneider, D. M. Lowe, R. A. Sayle, M. A. Tarselli and G. A. Landrum, *J. Med. Chem.*, 2016, **59**, 4385–4402.

25 F. Lovering, J. Bikker and C. Humblet, *J. Med. Chem.*, 2009, **52**, 6752–6756.

26 D. J. Foley, A. Nelson and S. P. Marsden, *Angew. Chemie - Int. Ed.*, 2016, **55**, 13650–13657.

27 A. Nadin, C. Hattotuwagama and I. Churcher, *Angew. Chemie - Int. Ed.*, 2012, **51**, 1114–1122.

28 K. R. Campos, P. J. Coleman, J. C. Alvarez, S. D. Dreher, R. M. Garbaccio, N. K. Terrett, R. D. Tillyer, M. D. Truppo and E. R. Parmee, *Science (80-.).*, 2019, **363**, eaat0805.

29 J. Twilton, C. (Chip) Le, P. Zhang, M. H. Shaw, R. W. Evans and D. W. C. MacMillan, *Nat. Rev. Chem.*, 2017, **1**, 0052.

30 M. H. Shaw, J. Twilton and D. W. C. MacMillan, *J. Org. Chem.*, 2016, **81**, 6898–6926.

31 R. Grainger, T. D. Heightman, S. V. Ley, F. Lima and C. N. Johnson, *Chem. Sci.*, 2019, **10**, 2264–2271.

32 S. L. Kidd, T. J. Osberger, N. Mateu, H. F. Sore and D. R. Spring, *Front. Chem.*, 2018, **6**, 460.

33 A. W. Hung, A. Ramek, Y. Wang, T. Kaya, J. A. Wilson, P. A. Clemons and D. W. Young, *Proc. Natl. Acad. Sci.*, 2011, **108**, 6799–6804.

34 S. Caputo, L. Banfi, A. Basso, A. Galatini, L. Moni, R. Riva and C. Lambruschini, *European J. Org. Chem.*, 2017, **2017**, 6619–6628.

35 D. A. Contreras-Cruz, M. A. Sánchez-Carmona, F. A. Vengoechea-Gómez, D. Peña-Ortíz and L. D. Miranda, *Tetrahedron*, 2017, **73**, 6146–6156.

36 H. S. G. Beckmann, F. Nie, C. E. Hagerman, H. Johansson, Y. S. Tan, D. Wilcke and D. R. Spring, *Nat. Chem.*, 2013, **5**, 861–867.

37 R. Doveston, S. Marsden and A. Nelson, *Drug Discov. Today*, 2014, **19**, 813–819.

38 J. Mayol-Llinàs, W. Farnaby and A. Nelson, *Chem. Commun.*, 2017, **53**, 12345–12348.

39 M. Mondal and A. K. H. Hirsch, *Chem. Soc. Rev.*, 2015, **44**, 2455–2488.

40 R. A. Goodnow, C. E. Dumelin and A. D. Keefe, *Nat. Rev. Drug Discov.*, 2017, **16**, 131–147.

41 D. A. Erlanson, S. W. Fesik, R. E. Hubbard, W. Jahnke and H. Jhoti, *Nat. Rev. Drug Discov.*, 2016, **15**, 605–619.

42 M. Baker, *Nat. Rev. Drug Discov.*, 2013, **12**, 5–7.

43 B. C. Doak, C. J. Morton, J. S. Simpson and M. J. Scanlon, *Aust. J. Chem.*, 2013, **66**, 1465–1472.

44 C. W. Murray and D. C. Rees, *Angew. Chemie, Int. Ed. English*, 2016, **55**, 488–492.

45 M. M. Hann, A. R. Leach and G. Harper, *J. Chem. Inf. Comput. Sci.*, 2001, **41**, 856–864.

46 D. E. Scott, A. G. Coyne, S. A. Hudson and C. Abell, *Biochemistry*, 2012, **51**, 4990–5003.

47 C. W. Murray, M. L. Verdonk and D. C. Rees, *Trends Pharmacol. Sci.*, 2012, **33**, 224–232.

48 D. Joseph-McCarthy, A. J. Campbell, G. Kern and D. Moustakas, *J. Chem. Inf. Model.*, 2014, **54**, 693–704.

49 D. C. Rees, M. Congreve, C. W. Murray and R. Carr, *Nat. Rev. Drug Discov.*, 2004, **3**, 660–672.

50 A. L. Hopkins, G. M. Keseru, P. D. Leeson, D. C. Rees and C. H. Reynolds, *Nat. Rev. Drug Discov.*, 2014, **13**, 105–121.

51 G. Bollag, J. Tsai, J. Zhang, C. Zhang, P. Ibrahim, K. Nolop and P. Hirth, *Nat. Rev. Drug Discov.*, 2012, **11**, 873–886.

52 A. J. Souers, J. D. Leverson, E. R. Boghaert, S. L. Ackler, N. D. Catron, J. Chen, B. D. Dayton, H. Ding, S. H. Enschede, W. J. Fairbrother, D. C. S. Huang, S. G. Hymowitz, S. Jin, S. L. Khaw, P. J. Kovar, L. T. Lam, J. Lee, H. L. Maecker, K. C. Marsh, K. D. Mason, M. J. Mitten, P. M. Nimmer, A. Oleksijew, C. H. Park, C. M. Park, D. C. Phillips, A. W. Roberts, D. Sampath, J. F. Seymour, M. L. Smith, G. M. Sullivan, S. K. Tahir, C. Tse, M. D. Wendt, Y. Xiao, J. C. Xue, H. Zhang, R. A. Humerickhouse, S. H. Rosenberg and S. W. Elmore, *Nat. Med.*, 2013, **19**, 202–208.

53 K. D. Collins and F. Glorius, *Nat. Chem.*, 2013, **5**, 597–601.

54 T. Chapman, *Nature*, 2003, **421**, 661–666.

55 S. V. Ley, D. E. Fitzpatrick, R. J. Ingham and R. M. Myers, *Angew. Chemie - Int. Ed.*, 2015, **54**, 3449–3464.

56 J. Li, S. G. Ballmer, E. P. Gillis, S. Fujii, M. J. Schmidt, A. M. E. Palazzolo, J. W. Lehmann, G. F. Morehouse and M. D. Burke, *Science (80-.).*, 2015, **347**, 1221–1226.

57 A. Buitrago Santanilla, E. L. Regalado, T. Pereira, M. Shevlin, K. Bateman, L.-C. Campeau, J. Schneeweis, S. Berritt, Z.-C. Shi, P. Nantermet, Y. Liu, R. Helmy, C. J. Welch, P. Vachal, I. W. Davies, T. Cernak and S. D. Dreher, *Science (80-.).*, 2015, **347**, 49–53.

58 D. Perera, J. W. Tucker, S. Brahmbhatt, C. J. Helal, A. Chong, W. Farrell, P. Richardson and N. W. Sach, *Science (80-.).*, 2018, **359**, 429–434.

59 K. Troshin and J. F. Hartwig, *Science (80-.).*, 2017, **357**, 175–181.

60 S. Chow, S. Liver and A. Nelson, *Nat. Rev. Chem.*, 2018, **2**, 174–183.

61 S. Y. F. W. Hawkes, M. J. V. Chapela and M. Montembault, *QSAR Comb. Sci.*, 2005, **24**, 712–721.

62 A. Baranczak, N. P. Tu, J. Marjanovic, P. A. Searle, A. Vasudevan and S. W. Djuric, *ACS Med. Chem. Lett.*, 2017, **8**, 461–465.

63 W. Czechtizky, J. Dedio, B. Desai, K. Dixon, E. Farrant, Q. Feng, T. Morgan, D. M. Parry, M. K. Ramjee, C. N. Selway, T. Schmidt, G. J. Tarver and A. G. Wright, *ACS Med. Chem. Lett.*, 2013, **4**, 768–772.

64 L. Guetzoyan, R. J. Ingham, N. Nikbin, J. Rossignol, M. Wolling, M. Baumert, N. A. Burgess-Brown, C. M. Strain-Damerell, L. Shrestha, P. E. Brennan, O. Fedorov, S. Knapp and S. V. Ley, *Medchemcomm*, 2014, **5**, 540–546.

65 L. Guetzoyan, N. Nikbin, I. R. Baxendale and S. V. Ley, *Chem. Sci.*, 2013, **4**, 764–769.

66 B. Desai, K. Dixon, E. Farrant, Q. Feng, K. R. Gibson, W. P. Van Hoorn, J. Mills, T. Morgan, D. M. Parry, M. K. Ramjee, C. N. Selway, G. J. Tarver, G. Whitlock and A. G. Wright, *J. Med. Chem.*, 2013, **56**, 3033–3047.

67 M. Werner, C. Kuratli, R. E. Martin, R. Hochstrasser, D. Wechsler, T. Enderle, A. I. Alanine and H. Vogel, *Angew. Chemie - Int. Ed.*, 2014, **53**, 1704–1708.

68 N. J. Gesmundo, B. Sauvagnat, P. J. Curran, M. P. Richards, C. L. Andrews, P. J. Dandliker and T. Cernak, *Nature*, 2018, **557**, 228–232.

69 J. B. Murray, S. D. Roughley, N. Matassova and P. A. Brough, *J. Med. Chem.*, 2014, **57**, 2845–2850.

70 D. J. Newman and G. M. Cragg, *J. Nat. Prod.*, 2012, **75**, 311–335.

71 T. Rodrigues, D. Reker, P. Schneider and G. Schneider, *Nat. Chem.*, 2016, **8**, 531–541.

72 R. D. Firn and C. G. Jones, *Nat. Prod. Rep.*, 2003, **20**, 382.

73 R. A. Maplestone, M. J. Stone and D. H. Williams, *Gene*.

74 Y. L. Huang and J. W. Bode, *Nat. Chem.*, 2014, **6**, 877–884.

75 P. Rugbjerg, M. Naesby, U. Mortensen and R. Frandsen, *Microb. Cell Fact.*, 2013, **12**, 1–9.

76 J. Lou, R. Yu, X. Wang, Z. Mao, L. Fu, Y. Liu and L. Zhou, *Brazilian J. Microbiol.*, 2016, **47**, 96–101.

77 H. M. L. Davies and D. Morton, *Chem. Soc. Rev.*, 2011, **40**, 1857–1869.

78 H. M. L. Davies and R. E. J. Beckwith, *Chem. Rev.*, 2003, **103**, 2861–2903.

79 D. Gillingham and N. Fei, *Chem. Soc. Rev.*, 2013, **42**, 4918–4931.

80 J. Kim, *J. Biomol. Screen.*, 2004, **9**, 375–381.

81 C. N. Johnson, F. Lima, R. Grainger, S. V. Ley and T. D. Heightman, *Chem. Sci.*, 2018, **00**, 1–3.

82 M. S. Khan, A. Haque, M. K. Al-Suti and P. R. Raithby, *J. Organomet. Chem.*, 2015, **793**, 114–133.

83 T. Gensch, M. N. Hopkinson, F. Glorius and J. Wencel-Delord, *Chem. Soc. Rev.*, 2016, **45**, 2900–2936.

84 Z. Chen, B. Wang, J. Zhang, W. Yu, Z. Liu and Y. Zhang, *Org. Chem. Front.*, 2015, **2**, 1107–1295.

85 D. Basu, S. Kumar, S. Sudhir and R. Bandichhor, *J. Chem. Sci*, 2039, **130**, 71.

86 J. Wencel-Delord and F. Glorius, *Nat. Chem.*, 2013, **5**, 369–375.

87 T. Cernak, K. D. Dykstra, S. Tyagarajan, P. Vachal and S. W. Krska, *Chem. Soc. Rev.*, 2016, **45**, 546–576.

88 T. Cernak, N. J. Gesmundo, K. Dykstra, Y. Yu, Z. Wu, Z. C. Shi, P. Vachal, D. Sperbeck, S. He, B. A. Murphy, L. Sonatore, S. Williams, M. Madeira, A. Verras, M. Reiter, C. H. Lee, J. Cuff, E. C. Sherer, J. Kuethe, S. Goble, N. Perrotto, S. Pinto, D. M. Shen, R. Nargund, J. Balkovec, R. J. DeVita and S. D. Dreher, *J. Med. Chem.*, 2017, **60**, 3594–3605.

89 J. Yang, *Org. Biomol. Chem.*, 2015, **13**, 1930–1941.

90 E. M. Beck, N. P. Grimster, R. Hatley and M. J. Gaunt, *J. Am. Chem. Soc.*, 2006, **128**, 2528–2529.

91 N. Lebrasseur and I. Larrosa, *J. Am. Chem. Soc.*, 2008, **130**, 2926–2927.

92 Y. Xu and G. Dong, *Chem. Sci.*, 2018, **9**, 1424–1432.

93 P. X. Shen, L. Hu, Q. Shao, K. Hong and J. Q. Yu, *J. Am. Chem. Soc.*, 2018, **140**, 6545–6549.

94 M. D. K. Boele, G. P. F. Van Strijdonck, A. H. M. De Vries, P. C. J. Kamer, J. G. De Vries and P. W. N. M. Van Leeuwen, *J. Am. Chem. Soc.*, 2002, **124**, 1586–1587.

95 H. Kim, K. Shin and S. Chang, *J. Am. Chem. Soc.*, 2014, **136**, 5904–5907.

96 H.-Y. Thu, W.-Y. Yu and C.-M. Che, *J. Am. Chem. Soc.*, 2006, **128**, 9048–9.

97 N. Umeda, K. Hirano, T. Satoh and M. Miura, *J. Org. Chem.*, 2009, **74**, 7094–7099.

98 C. Suzuki, K. Morimoto, K. Hirano, T. Satoh and M. Miura, *Adv. Synth. Catal.*, 2014, **356**, 1521–1526.

99 Z. Liang, L. Ju, Y. Xie, L. Huang and Y. Zhang, *Chem. - A Eur. J.*, 2012, **18**, 15816–15821.

100 L. Ackermann and J. Pospech, *Org. Lett.*, 2011, **13**, 4153–4155.

101 C. Zhu, Y. Zhang, J. Kan, H. Zhao and W. Su, *Org. Lett.*, 2015, **17**,

3418–3421.

102 H.-J. Xu, Y.-S. Kang, H. Shi, P. Zhang, Y.-K. Chen, B. Zhang, Z.-Q. Liu, J. Zhao, W.-Y. Sun, J.-Q. Yu and Y. Lu, *J. Am. Chem. Soc.*, 2019, **141**, 76–79.

103 J. Jiao, K. Murakami and K. Itami, *ACS Catal.*, 2016, **6**, 610–633.

104 H. Kim and S. Chang, *ACS Catal.*, 2015, **5**, 6665–6669.

105 C. Grohmann, H. Wang and F. Glorius, *Org. Lett.*, 2012, **14**, 656–659.

106 B. Haffemayer, M. Gulias and M. J. Gaunt, *Chem. Sci.*, 2011, **2**, 312–315.

107 F. Yang, F. Song, W. Li, J. Lan and J. You, *RSC Adv.*, 2013, **3**, 9649–9652.

108 R. B. Den and B. Lu, *Ther. Adv. Med. Oncol.*, 2012, **4**, 211–218.

109 A. D. Zuehlke, M. A. Moses and L. Neckers, *Philos. Trans. R. Soc. B Biol. Sci.*, , DOI:10.1098/rstb.2016.0527.

110 F. H. Schopf, M. M. Biebl and J. Buchner, *Nat. Rev. Mol. Cell Biol.*, 2017, **18**, 345–360.

111 A. J. Woodhead, H. Angove, M. G. Carr, G. Chessari, M. Congreve, J. E. Coyle, J. Cosme, B. Graham, P. J. Day, R. Downham, L. Fazal, R. Feltell, E. Figueroa, M. Frederickson, J. Lewis, R. McMenamin, C. W. Murray, M. A. O'Brien, L. Parra, S. Patel, T. Phillips, D. C. Rees, S. Rich, D. M. Smith, G. Trewartha, M. Vinkovic, B. Williams and A. J. A. Woolford, *J. Med. Chem.*, 2010, **53**, 5956–5969.

112 C. W. Murray, M. G. Carr, O. Callaghan, G. Chessari, M. Congreve, S. Cowan, J. E. Coyle, R. Downham, E. Figueroa, M. Frederickson, B. Graham, R. McMenamin, M. A. O'Brien, S. Patel, T. R. Phillips, G. Williams, A. J. Woodhead and A. J. A. Woolford, *J. Med. Chem.*, 2010, **53**, 5942–5955.

113 J. R. Huth, C. Park, A. M. Petros, A. R. Kunzer, M. D. Wendt, X. Wang, C. L. Lynch, J. C. Mack, K. M. Swift, R. A. Judge, J. Chen, P. L. Richardson, S. Jin, S. K. Tahir, E. D. Matayoshi, S. A. Dorwin, U. S. Ladror, J. M. Severin, K. A. Walter, D. M. Bartley, S. W. Fesik, S. W. Elmore and P. J. Hajduk, *Chem. Biol. Drug Des.*, 2007, **70**, 1–12.

114 S. D. Roughley and R. E. Hubbard, *J. Med. Chem.*, 2011, **54**, 3989–4005.

115 S. Roughley, L. Wright, P. Brough, A. Massey and R. E. Hubbard, *Top. Curr. Chem.*, 2012, **317**, 61–82.

116 J. Ren, J. Li, Y. Wang, W. Chen, A. Shen, H. Liu, D. Chen, D. Cao, Y. Li, N. Zhang, Y. Xu, M. Geng, J. He, B. Xiong and J. Shen, *Bioorganic Med. Chem. Lett.*, 2014, **24**, 2525–2529.

117 L. B. Peterson and B. S. Blagg, *Future Med. Chem.*, 2009, **1**, 267–283.

118 F. Ritossa, *Cell Stress Chaperones*, 1996, **1**, 97–98.

119 W. B. Pratt and D. O. Toft, *Endocr. Rev.*, 1997, **18**, 306–360.

120 P. C. Echeverría, A. Bernthaler, P. Dupuis, B. Mayer and D. Picard, *PLoS One*, 2011, **6**, e26044.

121 C. Prodromou, S. M. Roe, R. O'Brien, J. E. Ladbury, P. W. Piper and L. H. Pearl, *Cell*, 1997, **90**, 65–75.

122 S. F. Harris, A. K. Shiau and D. A. Agard, *Structure*, 2004, **12**, 1087–1097.

123 M. Jahn, A. Rehn, B. Pelz, B. Hellenkamp, K. Richter, M. Rief, J. Buchner and T. Hugel, *Proc. Natl. Acad. Sci.*, 2014, **111**, 17881–17886.

124 N. Wayne and D. N. Bolon, *J. Biol. Chem.*, 2007, **282**, 35386–35395.

125 M. P. Mayer and L. Le Breton, *Mol. Cell*, 2015, **58**, 8–20.

126 A. K. Shiau, S. F. Harris, D. R. Southworth and D. A. Agard, *Cell*, 2006, **127**, 329–340.

127 C. Prodromou, *Biochem. J.*, 2016, **473**, 2439–2452.

128 E. J. Solís, J. P. Pandey, X. Zheng, D. X. Jin, P. B. Gupta, E. M. Airoldi, D. Pincus and V. Denic, *Mol. Cell*, 2018, **69**, 534.

129 R. Voellmy and F. Boellmann, *Adv. Exp. Med. Biol.*, 2007, **594**, 89–99.

130 B. T. Scroggins and L. Neckers, *Expert Opin. Drug Discov.*, 2007, **2**, 1403–1414.

131 M. Mollapour, S. Tsutsumi, A. W. Truman, W. Xu, C. K. Vaughan, K. Beebe, A. Konstantinova, S. Vourganti, B. Panaretou, P. W. Piper, J. B. Trepel, C. Prodromou, L. H. Pearl and L. Neckers, *Mol. Cell*, 2011, **41**, 672–681.

132 M. Mollapour and L. Neckers, *Biochim. Biophys. Acta - Mol. Cell Res.*, 2012, **1823**, 648–655.

133 A. Röhl, J. Rohrberg and J. Buchner, *Trends Biochem. Sci.*, 2013, **38**, 253–262.

134 S. J. Felts and D. O. Toft, *Cell Stress Chaperones*, 2003, **8**, 108–113.

135 M. Taipale, I. Krykbaeva, M. Koeva, C. Kayatekin, K. D. Westover, G. I. Karras and S. Lindquist, *Cell*, 2012, **150**, 987–1001.

136 S. J. Park, B. N. Borin, M. A. Martinez-Yamout and H. J. Dyson, *Nat. Struct. Mol. Biol.*, 2011, **18**, 537–541.

137 G. E. Karagöz, A. M. S. Duarte, E. Akoury, H. Ippel, J. Biernat, T. Morán Luengo, M. Radli, T. Didenko, B. A. Nordhues, D. B. Veprintsev, C. A. Dickey, E. Mandelkow, M. Zweckstetter, R. Boelens, T. Madl and S. G. D. Rüdiger, *Cell*, 2014, **156**, 963–974.

138 E. Vartholomaiou, P. C. Echeverría and D. Picard, *Adv. Cancer Res.*, 2016, **129**, 1–30.

139 A. Rodina, T. Wang, P. Yan, E. D. Gomes, M. P. S. Dunphy, N. Pillarsetty, J. Koren, J. F. Gerecitano, T. Taldone, H. Zong, E. Caldas-Lopes, M. Alpaugh, A. Corben, M. Riolo, B. Beattie, C. Pressl, R. I. Peter, C. Xu, R. Trondl, H. J. Patel, F. Shimizu, A. Bolaender, C. Yang, P. Panchal, M. F. Farooq, S. Kishinevsky, S. Modi, O. Lin, F.

Chu, S. Patil, H. Erdjument-Bromage, P. Zanzonico, C. Hudis, L. Studer, G. J. Roboz, E. Cesarman, L. Cerchietti, R. Levine, A. Melnick, S. M. Larson, J. S. Lewis, M. L. Guzman and G. Chiosis, *Nature*, 2016, **538**, 397–401.

140 A. Kamal, L. Thao, J. Sensintaffar, L. Zhang, M. F. Boehm, L. C. Fritz and F. J. Burrows, *Nature*, 2003, **425**, 407–410.

141 C. G. Evans, S. Wisén and J. E. Gestwicki, *J. Biol. Chem.*, 2006, **281**, 33182–33191.

142 P. J. McLean, J. Klucken, Y. Shin and B. T. Hyman, *Biochem. Biophys. Res. Commun.*, 2004, **321**, 665–669.

143 X. Wang, J. Venable, P. LaPointe, D. M. Hutt, A. V. Koulov, J. Coppinger, C. Gurkan, W. Kellner, J. Matteson, H. Plutner, J. R. Riordan, J. W. Kelly, J. R. Yates and W. E. Balch, *Cell*, 2006, **127**, 803–815.

144 R. Geller, S. Taguwa and J. Frydman, *Biochim. Biophys. Acta - Mol. Cell Res.*, 2012, **1823**, 698–706.

145 N. Roy, R. K. Nageshan, S. Ranade and U. Tatu, *Biochim. Biophys. Acta*, 2012, **1823**, 707–11.

146 S. M. Roe, C. Prodromou, R. O'Brien, J. E. Ladbury, P. W. Piper and L. H. Pearl, *J. Med. Chem.*, 1999, **42**, 260–266.

147 P. Workman, F. Burrows, L. Neckers and N. Rosen, *Ann. N. Y. Acad. Sci.*, 2007, **1113**, 202–216.

148 T. W. Schulte and L. M. Neckers, *Cancer Chemother. Pharmacol.*, 1998, **42**, 273–279.

149 T. W. Schulte, S. Akinaga, S. Soga, W. Sullivan, B. Stensgard, D. Toft and L. M. Neckers, *Cell Stress Chaperones*, 1998, **3**, 100–108.

150 A. Khandelwal, V. M. Crowley and B. S. J. Blagg, *Med. Res. Rev.*, 2016, **36**, 92–118.

151 P. A. Brough, W. Aherne, X. Barril, J. Borgognoni, K. Boxall, J. E. Cansfield, K. M. J. Cheung, I. Collins, N. G. M. Davies, M. J. Drysdale, B. Dymock, S. A. Eccles, H. Finch, A. Fink, A. Hayes, R. Howes, R. E. Hubbard, K. James, A. M. Jordan, A. Lockie, V. Martins, A. Massey, T. P. Matthews, E. McDonald, C. J. Northfield, L. H. Pearl, C. Prodromou, S. Ray, F. I. Raynaud, S. D. Roughley, S. Y. Sharp, A. Surgenor, D. L. Walmsley, P. Webb, M. Wood, P. Workman and L. Wright, *J. Med. Chem.*, 2008, **51**, 196–218.

152 G. Chiosis, Y. Kang and W. Sun, *Expert Opin. Drug Discov.*, 2008, **3**, 99–114.

153 P. Krajewski and L. Kozerski, *Synth. Commun.*, 2004, **34**, 3737–3742.

154 I. Lalezari and H. Golgolab, *J. Chem. Eng. Data*, 1971, **16**, 117–117.

155 J. R. Lakowicz, *Princ. Fluoresc. Spectrosc.*, 2006, 1–954.

156 L. Llauger-Bufi, S. J. Felts, H. Huezo, N. Rosen and G. Chiosis, *Bioorganic Med. Chem. Lett.*, 2003, **13**, 3975–3978.

157 L. T. Gooljarsingh, C. Fernandes, K. Yan, H. Zhang, M. Grooms, K. Johanson, R. H. Sinnamon, R. B. Kirkpatrick, J. Kerrigan, T. Lewis, M. Arnone, A. J. King, Z. Lai, R. A. Copeland and P. J. Tummino, *Proc. Natl. Acad. Sci.*, 2006, **103**, 7625–7630.

158 R. Howes, X. Barril, B. W. Dymock, K. Grant, C. J. Northfield, A. G. S. Robertson, A. Surgenor, J. Wayne, L. Wright, K. James, T. Matthews, K.-M. Cheung, E. McDonald, P. Workman and M. J. Drysdale, *Anal. Biochem.*, 2006, **350**, 202–213.

159 S. M. Roe, C. Prodromou, R. O'Brien, J. E. Ladbury, P. W. Piper and L. H. Pearl, *J. Med. Chem.*, 1999, **42**, 260–266.

160 P. Gandeepan and C. H. Cheng, *J. Am. Chem. Soc.*, 2012, **134**, 5738–5741.

161 G. Liu, Y. Shen, Z. Zhou and X. Lu, *Angew. Chemie - Int. Ed.*, 2013, **52**, 6033–6037.

162 T. Hashimoto, N. Uchiyama and K. Maruoka, *J. Am. Chem. Soc.*, 2008, **130**, 14380–14381.

163 D. M. Hodgson and D. Angrish, *Chem. - A Eur. J.*, 2007, **13**, 3470–3479.

164 J. P. Wan, L. Gan and Y. Liu, *Org. Biomol. Chem.*, 2017, **15**, 9031–9043.

165 D. Y. K. Chen and S. W. Youn, *Chem. - A Eur. J.*, 2012, **18**, 9452–9474.

166 M. Makishima, H. Naitou, S. Arimoto-Kobayashi, K. Morishita, M. Nakayama, H. Tokiwa, T. Kobayashi, T. Oohashi, H. Kakuta, Y. Furusawa, A. Tai, E. Ishitsubo, K. Kawata and S. Yamada, *J. Med. Chem.*, 2014, **58**, 912–926.

167 I. González, J. Mosquera, C. Guerrero, R. Rodríguez and J. Cruces, *Org. Lett.*, 2009, **11**, 1677–1680.

168 Z. Nikolovska-Coleska, R. Wang, X. Fang, H. Pan, Y. Tomita, P. Li, P. P. Roller, K. Krajewski, N. G. Saito, J. A. Stuckey and S. Wang, *Anal. Biochem.*, 2004, **332**, 261–73.

Appendix A
Protection and Deprotection of Phenol Containing Hsp90 Fragments for C-H Functionalisation Reaction Arrays

A series of LC-MS and ^{1}H NMR (300 MHz) studies were performed to determine the deprotection of acetate-protected phenol Hsp90 fragments in parallel-based reaction format.

A.1 Acetate Protections and Deprotections

A.1.1 Fragment 92/F10

92/F10	LC-MS Analysis	^{1}H NMR (300 MHz)
Unprotected Start (**92**)	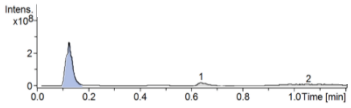 Mass Found $[MH]^+$: 221.3	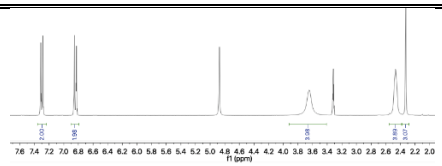
Protected (Purified **F10**)	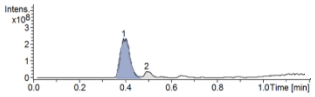 Mass Found $[MH]^+$: 263.4	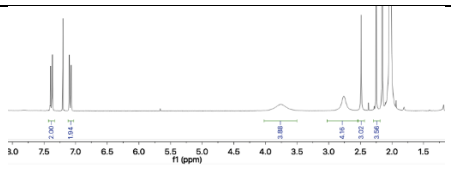
Deprotected (Purified **92**)	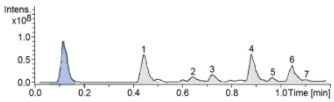 Mass Found $[MH]^+$: 221.3	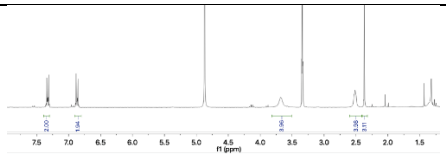
Deprotected in Plate (crude, **92**)	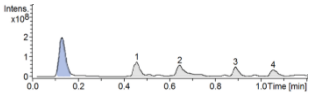 Mass Found $[MH]^+$: 221.3	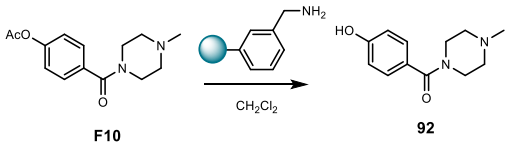

Table A1.1 LC-MS and ^{1}H NMR (300 MHz) for acetate protection and deprotection of phenol containing Hsp90 fragment **F10**. Protection was performed by reaction of phenol with acetic anhydride and pyridine and deprotection was performed with Na_2CO_3 in MeOH:THF:H_2O (2:1:1) and LC-MS and ^{1}H NMR (300 MHz) data collected. Deprotection was performed in plates with Quadrapure BzA resin (30 mg) and analysed by LC-MS. Calculated mass of unprotected **92** and protected **F10** fragment $[MH]^+$: 221.3 and $[MH]^+$: 263.3 respectively.

A.1.2 Fragment 88/F3

88/F3	LC-MS Analysis	^{1}H NMR (300 MHz)
Unprotected Start (**88**)	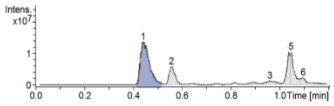 Mass Found [M-H]$^-$: 167.3	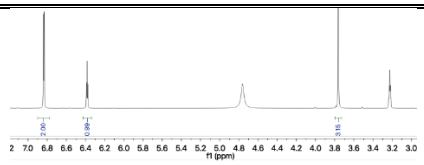
Protected (Purified **F3**)	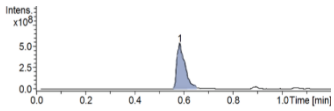 Mass Found [MH]$^+$: 253.3	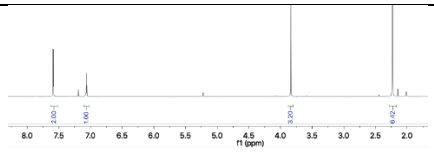
Deprotected (Purified **88**)	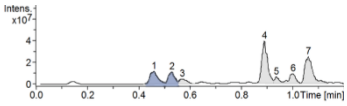 Mass: 1. [M-H]$^-$: 167.3 and 2. [MH]$^+$ 169.4	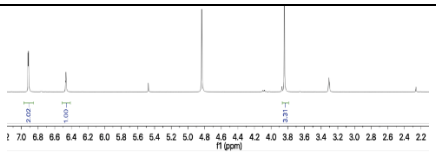
Deprotected in Plate (crude, **88**)	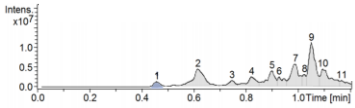 Mass Found [M-H]$^-$: 167.3	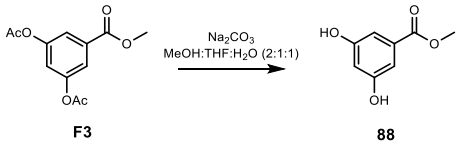
Deprotected in Plate (crude, **88**)	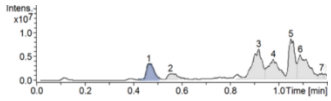 Mass Found [M-H]$^-$: 167.3	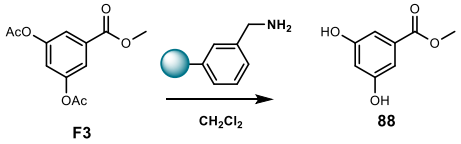

Table A1.2 LC-MS and ^{1}H NMR (300 MHz) for acetate protection and deprotection of phenol containing Hsp90 fragment **F3**. Protection was performed by reaction of phenol with acetic anhydride and pyridine and deprotection was performed with Na_2CO_3 in MeOH:THF:H_2O (2:1:1) and LC-MS and ^{1}H NMR (300 MHz) data collected. Deprotection was performed in plates with MeOH:THF:H_2O (2:1:1) and with Quadrapure BzA resin (30 mg) and analysed by LC-MS. Calculated mass of unprotected **88** and protected **F3** fragment [M-H]$^-$: 167.1 or [MH]$^+$: 169.2 and [MH]$^+$: 253.2 respectively.

A.1.3 Fragment 89/F5

89/F5	LC-MS Analysis	^{1}H NMR (300 MHz)
Unprotected Start (**89**)	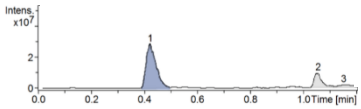 Mass Found [M-H]$^-$: 181.3	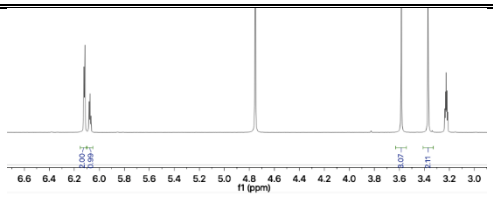
Protected (Purified **F5**)	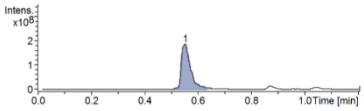 Mass Found [MH]$^+$: 267.3	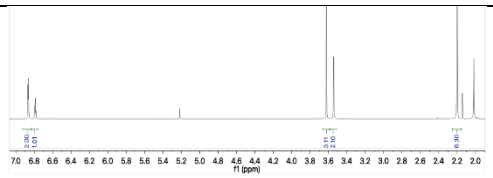
Deprotected (Purified **89**)	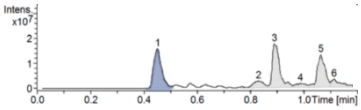 Mass Found [M-H]$^-$: 181.3	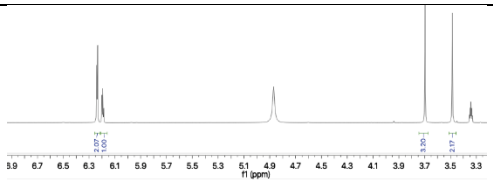
Deprotected in Plate (crude, **89**)	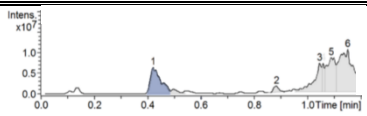 Mass Found [M-H]$^-$: 181.3	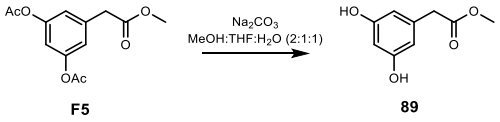
Deprotected in Plate (crude, **89**)	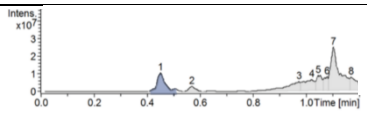 Mass Found [M-H]$^-$: 181.3	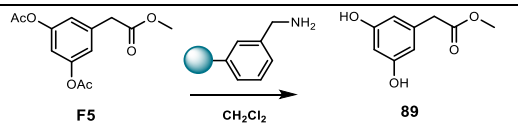

Table A1.3 LC-MS and ^{1}H NMR (300 MHz) for acetate protection and deprotection of phenol containing Hsp90 fragment **F5**. Protection was performed by reaction of phenol with acetic anhydride and pyridine and deprotection was performed with Na_2CO_3 in MeOH:THF:H_2O (2:1:1) and LC-MS and ^{1}H NMR (300 MHz) data collected. Deprotection was performed in plates with MeOH:THF:H_2O (2:1:1) and with Quadrapure BzA resin (30 mg) and analysed by LC-MS. Calculated mass of protected **F5** and unprotected fragment **89** [MH]$^+$: 267.3 and [M-H]$^-$: 181.2 respectively.

A.1.4 Fragment 94/F4

94/F4	LC-MS Analysis	^{1}H NMR (300 MHz)
Unprotected Start (**94**)	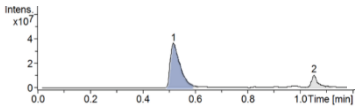 Mass Found $[MH]^+$: 151.5	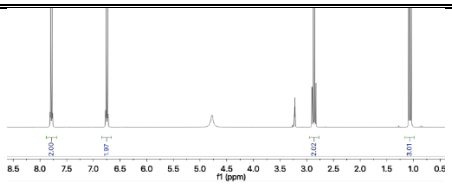
Protected (Purified **F4**)	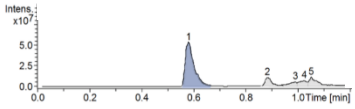 Mass Found $[M_2H]^+$: 385.2	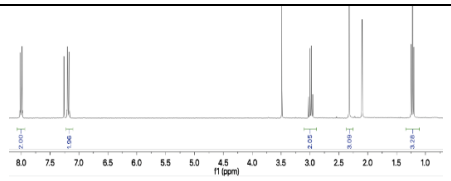
Deprotected (Purified **94**)	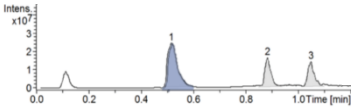 Mass Found $[MH]^+$: 151.5	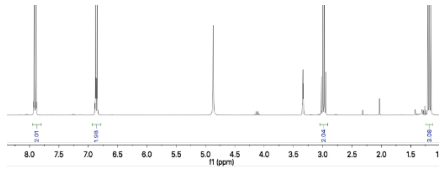
Deprotected in Plate (crude, **94**)	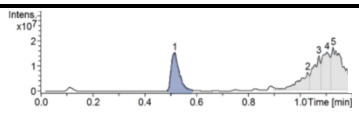 Mass Found $[MH]^+$: 151.4	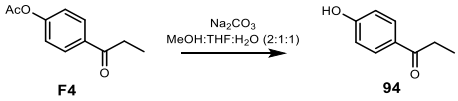
Deprotected in Plate (crude, **94**)	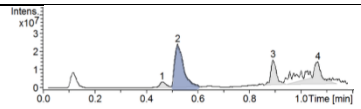 Mass Found $[MH]^+$: 151.4	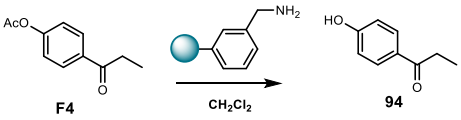

Table A1.4 LC-MS and ^{1}H NMR (300 MHz) for acetate protection and deprotection of phenol containing Hsp90 fragment **F4**. Protection was performed by reaction of phenol with acetic anhydride and pyridine and deprotection was performed with Na_2CO_3 in MeOH:THF:H_2O (2:1:1) and LC-MS and ^{1}H NMR (300 MHz) data collected. Deprotection was performed in plates with MeOH:THF:H_2O (2:1:1) and with Quadrapure BzA resin (30 mg) and analysed by LC-MS. Calculated mass of protected **F4** and unprotected fragment **94** $[M_2H]^+$: 385.4 and $[MH]^+$: 151.2 respectively.

A.1.5 Fragment 111/F6

111/F6	LC-MS Analysis	^{1}H NMR (300 MHz)
Unprotected Start (**111**)	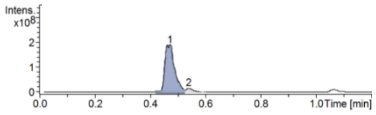 Mass Found $[MH]^+$: 161.4	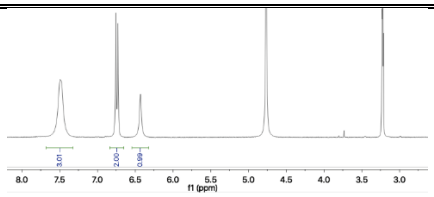
Protected (Purified **F6**)	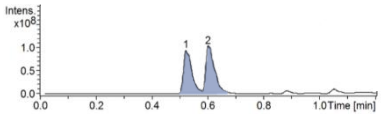 Mass Found $[MH]^+$: 203.4	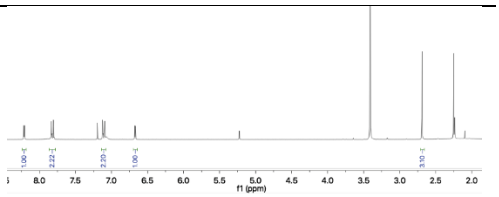
Deprotected (Purified **111**)	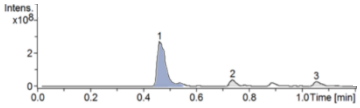 Mass Found $[MH]^+$: 161.4	
Deprotected in Plate (crude, **111**)	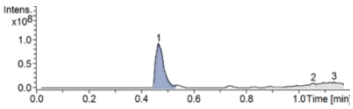 Mass Found $[MH]^+$: 161.4	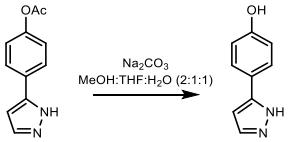
Deprotected in Plate (crude, **111**)	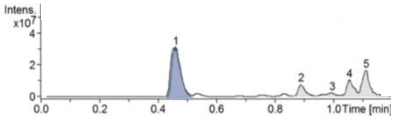 Mass Found $[MH]^+$: 161.4	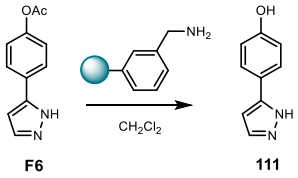

Table A1.5 LC-MS and ^{1}H NMR (300 MHz) for acetate protection and deprotection of phenol containing Hsp90 fragment **F6**. Protection was performed by reaction of phenol with acetic anhydride and pyridine and deprotection was performed with Na_2CO_3 in MeOH:THF:H_2O (2:1:1) and LC-MS and ^{1}H NMR (300 MHz) data collected. Deprotection was performed in plates with MeOH:THF:H_2O (2:1:1) and with Quadrapure BzA resin (30 mg) and analysed by LC-MS. Calculated mass of protected **F6** and unprotected fragment **111** $[MH]^+$: 203.2 and $[MH]^+$: 161.2 respectively.

Appendix B
Reaction Array Component Assay Controls

B.1 C-H functionalisation Reaction Arrays

B.1.1 Room Temperature Arrays

Component	Biological Activity, % (Relative to 10 μM Geldanamycin) Screened at 80 μM	Component	Biological Activity, % (Relative to 10 μM Geldanamycin) Screened at 80 μM
Catalyst 1	0.44	Catalyst 2	-2.79
Catalyst 3	-1.96	Catalyst 4	-1.86
Catalyst 5	0.44	Catalyst 6	-1.65
Catalyst 7	-0.42	Catalyst 8	-2.55
F1	-1.95	F2	-1.13
F3	-2.88	F4	-0.04
F5	-2.21	F6	-3.12
F7	-2.10	F8	-6.88
F9	0.75	F10	-4.48
S1	-0.15	S2	-1.42
S3	-0.76	S4	
S5	2.60	S6	0.31
S7	-2.12	S8	-1.81
S9	0.43	S10	
S11	-0.35	S12	-
S13	-1.83	S14	-1.86
S15	46.09	S16	-1.96
S17	-2.18	S18	-4.73
S19	-1.76	S20	0.18
S21	-	S22	-0.60
S23	0.64	S24	2.53
S25	29.30	S26	-2.41

S27	-3.32	S28	1.43
S29	-3.63	S30	-4.51
S31	-2.44	S32	-1.35
S33			

B.1.2 Heated Arrays

Component	Biological Activity, % (Relative to 10 μM Geldanamycin)	Component	Biological Activity, % (Relative to 10 μM Geldanamycin)
	Screened at 100 μM		Screened at 100 μM
F11	-8.44	F12	-7.67
F13	-7.75	F14	-8.35
F15	-8.87	F16	-4.93
R1	-5.64	R2	-4.86
R3	-5.50	R4	-7.16
R5	-2.93	R6	-5.29
R7	-6.08	R8	-2.68
R9	0.09	R10	-2.92
R11	-0.50	R12	-0.16
R13	2.39	R14	-3.07
R15	-9.70	R16	-4.88
R17	-10.10	R18	-5.29
R19	-14.74	R20	-10.88
R21	-5.51	R22	-1.71
R23	-6.00	R24	-5.05
R25	-9.72	R26	-1.93
R27	-4.26	R28	-0.93
R29	-1.97	R30	-1.64
R31	-4.49	R32	-12.85
R33	-6.63	R34	-2.11

R35	-7.47	R36	-4.95
R37	-3.68		

B.2 Metal-Catalysed Carbenoid α-Diazoamide Reaction Arrays

Component	Biological Activity, % (Relative to 10 μM Geldanamycin)	Component	Biological Activity, % (Relative to 10 μM Geldanamycin)
	Screened at 100 μM		Screened at 100 μM
C9	1.33	C10	0.45
D1	1.78	D2	-1.14
D3	-0.68	D4	-0.49
D5	0.70	D6	-1.11
D7	-0.60	D8	-0.41
D9	-1.10	D10	-0.71
D11	-0.35	D12	-0.29
DF1	2.55	DF2	3.15
CS1	3.26	CS2	-0.26
CS3	1.85	CS4	-1.44
CS5	-2.38	CS6	-1.35
CS7	0.23	CS8	3.72
CS9	0.96	CS10	-5.56
CS11	-3.84	CS12	-8.54
CS13	-3.70	CS14	-4.30
CS15	2.79	CS16	4.30
CS17	4.73	CS18	-3.28
CS19	3.84	CS20	8.98

Appendix C
Analysis of Crude Reaction Array Mixtures by LCMS for Detection of Elaborated Hsp90 Fragments

C.1 C-H Functionalisation Reaction Array Product Analysis

C.1.1 Reaction Array LCMS Analysis

Crude reaction array mixtures were analysed by LCMS (Experimental 6.2) by diluting reaction arrays stocks (100 mM, DMSO) into MeCN to give a final product concentration of 5 mM. LC-MS spectra were analysed by searching for the mass of the starting fragment (with deprotection of acetate), substrate and bimolecular reaction products ([F+S] – [H+X], F= Fragment, S = substrate and X = H, Cl, Br, I or $B(OH)_2$). The catalyst is listed to show the full reaction mixture but masses of catalysts and additives were not searched for. For each component, the component number is given, the molecular weight and whether the mass was (✓) or was not (✗) detected. For reactions where more than one possible reaction is possible, multiple masses are given. 10% of the reaction array mixtures were analysed.

C.1.1.1 Room Temperature Reaction Array

Fragment	Substrate	Catalyst	Product
F4	S3	C3	289.3
150.2	185.0	-	
×	×	N/A	×
F2	S14	C8	335.5
219.3	448.8	-	369.9
✓	×	N/A	×
F1	S2	C3	356.4
223.3	179.0	-	400.2
✓	×	N/A	×
F4	S27	C5	299.3
150.2	151.1	-	
✓	×	N/A	×
F3	S5	C5	294.3
168.2	207.0	-	
×	×	N/A	×
F4	S19	C7	360.8
150.2	212.7	-	326.4
×	×	N/A	×
F2	S23	C6	288.4
219.3	71.1	-	
✓	×	N/A	×
F3	S33	C4	252.2
168.2	86.1	-	
×	×	N/A	×
F4	S1	C3	266.3
150.2	162.0	-	310.1
×	×	N/A	×
F3	S18	C7	304.3
168.2	136.2	-	
×	✓	N/A	×
F5	S32	C1	321.4
182.2	141.2	-	
×	×	N/A	×
F5	S17	C7	305.3
182.2	204.0	-	384.2
×	×	N/A	×
F7	S8	C2	338.8
187.2	279.5	-	430.2
×	×	N/A	×
F5	S24	C5	349.4
182.2	169.2	-	
×	×	N/A	✓
F7	S31	C4	284.3
187.2	99.1	-	
✓	×	N/A	×
F6	S33	C4	266.3
160.2	86.1	-	
×	×	N/A	×
F5	S3	C4	321.3
182.2	185.0	-	
×	×	N/A	×
F1	S2	C3	356.4
223.3	179.0	-	400.2
×	×	N/A	×

Fragment	Substrate	Catalyst	Product
F7	S1	C3	303.3
187.2	162.0	-	347.1
✓	×	N/A	×
F7	S31	C6	284.3
187.2	99.1	-	
✓	×	N/A	×
F8	S24	C5	356.4
189.2	169.2	-	
✓	×	N/A	×
F7	S32	C1	326.4
187.2	141.1	-	
✓	×	N/A	×
F9	S30	C1	358.4
197.2	163.2	-	
✓	×	N/A	×
F9	S19	C7	407.9
197.2	212.7	-	373.5
✓	×	N/A	×
F10	S9	C2	503.3
220.3	285.1	-	377.5
×	✓	N/A	✓
F10	S23	C5	289.4
220.3	71.1	-	
×	×	N/A	×
F5	S1	C1	342.1
182.2	162.0	-	298.3
×	×	N/A	✓
F7	S11	C3	306.3
187.2	163.1	-	
✓	×	N/A	×
F9	S6	C4	395.5
197.2	200.1	-	316.4
✓	×	N/A	×
F9	S8	C5	440.2
197.2	279.5	-	348.8
✓	×	N/A	×
F6	S6	C2	358.2
160.2	200.1	-	279.3
×	×	N/A	×
F4	S8	C7	393.2
150.2	279.5	-	301.7
✓	×	N/A	×
F4	S1	C8	310.2
150.2	162.0	-	266.3
×	×	N/A	✓
F1	S6	C6	421.3
223.3	200.1	-	342.2
×	×	N/A	✓
F5	S7	C1	325.3
182.2	224.1	-	
×	×	N/A	×
F5	S22	C1	285.3
182.2	105.1	-	
×	×	N/A	×

Fragment	Substrate	Catalyst	Product
F5	S18	C1	318.3
182.2	138.2	-	
×	×	N/A	×
F8	S18	C2	325.4
189.2	138.2	-	
✓	×	N/A	×
F7	S22	C3	290.3
187.2	105.1	-	
×	×	N/A	×
F9	S16	C4	356.4
197.2	161.2	-	
✓	✓	N/A	✓
F9	S20	C5	368.4
197.2	173.2	-	
✓	✓	N/A	×
F1	S18	C6	359.4
223.3	136.2	-	
✓	×	N/A	×
F4	S22	C7	253.3
150.2	105.1	-	
×	×	N/A	×
F8	S25	C4	387.3
189.2	200.1	-	352.8
✓	×	N/A	×
F4	S23	C8	219.3
150.2	71.1	-	
×	×	N/A	✓
F3	S27	C8	317.2
168.2	151.1	-	
×	×	N/A	×
F1	S30	C6	384.4
223.3	163.2	-	
✓	×	N/A	✓
F8	S21	C2	386.5
189.2	199.1	-	
✓	×	N/A	×
F9	S30	C5	358.4
197.2	163.2	-	
✓	×	N/A	×
F3	S7	C1	390.2
168.2	224.1	-	
×	✓	N/A	×
F10	S30	C2	381.4
220.3	163.2	-	
×	×	N/A	×
F7	S8	C3	338.8
187.2	279.5	-	430.2
×	×	N/A	×
F1	S5	C7	330.4
223.3	207.0	-	
×	×	N/A	×
F4	S9	C8	433.3
150.2	285.1	-	307.4
×	✓	N/A	×

Fragment	Substrate	Catalyst	Product
F3	S7	C3	311.3
168.2	224.1	-	
×	×	N/A	×
F4	S9	C4	433.3
150.2	285.1	-	307.4
×	✓	N/A	×
F5	S8	C5	333.7
182.2	279.5	-	425.2
×	×	N/A	×
F9	S15	C3	329.4
197.2	134.2	-	
✓	×	N/A	×
F4	S28	C2	204.2
150.2	56.1	-	
×	×	N/A	×
F6	S29	C5	293.3
160.2	135.2	-	
×	✓	N/A	×
F10	S14	C4	370.8
220.3	152.6	-	336.4
×	×	N/A	×
F2	S6	C1	338.5
219.3	200.1	-	
✓	×	N/A	×
F1	S27	C8	327.3
223.3	151.1	-	
✓	×	N/A	×
F6	S29	C3	293.3
160.2	135.2	-	
×	×	N/A	×
F6	S33	C3	244.3
160.2	86.1	-	
×	×	N/A	×
F1	S31	C1	320.4
223.3	99.13	-	
✓	×	N/A	×
F10	S26	C2	391.5
220.3	173.2	-	
×	×	N/A	×
F5	S32	C6	321.4
182.2	141.21	-	
×	×	N/A	×
F4	S26	C5	321.4
150.2	171.2	-	
×	×	N/A	×
F7	S23	C2	256.3
187.2	71.1	-	
×	×	N/A	×
F6	S33	C8	244.3
160.2	86.1	-	
×	×	N/A	×
F4	S26	C3	321.4
150.2	171.2	-	
×	✓	N/A	×

C.1.1.2 Heated Reaction Array 1

Fragment	Substrate	Catalyst	Product
F1	S31	C4	320.4
189.2	99.13	-	
×	×	N/A	×
F3	S29	C4	301.3
168.2	135.2	-	
×	✓	N/A	×
F4	S30	C4	311.3
150.2	163.2	-	
×	×	N/A	×
F5	S24	C4	349.4
182.2	169.2	-	
×	×	N/A	×
F7	S26	C4	358.4
187.2	171.2	-	
✓	×	N/A	×
F2	S14	C8	369.9
219.3	152.6	-	335.5
×	×	N/A	×
F3	S15	C8	300.3
168.2	134.2	-	
×	×	N/A	×
F5	S23	C8	251.3
182.2	71.1	-	
×	×	N/A	×
F7	S19	C8	397.9
187.2	212.7	-	363.4
✓	×	N/A	×
F9	S26	C8	368.5
197.2	171.2	-	
✓	×	N/A	×

Fragment	Substrate	Catalyst	Product
F1	S8	C2	374.8
189.2	279.5	-	466.3
×	×	N/A	✓
F2	S10	C2	491.4
219.3	274.1	-	365.5
✓	×	N/A	×
F4	S5	C2	276.3
150.2	207.0	-	
×	×	N/A	×
F5	S6	C2	380.2
182.2	200.1	-	301.3
×	×	N/A	×
F9	S1	C2	313.4
197.2	162.0	-	
✓	×	N/A	×
F2	S30	C6	380.5
219.3	163.2	-	
×	×	N/A	×
F3	S29	C6	301.3
168.2	135.2	-	
✓	✓	N/A	×
F4	S32	C6	289.4
150.2	141.2	-	
×	✓	N/A	×
F7	S26	C6	358.4
187.2	171.2	-	
✓	×	N/A	×
F9	S31	C6	294.4
197.2	99.13	-	
✓	×	N/A	×

C.1.1.3 Heated Reaction Array 2

Fragment	Substrate	Catalyst	Product
F11	R1	C4	288.5
219.3	71.1	-	
✓	×	N/A	×
F12	R2	C4	274.4
219.3	57.1	-	
✓	×	N/A	×
F13	R3	C4	425.5
249.3	178.2	-	
✓	×	N/A	✓
F14	R4	C4	293.5
243.3	152.2	-	
✓	×	N/A	×
F15	R5	C4	387.5
255.3	134.2	-	
✓	×	N/A	×
F8	R6	C4	287.3
189.1	100.1	-	
✓	×	N/A	×
F11	R1	C6	288.5
219.3	71.1	-	
✓	×	N/A	✓
F12	R9	C6	380.4
219.3	163.2	-	
✓	×	N/A	×
F13	R10	C6	333.4
249.3	86.1	-	
✓	×	N/A	×
F14	R7	C6	380.5
243.3	139.2	-	
✓	×	N/A	×
F15	R11	C6	341.5
255.3	128.2	-	
✓	×	N/A	×
F8	R12	C6	273.3
189.1	86.1	-	
✓	×	N/A	×
F11	R15	C7	373.5
219.3	156.3	-	
✓	×	N/A	✓
F12	R2	C7	274.4
219.3	57.1	-	
✓	×	N/A	×
F13	R16	C7	352.4
249.3	105.1	-	
✓	×	N/A	×

Fragment	Substrate	Catalyst	Product
F14	R17	C7	316.4
243.3	75.1	-	
✓	×	N/A	×
F15	R18	C7	326.4
255.3	73.1	-	
✓	×	N/A	×
F8	R19	C7	284.3
189.1	91.1	-	
×	×	N/A	×
F11	R22	C2	455.7
219.3	272.9	-	364.3
✓	×	N/A	✓
F12	R23	C2	296.4
219.3	158.0	-	
✓	×	N/A	×
F13	R24	C2	350.4
249.3	182.2	-	
✓	×	N/A	×
F14	R25	C2	358.5
243.3	196.1	-	
✓	×	N/A	×
F15	R26	C2	361.5
255.3	187.0	-	
✓	×	N/A	×
F8	R27	C2	308.3
189.1	200.0	-	
✓	×	N/A	×
F11	R30	C8	335.4
219.3	161.1	-	
✓	×	N/A	×
F12	R31	C8	351.5
219.3	118.1	-	
✓	×	N/A	×
F13	R32	C8	370.5
249.3	118.1	-	
✓	×	N/A	×
F14	R33	C8	338.4
243.3	123.2	-	
✓	×	N/A	×
F15	R34	C8	415.3
255.3	162.0	-	380.9
✓	×	N/A	×
F8	R35	C8	337.4
189.1	150.2	-	
✓	×	N/A	×

C.2 Fragment and α-Diazoamide Reaction Array Product Analysis

Fragment	Substrate	Catalyst	Product
F17	D1	C9	459.0
235.3	251.7	-	
✓	×	N/A	✓
F5	D2	C9	369.4
182.2	215.3	-	
✓	×	N/A	×
F10	D3	C9	375.5
220.3	183.2	-	
×	×	N/A	×
F8	D4	C9	341.4
189.2	180.2	-	
✓	×	N/A	×
F17	D5	C9	422.6
235.3	215.3	-	
✓	×	N/A	✓

Fragment	Substrate	Catalyst	Product
F17	D6	C10	362.5
235.3	155.2	-	
✓	×	N/A	×
F5	D7	C10	323.4
182.2	169.2	-	
×	×	N/A	×
F10	D8	C10	353.4
220.3	161.2	-	
×	×	N/A	×
F8	D9	C10	390.4
189.2	220.6	-	
×	×	N/A	×
F17	D10	C10	436.5
235.3	229.2	-	
✓	×	N/A	×

C.3 Hsp90 α-Diazoamide Fragment and Co-Substrate Reaction Array Product Analysis

Fragment	Substrate	Catalyst	Product
DF1*	CS1	C9	343.5
219.2	152.1	-	
✓	×	N/A	×
DF1*	CS10	C9	364.5
219.2	173.1	-	
✓	×	N/A	×
DF1*	CS19	C9	364.5
219.2	173.1	-	
✓	✓	N/A	×
DF1*	CS4	C10	382.5
219.2	191.1	-	
×	✓	N/A	✓
DF1*	CS13	C10	355.4
219.2	164.1	-	
×	✓	N/A	✓

Fragment	Substrate	Catalyst	Product
DF2*	CS1	C9	357.5
233.3	152.1	-	
×	×	N/A	×
DF2*	CS10	C9	378.5
233.3	173.1	-	
×	×	N/A	×
DF2*	CS19	C9	378.5
233.3	173.1	-	
×	✓	N/A	×
DF2*	CS4	C10	396.5
233.3	191.1	-	
×	✓	N/A	×
DF2*	CS13	C10	369.5
233.3	164.1	-	
×	×	N/A	×

* Mass of diazo with TBS deprotected

Appendix D
Anisotropy Calculations

D.1 Calculations for Determination of Tracer Dissociation Constant

D.1.1 P channel

Fixed Tracer Concentration	50 nM										
p channel Protein Concentration	1	2	3	Blank 1	Blank 2	Blank 3	Average Blank		Corrected 1	Corrected 2	Corrected 3
15.0000	239468	169938	158955	6834	6639	6220	6564.333333	*Subtract average blank from each p value for each protein concentration to give corrected p value for each protein concentration*	232903.667	163373.667	152390.667
7.5000	187139	150088	142258	6665	5920	5412	5999		181140	144089	136259
3.7500	206083	160820	154812	5902	5492	5488	5627.333333		200455.667	155192.667	149184.667
1.8750	193374	167400	162440	5698	8437	5938	6691		186683	160709	155749
0.9375	186381	154147	160800	5733	5616	5816	5721.666667		180659.333	148425.333	155078.333
0.4688	198871	161253	166470	5987	5452	5792	5743.666667		193127.333	155509.333	160726.333
0.2344	191354	153027	158420	5947	5932	5654	5844.333333		185509.667	147182.667	152575.667
0.1172	182700	144560	151615	7420	5954	10657	8010.333333		174689.667	136549.667	143604.667
0.0586	179846	144631	153056	5883	6334	6568	6261.666667		173584.333	138369.333	146794.333
0.0293	165964	131782	137789	6138	6093	5330	5853.666667		160110.333	125928.333	131935.333
0.0146	144632	116200	124642	5685	5489	5599	5591		139041	110609	119051
0.0073	123222	101989	104999	5597	6310	6190	6032.333333		117189.667	95956.6667	98966.6667
0.0037	115134	93561	95073	5708	5593	6219	5840		109294	87721	89233
0.0018	116504	92457	93949	5821	5775	6929	6175		110329	86282	87774
0.0009	103890	84704	86918	5934	5723	5413	5690		98200	79014	81228
0.0005	100657	80292	84408	5223	5572	5173	5322.666667		95334.3333	74969.3333	79085.3333
0.0002	103259	83313	83445	5607	6607	5714	5976		97283	77337	77469
0.0001	99066	81253	84359	5964	5341	5645	5650		93416	75603	78709
0.0001	104335	87444	86214	5488	5425	5679	5530.666667		98804.3333	81913.3333	80683.3333
0.0000	95695	76951	87535	5359	5160	5357	5292		90403	71659	82243
0.0000	99745	78085	79722	5782	5574	5718	5691.333333		94053.6667	72393.6667	74030.6667
0.0000	97760	73210	74577	5711	5310	5378	5466.333333		92293.6667	67743.6667	69110.6667
0.0000	106140	78120	81659	5161	5030	5452	5214.333333		100925.667	72905.6667	76444.6667
0.0000	98885	75569	76689	5449	5019	5464	5310.666667		93574.3333	70258.3333	71378.3333

D.1.2 S channel

s channel Protein Concentration (μM)	1	2	3	Blank 1	Blank 2	Blank 3	Average Blank		Corrected 1	Corrected 2	Corrected 3
15.0000	358628	250976	233231	10775	10339	10034	10382.66667	*Subtract average blank from each s value for each protein concentration to give corrected s value for each protein concentration*	348245.333	240593.333	222848.333
7.5000	279443	223983	210061	9364	9025	9056	9148.333333		270294.667	214834.667	200912.667
3.7500	306442	239365	229314	8719	8842	8412	8657.666667		297784.333	230707.333	220656.333
1.8750	289690	252667	241672	9329	11971	9107	10135.66667		279554.333	242531.333	231536.333
0.9375	271705	227743	233774	8595	8827	9084	8835.333333		262869.667	218907.667	224938.667
0.4688	290163	238490	244935	9044	9199	8799	9014		281149	229476	235921
0.2344	276342	222557	226081	8879	9359	8766	9001.333333		267340.667	213555.667	217079.667
0.1172	257414	208260	215291	10097	9089	16482	11889.33333		245524.667	196370.667	203401.667
0.0586	244281	198747	206068	9224	9341	9983	9516		234765	189231	196552
0.0293	214051	170453	172344	9677	9233	8998	9302.666667		204748.333	161150.333	163041.333
0.0146	167032	136610	141171	8706	8447	8636	8596.333333		158435.667	128013.667	132574.667
0.0073	136253	113013	115331	8880	9639	9302	9273.666667		126979.333	103739.333	106057.333
0.0037	123475	99958	99719	9038	8712	9485	9078.333333		114396.667	90879.6667	90640.6667
0.0018	122545	96888	95450	8875	9193	10447	9505		113040	87383	85945
0.0009	107353	85751	87782	8631	8709	8893	8744.333333		98608.6667	77006.6667	79037.6667
0.0005	103457	82850	86267	8746	8735	8558	8679.666667		94777.3333	74170.3333	77587.3333
0.0002	104090	85674	84666	8673	9651	9095	9139.666667		94950.3333	76534.3333	75526.3333
0.0001	100784	82868	85352	9372	8466	9022	8953.333333		91830.6667	73914.6667	76398.6667
0.0001	106878	92229	86794	8607	8706	8498	8603.666667		98274.3333	83625.3333	78190.3333
0.0000	97289	78817	92202	8462	8529	8305	8432		88857	70385	83770
0.0000	101506	79597	80648	9532	8747	9154	9144.333333		92361.6667	70452.6667	71503.6667
0.0000	101162	75714	76621	8961	8416	8616	8664.333333		92497.6667	67049.6667	67956.6667
0.0000	110105	81784	84661	8616	8403	8176	8398.333333		101706.667	73385.6667	76262.6667
0.0000	107072	77237	78786	9452	8078	8909	8813		98259	68424	69973

D.1.3 Anisotropy

Calculate anisotropy for each set of corrected p and s values at each protein concentration

$$r = 1000 \times \frac{s - gp}{s + g2p} \quad \textbf{\textit{Equation 1}}$$

Calculate average and standard deviation for each protein concentration

Anisotropy	1	2	3		Average	Stand Dev
Protein Concentration (μM)						
15.0000	141.6882	136.1081	133.5362		137.1108	4.1674793
7.5000	140.9394	140.6439	136.5642		139.3825	2.4451919
3.7500	139.3005	139.5596	137.7035		138.8545	1.0051871
1.8750	142.2399	145.0881	139.5627		142.2969	2.7631413
0.9375	131.7076	136.6577	130.5568		132.974	3.2416148
0.4688	131.8867	136.8499	134.9089		134.5485	2.5011726
0.2344	128.1894	130.6758	123.5162		127.4605	3.6350398
0.1172	119.0696	127.4224	121.8827		122.7916	4.2499147
0.0586	105.1334	109.1523	101.5171		105.2676	3.8193674
0.0293	85.02978	85.28185	72.86279		81.05814	7.0984995
0.0146	44.43043	49.83702	36.48373		43.58373	6.7167925
0.0073	27.09127	26.32368	23.32528		25.58008	1.9900735
0.0037	15.32403	11.86034	5.230887		10.80509	5.1286502
0.0018	8.124112	4.235479	-6.99445		1.78838	7.8507298
0.0009	1.38527	-8.54058	-9.06994		-5.40842	5.8894572
0.0005	-1.95133	-3.56523	-6.35397		-3.95684	2.2272929
0.0002	-8.05712	-3.47162	-8.42936		-6.6527	2.7611768
0.0001	-5.68908	-7.49968	-9.88096		-7.68991	2.1024062
0.0001	-1.79125	6.918513	-10.4067		-1.75981	8.662654
0.0000	-5.73308	-5.96154	6.150909		-1.84791	6.9281185
0.0000	-6.03275	-9.01784	-11.5091		-8.85324	2.7418921
0.0000	0.736236	-3.42653	-5.59711		-2.76247	3.2184689
0.0000	2.57282	2.189811	-0.79423		1.322799	1.8433779
0.0000	16.41395	-8.77921	-6.60619		0.342849	13.960325

D.1.4 Ligand Bound

Convert anisotropy to ligand bound for each protein concentration (see experimental equations) and calculate average and standard deviation.

Ligand Bound	1	2	3	Average	Stand Dev
Protein Concentration (μM)					
15.0000	52.2796792	47.6424369	45.6652432	22.2699721	22.630894
7.5000	51.627706	51.3731208	48.0030775	20.4394376	26.908314
3.7500	50.2339502	50.4513164	48.9177913	18.4021678	27.789286
1.8750	52.7662483	55.3659812	50.4539319	20.0013742	30.629867
0.9375	44.3153659	48.0774003	43.4885151	17.4188384	26.576076
0.4688	44.4456169	48.2306512	46.70874	17.0668579	27.007762
0.2344	41.8399491	43.5732534	38.7785014	15.8142227	24.100082
0.1172	36.0810178	41.3203953	37.7644064	15.2291658	22.689955
0.0586	28.7594322	30.7136036	27.0963714	11.5305216	16.719116
0.0293	20.4831431	20.5737973	16.4279825	9.23386456	10.437383
0.0146	8.89567984	10.1566721	7.16247997	5.62937099	5.1577151
0.0073	5.27897375	5.13228521	4.56913672	2.37656097	2.5842476
0.0037	3.13918742	2.55096456	1.47303682	2.56109229	2.5625091
0.0018	1.93596126	1.31636964	-0.3644441	3.05631017	4.2037897
0.0009	0.87493534	-0.5840733	-0.658648	1.7687665	3.5805896
0.0005	0.37125683	0.1325348	-0.2726639	0.78676182	1.2492832
0.0002	-0.5156878	0.14629605	-0.5683641	0.96923391	1.5535857
0.0001	-0.1768831	-0.4365114	-0.7722956	0.55533641	1.3574717
0.0001	0.39510792	1.74167913	-0.8455786	3.46813013	4.5820979
0.0000	-0.183238	-0.2161952	1.61901312	2.23731731	4.0637913
0.0000	-0.2264549	-0.6513221	-0.9982561	0.69686143	1.8007422
0.0000	0.77587024	0.15292694	-0.1635938	1.123801	1.8156463
0.0000	1.05758509	0.99847952	0.54436162	0.94728701	0.9227528
0.0000	3.32801446	-0.6177289	-0.3088633	4.4475325	8.2441074

D.2 Calculations for array data for Figure 4.5

Plate layout for screening reaction arrays in triplicate:

	1	2	3	4	5	6	7	8	9	10	11	12
A	A1	A2	A3	A4	A5	A6	A7	A8	A9	A10	A11	A12
B												

96 TO 384 WELL SCREENING PATTERN

	1	2	3	4	5	6	7	8	9	10	11	12	13	14	15	16	17	18	19	20	21	22	23	24
A	A1	A2	A3	A4	A5	A6	A7	A8	A9	A10	A11	A12	A1	A2	A3	A4	A5	A6	A7	A8	A9	A10	A11	A12
B	A1	A2	A3	A4	A5	A6	A7	A8	A9	A10	A11	A12	A1 BLANK	A1 BLANK	A1 BLANK	A1 BLANK	A1 BLANK	A1 BLANK	A1 BLANK	A1 BLANK	A1 BLANK	A1 BLANK	A1 BLANK	A1 BLANK
C																								
D																								

P Values:

P Channel

	1	2	3	4	5	6	7	8	9	10	11	12	13	14	15	16	17	18	19	20	21	22	23	24
A	460782	543375	579593	504358	542351	594255	594362	455597	553532	585813	538059	316524	587937	534160	608946	498913	534278	565961	540702	476946	567434	529379	513604	335898
B	557666	551574	516840	570742	538128	516633	536954	478087	549203	548722	512262	329655	7698	6740	7529	7114	8217	6867	5390	8032	7059	7011	6937	6886
C	455528	559780	486442	527808	519845	578186	530993	553396	582172	568017	519501	482953	567518	525585	530953	475909	483666	519962	469853	525702	542323	366925	476287	560471
D	620981	549133	543237	569408	532348	490807	507666	521975	536345	512122	520414	555287	10439	8510	6239	6975	6433	6416	6830	27304	9125	7360	6862	7124
E	489933	479445	507340	535846	571300	564155	589844	479646	596550	573459	572538	316943	559125	569933	535008	551605	629282	511586	431985	428849	520390	530618	512518	325389
F	620495	571710	580180	546550	550635	524199	547212	426980	519535	532036	512607	321097	7264	8027	8015	8130	7818	7687	7363	8068	6210	6921	6793	6442
G	477755	469768	474325	506019	629460	589505	579204	656475	595671	567521	564985	497346	593283	560821	572659	524147	567553	516430	537119	523786	525027	495414	489162	505784
H	597326	564000	512792	539249	541583	486956	505450	565068	503373	517916	494098	553526	9623	8036	6500	6600	7519	7072	7068	59173	7675	7714	6129	6245
I	486601	479129	476358	533609	538421	614701	547252	468208	581232	633957	533111	302999	582129	569954	574955	543979	536815	560410	512483	453889	528413	542628	513638	312682
J	620742	562796	574281	550440	524152	499518	518908	520505	552535	539718	488793	325298	8316	6484	7342	7877	6680	7458	6750	7823	6993	19854	7367	5989
K	488404	469447	542368	507338	507924	542025	449427	582188	549795	554084	508474	515955	549780	528634	540226	457235	525219	484933	488477	495806	486601	476883	421063	496400
L	592355	563412	553326	534890	506496	504294	535507	501480	513001	501487	471425	493153	8732	6692	6799	7176	7079	6166	7832	33304	6670	7200	6992	6102
M	481504	498793	543287	498000	540067	541221	551621	472071	535865	550898	527115	300862	615642	483524	559895	480363	508299	488541	455873	459715	477174	521828	496874	312911
N	590728	604120	524810	506527	503604	497438	501621	454696	502139	494566	486946	287079	5881	5575	6238	5812	12330	6474	5456	8056	5723	5435	8143	6774
O	504907	544548	500231	499259	511840	544951	416667	573613	571140	521861	473953	465269	518822	491405	410581	473916	501215	475900	434322	497310	441233	460548	418510	461003
P	658320	545991	513718	506981	544158	520870	450074	510280	479543	459436	412746	476182	7519	6419	5849	6346	6100	6081	7313	29689	7312	6176	4195	5406

P Channel Corrected Values

	1	2	3	4	5	6	7	8	9	10	11	12	13	14	15	16	17	18	19	20	21	22	23	24
A	453084	536635	572064	497244	534134	587388	588972	447565	546473	578802	531122	309638	580239	527420	601417	491799	526061	559094	535312	468914	560375	522368	506667	329012
B	549968	544834	509311	563628	529911	509766	531564	470055	542144	541711	505325	322769												
C	445089	551270	480203	520833	513412	571770	524163	526092	573047	560657	512639	475829	557079	517075	524714	468934	477233	513546	463023	498398	533198	359565	469425	553347
D	610542	540623	536998	562433	525915	484391	500836	494671	527220	504762	513552	548163												
E	482669	471418	499325	527716	563482	556468	582481	471578	590340	566538	565745	310501	551861	561906	526993	543475	621464	503899	424622	420781	514180	523697	505725	318947
F	613231	563683	572165	538420	542817	516512	539849	418912	513325	525115	505814	314655												
G	468132	461732	467825	499419	621941	582433	572136	597302	587996	559807	558856	491101	583660	552785	566159	517547	560034	509358	530051	464613	517352	487700	483033	499539
H	587703	555964	506292	532649	534064	479884	498382	505895	495698	510202	487969	547281												
I	478285	472645	469016	525732	531741	607243	540502	460385	574239	614103	525744	297010	573813	563470	567613	536102	530135	552952	505733	446066	521420	522774	506271	306693
J	612426	556312	566939	542563	517472	492060	512158	512682	545542	519864	481426	319309												
K	479672	462755	535569	500162	500845	535859	441595	548884	543125	546884	501482	509853	541048	521942	533427	450059	518140	478767	480645	462502	479931	469683	414071	490298
L	583623	556720	546527	527714	499417	498128	527675	468176	506331	494287	464433	487051												
M	475623	493218	537049	492188	527737	534747	546165	464015	530142	545463	518972	294088	609761	477949	553657	474551	495969	482067	450417	451659	471451	516393	488731	306137
N	584847	598545	518572	500715	491274	490964	496165	446640	496416	489131	478803	280305												
O	497388	538129	494382	492913	505740	538870	409354	543924	563828	515685	469758	459863	511303	484986	404732	467570	495115	469819	427009	467621	433921	454372	414315	455597
P	650801	539572	507869	500635	538058	514789	442761	480591	472231	453260	408551	470776												

S Values:

S Channel

	1	2	3	4	5	6	7	8	9	10	11	12	13	14	15	16	17	18	19	20	21	22	23	24
A	578527	684731	690233	643768	670955	738508	714254	606708	663257	734653	659992	277403	716562	684266	729859	635212	659439	705756	662001	611508	672974	667254	624889	295919
B	687656	648296	619654	695182	670820	618628	680809	606494	700341	667674	656256	278468	14283	12829	13682	13064	14046	12228	12302	14925	12972	11810	13757	12340
C	569099	684946	604773	680350	636110	731368	643587	707707	702549	721103	635558	625397	689960	677452	653091	615007	596086	660165	579716	666788	657544	465106	583506	688238
D	742474	650734	688957	693113	689829	607127	639931	640839	683598	630532	660483	674455	16949	14828	11950	12840	12843	13288	13390	33282	15793	13731	13183	12809
E	600825	605043	623986	672902	695145	707761	713407	614479	710338	726418	689027	277806	692026	723830	659610	687851	739729	639680	527740	547316	615933	654599	615185	283111
F	761700	676927	722165	671374	709235	641441	687990	536497	656038	642916	649206	272036	13865	14060	13879	13524	13237	12128	12900	14715	12330	12772	13106	12638
G	595093	598543	582986	655933	752604	733909	694977	814690	717315	713158	677752	635827	719146	710953	692907	661762	669472	646201	644970	638675	622287	614185	580953	614146
H	740768	671610	641408	652040	687295	587797	651758	672579	643751	629069	630682	678728	15218	13611	12967	12660	13412	12679	14234	64489	13657	14050	12657	12853
I	598206	609099	590447	667747	660562	787775	661295	608524	694394	786700	656314	265117	697593	714563	690815	689579	636054	685841	613999	563193	626595	662630	609467	269224
J	751987	671528	714280	665815	666401	609694	655831	662018	692230	655810	621472	273773	13897	12915	14367	14377	13598	13069	13002	15113	12894	26807	13767	11382
K	599502	603622	668034	648021	628962	703327	548792	739266	667373	695220	623432	651355	667682	670258	653610	565601	628431	615896	594007	615211	581150	590261	507303	591683
L	719692	676558	690663	654846	640036	617562	692092	600820	649524	621608	598894	595725	15156	12478	12538	12627	13123	11680	14481	39526	13476	12970	12764	11864
M	593722	635529	664609	635516	666224	693899	662750	611576	647223	692856	649758	262207	737200	607005	673017	602720	618772	599966	549210	582648	580295	640916	589882	269479
N	720384	716674	650504	628414	635560	617690	651370	584723	637336	611356	613375	247427	11524	11043	11745	11975	22204	12274	12038	15628	11281	11564	14089	12689
O	618378	695519	615665	638671	637250	692831	504429	719204	681599	658446	579479	592341	638962	612471	506867	590765	607097	584784	530791	613575	547994	568236	509121	555235
P	801986	655169	638252	612413	673509	631425	566023	630573	601937	571046	513477	592096	13657	12265	11595	12286	11825	11865	16004	34752	13661	12124	10511	11329

S Channel Corrected Values

	1	2	3	4	5	6	7	8	9	10	11	12	13	14	15	16	17	18	19	20	21	22	23	24
A	564244	671902	676551	630704	656909	726280	701952	591783	650285	722843	646235	265063	702279	671437	716177	622148	645393	693528	649699	596583	660002	655444	611132	283579
B	673373	635467	605972	682118	656774	606400	668507	591569	687369	655864	642499	266128												
C	552150	670118	592823	667510	623267	718080	630197	674425	686756	707372	622375	612588	673011	662624	641141	602167	583243	646877	566326	633506	641751	451375	570323	675429
D	725525	635906	677007	680273	676986	593839	626541	607557	667805	616801	647300	661646												
E	586960	590983	610107	659378	681908	695633	700507	599764	698008	713646	675921	265168	678161	709770	645731	674327	726492	627552	514840	532601	603603	641827	602079	270473
F	747835	662867	708286	657850	695998	629313	675090	521752	643708	630144	636100	259398												
G	579875	584932	570019	643273	739242	721230	680743	750201	703658	699108	665095	622974	703928	697342	679940	649102	656060	633522	630736	574186	608630	600135	568296	601293
H	725550	657999	628441	639380	673883	575118	637524	608090	630094	615019	618025	665875												
I	584309	596184	576080	653370	646964	774706	648293	593411	681500	759893	642547	253735	683696	701648	676448	675202	622456	672772	600997	548080	613701	635823	595700	257842
J	738090	658613	699913	651438	652803	596625	642829	646905	679336	629003	607705	262391												
K	584346	591144	655496	635394	615839	691647	534311	699740	653897	682250	610668	639491	652526	657780	641072	552974	615308	604216	579526	575685	567674	577291	494539	579819
L	704536	664080	678125	642219	626913	605882	677611	561294	636048	608638	586130	583861												
M	582198	624486	652864	623541	644020	681625	650712	595948	635942	681292	635669	249518	725676	595962	661272	590745	596568	587692	537172	567020	569014	629352	575793	256790
N	708860	705631	638759	616439	613356	605416	639332	569095	626055	599792	599286	234738												
O	604721	683254	604070	626385	625425	680966	488425	684452	667938	646322	568968	581012	625305	600206	495272	578479	595272	572919	514787	578823	534333	556112	498610	543906
P	788329	642904	626657	600127	661684	619560	550019	595821	588276	558922	502966	580767												

Anisotropy Calculations:

Anisotropy Values

	1	2	3	4	5	6	7	8	9	10	11	12	13	14	15	16	17	18	19	20	21	22	23	24
A	109.398	111.347	90.8029	116.047	104.876	106.809	93.5731	131.19	93.0134	110.419	101.008	-20.164	99.1072	117.379	93.2691	115.086	103.99	107.974	100.104	117.152	89.328	112.124	97.8728	-17.931
B	103.267	85.8405	92.9593	99.0775	107.669	92.8923	112.952	113.207	115.896	99.226	116.921	-32.325												
C	108	100.669	106.244	119.815	100.189	112.452	96.712	119.909	95.5559	114.121	100.216	121.455	98.4466	119.777	102.531	120.523	102.604	113.529	102.89	116.815	97.0994	112.292	100.476	102.158
D	92.5196	88.8601	113.845	98.8666	121.411	103.728	111.036	104.391	115.547	102.553	113.762	98.1242												
E	100.812	111.799	102.524	110.603	99.0599	110.774	96.812	117.026	90.7223	113.539	94.4508	-20.942	104.584	114.541	103.54	108.067	86.6513	109.413	99.7428	115.286	88.1501	103.616	93.1819	-23.231
F	101.826	88.772	107.232	102.51	119.978	101.498	110.899	109.442	111.905	96.0299	112.938	-32.375												
G	107.464	115.595	101.514	121.634	92.6026	107.349	92.9712	112.479	95.0392	110.412	93.0536	116.083	97.8363	114.07	96.3168	111.961	87.4035	108.94	93.0092	106.628	88.9167	105.077	88.9419	97.1314
H	106.252	91.0689	108.211	96.1395	114.155	95.5629	119.124	96.6272	116.826	97.6526	115.51	100.997												
I	102.468	114.033	104.411	108.653	100.995	118.153	95.8551	121.889	92.0544	107.085	102.613	-20.829	93.4739	109.364	93.5477	113.483	88.2209	100.995	92.5313	104.536	89.0831	100.864	88.9804	-26.039
J	97.5775	91.1789	106.251	96.2264	114.075	99.754	112.235	114.156	109.371	98.9913	114.298	-33.407												
K	101.448	118.628	103.131	116.612	104.801	122.391	98.9971	117.887	97.2082	110.031	101.302	111.983	97.8311	113.71	96.5646	104.528	92.2791	114.219	97.7371	109.217	90.8559	104.656	94.3273	90.7834
L	98.1695	93.8793	108.073	101.082	112.279	100.885	120.531	95.6957	112.539	105.313	114.221	95.6575												
M	103.176	115.402	100.687	115.611	102.075	117.838	93.451	120.583	95.8975	110.464	103.408	-23.067	93.0531	109.855	94.3385	109.255	96.8738	101.71	93.8091	112.315	98.0997	101.603	89.4351	-26.776
N	99.6171	89.6694	105.436	105.246	110.315	105.832	121.776	117.695	113.967	103.813	111.222	-27.305												
O	100.729	116.415	102.525	116.728	106.866	114.698	93.9746	113.164	91.4079	111.712	99.3648	114.627	102.848	107.135	103.066	107.027	96.7115	101.81	97.6891	107.202	105.331	103.128	97.0599	94.1763
P	99.4026	93.4772	106.06	95.6467	104.849	97.0796	108.498	107.775	109.513	105.831	105.24	105.984												

Average Anisotropy / **Standard Deviation**

	1	2	3	4	5	6	7	8	9	10	11	12	1	2	3	4	5	6	7	8	9	10	11	12
A	103.924	104.855	92.3437	110.07	105.512	102.558	102.209	120.516	99.4124	107.256	105.267	-23.473	4.22662	13.6692	1.09688	7.78287	1.56795	6.85158	8.05021	7.71708	11.7523	5.72096	8.3393	6.32533
B	99.6554	103.102	107.54	113.068	108.068	109.903	103.546	113.705	102.734	109.655	104.818	107.246	6.37743	12.7383	4.70908	10.0462	9.48616	4.38863	5.86608	6.70619	9.08195	5.07705	6.32528	10.1817
C	102.407	105.037	104.432	107.06	101.897	107.228	102.484	113.918	96.9259	104.395	100.19	-25.516	1.59393	11.5557	2.02288	3.37983	13.7527	4.08994	6.06888	3.24386	10.644	7.1692	9.02915	4.93902
D	103.851	106.911	102.014	109.911	98.0536	103.95	101.701	105.245	100.261	104.381	99.1686	104.737	4.28152	11.2195	4.86861	10.5084	11.5813	5.96635	12.3196	6.54485	11.9773	5.23238	11.6765	8.1765
E	97.8399	104.859	101.403	106.121	101.097	106.301	100.207	113.527	96.8362	102.314	101.964	-26.758	3.67666	9.85905	5.60514	7.26885	10.555	8.3962	8.61255	7.09834	8.94614	3.45969	10.3462	5.16032
F	99.1494	108.739	102.59	107.407	103.119	112.498	105.755	107.6	100.201	106.667	103.283	99.4746	1.6309	10.6976	4.71397	6.65939	8.25091	8.86393	10.4606	9.1314	9.10137	2.39401	8.24166	9.06582
G	98.6153	104.975	100.154	110.037	103.088	108.46	103.012	116.865	102.655	105.293	101.355	-25.716	4.19281	11.0572	4.54612	4.26739	5.53379	6.84118	13.269	3.42602	8.04943	3.76584	9.01217	1.88561
H	100.993	105.676	103.884	106.467	102.809	104.529	100.054	109.381	102.084	106.891	100.555	104.929	1.41906	9.42085	1.5543	8.61568	4.3894	7.44513	6.16049	2.68554	7.73968	3.58338	3.44388	8.38221

Red = Negative controls, Green = Positive controls